Role of GTPases in Assembly of the Bacterial 30S Subunit

Aida Razi

Department of Anatomy and Cell Biology

McGill University, Montreal

Quebec, Canada

August 2018

A thesis submitted to McGill University in partial fulfillment of the requirements of the degree of Doctor of Philosophy.

There is no substitute for hard work.

- Thomas A. Edison

Table of Contents

Abstract

My PhD thesis aims to improve our understanding of the assembly process of the bacterial ribosome and the overarching goal of my research is to identify steps in this pathway that can be targeted with new molecular probes. Ribosome assembly in actively growing *Escherichia Coli* involves multiple events including synthesis of 54 ribosomal-proteins and their binding to ribosomal RNAs in a hierarchical manner. Many of these events are assisted by a number of accessory proteins known as assembly factors, making the process extremely fast and efficient. **My PhD thesis contributes new knowledge on the precise mechanism by which YjeQ and Era assist the ribosome assembly process.** Recent work indicates that both factors assist the late stages of the 30S subunit assembly. To reveal the precise role of YjeQ in the context of the mature 30S subunit, we solved the structure of the 30S subunit in complex with YjeQ by cryo-electron microscopy (Cryo-EM). Our data suggested that in addition to work as a maturation factor, YjeQ also functions as a checkpoint protein testing the proofreading ability of the ribosomal subunit prior to the particle's release into the pool of actively translating ribosomes. This work provides the first example of a bacterial assembly factor that tests a specific translation mechanism of the 30S subunit. To investigate the role of Era, we used quantitative mass spectrometry (qMS), microscale thermophoresis (MST) and cryo-EM techniques. We first determined using cryo-EM the structures of the assembly intermediate that accumulated in *E. coli* upon depletion of Era at 3.8Å resolution. In addition, we also solved the structure of the mature 30S subunit in complex with Era. We found that Era-depleted cells accumulated three assembly intermediates at different stages of maturation ranging from early stage of maturation to the late stage of 30S subunit with missing density both in the central and 3' minor domains of the 30S subunit. Densities for ribosomal proteins (r-proteins) bS21, bS1, uS3 and uS2 bound to the central domain were also missing from the late stage of 30S subunit. The

structure of the 30S subunit in complex with Era demonstrated that binding of this factor reverts the mature subunit to an immature state lacking density for the motifs integrating the decoding center. These results suggest that Era facilitates the proper folding of the platform region of the 30S subunit. In addition, Era may work as a placeholder for some of the late ribosomal proteins and prevent premature association of the 30S subunit with the 50S subunit. Finally, we tested whether YjeQ and Era exert their function in conjunction rather than independently. To this end, we obtained the cryo-EM structure of the 30S subunit in complex with Era and YjeQ at 3.5Å resolution. However, we couldn't observe any density for YjeQ in this structure. Moreover, we demonstrated Era binds to the cavity between head and platform and reverts the structure of the 30S subunit to its immature state. These results suggest that Era and YjeQ works subsequently during assembly. Era binds first to the assembling subunit and assists the folding of the platform region at the same time that it prevents the binding of YjeQ. Once Era is released, YjeQ binds assisting the maturation of the decoding center and testing the fidelity of the subunit before releasing it to the pool of fully active ribosomes. Overall, this thesis provides novel insights into the function of two important GTPases dedicated to the assembly process of the bacterial ribosome.

Résumé

Ma thèse de doctorat vise à améliorer notre compréhension des processus d'assemblage du ribosome bactérien et l'objectif global de mon travail de recherche est d'identifier les étapes de cette voie, qui peut être une cible potentielle pour de nouvelles molécules thérapeutiques. L'assemblage de ribosomes chez *Escherichia coli* en croissance active implique plusieurs évènements, dont la synthèse de 54 protéines ribosomales, et leur liaison aux ARN ribosomiques de façon hiérarchique. Plusieurs de ces évènements sont assistés par certain nombre de protéines accessoires, les facteurs d'assemblage, qui rendent le processus extrêmement rapide et efficace. **Ma thèse de doctorat contribue aux nouvelles connaissances sur le mécanisme précis par lequel YjeQ et Era assistent le processus d'assemblage du ribosome.** Des travaux récents indiquent que ces deux facteurs aident les dernières étapes de l'assemblage de la sous-unité 30S. Pour révéler le rôle précis de YjeQ dans le contexte de la sous-unité mature 30S, nous avons résolu la structure de la sous-unité 30S en complexe avec YjeQ, par Cryo-microscopie électronique (Cryo-EM). Nos données révèlent qu'en plus de fonctionner comme un facteur de maturation, YjeQ fonctionne également comme une protéine de contrôle qui teste la capacité de relecture de la sous-unité ribosomale, avant la libération de la particule dans le pool des ribosomes actifs. Ce travail fournit le premier exemple d'unfacteur d'assemblage bactérien qui teste un mécanisme de traduction spécifique de la sous-unité 30S. Pour examiner le rôle d'Era, nous avons utilisé la spectrométrie de masse quantitative (qSM), la thermophorèse à l'échelle microscopique (MST) et la technique de la cryo-EM. Nous avons d'abord déterminé, en utilisant la cryo-EM, les structures de l'intermédiaire d'assemblage accumulées dans *E. Coli* lors de la déplétion d'Era, à une résolution de 3.8Å. En outre, nous avons également résolu la structure de la sous-unité 30S mature dans le complexe avec l'Era. Nous avons trouvé que les bactéries déplétée en Era accumulaient principalement un intermédiaire d'assemblage avec des densités

manquantes à la fois dans les domaines central et 3' mineur de la sous-unité 30S. Les densités des protéines ribosomiques bS21, bS1, uS3 et uS2 liées au domaine central étaient également manquantes. La structure de la sous-unité 30S en complexe avec Era a démontré que la liaison de ce facteur ramène la sous-unité mature à un état immature auquel manquent les densités des motifs intégrant le centre de décodage. Ces résultats suggèrent qu'Era facilite le repliement correct de la région de la plateforme de la sous-unité 30S. En outre, Era peut agir comme un espace réservé pour certaines des protéines ribosomales tardives et empêcher l'association prématurée de la sous-unité 30S avec la sous-unité 50S. Enfin, nous avons testé si YjeQ et Era exerçaient leur fonction en conjonction plutôt qu'indépendamment. À cette fin, nous avons obtenu la structure en Cryo-EM de la sous-unité 30S dans le complexe avec Era et YjeQ à une résolution de 3.8Å. Cependant, nous n'avons pas pu observer de densité pour YjeQ dans cette structure. De plus, nous avons démontré qu'Era se lie à la cavité entre la tête et la plateforme et ramène la structure de la sous-unité 30S à son état immature. Ces résultats suggèrent qu'Era et YjeQ fonctionnent successivement pendant l'assemblage. Era se lie d'abord à la sous-unité d'assemblage et aide au repliement de la région de la plateforme en même temps qu'elle empêche la liaison de YjeQ. Une fois qu'Era est libérée, YjeQ se lie pour aider à la maturation du centre de décodage et tester l'efficacité de la sous-unité avant de la relâcher dans le pool de ribosomes actifs. Dans l'ensemble, cette thèse fournit de nouvelles pistes sur la compréhension de la fonction de deux GTPases importantes impliquées dans le processus d'assemblage du ribosome bactérien.

Acknowledgements

I am extremely grateful to my supervisor, Dr. Joaquin Ortega, who cared so much about my work, my future and my success. His deep insights guided my research at various stages and his vast knowledge, providing resolution to every issue. He taught me so much as a person. He is kind and considerate. I will really miss our conversations while collecting data for 24 hour stretches at the Hospital for Sick Children. Also, I would like to thank him for making my move to Montreal possible so that I could pursuit of my dreams. He was and remains my best role model as a scientist.

Special thanks to Dr. Alba Guarne for providing guidance, encouragement and advice during my graduate studies. I would like to thank her for teaching me protein purification. It was a privilege for me to experience and observe her extraordinary abilities.

I would like to thank my mentor Dr. Huy Bui for his valuable insights and advice that propelled my project's progress. Also, I will forever be thankful to my committee member Dr. Chantal Autexier. I will never forget her support and kindness since my move to McGill University.

I want to thank Dr. Jonathan Lovell for his collaboration in the liposomes work.

To Dr. John Rubinstein, I would like to express my gratitude for allowing me to use his lab's microscope. My first paper would not have been possible without his generosity.

I would like to thank all members of the Ortega's lab, past and present, for helpful discussions. Particularly, special thanks to Dr. Brett Thurlow and Dushyant Jahagirdar for their support and companionship.

To my friend Dr. Monica Pillon, thank you for listening to and supporting me through my graduate studies. I am also truly thankful to Dr. Kaustuv Basu for his selfless willingness to assist, whenever needed. I would like to thank Dr. Vargas for all of our insightful conversations.

I would like to thank my family: my mother, Sima Khoshand for teaching me to practice patience, my father Nezam Razi, who taught me perseverance, my sisters, Nahid, Mitra and Azita, my uncle Mehrdad Khoshand and my aunt Dr. Simin Khoshand, for their unconditional support, encouragement and love. I would like to thank my brother-in-law Behnam Kochnari for his guidance and support during my graduate studies.

Words fail to express my gratitude to my grandmother, who always gave me encouragement through all the challenges that I encountered during my PhD studies. She helped me to see the light at the end of the tunnel. I remember on the days that I was hopeless, she would ask me, “When am I visiting you in your office?”

I am truly grateful to my dear nephew, Arash Lotfi, for all his support and love. He always encouraged me to explore my potential and pursue my dreams.

Finally, I would like to acknowledge the most important person in my life - my husband, Mohammad Farjadnia. He experienced all of the ups and downs of my research with me. He has been my rock during the past five years of my graduate studies. Thank you for all your love and care and thank you for always believing in me. You always encouraged me to keep going and you were a constant source of strength to me. Thank you for supporting my relocation to Montreal to continue my education. Without you I would not have the strength to come this far.

First-Authored Manuscripts

The present thesis is submitted in a manuscript-based format. In accordance to the guidelines of the Faculty of Graduate and Postdoctoral Studies at McGill University, the thesis is composed of published or to be submitted first- authored manuscripts. The candidate is the first author of the two included manuscripts. The contributions of all authors to each article are stated in the Contribution of Authors section.

Chapter 2

The cryo-EM structure of YjeQ bound to the 30S subunit suggests a fidelity checkpoint function for this protein in ribosome assembly

Aida Razi, Alba Guarné and Joaquin Ortega

PNAS, 2017 April; 114(17): E3396-E3403.

Chapter 3

Role of Era in the assembly of the 30S subunit and ribosome homeostasis

Aida Razi, Joseph H. Davis, Dushyant Jahagirdar, Brett Thurlow, Kaustuv Basu, Nikhil Jain, Robert A. Britton, Javier Vargas, Alba Guarné, James R. Williamson and Joaquin Ortega

To be submitted

Contributions of Authors

Chapter 2

I designed experiments, purified proteins and ribosomes, performed cryo-EM sample preparation, EM data collection and image analysis. Dr. A. Guarné performed model building and real-space rigid body refinement of the atomic model. Dr. J. Ortega designed and supervised the study. The three authors wrote and edited the manuscript.

Chapter 3

I designed experiments, purified proteins and ribosomes, performed cryo-EM sample preparation, EM data collection and image analysis. J.D. performed the qMS experiments. D.J. performed MST experiments. B.T. obtained the Era depleted strain and contributed experiment in Figure 1A. K.B. designed and implemented strategies for cryo-EM data collection in the Titan Krios TEM (FEMR-McGill). N.J performed qPCR analysis. J.V. designed image processing approaches. A.G. performed model building of the atomic models. R.B, J.W and J.O. designed and supervised the study. A.R. and J.O wrote the manuscript and all authors contributed to editing.

Original Contributions to Knowledge

Chapter 2

Studying of the factors through investigating their role on the context of the mature 30S subunit gives an initial insight to the function and molecular mechanism of them. More specifically, studying the YjeQ factor in complex with the 30S subunit reveals the fact that YjeQ works as a checkpoint protein in addition to have a role in the maturation of the 30S subunit.

Chapter 3

Investigating the role of the assembly factors by removing of these factors in addition to analyze them on the context of the mature 30S subunit give an initial insight to the function of them. Studying of the $30S_{Era\text{-}depleted}$ particles, in addition to the complex of the Era with the 30S subunit reveal the fact that Era has a role as a local chaperon to facilitate the proper folding of specific motifs in the central domain of the 30S subunit. In addition, aiming to understand the functional interplay between Era and YjeQ, it was found that binding of Era to the mature 30S subunit reverts the 30S subunit back to the immature state that is no longer recognized by YjeQ. This finding suggests the function of Era is prior to YjeQ and likely both factors act sequentially during assembly rather than at the same time.

Collaborative Publications

I contributed intellectually, performed experiments such as cryo-EM, data collection and image analysis, or wrote drafts of the review papers for 12 studies, which resulted in peer-reviewed publications. These publications are listed below, and my first authors review papers are included in the appendix of this thesis.

1. Highly-Soluble Cyanine J-aggregates Entrapped by Liposomes for In Vivo Optical Imaging around 930 nm

Dyego Miranda, Haoyuan Huang, Homan Kang, Ye Zhan, Depeng Wang, Yang Zhou, Jumin Geng, Hailey Kilian, Wesley Stiles, Aida Razi, Joaquin Ortega, Jun Xia, Hak Soo Choi, Jonathan F Lovell

Theranostics, 2018 November; *In press.*

2. A malaria vaccine adjuvant based on recombinant antigen binding to liposomes

Wei-Chiao Huang, Bingbing Deng, Cuiyan Lin, Kevin Carter, Jumin Geng, Aida Razi, Xuedan He, Upendra Chitgupi, Jasmin Federizon, boyang sun, Carole Long, Joaquin Ortega, Sheetij Dutta, C King, Kazutoyo Miura, Shwu-Maan Lee, and Jonathan Lovell

Nature Nanotechnology, 2018 October; 10.1038/s41565-018-0271-3.

3. Ribosomal proteins: Their role in the assembly, structure and function of the ribosome

Aida Razi and Joaquin Ortega

eLS, 2017 September; 10.1002/978047001590 **(attached)**.

4. Final touches and quality control on the assembly of the eukaryotic ribosome

Aida Razi and Joaquin Ortega

EMBO J., 2017; 36(7):834-836 **(attached)**.

5. The Impact of recent improvements in cryo-electron microscopy technology on the understanding of bacterial ribosome assembly.

Aida Razi, Robert A. Britton and Joaquin Ortega

Nucleic Acid Research, 2016 November; 45(3):1027-1040 **(attached)**.

6. Design of Hydrated Porphyrin-Phospholipid Bilayers with Enhanced Magnetic Resonance Contrast

Shuai Shao, Trang Nhu Do, Aida Razi, Upendra Chitgupi, Jumin Geng, Richard J. Alsop, Boris G. Dzikovski, Maikel C. Rheinstadter, Joaquin Ortega, Mikko Karttunen, Joseph A. Spernyak, Jonathan F. Lovell

Small, 2017 January; 13(1).

7. YphC and YsxC GTPases assist the maturation of the central protuberance, GTPase associated region and functional core of the 50S ribosomal subunit.

Xiaodan Ni, Joseph H. Davis, Nikhil Jain, Aida Razi, Samir Benlekbir, Andrew G. McArthur, John L. Rubinstein, Robert A. Britton, James R. Williamson, and Joaquin Ortega

Nucleic Acids Research, 2016 July; 44:8442-55 **(attached)**.

8. Sphingomyelin Liposomes Containing Porphyrin-phospholipid for Irinotecan Chemophototherapy

Kevin A. Carter, Dandan Luo, Aida Razi, Jumin Geng, Shuai Shao, Joaquin Ortega, Jonathan F. Lovell

Theranostics, 2016 June; 6: 2329-2336.

9. Lack of Adipocyte AMPK Exacerbates Insulin Resistance and Hepatic Steatosis through Brown and Beige Adipose Tissue Function.

Emilio Mottillo, Eric M. Desjardins, Justin D. Crane, Brennan K. Smith, Alex E. Green, Serge Ducommun, Tora I. Henriksen, Irena A. Rebalka, Aida Razi, Kei Sakamoto, Camilla Scheele, Bruce E. Kemp, Thomas J. Hawke, Joaquin Ortega, James G. Granneman, and Gregory R. Steinberg

Cell Metabolism, 2016 July; 24:118-129.

10. Porphyrin Phospholipid Liposomes with Tunable Leakiness.

Dandan Luo, Kevin A. Carter, Aida Razi, Jumin Geng, Shuai Shao, Joaquin Ortega, Jonathan F. Lovell

Journal of Controlled Release, 2015 December; 220:484-494.

11. Doxorubicin Encapsulated in Stealth Liposomes Conferred with Light-Triggered Drug Release.

Dandan Luo, Kevin A Carter, Aida Razi, Jumin Geng, Shuai Shao, Daniel Giraldo, Ulas Sunar, Joaquin Ortega, Jonathan F. Lovell

Biomaterials, 2015 November; 75:193-202.

12. YjeQ zinc finger domain monitors the conformation of the decoding center and catalyzes the release of RbfA during 30S ribosome subunit assembly.

Ajitha Jeganathan, Aida Razi, Brett Thurlow and Joaquin Ortega

***RNA**, 2015;* 21: 1203-1216 **(attached)**.

List of Abbreviations

16S	mature 30S subunit rRNA molecule
17S	immature 30S subunit rRNA molecule
23S	mature 50S subunit rRNA molecule
2D	two-dimensional
30S	prokaryotic small ribosome subunit
$30S_{Era\text{-}depleted}$	30S particle that accumulates in Era-depleted strain
$30S_{\Delta rimM}$	immature 30S particles that accumulates in Δ*rimM* strain
$30S_{\Delta yjeQ}$	immature 30S particle that accumulates in Δ*yjeQ* strain
3D	three-dimensional
40S	eukaryotic small subunit
50S	prokaryotic large ribosome subunit
5S	mature 50S subunit rRNA molecule
60S	eukaryotic large ribosome subunit
70S	prokaryotic ribosome
80S	eukaryotic ribosome
A	adenine
A-site	aminoacyl site
A260	Light absorbance at 260 nanometres (wavelength)
BSA	Bovine serum albumin
C	cytosine
Cryo-EM	Cryo-electron microscopy
C-Terminal	Carboxyl-terminus
CTE	C-terminal extension (C-terminal helix of zinc-finger domain of YjeQ)
DNA	Deoxyribonucleic acid
DNAse	Deoxyribonuclease
DTT	Dithiothreitol
E.coli	*Escherichia coli*
EDTA	Ethylenediaminetetraacetic acid
EMDB	Electron Microscopy Data Bank
Era	*E.coli* ras-like protein
FPLC	Fast protein liquid chromatography
FT	flow-through
g	gravitational force
G	guanosine
GDP	Guanosine diphosphate
GTP	Guanosine-5'-triphosphate
GTPase	Guanosine triphosphate hydrolase
GMP-PNP	5'-Guanylyl imidodiphosphate – non-hydrolyzable analog of GTP
GDPNP	Guanosine 5'-(tetrahydrogen triphosphate) – non-hydrolyzable analog of GTP
h44	Helix 44 of the 16S rRNA of the 30S subunit
h45	Helix 45 of the 16S rRNA of the 30S subunit
IF2	Initiation factor 2
IF3	Initiation factor 3

IPTG	Isopropyl β-D-1-thiogalactopyranoside
KCAT	constant that describes the turnover rate of an enzyme- substrate complex to product and enzyme
KM	Michaelis constant that describes the amount of substrate needed for the enzyme to obtain half of its maximum rate of reaction
kDa	kilodalton
KH domain	RNA-binding K homology domain
KsgA	Kasugamycin resistance protein
LB	Luria-Bertani broth viii
MOPS	3-(N-morpholino)propanesulfonic acid
MDa	megadalton
MS	mass spectrometry
MST	microscale thermophoresis
MWCO	molecular weight cut-off
mRNA	Messenger RNA
Ni^{2+}	Nickel ion
N-terminal	Amino-terminal
OB-fold	Oligosaccharide-binding fold
OD600	Optical Density of light at wavelength 600 nanometres
PDB	Protein Data Bank
PEI	polyethyleneimine
PBS	Phosphate buffered saline
RbfA	Ribosome binding factor A
RbgA	Ribosome biogenesis GTPase A
RID	Ribosome interaction domain
RimM	Ribosome maturation factor M
RNA	Ribonucleic acid
RNase	Ribonuclease
r-protein	Ribosomal protein
rRNA	Ribosomal RNA
RsgA	Ribosome stimulated GTPase A (YjeQ)
S1-S21	Small ribosomal proteins 1 to 21
SDS-PAGE	Sodium dodecyl sulfate-Polyacrylamide gel electrophoresis
S.typhimurium	*Samonella typhimurium*
TEV	tobacco etch virus
tRNA	Transfer RNA
U	uracil
WT	Wild type (parental)
Zn^{2+}	Zinc ion

List of Tables

List of Figures

Chapter 1: Introduction and Literature Review

1.1 Structure of the prokaryotic ribosome

The bacterial 70S ribosome is a large ribonucleoprotein complex with a molecular mass of ~2.3 MDa and comprised of the 30S and 50S subunits (Figure 1.1). Both subunits work in conjunction during protein synthesis to translate the genetic code into functional proteins (Gilbert et al., 2004). The small 30S subunit monitors base pairing between the codon on the messenger RNA (mRNA) and the anticodon on the transfer RNA (tRNA) at the decoding center. The large 50S subunit is responsible for peptide bond formation at the peptidyl transferase center (PTC).

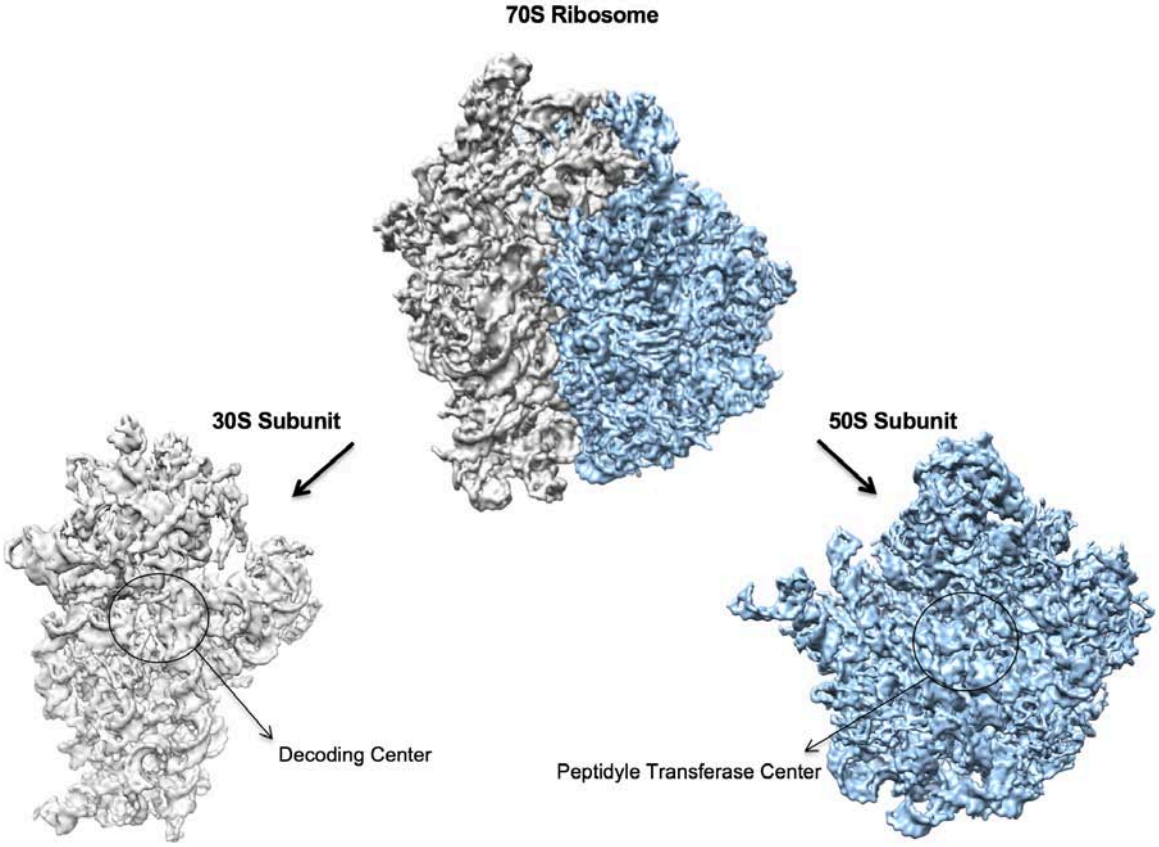

Figure 1.1: Structure of the prokaryotic ribosome. Structure of the 30S subunit (gray), 50S subunit (blue) and 70S ribosome. 30S subunit is responsible for base pairing of mRNA codon and tRNA anticodon at the decoding center (indicated with circle), and 50S subunit is responsible for peptide bond formation at the peptidyl transferase center (indicated with circle).

The 30S subunit, with a molecular weight of 0.85 MDa is made of 16S ribosomal RNA (rRNA) and 21 ribosomal proteins (r-proteins) named from S1 to S21 (with a ‘u’ or ‘b’ prefix)

(Ban et al., 2014; Earnest et al., 2015; Shajani et al., 2011). The 16S rRNA, which is composed of 1542 nucleotides folds into four-domains that constitutes the key landmarks of the 30S subunit: the body (5′ domain), the platform (central domain), the head (3′ major domain) and helix 44 (3′ minor domain) (Figure 1.2) (Wimberly et al., 2000). The four domains fold around the decoding center that constitutes the functional core of the 30S subunit. Two universally conserved residues Adenine 1492 and 1493 monitor the base pairing between mRNA codon and tRNA anticodon and are located on helix 44.

The 50S subunit is made of 23S and 5S rRNA with total of 3000 nucleotides, as well as ~34 r-proteins, variable at different bacteria species, named from L1 to L36 (with a 'u' or 'b' prefix) (Earnest et al., 2015; Shajani et al., 2011). Front view of the 50S subunit is called "crown view" of the 50S subunit, the bottom is the body and the top is the central protuberance of the 50S subunit. This front side of the 50S subunit is flat and it is an association side of the 50S subunit with the 30S subunit. PTC, the functional core of the large subunit, is located in interface side of 50S subunit (Figure 1.2). On the other hand, the back of the 50S subunit is round and most of the r-proteins bind to this solvent exposed side. In addition, the 50S subunit is made of uL1 stalk and bL7/L12 stalk (Nissen et al., 2000).

In general, rRNAs are involved in scaffolding r-proteins, decoding fidelity, binding of elongation factors and controlling the access of the nascent peptide chain into the exit channel. R-proteins typically contain long amino acid extensions inserted into the internal parts of the ribosome, which contact the rRNA. Moreover, structurally they are mostly located at the periphery side of the ribosome.

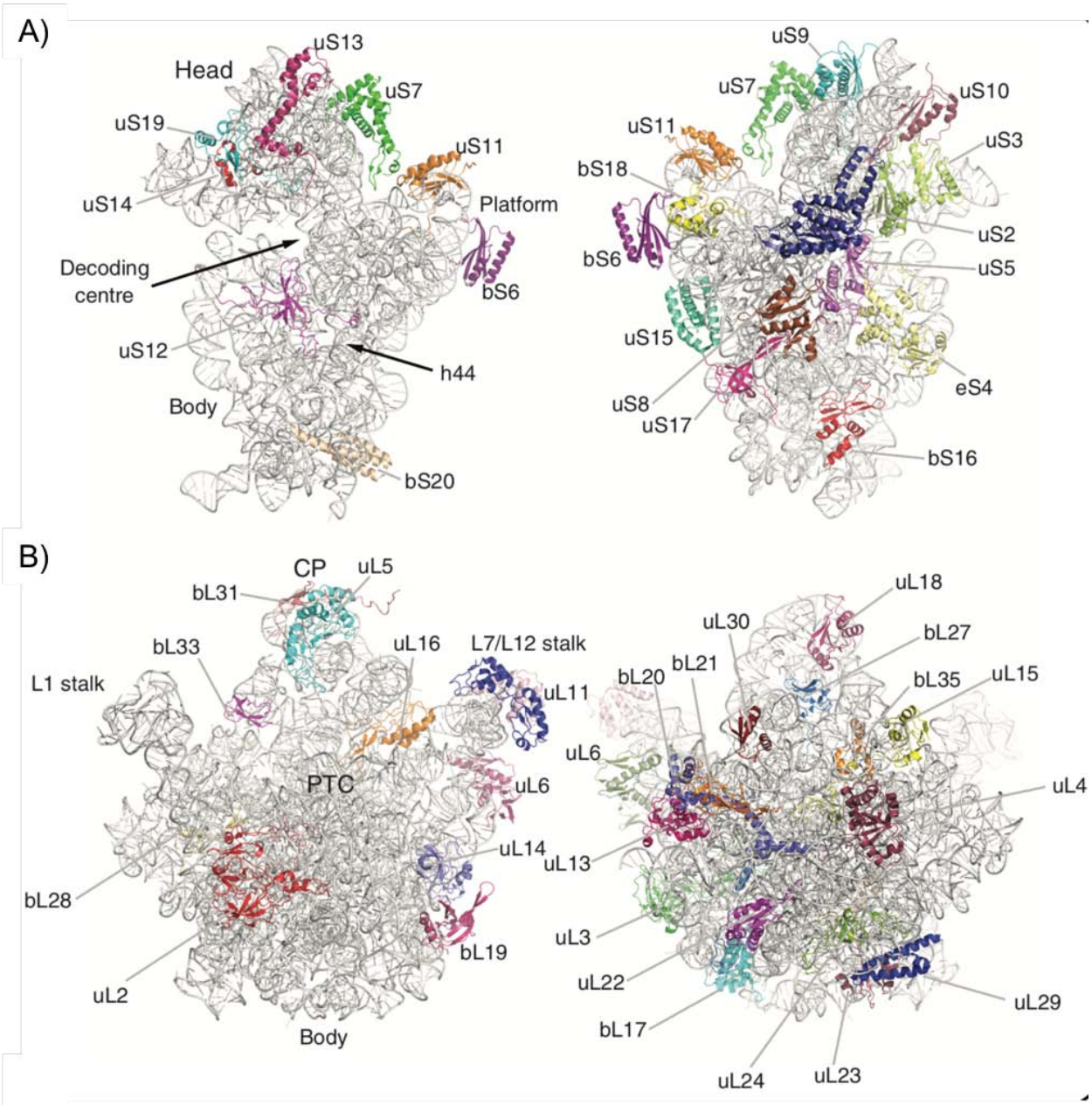

Figure 1.2: Structure and main landmarks of the bacterial ribosomal subunits. A) Front (left) and back (right) views of the structure of the 30S subunit. Labels indicate the main landmarks of the ribosomal subunit and the r-proteins. Panel B) shows the 'crown view' (left) and solvent (right) view of the 50S subunit of *Bacillus subtilis*, respectively. Figure taken from (Razi *et al*., 2017) with permission eLS publisher.

30S and 50S subunits associate together during translation forming the 70S ribosome through inter-subunit bridges. These bridges are formed by RNA-RNA, RNA-protein and protein-protein interactions (Dunkle and Cate, 2013; Gao et al., 2003; Yusupov et al., 2001). These inter-subunit bridges can be categorized into three different groups, based on the contact

points that they make between two subunits. There are three bridges, B1a, B1b and B1c, between the head of the 30S subunit and the central protuberance of the 50S subunit. A second group of bridges are B2a, B3, B4, B5, B6, B8, which forms an interaction between helix 44 of the 30S subunit and the PTC of the 50S subunit. Among these bridges B3 are located at the top of helix 44, which works as the pivot point during the ratcheting motion in translation (Yusupov et al., 2001). The third category of the bridge is B7a that holds the platform of the 30S subunit and L1 stalk of the 50S subunit.

1.2 Differences between prokaryotes and eukaryotes ribosome

In all living organisms, the ribosomes are composed of two subunits: a small subunit responsible for monitoring codon-anticodon base pairing and a large subunit responsible for performing peptide bond formation. However, there are species differences in terms of ribosome size and complexity. As opposed to 70S bacteria ribosome, which is described above, the eukaryotic ribosome is composed of a 40S small subunit and a 60S large subunit. The fully assembled ribosome sediments as the 80S ribosome with the molecular weight of 3.3 MDa in lower eukaryotes to 4.3 MDa in higher eukaryotes (Figure 1.3). The 40S small subunit consists of ~ 33 r-proteins and 18S rRNA. The 60S large subunit is composed of ~47 r-proteins and three different rRNA molecules (25S rRNA, 5.8S rRNA and 5S rRNA). Both 40S and 60S subunits have similar structural landmarks to the 30S and 50S subunits in bacteria. The 40S small subunit contains the body, head, platform and helix 44, while the large 60S subunit is composed of the body, central protuberance and two stalks (L1 and P-stalks).

In *Saccharomyces cerevisiae*, the 80S ribosome contains 79 r-proteins and 5500 rRNA bases. R-proteins contain long tails and loops, which are extended from the globular domains of the r-proteins located at the surface of the ribosome (Ben-Shem et al., 2011). The extended

domains are inserted into the rRNA and they are located at the same interface side of the ribosome, as in bacteria.

Human 80S ribosomes have over 80 r-proteins, with an additional protein, eL28, compared to the yeast ribosome. In addition, human mitochondrial ribosome r-proteins are extensively interconnected, and they have a distinct morphology contains three rRNA molecules as the bacterial ribosome (Amunts et al., 2015).

The focus of my thesis is on the bacterial ribosome.

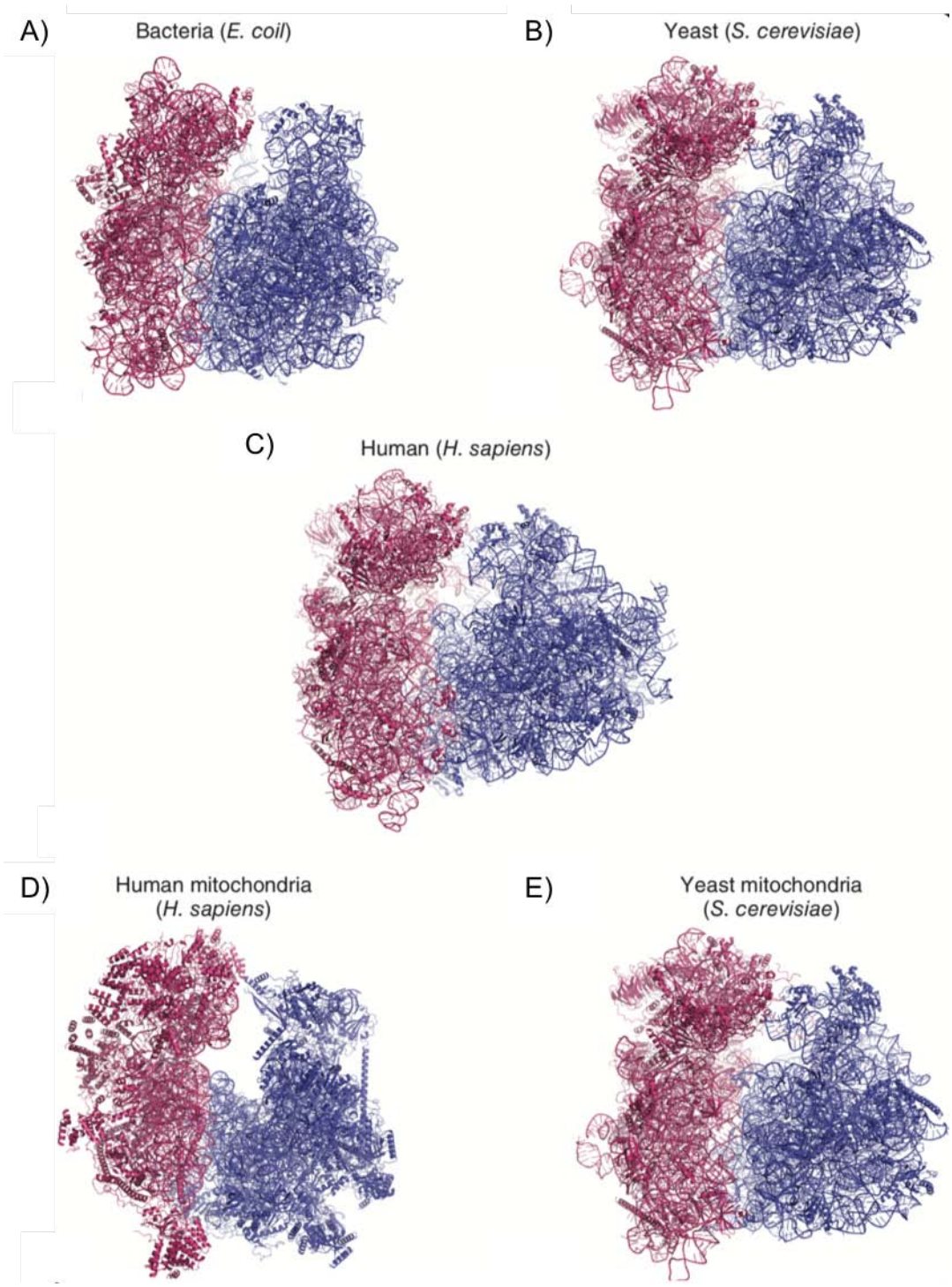

Figure 1.3: Gallery of ribosomal structures. A side-by-side comparison of the structures of the bacteria (*E. coli*) (PDB ID: 4v4q) (A), yeast (*S. cerevisiae*) (PDB ID: 4v88) (B) and human (PDB ID: 4ug0) (C) ribosomes. Panel (D) and (E) show the structures of the mitochondrial ribosome from human (PDB ID: 3j9m) and yeast (PDB ID: 5mrf), respectively. Figure taken from (Razi *et al*., 2017) with permission eLS publisher.

1.3 Function of the ribosome

The function of the ribosome is to synthesize proteins during translation. To achieve this goal translation has three steps: initiation, elongation, and termination.

Each subunit of the ribosome has three major sites involved in translation. These are aminoacyl (A)-site, peptidyl (P)-site and exit (E)-site (Dauphin and Hamel, 1992; Frank, 2003; Gao et al., 2003; Ramakrishnan, 2002; Rasmussen et al., 1991). A site is responsible for entering the aminoacyl-tRNA, P site has a role in locating peptidyle-tRNA, and E site is accountable for keeping deacylated tRNA before releasing from the ribosome.

Initiation of the protein synthesis starts with the recruitment of mRNA to the 30S subunit and binding of the Shine-Dalgarno sequence of the mRNA to the anti-Shine-Dalgarno sequence on the 16S rRNA (Shine and Dalgarno, 1974). Then tRNA loaded with an amino acid (charged tRNA) is bound to the P-site with the assistance of initiation factors I, II and III. Initiation factors II and III facilitate the association of the 30S and 50S subunit and trigger the initiation process.

Then, the initiation complex is formed, by base pairing between the mRNA codon and tRNA anticodon at the A-site. The decoding center of the 30S subunit is responsible for monitoring the geometry of the canonical codon and anticodon base pairing by nucleotides A1492 and A1493 located in helix 44 in a proofreading step (Ogle et al., 2001; Yoshizawa et al., 1999).

Subsequently, the elongation of the polypeptide chain occurs with the assistance of two protein factors. Elongation factor Tu (EF-Tu), which is responsible for recruiting of the aminoacyl-tRNA to the A site, and elongation factor G (EF-G), which is responsible for the translocation mechanism that shift tRNA from the A site to the P site and simultaneously shifts mRNA from the P site into the E site. Subsequently, the bound tRNA in E site will get released. When a stop codon reaches the A site, release factor I or II binds to the A site and facilitates the

release of deacylated peptidyl-tRNA. Then the recycling factor promotes the dissociation of the release factor and the dissociation of two ribosomal subunits.

1.4 The ribosome is a major target for antimicrobials

Emergence of antibiotic resistance among organisms responsible for infectious disease has outpaced new antibiotic development posing a serious health problem. Antibiotics are losing their ability to control even common bacterial pathogens and of increasing concern are "superbugs", bacteria that carry resistance genes for multiple antibiotics. The ribosome has traditionally been used as a major antibiotic target and as a such, antibiotics targeting the ribosome interact with either the 30S or 50S subunit of the 70S ribosome and inhibit and impair protein synthesis.

The Ramakrishnan group solved the X-ray structure of the ribosomal subunits in complex with various antibiotic families (Carter et al., 2000). Some of these antibiotics such as Spectinomycin bind to the 50S subunit at H34 and inhibit elongation factor G, thus blocking translocation of tRNA. Streptomycin and paromomycin bind to the helix 44 of the 30S subunit and thus affect the proof-reading step during translation. Binding of these antibiotics induces conformational changes that prevent the association of the 30S subunit to the 50S subunit and therefore cease translation.

However, there are no drugs that specifically target the process of ribosome assembly. This process is assisted by protein factors that ensure proper folding of the rRNA and other events necessary for the maturation of the ribosomal subunits. In theory, each step of assembly catalyzed by a protein factor provides a potential platform to develop new antibiotics against bacteria. However, an essential pre-requisite to leverage these assembly factors as new antimicrobial targets is to understand their exact role.

1.5 The Assembly of the bacterial ribosome

Ribosome biogenesis is a highly-regulated and multistep process. This assembly process was examined for the past 50 years by different techniques such as chemical footprinting (Adilakshmi et al., 2008), pulse chase monitored with mass spectrometry (Mulder et al., 2010), microscale thermophoresis (MST) (Thurlow et al., 2016b), analytical ultracentrifugation (Jeganathan et al., 2015) and cryo-EM. These techniques reveal that ribosome biogenesis starts with transcription of rRNA and subsequently this nascent rRNA undergoes modifications of precursor sequences to form the backbone of each ribosome subunit.

Initially the three rRNAs (16S rRNA, 23S rRNA, and 5S rRNA) and tRNA are transcribed from a single pre-rRNA transcript. This transcript is cleaved by RNase III into the precursor of all three rRNAs (Figure 1.4) (Shajani et al., 2011).

The 17S rRNA, precursor of 16S rRNA, contains an additional 115 nucleotides at the 5' end and 33 nucleotides at the 3' end. RNase E cleaves the 5' end of the 17S rRNA to 66 nucleotides and RNase G further processes the 5' end (Li et al., 1999b). Maturation of the 5' end happens before maturation of the 3' end of the 16S rRNA (Al Refaii and Alix, 2009; Li et al., 1999b). The cleavage of the 3' end is less characterized, however recent studies have shown that there are at least four exonucleases (RNase II, RNase R, RNase PH and PNPase), in addition to YebY (Figure 1.4) (Sulthana and Deutscher, 2013).

The 23S rRNA precursor contains between 3 to 7 additional nucleotides at the 5' end and from 7 to 9 additional nucleotides at the 3' end (King et al., 1986; Sirdeshmukh and Schlessinger, 1985). The details of 5' end maturation are unknown. However, RNase T processes the 3' end (Figure 1.4) (Li et al., 1999a).

The 5S rRNA precursor contains an additional 84 and 42 nucleotides at the 5' and 3' ends, respectively. RNase E is essential to cleave the extra nucleotides at both ends of the 5S rRNA.

However, processing by this enzyme leaves 3 extra nucleotides at each end of the 5S rRNA. The maturation of the 5' end of the 5S rRNA is still unknown. In addition, the 3' end of the 5S rRNA can be further cleaved by RNase T (Figure 1.4) (Misra and Apirion, 1979).

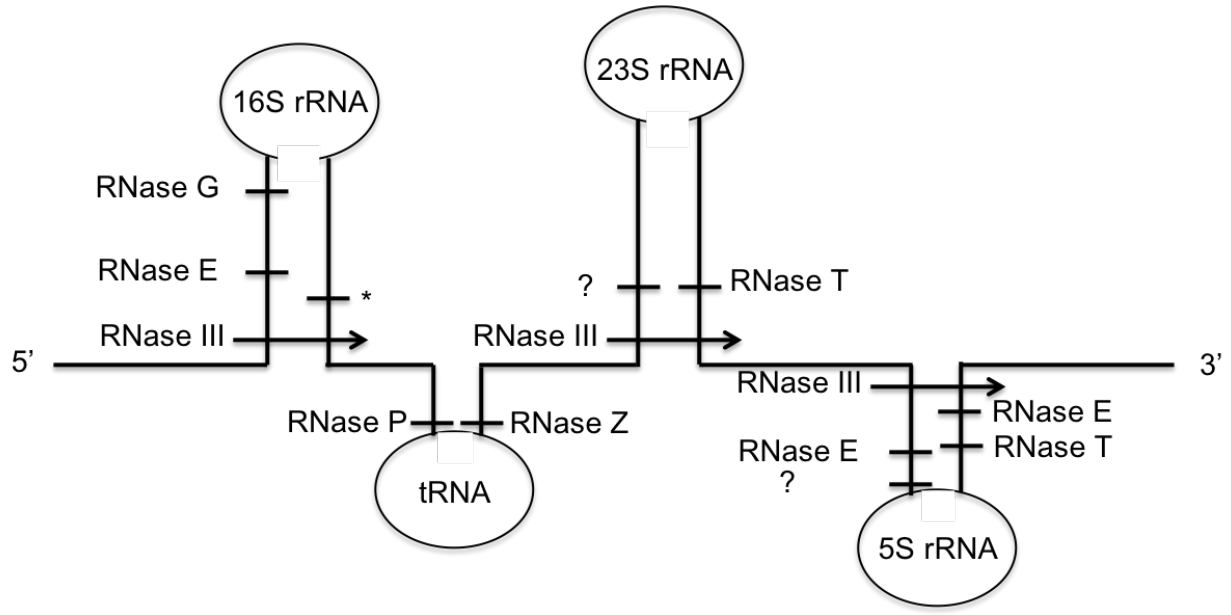

Figure 1.4: rRNA processing. rRNA contains 17S rRNA, 23S rRNA, 5S rRNA and one tRNA molecule. Shown here is rRNA transcript in 5' to 3' direction with known cleavage sites. The site marked with an asterisk (*) is suggested to be processed by sevral enzymes (RNase II, RNase R, RNase PH, RNPase). The sites marked with a question mark (?) are cleaved by unknown nucleases.

Simultaneously, r-proteins are synthesized, modified, and folded, and they bind to the rRNA backbone. Hierarchical binding of r-proteins results in stabilization of rRNA that aids further r-protein binding, until subunits are fully matured. By varying the order in which r-proteins were added *in vitro* studies by the Nomura and Nierhaus groups created a hierarchal map of r-proteins binding to the rRNA scaffold. First primary r-proteins bind directly to the rRNA and stabilize their folding, then secondary r-proteins bind to the primary proteins and further assist in the folding of the rRNA, and finally the tertiary r-proteins bind to the secondary proteins (Figure 1.5) (Mizushima and Nomura, 1970; Nomura, 1970). Thus, the role of r-proteins in ribosome

assembly can be viewed as factors that facilitate and stabilize rRNA folding into the proper and functional conformation. The assembly of each subunit occurs separately. The focus of my dissertation is on 30S subunit assembly.

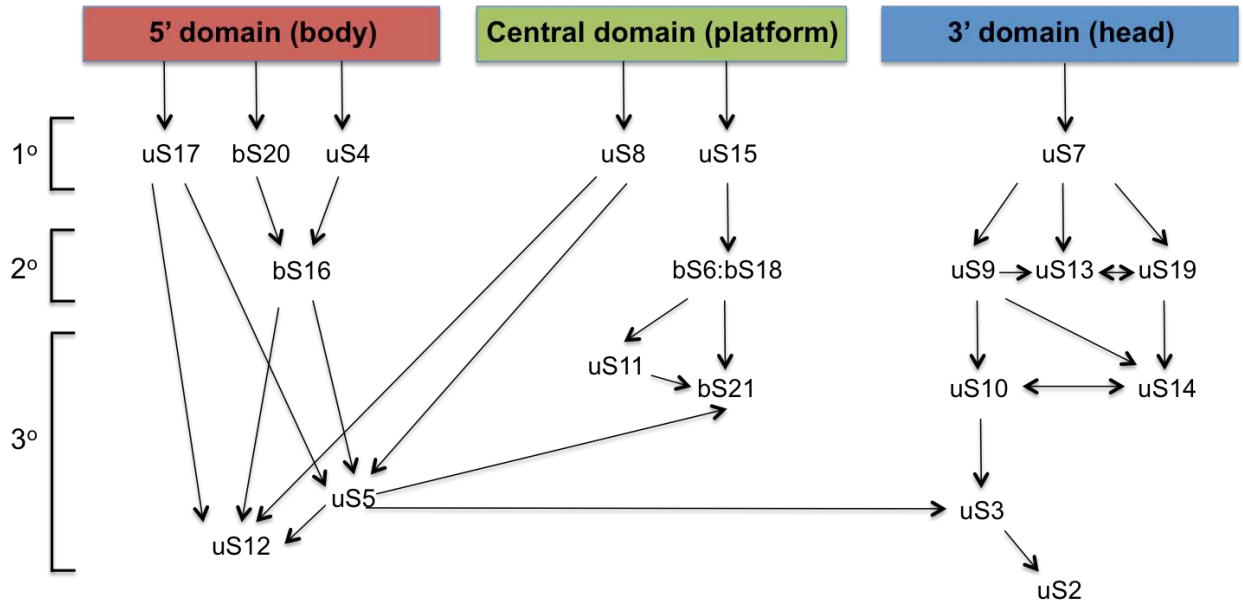

Figure 1.5: Nomura assembly map. This is the hierarchical order of r-proteins binding to the 16S rRNA. Arrows represent protein binding dependencies. Primary r-proteins (1°) require only the presence of rRNA. Secondary r-proteins (2°) require the presence of primary proteins. Tertiary proteins (3°) require the presence of secondary proteins to bind.

1.6 Assembly factors provide speed and directionality to the assembly process

The Nomura group showed that the 30S subunit can be reconstituted in vitro in the presence of r-proteins and rRNA under non-physiological conditions such as high temperature and buffer containing high salt concentrations (Nomura, 1969). These *in vitro* reconstitution experiments revealed that all of the information necessary to assemble the ribosome is contained in its RNA and protein components (Nomura, 1969; Nomura and Traub, 1968). In these *in vitro* reconstitution experiments two intermediates of the 30S subunit were isolated. The first intermediate known as 21S reconstitution intermediate (RI) with 15 r-proteins bound to the 16S

rRNA, accumulates when the experiment is performed at low temperature (0 -15 ^{o}C). Subsequently, exposure of the reaction to higher temperature (40 ^{o}C) enhances the conformational changes that cause the formation of the second intermediate as 25S (RI*). This intermediate eventually leads to the formation of the mature 30S subunit. Thus, it was originally theorized that the assembly process occurs through a linear pathway (Figure 1.6).

However, subsequent pulse-chase quantified by mass spectrometry experiments performed by the Williamson group, revealed various rates of association of r-protein binding to rRNA (Talkington et al., 2005). In addition, rRNA folding as a result of r-protein binding was examined through hydroxyl radical foot-printing by the Woodson lab. These experiments demonstrate that local transformations in biogenesis have similar but distinct activation energies. That indicates the assembly process occurs through multiple simultaneous folding pathway (Talkington et al., 2005). Local folding of rRNA creates the binding position for r-proteins. Binding of r-proteins to rRNA generates large changes in the landscape of energy. Sequential protein binding eventually stabilizes the native 30S conformation (Figure 1.6). The folding events at the late stages of maturation have a strong tendency to fall into local energy minima, although this process in the cell is fast and efficient.

Conversely, the in vitro reconstitution experiments showed that the entire process of ribosome maturation in the cell, including synthesis of components as well as folding and assembly, occurs in less than 2 minutes in actively growing *E. coli*. Cell achieves this high efficiency through the action of assembly factors that expedite the process (Culver, 2003; Talkington et al., 2005). There are over 20 assembly factors that help the maturation of the 30S subunit. Unlike ribosomal proteins, these assembly factors are not part of the final structure of the ribosome (Wilson and Nierhaus, 2007). These assembly factors can be broadly characterized as helicases, chaperons, RNA modification enzymes, and GTPases (Shajani et al., 2011;

Woodson, 2011). Assembly factors have structural and catalytic roles in ribosome maturation. These assembly factors help the proper folding of rRNA motifs with r-proteins and prevent them from becoming trapped in local energy minima (Connolly and Culver, 2009). Helicases are involved in RNA unwinding and RNA folding (Jankowsky et al., 2001). Chaperones have a role in ribosome biogenesis, since deletion of genes that express heat shock protein 70, causes an accumulation of immature 30S subunits (El Hage et al., 2001). RNA modification enzymes catalyze post transcriptional modifications, primarily methylation of 16S rRNA (Nesterchuk et al., 2011).

Some of these assembly factors have been implicated in the late stages of maturation (Britton, 2009; Shajani et al., 2011). Our lab focuses on the function and role of YjeQ, Era, RbfA and RimM. Among these assembly factors, GTPases are an important driving force for conformational changes that lead to functional subunits. My PhD dissertation focuses on the role of two of these GTPase proteins: YjeQ and Era.

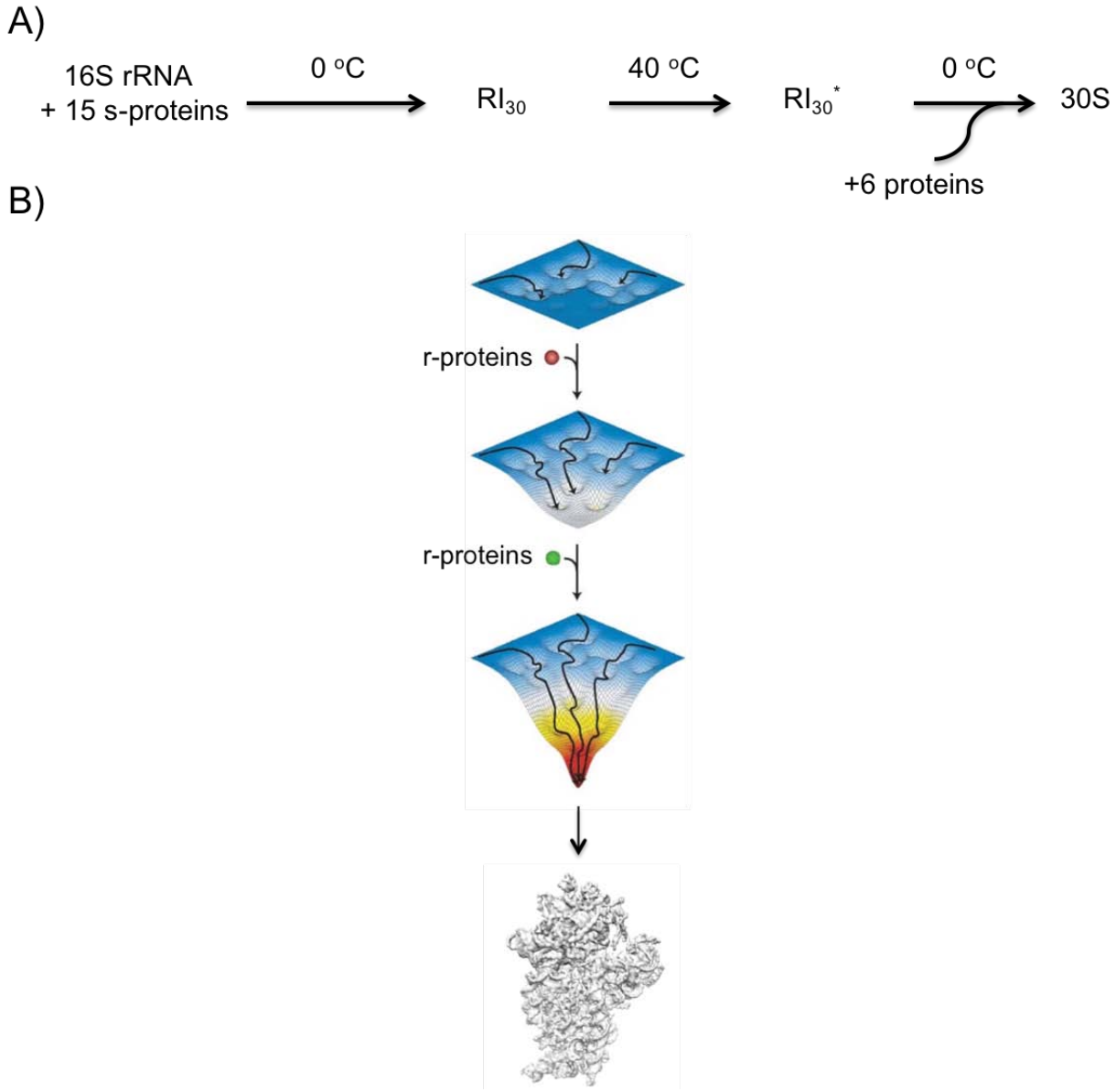

Figure 1.6: Assembly pathway of the 30S subunit. A) The assembly of the 30S subunit was believed to follow a single linear pathway with two rate limiting steps. B) Binding of r-protein changes the energy landscape of the ribosome assembly (Adapted from Williamson JR. 2005; Nature)

1.7 GTPase assembly factors

GTPases are universally conserved and have diverse roles in cell function regulation, signal transduction, translation, hormonal and sensory signals (Caldon et al., 2001). Previous

work suggests that GTPases are also essential factors that facilitate the maturation of the bacterial ribosomes (Britton, 2009; Shajani et al., 2011).

There are two large GTPase classes: TRAFAC, which includes factors involved in translation and signal transduction and SIMIBI, which consists of signal recognition particle GTPases and metabolic enzymes (Leipe et al., 2002). GTPase factors that are involved in ribosome maturation belong to the TRAFAC family. More specifically, they belong to the Ras superfamily and play a role in signal transduction by acting as an on and off switch (Karbstein, 2007). The general structure of the GTPase domain contains five conserved motifs, G1-G5. These motifs are involved in nucleotide binding and Mg^{2+} ion binding. Also, they contain switch I and II that adopt large conformational changes when they are bound to GTP versus GDP.

1.7.1 YjeQ

YjeQ (RsgA) is a 39 KDa highly conserved GTPase, only present in bacteria. YjeQ has low intrinsic GTPase activity that gets stimulated upon binding to the 30S subunit by 160-fold (Daigle et al., 2002). YjeQ is comprised of three domains: the N-terminal OB-fold (oligonucleotide/oligosacharide binding fold) domain, the GTPase domain and the C-terminal zinc-binding domain (Daigle et al., 2002; Levdikov et al., 2004; Nichols et al., 2007; Shin et al., 2004). The OB fold domain consists of antiparallel β-sheets that form a β-barrel. This domain is an RNA binding domain, which is required for binding to the 30S subunit in *E. Coli* and for the protein to stimulate GTPase activity (Daigle and Brown, 2004). OB fold domains are found in translation factors, as well. In addition, there is an extra 24 amino acid extension at the N-termini of E. coli YjeQ (Figure 1.7) (Razi et al., 2017b).

The GTPase domain has the characteristic G motifs mediating the nucleotide binding and hydrolysis (G1-G2-G3-G4-G5). However, they are circularly permutated and adopt a G4-G5-G1-

G2-G3 pattern. Work on the prototype ras GTPase showed that nucleotide binding and hydrolysis leads to conformational changes typically confined to two loops in the GTPase domain, known as switch I and switch II, which make contact with the phosphate groups of the nucleotide and undergo large conformational changes upon GTP hydrolysis (Anand et al., 2006). Switch I in YjeQ encompasses the G2-loop and it is disordered in the YjeQ structure. The G3 loop constitutes the switch II, which in this case is a long stretch of amino acids connecting the GTPase domain with the C-terminal zinc finger domain. Therefore, switch I and II are well positioned in YjeQ to propagate the conformational changes occurring as a result of GTP hydrolysis to the upstream and downstream domains, respectively. Finally, the C-terminal zinc-finger domain contains 3^{10}-helix and a long loop containing three cysteine and a histidine that coordinate the zinc ion. Zinc-finger motifs are present in proteins that bind to RNA. There is also a helical extension that has been referred to as the C-terminal extension (CTE) (Nichols et al., 2007).

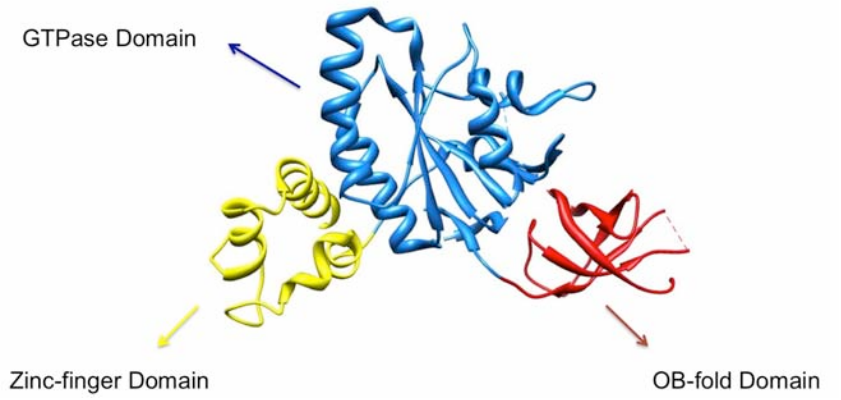

Figure 1.7: Crystal structure of YjeQ S. typhirmurium. Crystal structure of YjeQ showing the three domains in the protein: Zinc-finger domain, GTPase domain and OB-fold domain (Figure made from PDB ID 2RCN).

Binding of YjeQ to the 30S subunit has previously been verified by filtration assay and MST (Jeganathan et al., 2015; Thurlow et al., 2016b). Filtration assays showed that YjeQ can bind to the mature 30S subunit with three different nucleotides. However, the binding of YjeQ to the mature 30S subunit is the highest in the presence of GMPPNP (non-hydrolyzable analog of

GTP) (Jeganathan et al., 2015). Previous MST results indicate that YjeQ is able to bind to the 30S subunit with high affinity of 66.2 nM. However, binding of YjeQ to mature 30S subunits in the presence of GDP was not observed with this technique (Thurlow et al., 2016a).

To test whether the zinc finger domain of YjeQ is important for binding to the 30S subunit, our laboratory constructed three YjeQ variants with different truncations in the C-terminal region. In the first variant (YjeQ M1), the entire zinc-finger domain was removed. For the second variant (YjeQ M2), the stop codon was introduced right after the 3^{10}-helix to remove the loop coordinating the zinc ion. Finally, for the third variant (YjeQ M3) the stop codon was introduced at the position removing the CTE but not the loop coordinating the zinc ion. Binding assays of these variants in complex with the 30S subunits were then performed. Results showed that the YjeQ M1 variant and the YjeQ M2 variant had decreased binding to the mature 30S subunit compared to the wt YjeQ. However, the YjeQ M3 variant showed enhanced binding to the 30S subunit compared to wt YjeQ (Jeganathan et al., 2015). This finding suggests that the zinc finger domain (except its C-terminal helix) contributes to the binding of YjeQ to the 30S subunit.

Cryo-EM has been used to generate a 3D structure of YjeQ in complex with the 30S subunit from two groups (Guo et al., 2011; Jomaa et al., 2011c) and described that YjeQ binds to the decoding center of the mature 30S subunit. According to one of these structures, the N-terminal OB-fold domain of YjeQ-GMPNP interacted with helix 44, while C-terminal zinc-finger domain interacted with the head of the 30S subunit (Guo et al., 2011). In addition, its GTPase domain covers the decoding center and interacts with the helix 44.

Based on the second structure, the N-terminal OB-fold of YjeQ interacted with the head of the 30S subunit and the C-terminal zinc-finger domain interacted with helix 44 (Jomaa et al.,

2011c). In this structure, the density representing the upper domain of helix 44, which constitutes the binding site of RbfA, is lacking (Datta et al., 2007). It is interesting that negatively charged residues in the surface of the zinc-finger domain face the negatively charged phosphate-oxygen backbone of nucleotides of helix 44 in the native 30S subunit. This charge distribution suggests the necessity of a shift in the helix 44 motifs to avoid electrostatic repulsion.

In 2017, two additional structures of the 30S in complex with YjeQ were solved with much higher resolution (Lopez-Alonso et al., 2017; Razi et al., 2017b). The Connell group solved the structure with a resolution of 5.2Å and demonstrated that YjeQ binding introduces conformational changes to the 30S subunit and in its late ribosomal proteins. In this study, they demonstrated the binding of YjeQ to the decoding center of the 30S subunit. In this complex, the OB fold domain of YjeQ interacts with the body and the Zinc finger domain contacts the head of the 30S subunit. In addition, they observed underrepresentation of several late ribosomal proteins such as uS2, uS3, uS7, uS12 and bS21 upon binding of YjeQ to the 30S subunit. Also, they observed that YjeQ locks helix 44 into a conformation which is consistent with the previous x-ray structure of the 30S subunit, representing the mature orientation ready to be associated with the 50S subunit.

On the other hand, deletion of YjeQ causes a slow-growth phenotype of cells and accumulation of the immature 30S subunit with unprocessed 17S rRNA (Himeno et al., 2004; Jomaa et al., 2011a) (Table 1.1). Our laboratory previously characterized the intermediates that accumulate upon deletion of *yjeQ* by cryo-EM and qMS (Leong et al., 2013; Thurlow et al., 2016a). Cryo-EM analysis revealed distortion at the 3' domain of the 16S rRNA and qMS demonstrated depletion of secondary and tertiary ribosomal proteins such as uS10, uS3, uS2, uS14, uS5, bS21 and uS9. In addition, the cryo-EM structure showed that these immature particles have a highly flexible helix 44. This intermediate structure shares similar features with

the intermediate particles that accumulate in the *ΔrimM* strain, which is characterized by a distortion at the decoding center of the 30S subunit (Leong et al., 2013).

Factor	Function	Growth	RNA	Ribosome profile
YjeQ	GTPase	Slow	17S rRNA	30S increased and 70S decreased
Era	GTPase	Essential	17S rRNA	30S increased and 70S decreased

Table 1.1: Phenotypic characteristics of the *ΔyjeQ* and *ΔrimM* strains.

1.7.2 Era

Era (*E. coli* ras like protein) is an essential 33 kDa GTPase protein. Era is a pleiotropic protein with multiple functions in the cell. It is involved in cell division (Britton et al., 1997; Britton et al., 1998), chromosome segregation (Lerner et al., 1992), cell homeostasis (Gollop and March, 1991a, b), carbon metabolism (Lerner and Inouye, 1991) and ribosome biogenesis (Sharma et al., 2005).

Era is found in both prokaryotes and eukaryotes. It consists of two domains: The N-terminal GTP-binding and the C-terminal KH RNA-binding domains (Comartin and Brown, 2006). These two domains are connected through a flexible linker, which is 17 amino acid residues in length. The N-terminal domain consists of a 6 stranded B-sheet flanked by five helices and it contains a phosphate binding loop. The C-terminal consists of a 3 stranded B-sheet and 3 helices responsible for nucleotide binding (Figure 1.8) (Chen et al., 1999). Era has slow GTPase activity. However, its GTPase activity gets stimulated upon binding to RNA (Meier et al., 2000; Sullivan et al., 2000).

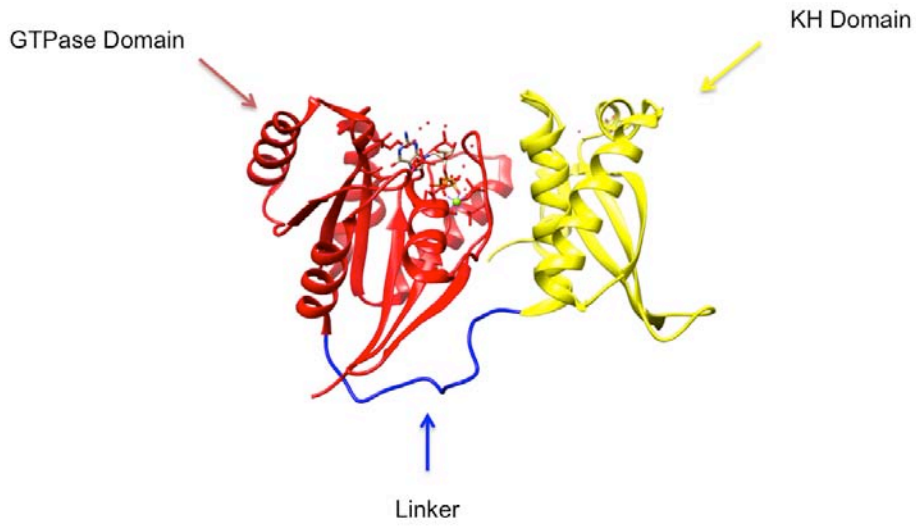

Figure 1.8: Crystal structure of Era. Crystal structure of Era protein showing its two domains: N-terminal GTP-binding domain, and C-terminal KH RNA-binding domain (Figure made from PDB ID 3IEV).

It was shown by sucrose gradient ultracentrifugation followed by western blot analysis with an anti-Era antibody, that Era co-sediments with the 30S subunit. In addition, they showed that binding of Era to the 30S subunit is possible in the presence of GMPPNP and this binding was inhibited in the presence of GTP and GDP (Boriack-Sjodin et al., 1998; Sayed et al., 1999). Thus, Era is able to bind to the 30S subunit in nucleotide dependent manner and may have a role as a small subunit assembly factor (Hang et al., 2001; Hang and Zhao, 2003; Inoue et al., 2003; Zhao et al., 1999).

The Cryo-EM structure of Era in complex with the 30S subunit in *T. Thermophilus* reveals that Era binds to the 30S ribosomal subunit between the head and platform, where the 3' terminus of the 16S rRNA is located. Furthermore, binding of Era blocks association of the 30S

and 50S subunits through conformational changes on the 30S subunit rather than stereochemically (Sharma et al., 2005).

These findings suggest Era has a role as an RNA chaperon to process rRNA or facilitate 30S subunit maturation by inducing conformational changes to the RNA. In addition, Era may act as a placeholder for ribosomal proteins and therefore prevent binding of the premature 30S subunit to the 50S subunit (Tu et al., 2009).

Although there are many findings regarding the function of Era in 30S subunit assembly, there is little known about the immature 30S particles that accumulate upon depletion of Era (Inoue et al., 2003; Sayed et al., 1999; Sharma et al., 2005) (Table 1.1).

1.8 Functional interplay between assembly factors

Interactions between assembly factors are essential for their function and synthesis. Genetics, binding assays and affinity measurements using MST have been used to assess the functional interplay between factors. For example, slow growth caused by deletion of YjeQ can be suppressed by overexpression of Era (Figure1.9) (Inoue et al., 2003).

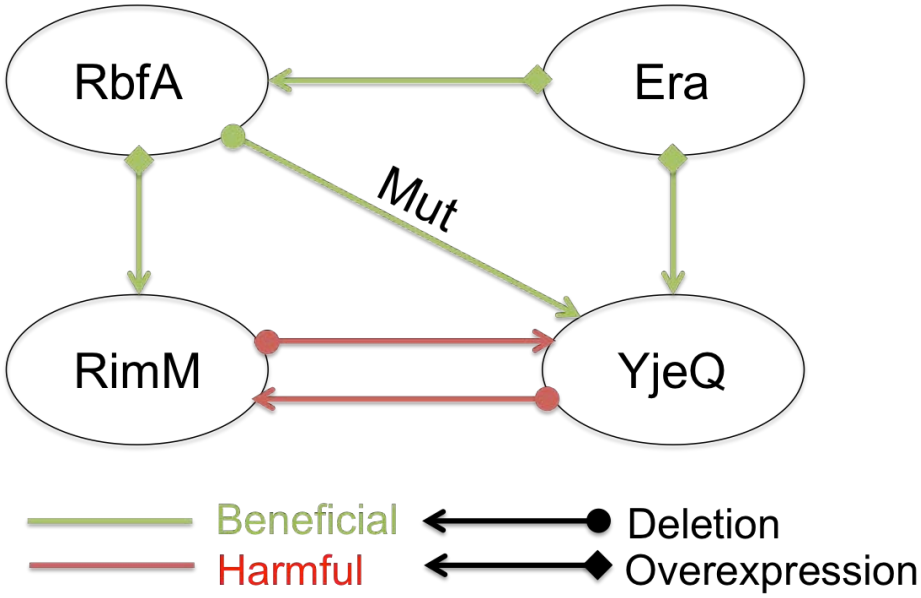

Figure 1.9: Genetic functional interplay between factors. Functional interplay between factors that show overexpression or mutation (Mut) of assembly factors can compensate for deletion of other factors. Green arrows indicate the effects are beneficial and red arrows indicate the effects are harmful.

The Inouye group also has previously shown that RbfA is essential for cell growth at low temperature (Inoue et al., 2006). Deletion of RbfA causes an accumulation of 30S and 50S subunits, however, overexpression of Era suppresses the cold sensitive and slow growth phenotype in the RbfA deletion strain (Inoue et al., 2006). This suggests a possible functional interplay between Era and RbfA, two of the assembly factors with roles during late stage of 30S maturation. Additionally, the slow growth phenotype in Δ*rimM* cells can be suppressed by overexpression of *rbfA* and deletion of rimM enhances the slow growth in Δ*yjeQ* cells (Bylund et al., 1998; Campbell and Brown, 2008).

All together, these evidences suggest that functional interplays between YjeQ, RbfA, RimM and Era are important for the maturation of the 30S subunit.

Functional interplays may also play an essential role during factor release (Campbell and Brown, 2008). Biochemical work from the Himeno group described that YjeQ assists the release

of RbfA once the maturation of the 30S subunit is completed (Goto et al., 2011). Furthermore, our previously published work (Jeganathan et al., 2015) identified that the zinc finger domain of YjeQ mediates the process of releasing RbfA. However, the detailed mechanism of how YjeQ implements the release of RbfA and the conformational changes that YjeQ or the 30S subunit undergoes to facilitate the release of RbfA have not been described. To understand the mechanisms through which YjeQ facilitates the release of RbfA from the mature 30S subunit, our laboratory performed binding assays of these two factors to both mature 30S subunits and immature 30S subunits purified from *Δyjeq E. coli* strains. The results showed that YjeQ was able to efficiently remove RbfA from the mature 30S subunit in a GTP dependent manner. The removal of RbfA was very efficient in the presence of GTP and GMP-PNP. In the presence of GDP, YjeQ was not capable of displacing the factor and RbfA remained bound to the mature 30S subunit. Therefore, we proposed a model on how YjeQ may release RbfA from the mature 30S subunit. In this model, first RbfA binds to the immature 30S subunit and coordinates the maturation of the decoding center of the 30S subunit. At this point YjeQ is able to bind to the mature 30S subunit in the presence of GTP. However, binding of YjeQ facilitates the release of RbfA from the mature 30S subunit (Figure1.10).

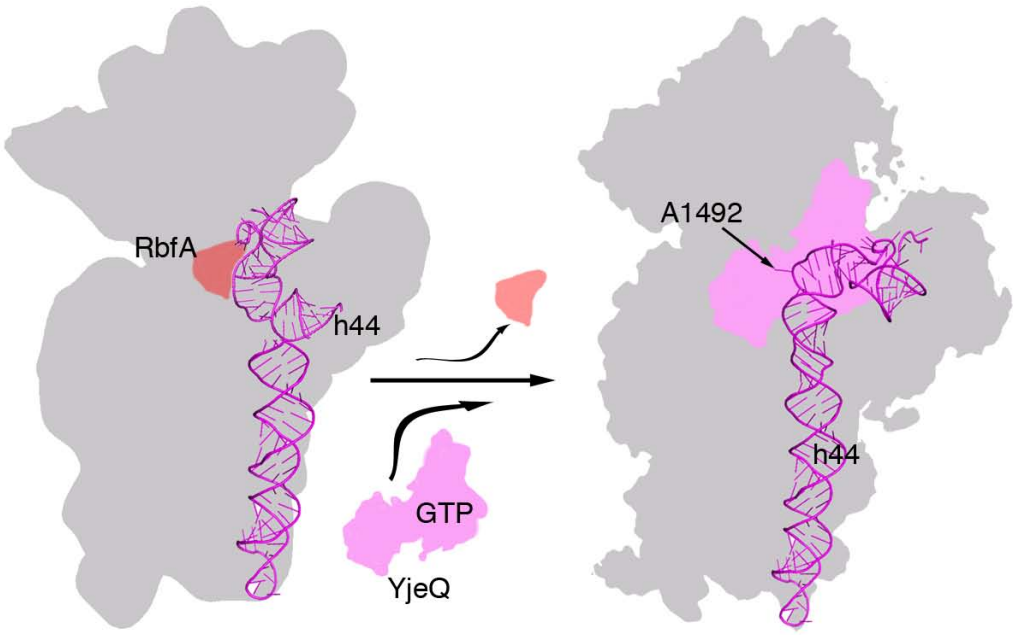

Figure 1.10: Diagram illustrating the Release of RbfA by YjeQ. RbfA binds to the immature 30S subunit. Subsequently, binding of YjeQ in the presence of GTP to the mature 30S subunit triggers the release of RbfA. Adapted from (Razi et al., 2017b) with permission PNAS publisher.

1.9 Assembly factor knockout strains studied by cryo-EM provide a powerful tool for investigating maturation

Historically, X-ray crystallography and cryo-electron microscopy have frequently been used to study the assembly process of macromolecular complexes. The study of the ribosome maturation process is illustrative of the potential of cryo-EM to directly visualize assembly of this macromolecular complex. Atomic resolution structures of the ribosome during its assembly provide unprecedented opportunity for drug development. However, most of the structures populating the assembly process are intrinsically flexible and standard approaches like X-ray crystallography are not useful. An ideal tool to obtain these structures is cryo-EM. In cryo-EM the sample is vitrified in a thin layer of ice and maintained in its fully hydrated state. Ribosome

motion and different conformations can be captured since it is not stabilized by a crystal lattice. Additionally, advanced classification tools, are able to identify unique conformations and categorize them into separate classes. However, until recently, cryo-EM was only capable of obtaining the structure of essential cellular complexes at moderate resolution (~10 Å). The advent of direct electron detector cameras has revolutionized structural biology. Cryo-EM can now obtain the structure of proteins and potentially resolve the multiple conformations that a protein complex may adopt in solution at high resolution (3 Å or better). This level of detail allows for the development of new antibiotics against these targets (Kuhlbrandt, 2014; Schluenzen et al., 2000; Smith and Rubinstein, 2014; Yusupov et al., 2001).

Nevertheless, visualizing the ribosome assembly process and how protein factors assist maturation is quite challenging. The process is continuous, and bacteria are extremely efficient at assembling ribosomes, thus it is very difficult to isolate and characterize ribosomal intermediates. To overcome this challenge, identifying small molecule inhibitors specific to ribosome biogenesis has been attempted. By screening thousands of various compounds, the Brown group identified lamotrigine, which is a chemical probe to perturb the bacterial ribosome biogenesis (Stokes et al., 2014). So far, this is the only small molecule found targeting biogenesis. Thus, the applicability of this approach for studying ribosome biogenesis is very limited at the moment.

Another well-established method developed by our laboratory (Guo et al., 2013; Jomaa et al., 2011a; Leong et al., 2013) revealed that mutations directed to assembly factors slow down ribosome assembly and enable the accumulation and isolation of ribosomal intermediates (Figure 1.11). Using this approach, our laboratory produced the first structures of *in vivo* assembled immature ribosomal subunits (Jomaa et al., 2014; Jomaa et al., 2011a; Leong et al., 2013). These structures constitute the first visual representations of discrete ribosome subunit assembly steps.

Also, structures of immature 30S subunits that accumulate in knockout strains lacking one of the genes for these assembly factors such as YjeQ, RbfA and RimM (Leong et al., 2013; Yang et al., 2014) along with their putative binding sites, indicate these factors may be involved in the maturation of the decoding center. Their roles in the maturation of the functional core of the 30S subunit may entail facilitating proper processing and folding of the 16S rRNA precursor (17S rRNA), or mediating protein-rRNA interactions. Also, binding of these factors to or around the decoding center blocks essential intersubunit bridges (B3, B2a and B7a), preventing the premature association of 30S and 50S particles before the maturation process is complete. Therefore, a key step to allow the 30S subunit to enter the pool of actively translating ribosomes is the release of these factors.

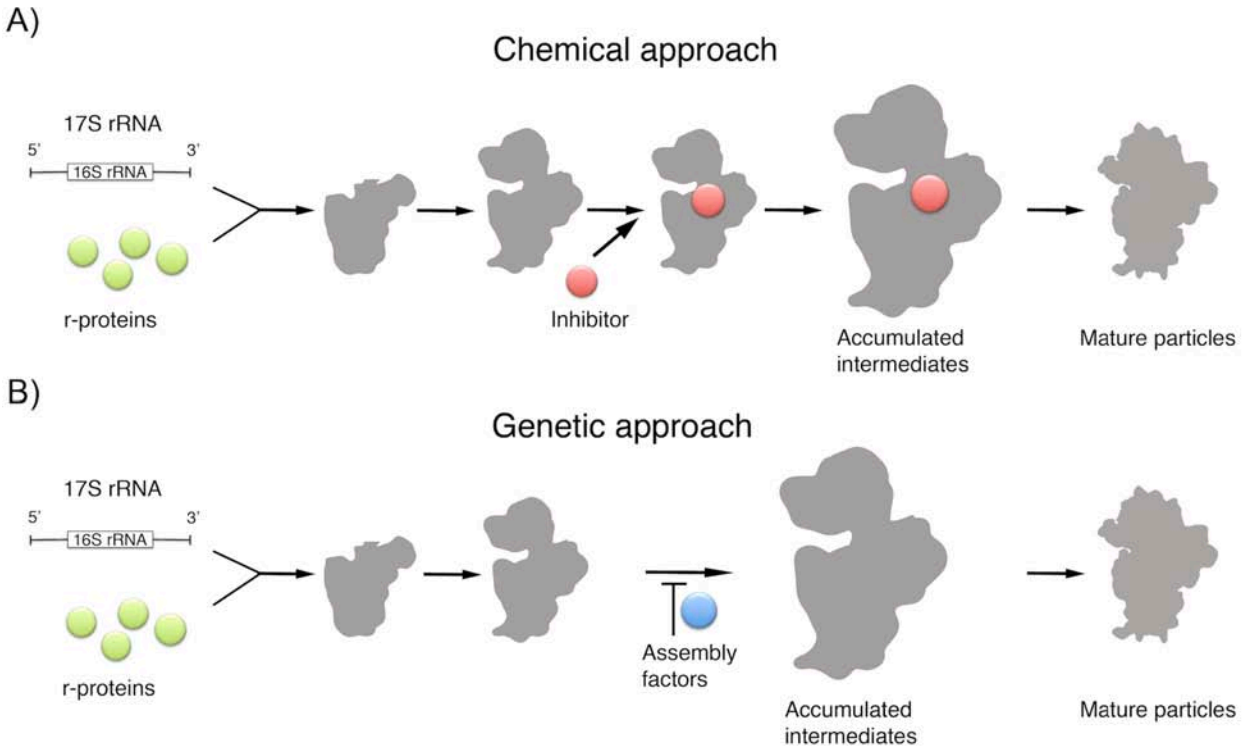

Figure 1.11: Chemical and genetic approaches to capture in vivo assembled ribosomal subunit intermediates. (A) The diagram represents the assembly line of the 30S subunit. Chemical approaches use small-molecule inhibitors to block a specific step in the ribosome assembly process, which leads to the accumulation of immature subunits. (B) In genetic approaches single-gene deletion strains are created by homologous recombination where the

open-reading frame coding region of the gene for an assembly factor is replaced with a marker cassette. Absence of a particular assembly factor causes a slowdown of the specific assembly steps assisted by this factor, which eventually leads to accumulation of assembly intermediates that are possible to purify for subsequent analysis. Figure taken from (Razi et al., 2017a) with permission NAR publisher.

1.10 Aims of this thesis

My working hypothesis is that, in addition to being maturation factors, Era and YjeQ function as quality control factors probing the functionality of the 30S subunit before it is released to the pool of actively translating ribosomes. The main objective of my thesis is to determine the precise function and mechanism of Era and YjeQ in assisting the assembly of the 30S subunit and assessing its functionality.

The specific aims of this study are listed below:

1) Uncovering the function of YjeQ in the maturation of the 30S subunit (Chapter 2).

2) Identifying the mechanism of Era in the maturation of the 30S subunit (Chapter 3).

3) Investigating the functional interplay between YjeQ and Era (Chapter 3).

Chapter 2: **The cryo-EM structure of YjeQ bound to the 30S subunit suggests a fidelity checkpoint function for this protein in ribosome assembly**

Aida Razi[a,b], Alba Guarné[a] and Joaquin Ortega[a,b,1]

PNAS, 2017 April; 114(17): E3396-E3403

[a]Department of Biochemistry and Biomedical Sciences, McMaster University, Hamilton, ON, Canada L8S4K1

[b]Michael G. DeGroote Institute for Infectious Diseases Research, McMaster University, Hamilton, ON, Canada L8S4K1

1. Edited by Harry F. Noller, University of California Santa Cruz, Santa Cruz, CA, and approved March 16, 2017 (received for review October 30, 2016)

2.1 Abstract

Recent work suggests that bacterial YjeQ (RsgA) participates at the late stages of assembly of the 30S subunit and assists the assembly of the decoding center, but YjeQ also binds the mature 30S subunit with high affinity. To determine the function and mechanisms of YjeQ in the context of the mature subunit, we determined the cryo-EM structure of the fully assembled 30S subunit in complex with YjeQ at 5.8 Å resolution. We found that binding of YjeQ stabilizes helix 44 into a conformation similar to that adopted by the subunit during proofreading. This finding indicates that, in addition to its role as an assembly factor, YjeQ has a role as a checkpoint protein consisting of testing the proofreading ability of the 30S subunit. The structure also informs on the mechanism by which YjeQ implements the release from the 30S subunit of a second assembly factor called RbfA. Finally, it reveals how the 30S subunit stimulates YjeQ GTPase activity and leads to the release of the protein. Checkpoint functions have been described for eukaryotic ribosome assembly factors. However, this work provides the first example of a bacterial assembly factor that tests a specific translation mechanism of the 30S subunit.

2.2 Introduction

Understanding how the components of the bacterial ribosome come together and organize themselves remain a daunting challenge. The assembly of the simplest of its subunits, the 30S ribosomal subunit, is a multi-step process that starts with transcription of the 16S ribosomal RNA (rRNA) and synthesis of the ribosomal proteins (r-proteins). Folding of the 16S rRNA starts before transcription is completed. This process is intimately coupled with modifications to the RNA and the processing of the precursor sequences (Connolly and Culver, 2009; Shajani et al., 2011). Binding of its 21 r-proteins to the 16 rRNA occurs in a hierarchical manner (Hosokawa et al., 1966; Traub and Nomura, 1968a, b, 1969) and their binding stabilizes the 3D interactions encoded by the sequence of the rRNA and simultaneously suppresses RNA misfolding (Woodson, 2008, 2011).

Ribosome assembly is a much more efficient process in the cell than in *in vitro* reconstitution experiments. The entire process of synthesis, folding, assembly and maturation occur in less than 2 min in actively growing *Escherichia coli* (Lindahl, 1975). Cells achieve this higher efficiency due to the existence of nonspecific RNA and protein chaperones assisting early stages of assembly and more importantly, through the action of specific assembly factors that mainly act at the later stages of the process (Connolly and Culver, 2009; Shajani et al., 2011). There are three protein factors (YjeQ (RsgA), Era and RbfA) involved in the late stages of assembly of the 30S subunit and their functions in ribosome maturation have been extensively studied in the last decade (Guo et al., 2013; Jeganathan et al., 2015; Jomaa et al., 2011a; Leong et al., 2013). Recent work indicates that these factors bind the 30S subunit at or near the decoding center and assist its folding (Datta et al., 2007; Guo et al., 2011; Jomaa et al., 2011b, c; Sharma et al., 2005). However, the precise mechanisms and the functional interplays between them remains unclear.

This study focuses on YjeQ, a protein that exhibits weak intrinsic GTPase activity (Daigle et al., 2002). Association of YjeQ with the 30S subunit results in a 160-fold stimulation of its GTPase activity (Daigle and Brown, 2004; Himeno et al., 2004). A defining feature of YjeQ, along with other GTPases involved in ribosome biogenesis (RbgA and YqeH), is that its GTPase domain presents a permutation in the order of the characteristic GTPase loops (Levdikov et al., 2004; Nichols et al., 2007; Shin et al., 2004). The canonical G motifs, mediating the nucleotide binding and hydrolysis, (G1 (Walker A, P-loop)-G2 (T)-G3 (Walker B)-G4 (N/TKxD)-G5 [(T/G)(C/S)A]) are circularly permutated and adopt a G4–G5–G1–G2–G3 pattern. A N-terminal oligonucleotide / oligosaccharide binding (OB-fold) domain and a C-terminal zinc-finger domain flank the GTPase domain. The OB-fold domain consists of antiparallel β-sheets defining a β-barrel. The carboxy-terminal zinc-finger domain in YjeQ is comprised of a 3^{10}-helix, a long loop mediating the tetrahedral coordination of a zinc metal ion and two additional α-helices. Two important functional GTPase elements of YjeQ are switch I (G2-loop) and switch II (G3-loop). Structural work in the ras GTPase has shown that nucleotide binding and hydrolysis in GTPases of this family causes conformational changes in these two switches. In YjeQ switch I and II are ideally positioned to propagate conformational changes between the GTPase domain and the other two domains in YjeQ.

The precise function of YjeQ in assisting the late stages of maturation of the 30S subunit is largely unknown. Structural characterization of a late 30S assembly intermediate that accumulate in an *E. coli yjeQ* null (Jomaa et al., 2011a) strain initially suggested that YjeQ may first bind to the 30S subunit when it is still in an immature state to act as a RNA chaperone assisting the folding of the upper region of helix 44 – an essential component of the decoding center. However, recent experiments revealed that the binding affinity of YjeQ to these immature

particles is weak suggesting that they transition to a more thermodynamically stable assembly intermediate that is no longer recognized by YjeQ (Thurlow et al., 2016a).

Unexpectedly for an assembly factor, YjeQ binds to mature 30S subunits with high affinity (Thurlow et al., 2016a). This property hints to the possibility that YjeQ function in ribosomal assembly may not be limited to late assembly intermediates, but rather act on both immature and mature 30S subunits. In this context, work from the Himeno group suggested that one of the functions of YjeQ is assisting in the release of RbfA once maturation of the ribosomal particle is complete (Goto et al., 2011). Another possible checkpoint role of YjeQ could be blocking the binding of initiation factors to premature 30S subunits and ensure quality control of the 30S subunit production (Guo et al., 2011). The role of the GTPase activity in these functions of YjeQ remains unclear.

A structure of YjeQ bound to a *bona fide* immature 30S particle has yet to be obtained. However, two independently produced cryo-electron microscopy (cryo-EM) structures show that YjeQ binds to the decoding center of the mature 30S subunit (Guo et al., 2011; Jomaa et al., 2011c). Interestingly, these two cryo-EM structures proposed different binding orientations for YjeQ. In one of the structures, the OB-fold domain interacts with the decoding center and the zinc-finger domain contacts the head of the 30S subunit (Guo et al., 2011). The second structure suggests a different orientation with the OB-fold interacting with the platform, the zinc-finger domain binding helix 44 and the GTPase domain largely covering the decoding center (Jomaa et al., 2011c). The moderate resolution (10-16Å) of both cryo-EM structures, however, precluded the identification of essential cues necessary to understand the function and molecular mechanisms of YjeQ, including specific amino acids and individual rRNA helices that mediate the interactions between the protein and ribosomal particle. Furthermore, the existing cryo-EM structures or any of the available X-ray structures of YjeQ do not provide an accurate description

of important functional motifs of YjeQ. These motifs include the first 34 N-terminal amino acids of *Escherichia coli* YjeQ that are essential for binding to the 30S subunit (Daigle and Brown, 2004), as well as switch I. Therefore, it is difficult from the existing cryo-EM and X-ray structures to derive precise testable models about the function of YjeQ.

To gain new key insights regarding the function of YjeQ in the context of the mature 30S subunit, we have obtained the 3D structure of the mature 30S subunit in complex with YjeQ at 5.8 Å resolution using an electron microscope equipped with a direct electron detector. Consistent with previous structural work (Guo et al., 2011; Jomaa et al., 2011c), the cryo-EM map shows that YjeQ binds to the decoding center. The much higher resolution of this structure allows the identification of specific secondary structure elements of YjeQ. Consequently, the binding orientation of YjeQ to the 30S subunit can be precisely established. The structure shows that YjeQ anchors tightly to the three domains of the subunit, mainly through its N- and C-terminal domains. The OB-fold contacts the body of the 30S subunit, while the zinc-finger domain anchors the protein to both the head and platform domains of the 30S particle. The GTPase domain almost completely covers the decoding center and contacts the platform through a long loop. The 34 N-terminal amino acids of YjeQ are clearly visible in the EM map and its location explains how this motif is essential for YjeQ binding to the 30S subunit. Switch I is also partially visible in the cryo-EM map revealing a possible mechanism for the ribosome activated GTPase activity of YjeQ. In addition, we obtained the cryo-EM map of free 30S mature subunit allowing us to visualize the structure of this particle when it is not confined in a crystal lattice. Surprisingly, we found that a long stretch of helix 44 is flexible and does not adopt the conformation described by the 30S subunit X-ray structure. However, binding of YjeQ to the free 30S subunit stabilizes helix 44 into a conformation that is similar to that on the X-ray structure. The specific interactions between the OB-fold of YjeQ and helix 44 indicate that YjeQ

has a role as a checkpoint protein dedicated to test the decoding fidelity of the 30S subunit before the particle is released to the pool of actively translating ribosomes.

2.3 Materials and Methods

2.3.1 Cell strains and protein overexpression clones

The parental strain *Escherichia coli* K-12 (BW25113) use to produce the mature 30S subunits was obtained from the Keio collection, a set of *E. coli* K-12 in-frame, single gene knockout mutants (Baba et al., 2006).

The pDEST17-*yjeQ* plasmid used to overexpress YjeQ protein with a amino-terminal His_6 tag cleavable by tobacco etch virus (TEV) protease was generated as previously described (Daigle and Brown, 2004).

2.3.2 Protein overexpression and purification

YjeQ protein was overexpressed as an amino-terminal His_6-tag protein by transforming *E. coli* BL21-A1 with the pDEST17-*yjeQ* plasmid described above. Typically, one liter of LB medium was inoculated with 10 ml of saturated overnight culture and cells were grown to OD_{600} = ~0.6 by incubation at 37 °C. Expression was induced with 0.2% L-arabinose. Cells were then induced for 3 hours at 37 °C and harvested by centrifugation at 3,700*g* for 10 min. Cell pellets were washed with 1 X PBS buffer (137 mM NaCl, 2.7 mM KCl, 8.1 mM Na_2HPO_4 at pH 7.4) and resuspended in 20 ml of buffer A (50 mM Tris-HCl at pH 8.0, 500 mM NaCl, 5% [v/v] glycerol) containing a protease inhibitor cocktail (Complete Protease Inhibitor Cocktail Tablets, Roche). Cells were lysed by sonication and the lysates were spun at 39,200*g* for 45 min to clear cell debris and the supernatant was collected. The lysate was then filtered with a 0.45-µm syringe filter (Millipore) and loaded onto a HiTrap Nickel Chelating Column (GE Healthcare Life Sciences) previously equilibrated with 50 mM Tris-HCl at pH 8.0, 0.5 M NaCl and 5% [v/v] glycerol. Non-specifically bound proteins were washed with 45 mM to 90 mM imidazole. YjeQ was eluted with 180 mM imidazole. Purity of the fractions was monitored by SDS-PAGE and

fractions containing each respective protein were collected and pooled together to dialyze overnight in buffer containing 50mM Tirs-HCl at pH 8.0, 200mM NaCl and 5% (v/v) glycerol.

The amino-terminal His_6-tag was removed by digestion with TEV protease at a ratio of 10:1 (YjeQ:TEV). Following digestion, the reaction was loaded onto a HiTrap Metal Chelating Column previously equilibrated with 50 mM Tris-HCl at pH 8.0, 0.5 M NaCl and 15 mM imidazole. Fractions were collected and their purity evaluated by SDS-PAGE and Coomassie Brilliant Blue staining. Fractions containing pure untagged YjeQ were pooled and dialyzed against 50 mM Tris-HCl at pH 8.0, 150mM NaCl and 5% [v/v] glycerol overnight. To concentrate the protein we used a 10 kDa-cutoff filter (Amicon) and the purified YjeQ was frozen in liquid nitrogen and stored at -80 °C.

2.3.3 Purification of 30S ribosomal subunits

The parental strain (BW25113) was used for purification of the mature 30S subunits. One liter of LB media was grown at 37°C to an OD_{600} of 0.6. Cells were harvested by centrifugation at 3,700*g* for 10 min. Cell pellets were resuspended in 7ml of buffer containing 20mM Tris-HCl at pH 7.5, 10 mM magnesium acetate, 100 mM NH_4Cl, 0.5mM EDTA, 3mM 2-mercaptoethanol containing a protease inhibitor cocktail (cOmplete Protease Inhibitor Cocktail Tablets, Roche) and DNaseI (Roche). All of the following steps were performed at 4 °C. The cell suspension was passed through a French pressure cell at 1400 kg/cm^2 three consecutive times to lyse the cells. The lysate was spun at 30,000*g* for 40 min to clear cell debris. The clarified lysate was collected and spun down at 138,488*g* for 132 minutes to pellet the ribosome. The pellet was resuspended in the buffer containing (10mM Tris-HCl at pH 7.5, 10 mM magnesium acetate, 500 mM NH_4Cl, 0.5mM EDTA and 3mM 2-mecaptoethanol). The resuspended solution was spun down at 30,000*g* for 15 minutes and then the supernatant was loaded onto a sucrose buffer containing

(30% sucrose, 20mM Tris-HCl at pH 7.5, 10 mM magnesium acetate, 500 mM NH_4Cl, 0.5 mM EDTA, 3 mM 2-mecaptoethanol) and spun down for 16hr at 100,000*g*. The washed ribosome pellet was resuspended in the buffer F containing (10 mM Tris-HCl at pH 7.5, 1.1 mM magnesium acetate, 60 mM NH_4Cl, 0.1mM EDTA, 3 mM 2-mecaptoethanol) that caused dissociation of subunits. Approximately 120 A_{260} units of resuspended crude ribosomes were then applied to 34 ml 10%-30% (w/v) sucrose gradients prepared with buffer F. The gradients were centrifuged for 16h at 40,000*g* on a Beckman SW32 Ti rotor. Gradients were fractionated using a Brandel fractionator apparatus and an AKTAprime FPLC system (GE Healthcare). The elution profile was monitored by UV absorbance at A_{260}, and fractions corresponding to the 30S subunit peak were pooled and spin down for another 16h at 40,000*g* on a Beckman SW32 Ti rotor. Pellet containing the purified 30S subunits were resuspended in buffer E containing (10mM Tris-HCl at pH 7.5, 10 mM magnesium acetate, 60 mM NH_4Cl, 3mM 2-mecaptoethanol) and stored at -80 °C.

2.3.4 Cryo-electron microscopy

The entire data set of images was collected over ten cryo-EM sessions. Assembly of the 30S+YjeQ complexes for these experiments was done in 20 µl reactions containing assembly buffer (10 mM Tris–HCl at pH 7.5, 10 mM magnesium acetate, 150 mM NH_4Cl, 3mM 2-mercaptoethanol and 2 mM GMP-PNP). The concentration of the 30S subunits in the assembly reactions for the multiple cryo-EM sessions was always maintained at 1µM whereas the concentration of YjeQ was either 5 µM or 7 µM depending on the reactions. The assembly reaction was incubated for 30 min at 37 ºC and then diluted in the same buffer between 10 to 20 times before the reaction was applied to the grid. Using these assembly and dilution conditions depending on the cryo-EM session the concentration of 30S subunits in the sample applied to the

grid ranged from 50 nM to 100 nM and for YjeQ from 300 nM to 700 nM. Concentrations of YjeQ higher than 700 nM in the reaction applied to the grid caused a significant drop in the number of 30S subunit particles absorbed to the grid. Approximately 4 µl of the diluted sample was applied in the holey carbon grids (c-flat CF-2/2-2C-T) with an additional layer of continuous thin carbon (5-10nm).

The data set from the sample containing only free 30S subunits was obtained in one single cryo-EM session from cryo-EM grids prepared in the same manner as those used in the 30S+YjeQ sample. Purified 30S subunits were diluted in assembly buffer to a concentration of 50 nM and directly applied to the grid as described above.

Before the samples were applied, grids were glow discharged in air at 5 mA for 15 seconds. Vitrification of samples was performed in a Vitrobot (FEI) by blotting the grids once for 15 seconds and with an offset of 0 before they were plunged into liquid ethane. Grids were loaded into the FEI Tecnai F20 electron microscope operated at 200kV using a Gatan 626 single tilt cryo-holder. Images were collected in a Gatan K2 Summit direct detector camera. This detector was used in counting movie mode with five electrons per pixel per second for 15 seconds exposures and 0.5 seconds per frame. This method produced movies containing 30 frames with an exposure rate of one electron per square angstrom. Movies were collected with a defocus range of 1 to 2.5 µm and a nominal magnification of 25,000x, which produced images with a calibrated pixel size of 1.45Å.

2.3.5 Image processing

The 30 frames in each movie were aligned using the program alignframesleastsquares_list (Rubinstein and Brubaker, 2015) and averaged into one single micrograph with the shiftframes_list program (Rubinstein and Brubaker, 2015). The averaged

frames were used for determination of the transfer function (CTF) parameters with CTFFIND3 (Mindell and Grigorieff, 2003). Coordinates of each particle image were selected from these averaged frames and extracted as 220 × 220 pixels particle images. The motion of the individual particles in the frames was tracked and corrected using alignparts_lmbfgs algorithm (Rubinstein and Brubaker, 2015). This procedure produced one stack of particle images fully corrected from beam-induced motion from the first 20 frames of each movie. The total accumulated dose to produce each particles image was 20 electrons per square angstrom. From here all processing was done with Relion 1.4 program.

The initial dataset from the grids containing 30S+YjeQ mixture after particle extraction contained 417,018 particles ('dirty' dataset). These images were subjected to 2D and 3D classification (Class3D 1st iteration), which resulted in a 'clean' dataset comprised of 273,407 particles. The 'clean' dataset was run through a second cycle of 3D classification (Class3D 2nd iteration) using the entire signal in the particle images (Figure S2.2A). This classification produced two 3D classes representing the 30S+YjeQ complex and the 30S subunit. Each class was separately refined using a binary mask with a soft edge. This approach produced the best map for the 30S+YjeQ complex (displayed in figures) and a map for the 30S subunit that we called the '30S subunit consensus structure'. These cryo-EM maps were produced from 130,462 and 142,945 particle images, respectively.

In a parallel approach (Figure S2.2B), the 'clean' dataset plus some additional particle images not initially selected in the approach below (total number of particles was 299,825) was subjected to focused classification with subtraction of the residual signal using Relion (Scheres, 2012) following an approach previously described (Bai et al., 2015a, b). To this end, we applied a low pass filter to the atomic model of the 30S+YjeQ complex (PDB 2YKR) (Guo et al., 2011) after we remove the head domain and lower part of the body. This procedure produced a density

map that was used to create a soft-edge mask for the focused classification and also for the signal subtraction in the experimental particles. The newly created stacks of particles after signal subtraction and the mask were used as input for the focused classification run. During the classification step, we kept all orientations fixed at the values determined in the refinement of the consensus maps. The classification produced three distinct classes that were refined independently using a binary mask with a soft edge. One of the classes represented the 30S+YjeQ complex (167,299 particles). The remaining classes were two distinct subpopulations of the 30S subunit that we called 30S subclass I (78,440 particles) and 30S subclass II (54,086 particles).

In the case of the grids containing free 30S subunits only, the initial dataset after particle extraction contained 90,417 particles ('dirty' dataset). These images were subjected to 2D and 3D classification (Class3D 1st iteration), which resulted in a 'clean' dataset comprised of 66,493 particles. The 'clean' dataset was run through a second cycle of 3D classification (Class3D 2nd iteration) using the entire signal in the particle images. This classification produced three 3D classes (Figure S2.6). Each class was separately refined using a binary mask with a soft edge. This approach produced three maps for the free 30S subunit that we called subclass Ia, subclass IIa and subclass IIIa. These cryo-EM maps were produced from 15,088, 17,443 and 33,962 particle images, respectively

Sharpening of the cryo-EM maps was done by applying a negative B-factor estimated using automated procedures (Rosenthal and Henderson, 2003). Relion processes were calculated using the SciNet cluster. We used the program ResMap (Kucukelbir et al., 2014) to estimate the local resolution of the structures.

2.3.6 Map analysis and Atomic model building

To build the atomic model for the 30S+YjeQ complex we first obtained the atomic model of *E. coli* YjeQ using I-TASSER (Roy et al., 2010). To this end we used the YjeQ primary sequence (GenBank: BAE78165) and the crystal structure of *Salmonella typhymurium* as a template. Using Chimera (Pettersen et al., 2004), the resulting YjeQ atomic model was docked as a rigid body into the 30S+YjeQ cryo-EM map along with one of the available structures for the 30S subunit from *E. coli* (PDB ID 2AVY) (Schuwirth et al., 2005). Docking was optimized by a flexible fitting approach based on molecular dynamics simulation (Trabuco et al., 2008). The flexible fitted model was examined and used as the starting point for manual model building in Coot (Emsley et al., 2010).

2.4 Results

2.4.1 Cryo-EM structure of the 30S+YjeQ complex

Previous biochemical work (Daigle and Brown, 2004; Himeno et al., 2004; Jeganathan et al., 2015; Thurlow et al., 2016a) revealed that the highest affinity binding of YjeQ to the mature 30S subunit occurs in the presence of GMP-PNP. Thus, 30S+YjeQ complexes were assembled in the presence of this nucleotide analogue and imaged by cryo-EM using a direct electron detector camera (Figure S2.1A). This device allows for full-correction of the beam-induced motion that the individual ribosomal particles experience during the image acquisition process (Figure S2.1B). Performing a three dimensional classification of all the particles in the dataset using the entire signal in the particles revealed the presence of both free 30S subunits and 30S+YjeQ complexes (Figure S2.2A).

The cryo-EM map of the 30S+YjeQ complex was refined to a mean resolution of 5.8 Å (Figure S2.3A) and revealed an additional density corresponding to YjeQ that almost completely covered the decoding center (Figure 2.1). Local resolution analysis revealed that the map exhibited isotropic resolution with both the areas representing the 30S subunit and YjeQ refining to resolution values around the mean value. None of the areas of the map refined to resolution values significantly lower than the mean resolution (Figure S2.3B and S2.3C), implying that YjeQ binds the 30S subunit tightly and adopting a single conformation.

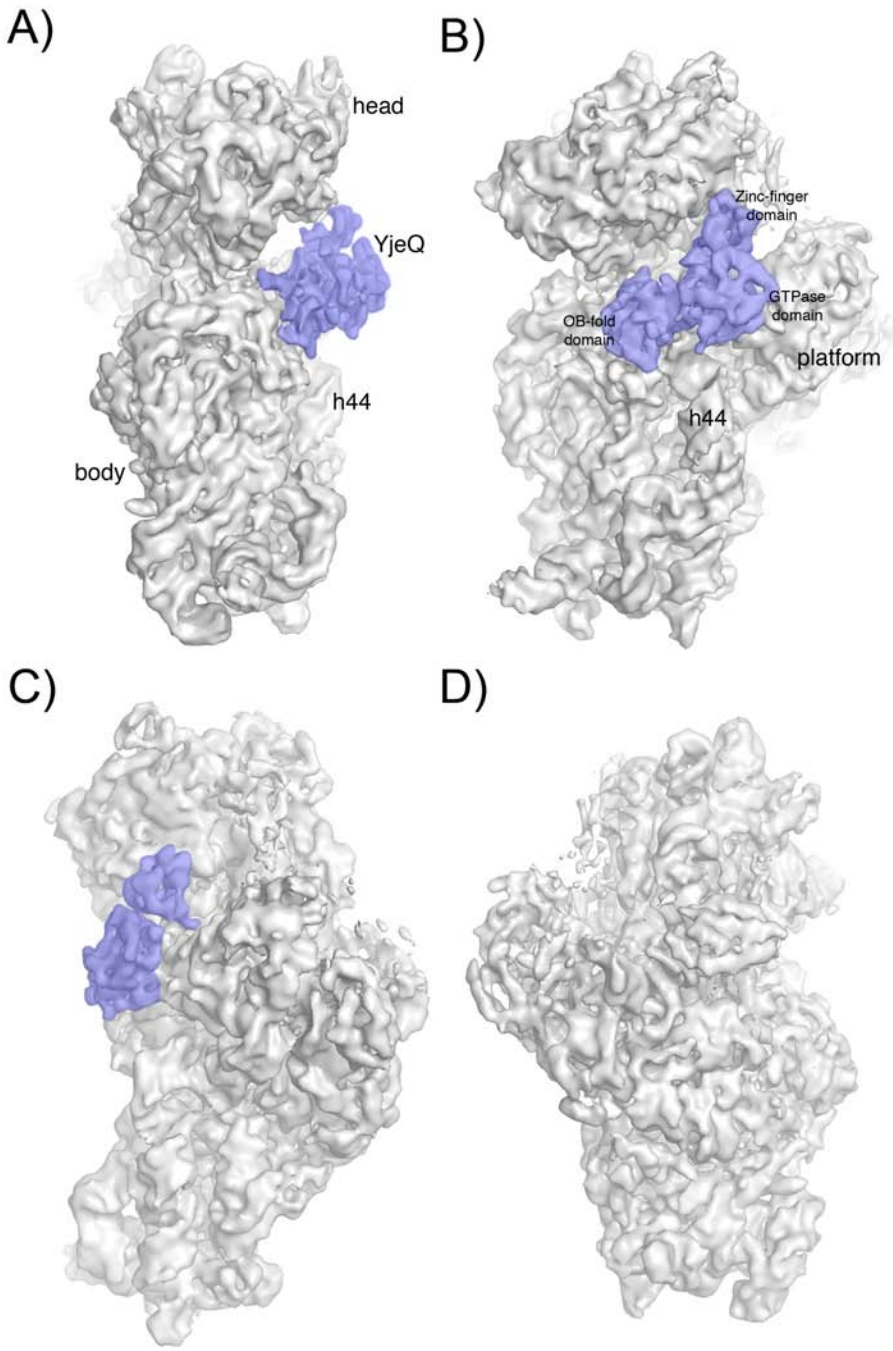

Figure 2.1: Cryo-EM structure of the 30S+YjeQ complex. Side (A), front (B), platform (C) and back (D) views of the 30S+YjeQ complex. Important landmarks of the 30S subunit and the three domains of the YjeQ protein are indicated. h44 stands for helix 44.

The entire 16S RNA fits perfectly in the electron density map (Figure 2.2A and 2.2B), albeit with minor rigid body movements of the head and platform domains with respect to the body suggesting that binding of YjeQ causes a small movement of the head backwards and of the platform forward (Figure S2.4). The main chain, and even some side chains, for 18 ribosomal proteins are well defined in the electron density map (Figure 2.2C and 2.2D). The remainder three proteins (bS1, uS7 and bS21) showed poor or no electron density in the structure. uS7 shows good electron density at its N-terminus –the region that anchors the protein to the head domain. The C-terminus is highly exposed to the solvent and, thus, the poor quality of the electron density likely reflects the intrinsic flexibility of this region of uS7 (Figure 2.2E). bS1 is normally lost during ribosome purification (Sengupta et al., 2001), therefore we were not surprised to only find residual density for this protein (Figure 2.2F). More surprising, was the absence of bS21 (Figure 2.2G). However, this protein is also absent in the two previously obtained cryo-EM structures of this complex (Guo et al., 2011; Jomaa et al., 2011c) and in some of the available X-ray structures of the mature 30S subunit (See for example PDB IDs: 1FKA, 2UXD, 2VQE).

The power of this structure is reflected on regions of the ribosomal proteins that were missing in previous crystal structures, but are visible in this one. For instance, the C-terminal helix of uS2 was missing in previous ribosome structures, but it could readily be traced in our structure using the structure of the S2-S1 complex from *E. coli* (Byrgazov et al., 2015) (Figure 2.2F). Furthermore, r-protein uS5 that could only be traced up to residue Lys159 in previous crystal structures has additional electron density at its C-terminus and residues Ser160-Leu165 are well defined in our map.

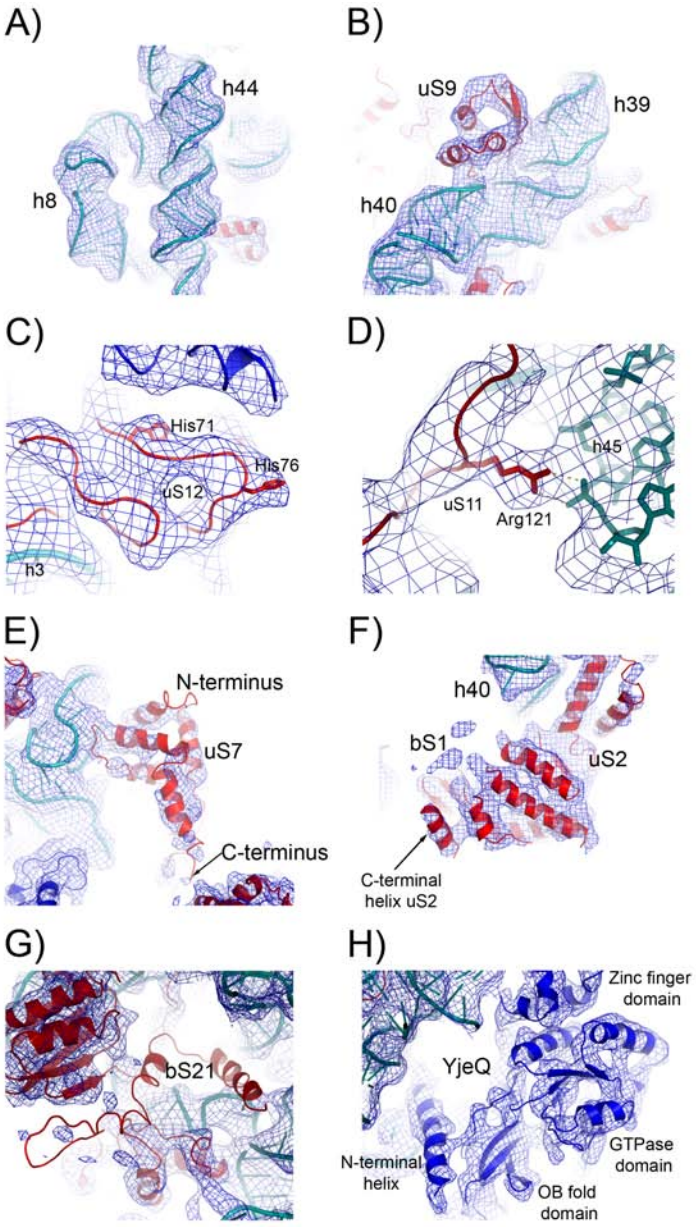

Figure 2.2: Structural details of the 30S+YjeQ cryo-EM map. Densities of several structural elements of the 30S+YjeQ cryo-EM map with the derived atomic model shown as colour-coded ribbons. (A) and (B) Regions of the cryo-EM map showing the quality of the density around the indicated 16S rRNA helices. (C) and (D) Closed up view of specific regions of the 30S+YjeQ cryo-EM map where side chains of amino acids are visible. (E) and (F) Zoomed in view of the density representing r-proteins uS7 and uS2. The C-terminal helix of uS2 (labeled) is not present in the X-ray crystal structure (Schuwirth et al., 2005), but it is visible in the cryo-EM map. Residual density observed for bS1 is labeled. (G) A density representing bS21 is not present in the cryo-EM map. (H) Density corresponding to YjeQ.

2.4.2 YjeQ binds to the decoding center of the 30S subunit in one single orientation

The electron density for YjeQ was of excellent quality and allowed us to trace almost the entire polypeptide chain, including an N-terminal helix spanning residues 7-28 that is disordered in all other YjeQ crystal structures (Levdikov et al., 2004; Nichols et al., 2007; Shin et al., 2004) (Figure 2.1 and Figure 2.2H). The cryo-EM structure also showed that the three structural domains (OB-fold, GTPase and zinc-finger domains) that are present in all YjeQ homologs (Levdikov et al., 2004; Nichols et al., 2007; Shin et al., 2004) also exist in *E. coli* YjeQ.

The high resolution of the cryo-EM map allowed us to unambiguously determine the relative binding orientation of YjeQ to the 30S subunit (Figure 2.3). The orientation in this structure was consistent with one of the previously published cryo-EM structures (Guo et al., 2011). This structure clearly shows that the N-terminal OB-fold of YjeQ interacts with the body of the 30S subunit mainly through helix 18 (Figure 2.3A), the GTPase domain contacts helix 44 and helix 24 (Figure 2.3B) in the platform and the C-terminal zinc finger domain anchors the protein to the head through helices 29 and 30 and to the platform by contacting helix 45 (Figure 2.3C). The relative orientation of YjeQ in this structure is different from that proposed in the cryo-EM map previously reported by our group (Jomaa et al., 2011b, c), which places YjeQ with a 180º rotation around an axis perpendicular to the interface surface of the 30S subunit with the large subunit. With the limited resolution of our previous structure (Jomaa et al., 2011b), rigid body docking of the YjeQ X-ray structure in the cryo-EM map produced multiple solutions with similar fitting scores preventing the unequivocal positioning of YjeQ in the map.

To explore the possibility that YjeQ may be binding the 30S subunit in more than one orientation, we performed focused classification with the entire dataset (Figure S2.2B). To this end, we kept the signal in the particle images corresponding to YjeQ and its binding area in the decoding center. The remaining part of the 30S subunit was masked out and subtracted from the

particle images. A 3D classification with the signal subtracted particle data set rendered a similar result to the classification performed with the entire signal in the particles (Figure S2.2A). One class presented an extra density identical to that described for YjeQ above. The other two obtained classes lack of any additional density and were consistent with free 30S subunits. However, no class presented an additional density that could be consistent with alternative binding orientations for YjeQ.

Therefore, the conclusion from this analysis is that YjeQ binds to the mature 30S subunit in only one orientation (Figure 2.1). This orientation is consistent with one of the previously published cryo-EM structures (Guo et al., 2011) and chemical modification experiments (Kimura et al., 2008) showing enhanced protection of 16S rRNA bases localized at the interface between YjeQ and the 30S ribosomal subunit.

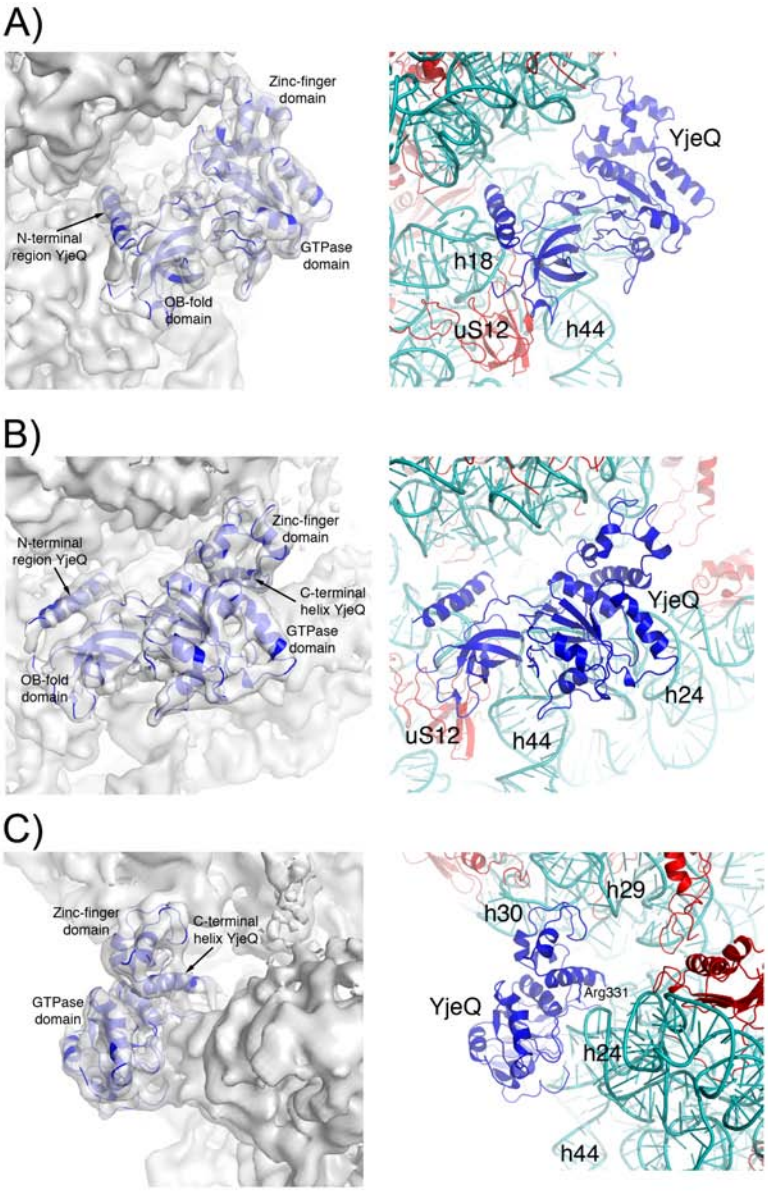

Figure 2.3: Cryo-EM structure and atomic model of YjeQ bound to the 30S subunit. (A) The left panel shows a zoomed in view of the density representing YjeQ in the cryo-EM map of the 30S+YjeQ complex. The atomic model of YjeQ is shown superimposed in the cryo-EM map. The right panel depicts the equivalent closed-up view of the atomic model of the 30S+YjeQ complex with the assembling factor binding to the decoding center of the 30S subunit. The rRNA and r-proteins interacting with YjeQ are labeled. (B) Front view of density representing YjeQ in the cryo-EM map and the atomic model. (C) Platform view of the YjeQ density in the cryo-EM map and the corresponding atomic model. All panels show equivalent orientations to Figure 2.1.

2.4.3 The structure of the mature 30S subunit in solution differs from that described by X-ray crystallography

The structure of the entire 30S subunit at atomic resolution was first described using X-ray crystallography (Wimberly et al., 2000). This structure demonstrated that the 16S rRNA largely determines the overall shape of the 30S subunit, which folds into four different domains. In the canonical front view of the 30S subunit (Figure 2.4A), the 5' domain forms the body of the particle with the shoulder at the top left side and the spur at the lower left. The central domain of the 16S rRNA forms the platform that occupies the top right side of the particle. The 3' major domain constitutes the bulk of the head and the 3' minor domain is also integral part of the body. In this structure, the 3' minor domain of the 16S rRNA consisting of helices 44 and 45 occupies the subunit interface with the 50S subunit and both helices are perfectly structured. Helix 44 stretches from the bottom of the body to the bottom of the head and helix 45 is connected to the top end of helix 44 adopting an orientation almost perpendicular to the preceding helix.

The presence of both 30S+YjeQ complexes (48% of the particles) and free 30S subunits (52% of the particles) in our sample provided the opportunity to obtain the structure of the free 30S subunit (Figure S2.2A). This cryo-EM structure showed no substantial differences from the crystal structure in the body, platform and head domains. However, helix 44 in the 3' domain showed significant discrepancies. We called this cryo-EM map the '30S subunit consensus structure'. In the X-ray structure, helix 44 represents the single longest helix in the subunit and runs in a defined single conformation from the bottom of the body to the neck region of the 30S subunit (Figure 2.4A). However, a defined density representing the upper region of helix 44 is completely absent in the cryo-EM map, although helix 45 still adopts similar conformations in both the cryo-EM map and the X-ray structure of the 30S subunit (Figure 2.4B).

To investigate whether the upper region of helix 44 was present in several discrete conformations or rather was a continuous of multiple conformations we analyzed the two classes representing free 30S subunits in the focused classification performed with all the particles in the dataset (Figure S2.2B). One of the classes (subclass I) was very similar to the '30S consensus structure' described above, with most of the density representing the upper motif of helix 44 missing (Figure 2.4C and Figure S2.2B). Interestingly, in the second class (subclass II) the entire length of helix 44 was visible. However, the upper region of helix 44 was not latched to the decoding center as described by the crystal structure. Instead, this entire section of the helix protruded from the surface of the 30S subunit, thereby distorting the interface with the 50S subunit (Figure 2.4D and Figure S2.2B). We found no class in which helix 44 adopted the conformation displayed in the X-ray crystal structure (Figure 2.4A and Figure S2.2B).

Local resolution analysis of the consensus 30S subunit, subclass I and subclass II maps (Figure S2.5B and 2.5C) revealed that the resolution of the structures was isotropic with most areas exhibiting resolutions values similar to the mean resolution value measured for the entire map (Figure S2.5A). Only isolated areas on the platform, back of the head and neck showed slightly lower resolution. More importantly, in the consensus and subclass I structures, the part of helix 44 that was visible showed a resolution value close to the mean resolution. However, In the case of the map obtained for subclass II, with the entire helix 44 defined by density, its upper domain refined to a slightly lower resolution suggesting that this region is partially flexible.

To establish whether any of the helix 44 conformations observed in the free 30S particles were induced by the presence of YjeQ, we imaged a sample containing purified mature 30S subunits in the absence YjeQ. Using all particle images in the data set produced a cryo-EM map similar to the '30S subunit consensus structure' described above. We named it '30S subunit average structure' (Figure S2.6, top panel). Performing image classification revealed the

existence of three subpopulations. One class (subclass Ia) representing a 22% of the population was equivalent to the 30S subclass I (Figure 2.4C and Figure S2.2B) and lacked the density for the upper section of helix 44 (Figure S2.6, bottom panel). The second class (subclass IIa) had the upper region of helix 44 unlatched from the decoding center (Figure S6, bottom panel) and thus, it was similar to the 30S subclass II (Figure 2.4D and Figure S2.2B). A 26% of the particle images belonged to this class. The third subpopulation was unique to this sample and produced a cryo-EM map that lacked density for the entire helix 44 (subclass IIIa) (Figure S2.6, bottom panel). Interestingly, these particles represented a 51% of the population, which is similar to the percentage of particles representing 30S+YjeQ complexes in the sample containing both 30S subunits and YjeQ (48%). This result suggests that YjeQ may predominantly bind 30S subunits with helix 44 in a flexible conformation. Intriguingly, these 30S particles are the most resembling to immature assembly intermediates (Guo et al., 2013; Jomaa et al., 2011a; Leong et al., 2013).

We concluded that when the 30S subunit is in solution and free of the stabilizing contacts provided by a crystal lattice or the 50S subunit, helix 44 adopts multiple conformations. These conformations do not seem to be induced by YjeQ as they are also present in the absence of the factor. Surprisingly, the specific conformation described by the crystal structure of the 30S subunit was not observed among the population of free 30S subunits in our sample.

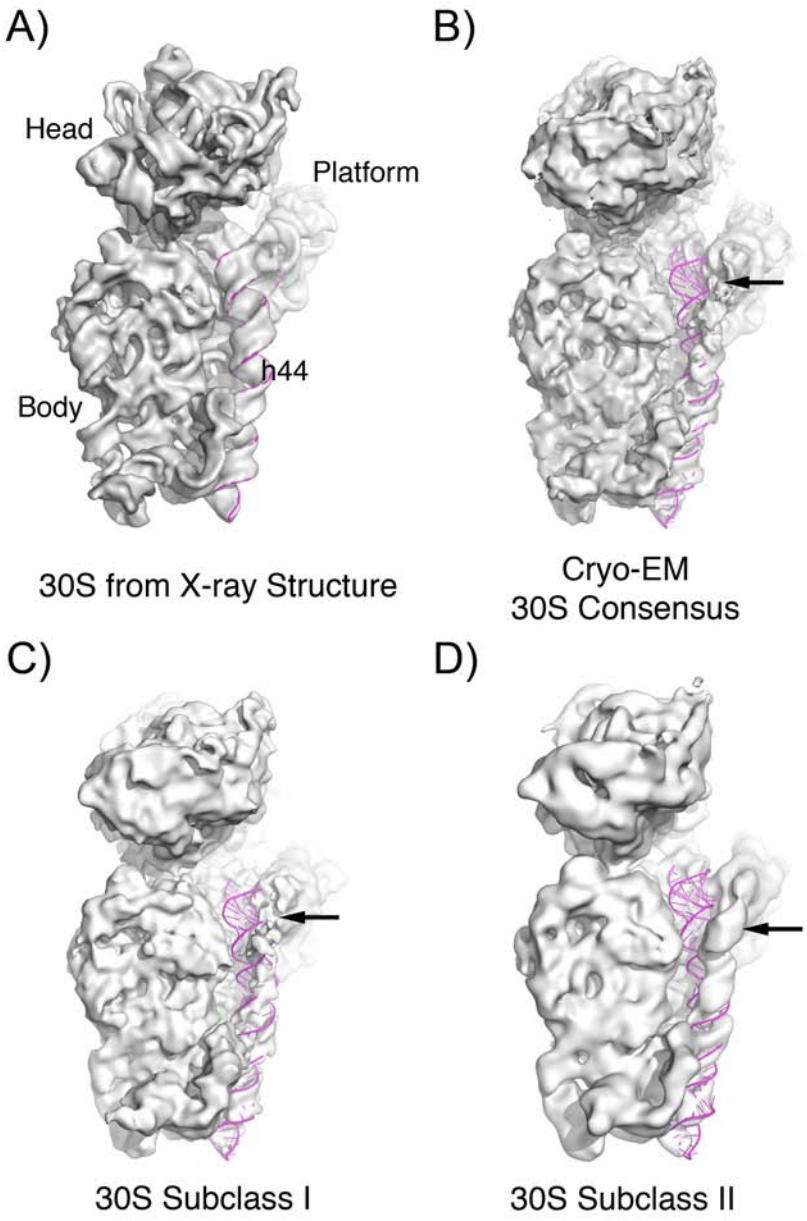

Figure 2.4: Cryo-EM structure of the 30S subunit. (A) Density map of the 30S subunit obtained by applying a low pass-filter at 7Å resolution to the X-ray structure PDB ID: 2AVY. Structural landmarks of the 30S subunit are labeled. (B) Consensus cryo-EM structure obtained for the 30S subunit. (C) Cryo-EM structure of the 30S subunit subclass I obtained from focused classification. (D) Cryo-EM structure of the 30S subunit subclass II obtained from focused classification. The region of helix 44 showing missing density or protruding outward is indicated with an arrow in panels (B) to (D).

2.4.4 YjeQ stabilizes helix 44 in a conformation suggesting a checkpoint role in ribosome fidelity

Previous structural work has established an essential role of the universally conserved A1492 and A1493 nucleotides in the decoding process and proofreading mechanisms of the ribosome (Carter et al., 2000). Decoding the mRNA requires the correct recognition of each A-site codon by the anticodon of the corresponding aminoacyl-tRNA (aa-tRNA). Interestingly, the ribosome performs this step with a much higher level of accuracy than the difference in binding energy between the cognate and non-cognate codon-anticodon pairing can explain (Green and Noller, 1997). This observation suggested early on that the ribosome possesses built-in proofreading capabilities. Nucleotides A1492 and A1493 in helix 44 mediate one of these mechanisms. During the decoding process these two bases swivel out and their N1 atoms form hydrogen bonds with the 2' OH groups on both sides of the codon-anticodon helix. Through the simultaneous interaction with both strands of the codon-anticodon helix, these two adenines can monitor the base-pairing geometry of the codon-anticodon and sense the distortions arising from mispairing (Carter et al., 2000; Yoshizawa et al., 1999).

Interestingly, when we compared the cryo-EM structures of the 30S+YjeQ complex with the structure of the free 30S subunit both obtained from the same set of images, we found that the binding of YjeQ stabilizes helix 44 in a conformation similar to that observed in the X-ray structure (Figure 2.4A). The assembly factor sits over the decoding center interacting mainly through the GTPase and OB-fold domains (Figure 2.3). The GTPase domain interacts with helix 44 mainly through switch I, switch II and the loop connecting the β6 and β7 strands in this domain (Figure 2.5A and 2.5B). These contacts occur in the last turn of helix 44, right before the rRNA continuous towards helix 45. In the OB-fold, the loop connecting strands β1 and β2 impinges on the last turn of helix 44 causing a reorganization of the electron density in the area

surrounding A1492 (Figure 2.5A and 2.5C). Analysis of this region on the cryo-EM map revealed that the density corresponding to the adenine moiety of A1492 is outside the helical axis (Figure 2.5C and 2.5D), indicating that A1492 flips out from the helix. This conformation is stabilized through hydrophobic interactions between the adenine moiety and the OB-fold of YjeQ, as well as π-stacking interactions between the side chain of Phe48 and A1408 (Figure 2.5D). The Phe-mediated stabilization of the unpaired nucleotide resembles the structure of the mismatch repair protein MutS in complex with a DNA including a one-nucleotide insertion, where the side chain of Phe36 promotes the extrusion of the unpaired nucleotide through an aromatic-ring stacking with the complementary DNA strand (Obmolova et al., 2000).

The conformation of A1492 resembles that exhibited by nucleotides A1492-A1493 during proofreading of the codon-anticodon pairing (Carter et al., 2001). In our structure, however, base A1493 did not swivel out of the helix. This finding suggests that YjeQ plays a role as a checkpoint protein in the mature 30S subunit by testing the ability of the 30S subunit to perform proofreading before the subunit is released to the pool of actively translating ribosomes. Simultaneously, the binding location of YjeQ covering essential inter-subunit bridges also prevents premature association with the 50S subunit.

This function of YjeQ suggests that similarly to the eukaryotic ribosome, bacteria also have specific quality control mechanisms to survey nascent ribosomes and test their functionality. In eukaryotic cells, quality control mechanisms during ribosome maturation have been extensively studied (Karbstein, 2013). In these cells, some factors simply prevent nascent subunits from entering the translation by sterically and allosterically blocking binding of initiation factors, tRNA or 60S subunits (Strunk et al., 2011). However, there are also other factors that perform functional checks in the assembling ribosomes by mimicking elements or steps of the translational cycle. The best-characterized example of this type of assembly factors

is that of the pre-40S subunit in yeast (Strunk et al., 2012). During the late stages of assembly of this ribosomal particle seven different factors bind to the subunit interface (Tsr1, Rio2, Dim1, Nob1, Pno1 and Enp1/Ltv1) of the 40S particle and cooperate to block every step in the translation initiation pathway. Interestingly, release of these assembly factors requires a translation-like cycle, during which translation factors must function. This cycle probes key functional properties on the pre-40S particle, including the ability to associate and position correctly the 60S subunit and the ability to bind important elements in the translation cycle (eIF5B, Fap7, Rli1 and Dom34).

To date, multiple studies (Guo et al., 2011; Jomaa et al., 2011c) have suggested a checkpoint function for YjeQ or other factors (Guo et al., 2013; Leong et al., 2013; Sharma et al., 2005) assisting the assembly of the bacterial ribosome. However, none of these studies had been able to pinpoint to a specific checkpoint function in which the factor performs a functional check in the assembling ribosomal particle. Previous structural work has suggested a general checkpoint role for YjeQ by sterically blocking the binding of initiation factors to the 30S subunit or its association with the large 50S subunit (Guo et al., 2011). The cryo-EM structure presented here provides for the first time evidence of a bacterial assembly factor testing a specific translation mechanism of the 30S ribosomal subunit before the particle is released to the pool of actively translating ribosomes. The remaining question is how deleterious eliminating these quality control mechanisms is for bacterial fitness, pathogenicity and survival. It will be exciting to test whether their suppression or inhibition leads to large populations of malfunctioning ribosomes, affecting the bacterial proteome and, in turn, creating an observable phenotype in these bacterial cells.

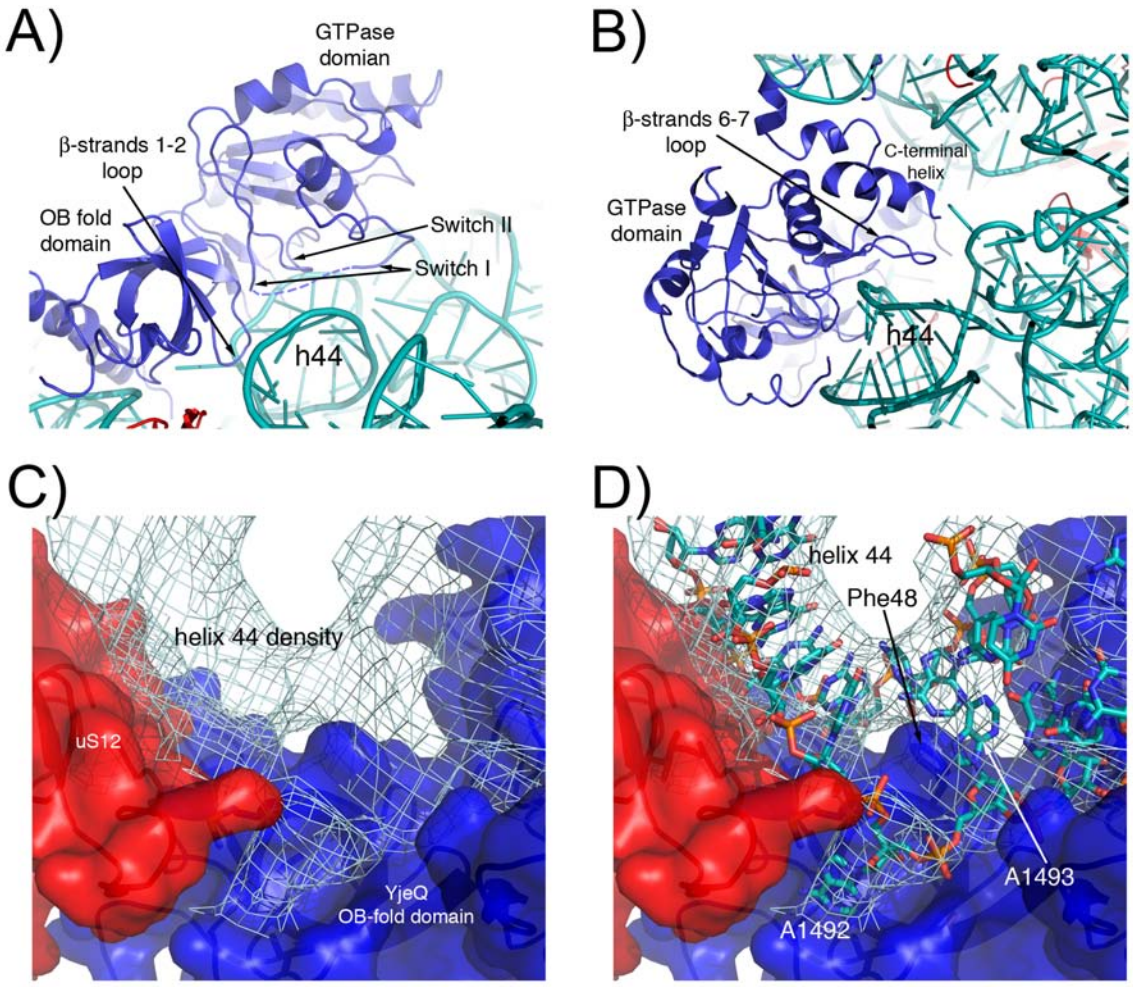

Figure 2.5: YjeQ checkpoint role in ribosome fidelity. (A) Interactions of YjeQ switch I and switch II with helix 44 of the 16S rRNA. (B) Loop between strands β6 and β7 in the GTPase domain of YjeQ interacting with helix 44. (C) Density representing helix 44 in the 30S+YjeQ cryo-EM map showing a disruption of the rRNA ribbon in this region. (D) Atomic model fitted into the cryo-EM density map showing that A1492 on the 16S rRNA adopts a flip out conformation. A1493 adopts the standard configuration seen in the X-ray structure of the free 30S subunit. Phe48 in the loop connecting strands β1 and β2 in the OB-fold domain of YjeQ inserts itself into helix 44 and stabilizes adenosine 1408 through π--stacking interactions.

2.4.5 The cryo-EM structure of the 30S+YjeQ complex suggest a role for the N-terminal region of YjeQ at promoting the release of RbfA.

One specific function that has been attributed to YjeQ during ribosome biogenesis is assisting on the release of RbfA from the mature 30S subunit once the maturation of the particle

is completed (Goto et al., 2011; Jeganathan et al., 2015). However, it is still unclear how this functional interplay between YjeQ and RbfA is implemented. The RbfA protein binds to the small ribosomal subunit at the junction between the body and head and alters dramatically the position of helix 44 and 45 (Figure S2.7), placing this region in a conformation unsuitable for the subunit's participation in protein synthesis (Datta et al., 2007).

The cryo-EM structure of the 30S+YjeQ complex presented here suggests a dual mechanism through which YjeQ may facilitate the release of RbfA from the 30S subunit. We find that binding of YjeQ to the 30S subunit has a significant stabilizing effect in the upper region of helix 44 (Figure 2.1 and 2.4). This is the same rRNA motif that appears severely disrupted upon RbfA binding (Figure S2.7). Therefore, it is likely that binding of YjeQ to the 30S subunit forces helix 44 back into the normal decoding position and triggers the release of RbfA. In addition, *E. coli* YjeQ includes a 34 amino acid N-terminal extension immediately preceding the OB-fold domain. In the cryo-EM map, this N-terminal region is visible and defines an α-helix that points into the neck region in the same area that has been described as the binding site for RbfA (Figure 2.3A). We concluded that the stabilizing effect of YjeQ in the conformation of helix 44 combined with the insertion of the N-terminal α -helix of YjeQ in the binding site of RbfA likely creates the necessary conditions to force the removal of RbfA factor from the mature 30S subunit.

Interestingly, this N-terminal stretch of amino acids is not conserved among all bacterial species. It is present in *E. coli* and *Salmonella typhimurium* YjeQ proteins. In the case of *S. typhimurium*, the N-terminal region is eight amino acids longer (Nichols et al., 2007). However, this region is disordered in the X-ray structure of *S. typhimurium* YjeQ and, therefore, the conformation and relative orientation with respect to the other protein domains remains unknown. YjeQ orthologs from bacterial species including *Thermatoga maritima*, *Bacillus*

subtilis (called YloQ), *Pseudomonas putida*, *Mycoplasma pneumoniae* and others all lack this N-terminal motif (Levdikov et al., 2004; Shin et al., 2004). In these species, it is not known whether YjeQ can remove RbfA from the 30S subunit, but the absence of this N-terminal motif may suggest that it is not essential for this function.

The C-terminal helix in the zinc-finger domain of YjeQ is also essential for its ability to remove RbfA from the 30S subunit (Jeganathan et al., 2015). Interestingly, when YjeQ is bound to the 30S subunit this C-terminal helix lies far away from the RbfA binding site (Figure 2.3B and 2.3C). Nevertheless, our cryo-EM map reveals that the zinc-finger domain of YjeQ constitutes a major anchor point of the protein to the 30S subunit head and platform. In this domain, the long loop that mediates the tetrahedral coordination of the zinc ion mediates strong interactions with helices 29 and 30 in the 16S rRNA head domain (Figure 2.3C). The interaction with the platform occurs mainly through the C-terminal helix of the zinc-finger domain. The main interactions between this motif of YjeQ and the platform include the side chain of Arg331 interacting with the backbone of helix 24 and the C-terminus of the protein interacting with the rRNA loop connecting helices 44 and 45 (Figure 2.3C). These interactions along with the previous mutational study (Jeganathan et al., 2015) suggest that the zinc-finger domain anchors YjeQ on its binding site allowing for the proper positioning of the OB-fold and GTPase domains. The OB-fold and GTPase domains, in turn, function as effector elements for the release of RbfA from its binding site.

In conclusion, this structure of the 30S+YjeQ complex provides for the first time a detailed specific testable model describing the functional interplay between YjeQ and RbfA.

2.4.6 Role of the GTPase activity in the YjeQ function

Although the GTPase activity of YjeQ was characterized early on (Daigle and Brown, 2004; Daigle et al., 2002; Himeno et al., 2004), the role of this activity in the overall function of

YjeQ and its regulation is still unclear. The present cryo-EM structure of the 30S+YjeQ complex shows that through extensive interactions involving the OB-fold and zinc finger domains, YjeQ interacts with three out of the four domains of the 30S subunit (body, head and platform) (Figure 2.1). These interactions are important for the functionality of YjeQ (Daigle and Brown, 2004). For example, deletion of the first N-terminal 20 amino acids of YjeQ significantly decreases the binding of YjeQ to the 30S subunit, while removal of the OB-fold domain completely suppresses any association with the ribosomal particle. Similarly, partial or complete removal of the C-terminal zinc finger domain also abolishes YjeQ binding (Jeganathan et al., 2015).

The interaction of YjeQ with the 30S subunit places the GTPase domain in direct contact with the upper part of helix 44 (Figure 2.3B). This area of helix 44 constitutes the ribosomal motif undergoing the largest conformational change upon YjeQ binding. Consequently, in the 30S+YjeQ complex, the GTPase domain of YjeQ is ideally placed to monitor these changes. The atomic model of the 30S+YjeQ complex describes the structural determinants of YjeQ that are likely probing the conformation of helix 44. Upon YjeQ binding, switch I and switch II lay at the interface with the 30S subunit (Figure 2.5A). The tip of the loop between strands β6 and β7 in the GTPase domains reaches helix 44 and may also be involved in the monitoring function (Figure 2.5B).

The GTPase activity of YjeQ is stimulated over 160-fold in the presence of mature 30S subunits (Daigle and Brown, 2004; Daigle et al., 2002; Himeno et al., 2004). Although the structure does not reveal what triggers this stimulation, it is plausible that the restrained conformation of helix 44 may stimulate the GTPase activity in YjeQ. If this is the case, the conformational change would be first sensed by switch I. Consistently, the crystal structure of YjeQ implies that the flexible switch I region of YjeQ must experience conformational changes to stimulate the GTPase activity (Shin et al., 2004). Once GTP hydrolysis has occurred,

additional conformational changes in switch I and switch II trigger a reorganization of their interactions with the 30S subunit causing an overall decrease in the binding affinity of YjeQ (Daigle and Brown, 2004; Thurlow et al., 2016a) and its release from the 30S subunit.

This model is supported by the conformational differences existing between YjeQ in our cryo-EM structure (GMP-PNP-bound form that mimics the GTP state) and that observed in the YjeQ crystal structure of *Thermotoga maritima* YjeQ (GDP-bound form) (Shin et al., 2004). Superimposition of the GTPase domain of these two structures yielded a 1.6 Å root-mean square deviation (r.m.s.d.) for over 500 atoms and revealed the re-orientation of both the OB fold and zinc-finger domains (Figure 2.6). The large contact area and weak interactions existing between YjeQ domains (Levdikov et al., 2004) allow for an easy propagation of the conformational changes from the GTPase domain to neighboring domains.

Therefore, we concluded that the GTPase activity of YjeQ functions as a sensor to facilitate the release of the protein factor from the 30S subunit once YjeQ has performed its functions. Our structure suggests that a specific conformation of helix 44 stimulates the GTPase activity of YjeQ. Hydrolysis of GTP and the associated conformational changes in YjeQ then lead to the reorganization of the interface of the complex and, in turn, the release of the factor. Our structure also rules out that the energy from GTP hydrolysis is necessary to place helix 44 in its normal decoding position.

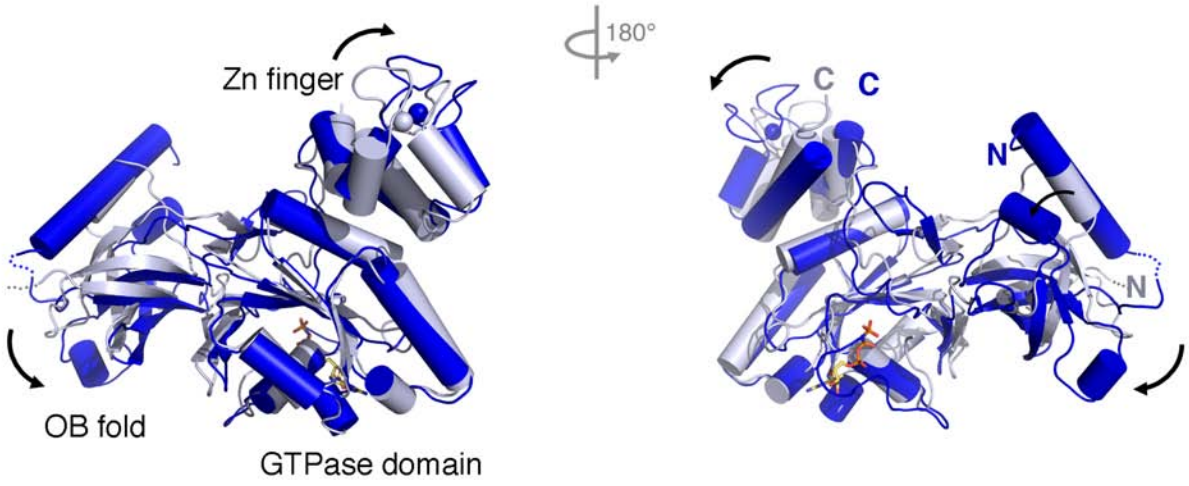

Figure 2.6: Conformational change of YjeQ upon GTP hydrolysis. Opposite views of YjeQ from *Thermotoga maritima* (PDB ID: 1u0l; white) (GDP bound) superimposed onto the structure of *E. coli* YjeQ bound to the 30S ribosome (blue) (GMP-PNP bound) from the cryo-EM structure. The zinc metal ions are shown as spheres and the GMP-PNP molecule bound to YjeQ is shown as color-coded sticks.

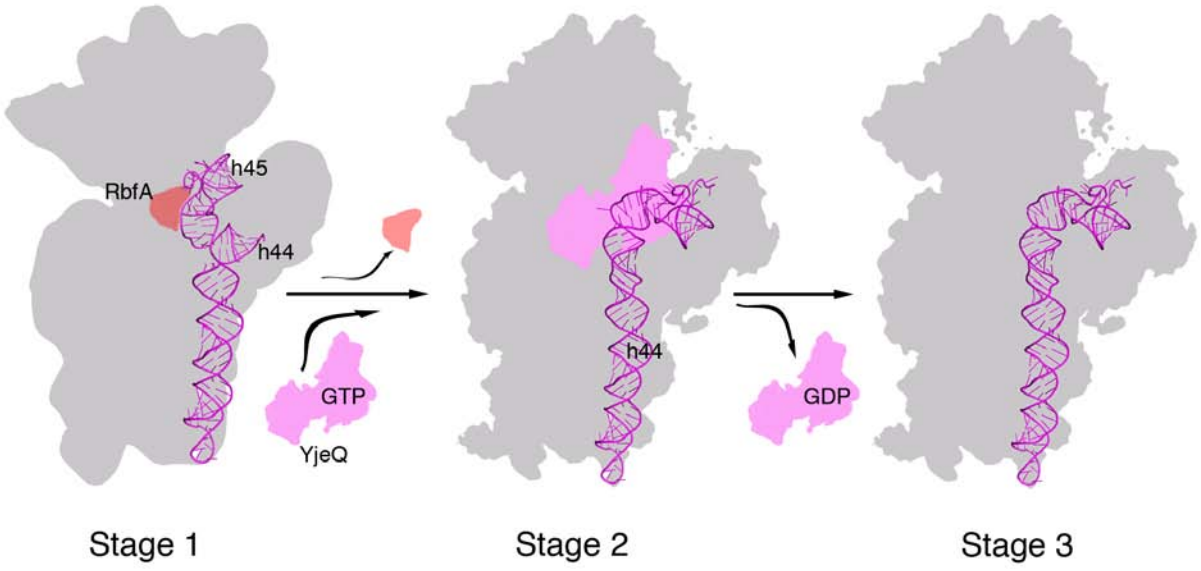

Figure 2.7: Diagram illustrating the function and mechanism of YjeQ. YjeQ likely binds to the pre-30S subunit when it is still bound to RbfA. RbfA binding alters dramatically the position of helix 44 and 45 (Stage 1). Binding of YjeQ to the 30S subunit forces helix 44 back into the normal decoding position and triggers the release of RbfA. YjeQ also causes A1492 to flip out from helix 44 to test the proofreading ability of the 30S subunit (Stage 2). This conformation of helix 44 may trigger the ribosome-activated GTPase activity in YjeQ. Hydrolysis of GTP causes a reorganization of the interactions between YjeQ and the 30S subunit that leads to the release of the factor. The 30S subunit is then free to join the pool of actively translating ribosomes (Stage 3).

2.5 Data Deposition

The EMDB IDs assigned to the structures presented here are: 30S+YjeQ (8621), 30S subunit consensus structure (8626), 30S subunit subclass I (8627) and 30S subunit subclass II (8628). The coordinates for the atomic model built for the 30S+YjeQ complex have been deposited in the Protein Data Bank with accession code (5UZ4).

2.6 Acknowledgment

We acknowledge the SciNet General Purpose Cluster (GPC) from Compute Canada for providing computer resources for this project. We are grateful to Dr. Brandon Aubie for technical assistance with the MSLR computing cluster. We acknowledge Dr. John Rubinstein at the Hospital for Sick Children in Toronto for granting us access to the Electron Microscopy Facility. We also thank Dr. Samir Benlekbir for assistance with the electron microscope. This work was supported by grants from the National Science and Engineering Research Council of Canada [RGPIN288327-07 to J.O.] and Canadian Institutes of Health Research [MOP-82930 to J.O. and MOP-67189 to A.G.]. Canadian Institutes of Health Research provided the funds for open access charges.

2.7 Supplemental Materials

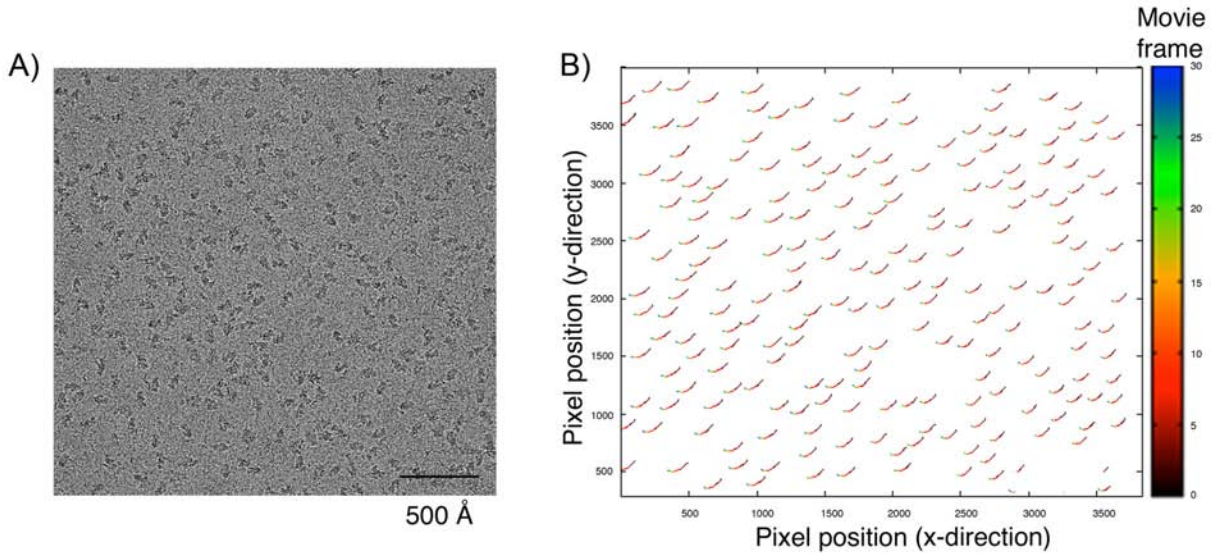

Figure S2.1: Cryo-EM images of the 30S+YjeQ complex and beam induced motion correction. (A) The left panel shows a representative cryo-EM image of the 30S+YjeQ assembly reaction. This image was obtained using a Gatan K2 direct electron detector in counting mode and the displayed image was produced after whole frame alignment (Li et al., 2013) of the 30 frames contained in the original movies. (B) The vector map displays the particle trajectories during the 15 seconds exposure used to collect the movies. Trajectories are exaggerated by a factor of 5 to allow visualization. Beam induced motion correction was performed in individual particle images using the calculated trajectories (Rubinstein and Brubaker, 2015).

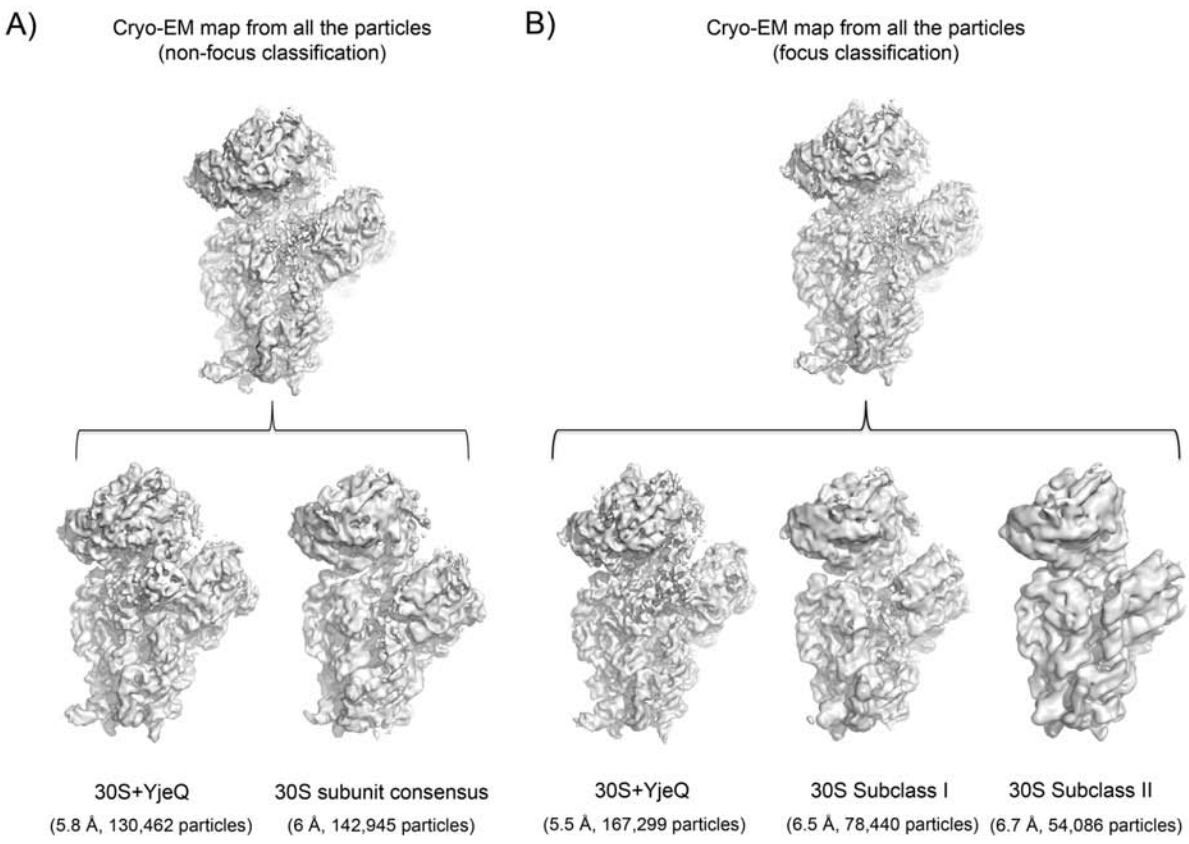

Figure S2.2: 3D particle classification. (A) 3D classification of the data set using the entire signal in the particles. The cryo-EM map obtained from all the particles in the data set is shown in the top row of the panel. The two classes obtained in this classification are shown in the bottom row. One of the classes represents the 30S+YjeQ complex with a clear additional density attached to the decoding center. The second class represents free 30S subunits (30S subunit consensus structure) that are also present in the assembly reaction. (B) The panel shows a 3D classification of the same data set but in this case it was performed using a focused classification approach (Bai et al., 2015a). During this classification only the signal around the decoding center was considered. The consensus structure obtained from all the particles in the data set is shown in the top row of the panel. The classification produces three classes that are show in the bottom row. One of the classes has additional density in the decoding center and represents the 30S+YjeQ complex. The other two classes represent two different conformational subpopulations of the 30S subunit that we name 30S subclass I and 30S subclass II.

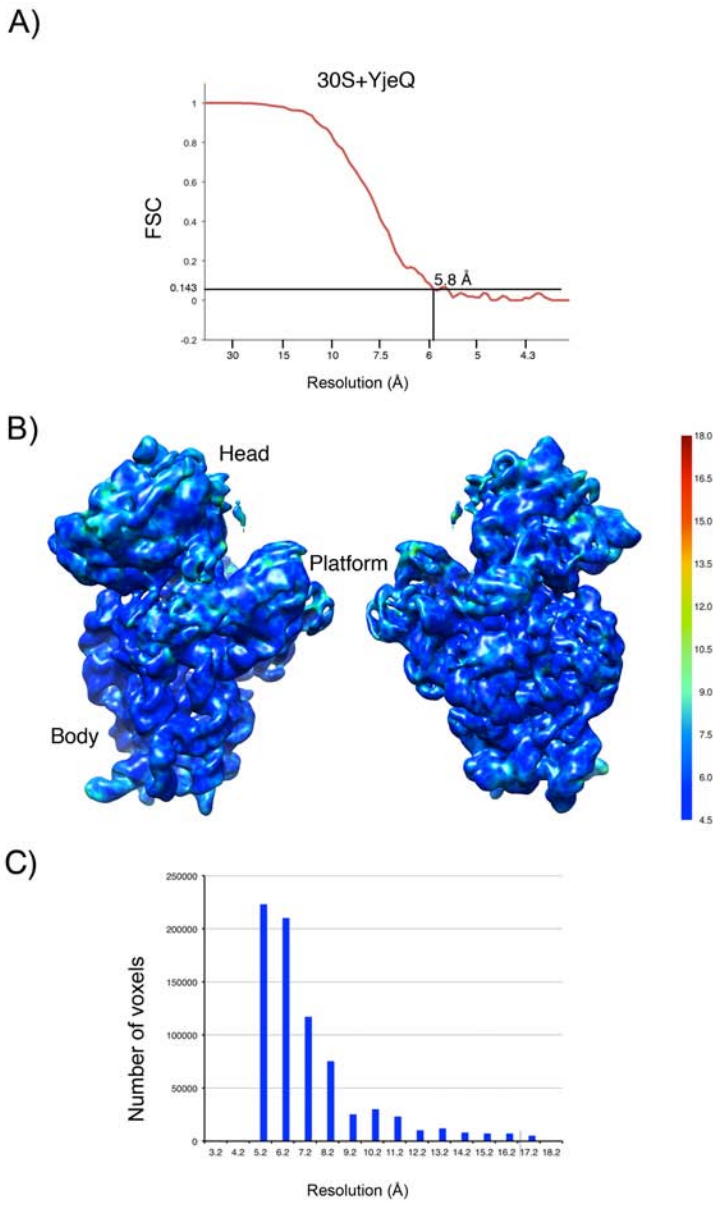

Figure S2.3: Resolution analysis of the 30S+YjeQ structure. (A) Fourier Shell Correlation (FSC) plot for the 30S+YjeQ structure. We used a FSC value of 0.143 to report the resolution. (B) Local resolution analysis of the 30S+YjeQ structure performed with ResMap (Kucukelbir et al., 2014). (C) The histogram shows the number of voxels in the map at each resolution after local resolution analysis

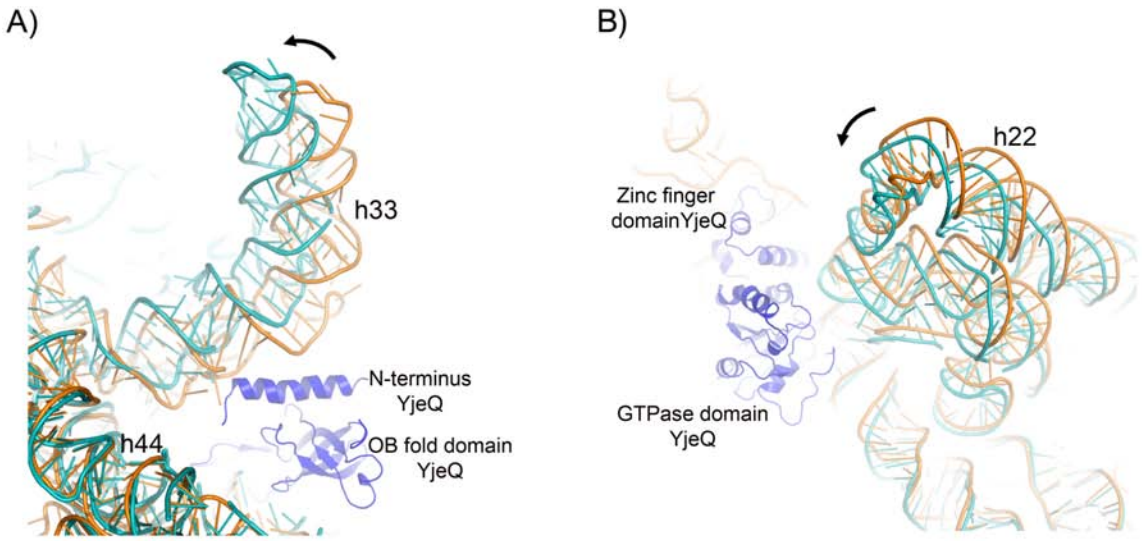

Figure S2.4: Binding of YjeQ changes the relative orientation of the domains in the 30S subunit. Overlap of the atomic model of the 30S+YjeQ complex overlapped with the X-ray structure of the free 30S subunit (PDB ID 2AVY) (Schuwirth et al., 2005) showing the displacement of the head (A) and platform (B) domain of the 30S subunit upon binding of YjeQ.

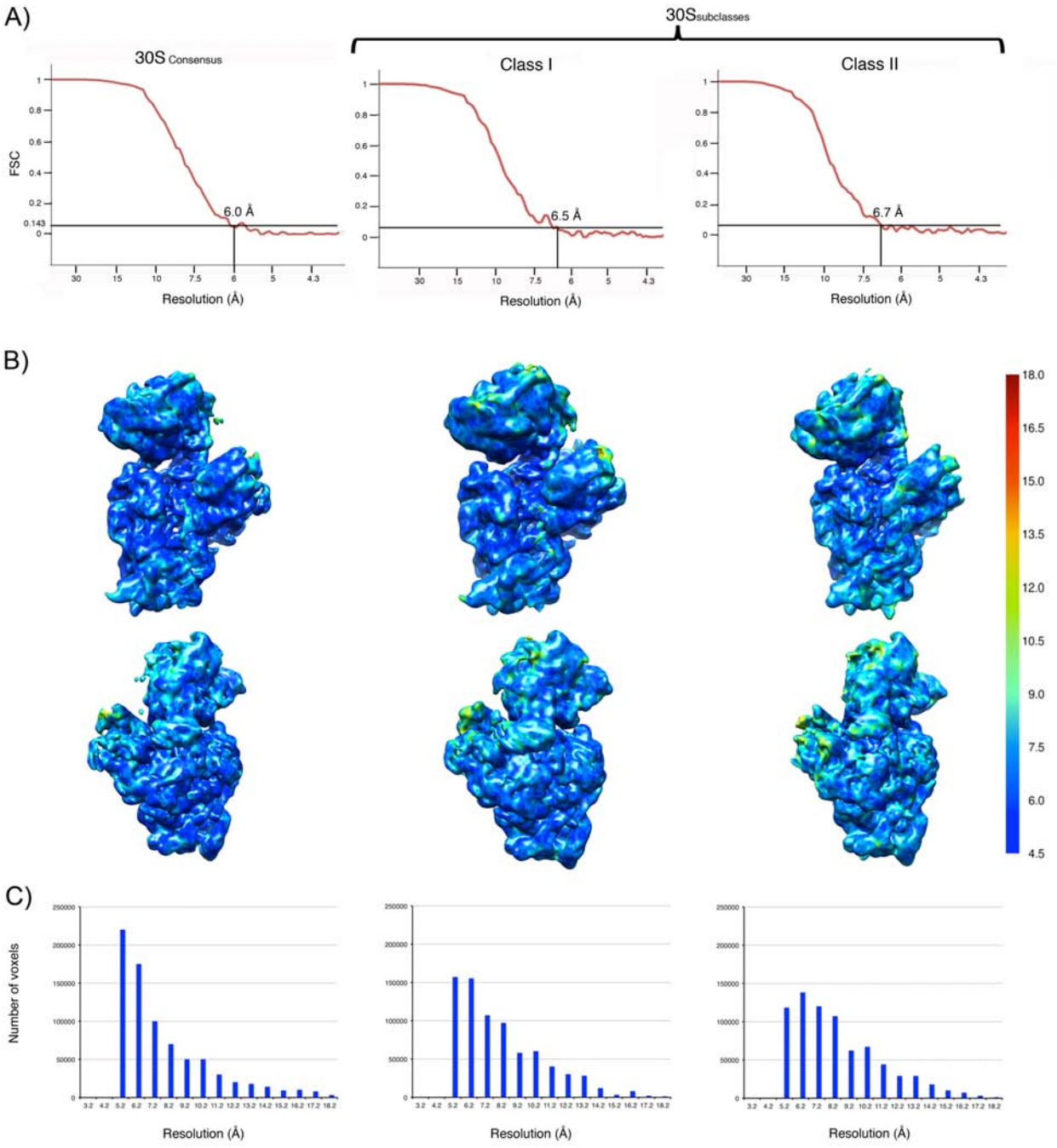

Figure S2.5: Resolution analysis of the 30S subunit structure. (A) This panel shows the Fourier Shell Correlation (FSC) plots for the 30S subunit consensus, the 30S subunit subclass I and 30S subunit subclass II structures. A FSC value of 0.143 was used to report the resolution. (B) Local resolution analysis of the three structure performed with ResMap (Kucukelbir et al., 2014). (C) The histogram shows the number of voxels in the maps at each resolution after local resolution analysis.

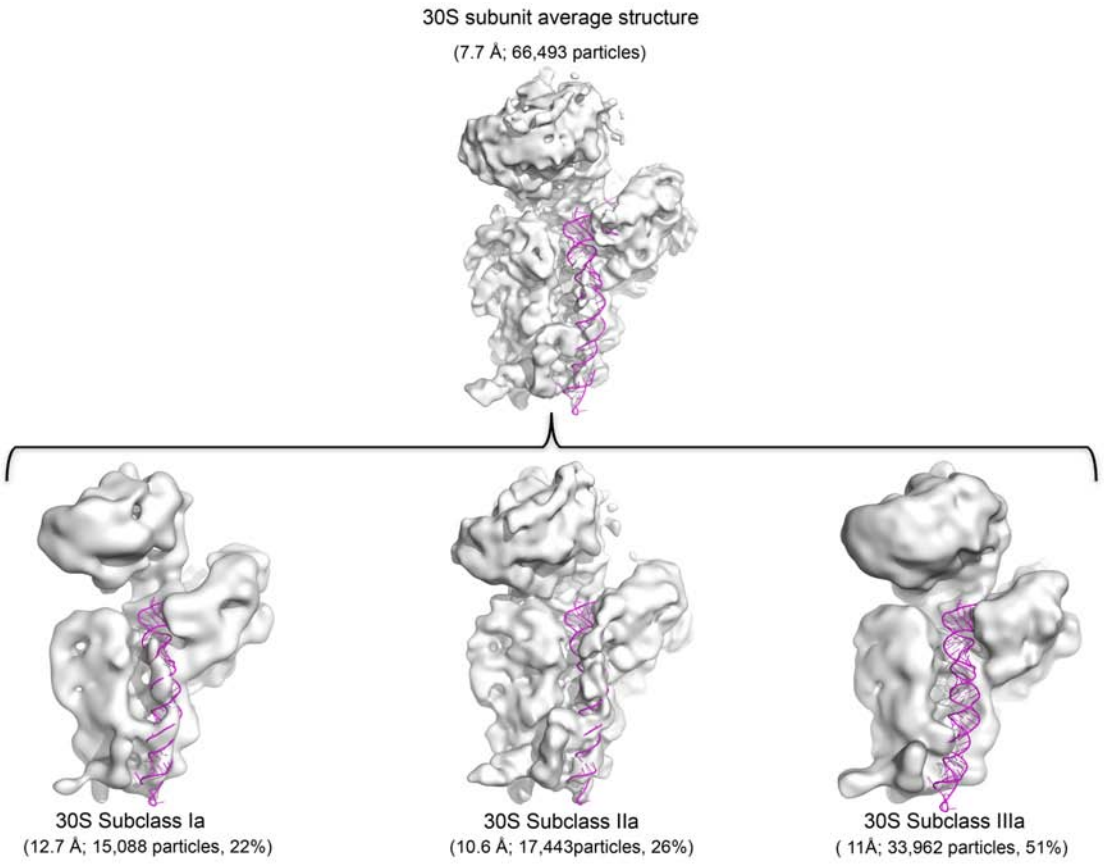

Figure S2.6: Cryo-EM structures of 30S subunit subpopulations in a sample containing mature 30S subunits. A sample containing purified mature 30S subunits was imaged by cryo-EM and subjected to image classification. The 3D reconstruction at the top was named '30S subunit average structure' and was obtained by combining all the particle images in the data set. The cryo-EM maps at the bottom represent the three identified conformational subpopulations in this sample. The conformation of helix 44 is different in the three cryo-EM maps. Labels indicate the number of particles used for each structure and the percentage of the total population they represent.

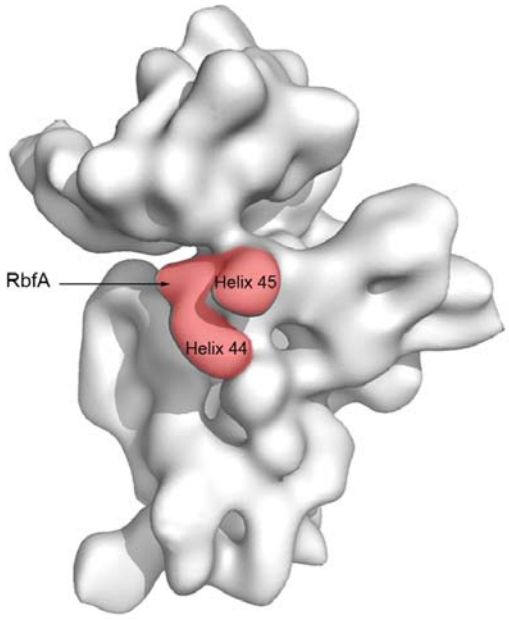

Figure S2.7: Structure of the mature 30S subunit in complex with RbfA. RbfA binds to the small ribosomal subunit at the junction between the body and head and alters dramatically the position of helix 44 and 45 (Datta et al., 2007).

Connecting Text

The previous chapter identified the role of YjeQ in the context of the mature 30S subunit by solving the structure of the 30S subunit in complex with YjeQ using cryo-EM (Razi et al., 2017b). We found that in addition to work as a maturation factor, YjeQ also functions as a checkpoint protein testing the proofreading ability of the ribosomal subunit prior to the particle's release into the pool of actively translating ribosomes. This work provides the first example of a bacterial assembly factor that tests a specific translation mechanism of the 30S subunit.

In the present study, we investigated the role of Era, another important assembly factor contributing to the assembly of the 30S subunit through qMS, MST and cryo-EM techniques. We then tested whether YjeQ and Era, two assembly factors, exert their function in conjunction rather than independently.

Chapter 3: Role of Era in the Assembly of the 30S Subunit and Ribosome Homeostasis

Aida Razi[1], Joseph H. Davis[2,3], Dushyant Jahagirdar[1], Brett Thurlow[1], Kaustuv Basu[1], Nikhil Jain[4,5], Robert A. Britton[4,5], Javier Vargas[1], Alba Guarné[6], James R. Williamson[2,3] and Joaquin Ortega[1*]

To be submitted

[1]Department of Anatomy and Cell Biology, McGill University, Montreal, Quebec, Canada. [2]Department of Molecular Biology, [3]Department of Chemistry and The Skaggs Institute for Chemical Biology, The Scripps Research Institute, La Jolla, CA, USA. [4]Department of Molecular Virology and Microbiology, [5]Center for Metagenomics and Microbiome Research, Baylor College of Medicine, Houston, TX, USA. [6]Department of Biochemistry, McGill University, Montreal, Quebec, Canada.

3.1 Abstract

The assembly of the ribosomal subunit is one of the most fundamental processes in all living organisms. Although much is known about the function and structure of the ribosome, there is little information about the mechanistic contribution of the assembly process. Here, we used quantitative mass spectrometry (qMS), microscale thermophoresis (MST) and cryo-electron microscopy (cryo-EM) to reveal the function of Era, as an essential assembly factor. We characterized the 30S particles accumulated upon depletion of Era that converged to one intermediate. The 3.8Å resolution cryo-EM map defines the role of Era as a local chaperone that facilitates the maturation of the 30S subunit platform region. In addition, we solved the structure of the mature 30S subunit in complex with Era and in complex with Era and YjeQ. Our 4.2Å and 3.5Å structures disclose that binding of Era reverts back the structure of the mature 30S subunit to an immature state, which can no longer be bound by YjeQ. These results define the timeline for Era and YjeQ in the assembly process of the 30S subunit. Era binds first to the immature 30S subunit and facilitates the folding of helices 23 and 24 in the platform. Once Era is released, YjeQ binds, assisting the maturation of the decoding center and testing the fidelity of the subunit before releasing it to the pool of fully active ribosomes.

3.2 Introduction

The ribosome is the enzyme responsible for protein synthesis in all cells. In *Escherichia coli* the ribosome is made from more than 50 different components organized into the small (30S) and large (50S) ribosomal subunits. Our understanding of how the components of the bacterial ribosome come together is still limited. In spite of its complexity, each bacterial cell assembles more than 20,000 ribosomes in less than 30 minutes (Connolly and Culver, 2009; Shajani et al., 2011; Sykes and Williamson, 2009). Cells are able to maintain this assembly rate because a number of auxiliary factors make the process extremely efficient. The focus of this study is in one of this assembly factors, the Era protein.

Era is an essential protein for cell survival. This protein has been implicated in carbon metabolism, cell cycle regulation (Britton et al., 1998; Gollop and March, 1991a) and ribosome biogenesis (Sayed et al., 1999). It is composed of two domains: a N-terminal GTPase domain, which has a role in GTP hydrolysis and a C-terminal KH domain, which is responsible for RNA binding. These two domains are connected through a flexible linker of 17 amino acids long. The GTP binding domain is composed of a six-stranded β-sheet flanked by five helices. The RNA binding domain consists of a three-stranded β-sheet and three helices. Previous studies demonstrate that Era binds to the helix 45 at the 3' end of the 16S rRNA in the 30S subunit (Sharma et al., 2005; Stewart et al., 2009).

Crystallography studies with purified Era and RNA fragments representing the 3' end of the 16S rRNA have revealed that the two domains of Era can adopt two distinct topologies: the so called ‘closed’ and ‘open’ conformations. In the absence of nucleotide or when Era is bound to GDP, the domains adopt the open conformation in which the nucleotide binding site is accessible but the RNA binding site in the KH domain is occluded. Binding of GTP drives the

Era conformation from open to close restricting access to the nucleotide binding site and unveiling the RNA binding motif (Chen et al., 1999; Ji, 2016; Tu et al., 2009). Subsequent binding of an RNA fragment representing the 3' end of the 16S rRNA (Tu et al., 2009) stimulates GTP hydrolysis and causes the reversal of the conformation to an open state with the occlusion of the RNA-binding site and thus the release of Era from the rRNA.

Most likely the functional cycle of Era in the presence of complete 30S subunits occurs differently than what can be inferred from the crystal structures containing only isolated fragments of rRNA. Biochemical studies have shown that the binding affinity of Era to fully assembled 30S subunits decreases in the presence of either GTP or GDP, but not GDPNP (Sayed et al., 1999; Thurlow et al., 2016a). Furthermore, a low resolution cryo-EM structure shows that neither the open nor closed conformations displayed by the crystal structures are compatible with the cleft region between the head and platform where Era binds to the mature 30S subunit (Sharma et al., 2005).

However, there is a contradiction to this model, which is proposed by another group. They demonstrate via sucrose gradient ultracentrifugation followed by western blot analysis that Era in the presence of GTP and GDP is unable to bind to the 30S subunit (Sayed et al., 1999) and binding of Era to the rRNA is possible only in the presence of GMPPNP. In this study, the fully assembled 30S subunits was used to test the binding of Era versus the fragment of rRNA used in the first study.

Moreover, genetic, biochemical and structural studies suggest that there is a functional interplay between Era and other assembly factors. Genetic studies demonstrated that overexpression of Era suppresses the slow growth phenotype caused by deletion of *rbfA* (Inoue et al., 2003) or *yjeQ* (Campbell and Brown, 2008). In addition, the overexpression of RbfA

suppresses the slow growth of Δ*rimM* strain (Bylund et al., 1998). Also, it was shown biochemically that YjeQ is able to release RbfA from the mature 30S subunit (Goto et al., 2011) (Jeganathan et al., 2015). In addition, Cryo-electron microscopy (cryo-EM) revealed that at least three of these factors (YjeQ, RbfA and Era) bind at or in close proximity to the decoding center at non-overlapping sites, indicating that simultaneous binding is stereochemically possible (Datta et al., 2007; Guo et al., 2011; Jomaa et al., 2011c; Leong et al., 2013; Sharma et al., 2005).

These findings suggest that Era has a role in the maturation of the 30S subunit and it may perform its function in conjugation with other assembly factors. However, there is little information on the precise role of Era in the maturation of the 30S subunit and its functional interplay with other factors. To study how a biological system works, others have used deletion or depletion of a key factor from that system to observe consequences and understand the role of that factor. A few groups (Stokes et al., 2015) have attempted with limited success to use small inhibitory compounds to perturb the bacterial ribosome maturation process. However, a well-established method for studying ribosome biogenesis has been using assembly factor knockout or depletion bacterial strains that disrupt the maturation pathway and cause an accumulation of *in vivo* assembled precursors. This method has been used in the past to study the immature 30S particles accumulating in Δ*yjeQ*, Δ*rimM* and Δ*yjeQ*Δ*rbfA* bacterial strains and has proven to be a powerful tool for investigating the late stages of 30S assembly (Guo et al., 2013; Jomaa et al., 2011a; Leong et al., 2013; Yang et al., 2014). For instance, cryo-EM structures of an immature ribosome particles from *yjeQ* null strains have revealed a distortion at the decoding center. This suggests the possible role of the YjeQ protein in the maturation of the functional core of the 30S subunit.

Here, we are using a similar approach to gain initial insights into the function of Era in the maturation of the 30S subunit. We are elucidating the role of Era by depleting this factor from *E. coli* cells. We used a multidisciplinary approach comprising genetics, biochemistry, quantitative mass spectroscopy (qMS) and structural biology to analyze the intermediates that accumulate upon depletion of Era. Our biochemical and structural analysis of these ribosomal particles ($30S_{Era\text{-}depleted}$) indicated the assembly intermediate that accumulates in the Era-depletion strain is at the late stages of maturation. More specifically, our 3.8Å structure of the 30S particles accumulating in the Era depleted strain showed missing density for rRNA helices 23 and 24, located at the central domain. Also, critical helices involved in mRNA decoding, helix 44 and helix 45, are not properly folded in, and several tertiary r-proteins had missing density in the accumulated intermediates. These findings reveal the possible role of Era as a local chaperon that facilitates the proper folding of RNA motifs at the platform and decoding center of the 30S subunit.

In addition, we investigated the possibility that Era may exert its function in conjunction with YjeQ, rather than independently. To this end, we obtained the cryo-EM structure of 30S in complex with Era and YjeQ, in addition obtaining the structure of the 30S subunit in complex with Era as a control. In summary, we obtained two subpopulations from the 30S subunit in complex with Era and YjeQ at 3.5Å and 4Å. One class revealed the structure of the immature 30S subunit bound with Era. In this class, the density for the helices on the decoding center of the 30S subunit were missing. These data suggest that Era binds to immature 30S subunit and causes conformational changes at the association site of the 30S subunit to the 50S subunit that prevents binding of premature 30S subunit to the 50S subunit. Also, YjeQ cannot recognize this immature state of the 30S subunit. The other class demonstrates the mature 30S subunit without any factor bound. Structural analysis of the 30S subunit in the presence of Era demonstrated two

classes at two different stages of maturation (subclass I and subclass II). Subclass I represents the immature 30S subunit with no density correspond to the 3' minor domain of the 30S subunit (helix 44 and helix 45). Subclass II represents similar distortion at the 3' minor domain of the 3S subunit. However, helix 44 starts to fold and thus represents particles at the later stage of maturation compare to subclass I. We could not capture any density for Era in subclass I and II.

Using these data, we propose a model and a timeline for how Era assists in maturation of the 30S subunit. Era first binds to the immature 30S subunit and facilitates the maturation and folding of rRNA, and binding of r-proteins at the platform and decoding center of the 30S subunit. Subsequently, it triggers its own release from the mature 30S subunit. At the last stage, YjeQ bind to the mature 30S subunit and tests the fidelity of the ribosome.

3.3 Materials and Methods

3.3.1 Cell strains and protein overexpression clones

The parental *E. coli* K-12 (BW25113) strain was obtained from the Keio collection, a set of *E. coli* K-12 in-frame, single gene knockout mutants (Baba et al., 2006).

The pET15b-*era* plasmids used for overexpression of Era were produced as previously described (Thurlow et al., 2016a).

3.3.2 Protein overexpression and purification

Overexpression and purification of Era (Thurlow et al., 2016a) and YjeQ (Razi et al., 2017b) proteins was done as previously described.

3.3.3 Purification of 30S ribosomal subunits and Era depleted 30S subunits

Purification of 30S ribosomal subunits (Razi et al., 2017b) and Era depleted 30S subunits (Thurlow, 2016) was done as previously described.

3.3.4 Strain growth experiments

Obtaining the growth curves for the parental and Era-depleted strains was done as previously described (Thurlow, 2016).

Dilution plating experiments were performed by inoculating 0.5 mL of a saturated overnight culture in 50 mL of fresh LB media. Cultures were grown at 37°C with shaking until an OD_{600} of 0.2. Then, serial dilutions were made in 10-fold increments, and 5 µL of each dilution was immediately spotted onto LB agar plates and incubated at 37°C. The plates were incubated until isolated colonies of the parental strain reached 2 mm in diameter.

3.3.5 Preparation of cell lysates for quantitative mass spectrometry

Cultures (40 mL) with the parental and Era-depleted strain for mass spectrometry analysis were prepared as described in the previous section. Cells were harvested by centrifugation at 3,300*g* for 15 min and the cell pellet was washed in buffer QPA (10 mM Tris-HCl, pH 7.5, 10.5 mM $MgCl_2$, 60 mM KCl). Cell pellets were resuspended in 6 mL lysis buffer (10 mM Tris-HCl, pH 7.5, 10.5 mM $MgCl_2$, 60 mM KCl, 0.5% Tween 20 (v/v) and 1 mM dithiothreitol (DTT)) with the addition of cOmplete™ Mini protease inhibitor cocktail and DNaseI (Roche). Cell lysis was performed by passing the suspension through a French pressure cell at 1400 kg/cm^2 three consecutive times. Cellular debris was clarified by spinning the lysate at 27,700*g* for 20 min. Recovered supernatant was loaded into an Amicon Ultra 10 kDa MWCO filter (Millipore) and spun at 3,400*g* for 25 min to concentrate the volume to ~ 1 ml.

The sample pellet was resuspended in 1mL of 8M urea, following with 10 times sonication. Then the sample was clarified for 11 minutes, at 20,000 rmp using MLA130. The supernatant was sent for qMS.

3.3.6 Sample preparation for qMS analysis

3.3.6.1 Generation of 15N-labeled isotopic spikes

Whole cell lysates spikes were generated by growing strain JD0189 (*E. coli* NCM3722(Brown and Jun, 2015)) to OD 0.4 in ^{15}N-labeled minimal media at 37 C as described previously (Davis et al., 2015). Cells were pelleted and resuspended in 50 mM Tris, 100 mM NH4Cl, 10 mM MgCl2 pH 7.8 to a concentration of 3.0 OD600 units/mL, which corresponds to ~0.05 μM ribosomes, assuming 5e8 cells/OD600/mL; 20,000 ribosomes/cell.

^{15}N-labeled 70S particles spikes were generated by growing strain JD0189 to OD 0.7 in 15N-labeleled media as described above. Cells were lysed, and 70S particles were purified on a

10%-40% sucrose gradient as described (Davis et al., 2015), and fractions bearing monosomes or polysomes were pooled and saved at -80C at 0.055 μM.

3.3.6.2 Generation of tryptic peptides

Particles were isolated from a sucrose gradient and concentrated to 0.5 μM. To each sample (10 pmols), an equimolar 15N-labeled spike sample (either purified ribosomal particles or lysate bearing ~10 pmols of ribosomes) was added and mixed, and TCA was added to 13% final concentration. After overnight precipitation at 4 C, pellets were sequentially washed with 10% TCA, 100% Acetone and were dried before they were resuspended in 40 μL buffer B (100 mM NH4CO3, 5% acetonitrile, 5 mM dithiothreitol) as described(Jomaa et al., 2013). After reduction for 10 minutes at 65 C, cysteines were alkylated by addition of iodoacetamide to 10 mM and incubation at 30 C for 30 mins. 0.2 μg trypsin was then added and protein digestion proceeded at 37 C overnight. Tryptic peptides were purified on C18 PepClean columns, and ~1 μg of peptides were mixed with 500 fmol iRT retention time standards (Pierce) and injected onto the LC/MS.

3.3.6.3 Quantitative mass spectrometry

Peptides were trapped on a ChomXP C18 cHiPLC column (Sciex) and resolved on a 15 cm ChromXP C18 cHiPLC analytical column using a 120 minute 5-35% linear acetonitrile gradient with a flowrate of 300 nL/min. Data was acquired in replicate with either data-dependent acquisitions or in SWATH data-independent acquisition (DIA) mode. Briefly, data-dependent acquisitions included one MS1 scan (200 msec accumulation time) followed by 30 MS2 scans (100 msec accumulation time). The SWATH DIA method consisted of one MS1 scan (200 msec accumulation time) followed by 32 MS2 scans (25 m/z wide, 100 msec accumulation time) covering the range 400-1200.

3.3.6.4: Ribosomal protein abundance analysis

DDA datasets were searched with comet (Eng et al., 2013), peptide-spectra matches (PSM) were scored with PeptideProphet (Deutsch et al., 2010), and scored PSMs were combined with iProphet (Keller and Shteynberg, 2011). A consensus spectral library was generated using Spectrast. Using this spectral library, a target list bearing ^{14}N- and ^{15}N-labeled precursor (Lam et al., 2007) and product ions corresponding to ribosomal proteins of interest was generated using Skyline (Escher et al., 2012), and ion chromatograms were extracted in regions of the chromatogram near the predicted elution time as determined using the iRT standards (Escher et al., 2012). Extracted ion chromatograms were filtered for interfering ions at both the MS1 and MS2 level, and relative peptide abundance was calculated as ^{14}N_total_area/^{15}N_total_area. For each sample and for each protein, the median peptide abundance ratio was then calculated and these values were clustered across both samples and proteins using the ward linkage method and the Euclidean distance metric (Sturn et al., 2002).

Non-ribosomal proteins were analyzed as described using a spectral library focused on assembly co-factors (Davis, Williamson Manuscript in preparation, (Davis et al., 2016)).

3.3.7 Microscale Thermophoresis

Mature 30S subunits were fluorescently labeled as previous mentioned in (Thurlow et al., 2016a). Prior to each MST experiment, all samples were centrifuged at 14000g for 10 min to remove any aggregates. Further, all reaction and titrations series were prepared in MST buffer (20 mM Tris–HCl pH 7.5, 150 mM NaCl, 10 mM MgCl2, 1 mM DTT, 0.05% Tween-20, 0.4 mg/ml BSA) and were incubated in in 0.5 ml Protein LoBind eppendorf tubes. 0.5 μM fluorescently labeled mature 30S subunits were incubated with 5 μM and 10 μM Era separately in presence of 1mM GMP-PNP and incubated for 15 minutes at room temperature. A 1:1 serial dilution of non-labelled YjeQ was then prepared in MST buffer starting at 4 μM. The 30S+Era

reaction mixture was then diluted in such that the concentration of 30S subunit was 40nM and was additionally supplemented 1mM GMP-PNP. Ten microliters of the serial dilution of the non-labeled assembly factor was mixed with 10 µl of the fluorescently labeled 30S subunit pre-bound with Era and these titration reactions were incubated for 10 min at room temperature. Mixed samples were then loaded into premium glass capillaries (NanoTemper Technologies) and MST analysis was performed using the Monolith NT.115 MST instrument (NanoTemper Technologies) at ambient temperature. Using the MO Control software an LED power of 100% and high MST power were used. The resulting binding curves were obtained by plotting the normalized fluorescence (Fnorm (‰) = F1/F0) versus the logarithm of assembly factor concentrations. Kds were calculated using the NanoTemper MO Affinity Analysis software. Experiments were performed in triplicate.

3.3.8 Cryo-electron microscopy

The entire data set of images was collected in one cryo-EM session. The $30S_{Era\text{-}depleted}$ sample and the assembly of the 30S+Era and 30S+Era+YjeQ were setup in 20 ml reactions containing assembly buffer (10 mM Tris–HCl at pH 7.5, 10 mM magnesium acetate, 150 mM NH_4Cl, 3mM 2-mercaptoethanol and 2 mM GMP-PNP). The concentration of the $30S_{Era\text{-}depleted}$ and 30S subunits in the assembly reactions for all samples was always maintained at 1mM. The concentration of YjeQ and Era was 3 mM and 20mM respectively. The assembly reaction was incubated for 30 min at 37 ºC and then diluted in the same buffer between 10 to 20 times before the reaction was applied to the grid. Using these assembly and dilution conditions depending on the cryo-EM session the concentration of $30S_{Era\text{-}depleted}$ and 30S subunits in the sample applied to the grid ranged from 50 nM to 100 nM and for YjeQ and Era, 350 nM and 4 µM, respectively. Approximately 4 µl of the diluted sample was applied in the holey carbon grids (c-flat CF-2/2-2C-T) with an additional layer of continuous thin carbon (5-10nm), except for the 30S subunit in

complex with Era and YjeQ, which was done without any extra layer of the carbon.

C-Flat holey carbon-coated TEM support grids (C-Flat R2/2, Protochips, Morrisville, NC USA) were glow discharged using the EMS 100 glow discharge system at 15 mA for 15 seconds (Electron Microscopy Sciences, Hatfield, PA USA). A three µl drop of sample was applied to the grid, blotted and frozen in liquid ethane using the Vitrobot Mark IV automated grid plunging system (Thermo Fisher Scientific, Hillsboro, OR USA).

Movies were obtained at 75kx nominal magnification with the Falcon II direct electron detector on the FEI Titan Krios cryo-TEM (Thermo Fisher Scientific, Hillsboro, OR USA) operated at an accelerating voltage of 300 kV, using a total dose of 45 electrons/Å^2 and seven frames (calculated pixel size of 1.073 Å/pixel). The defocus range was between −1.25 and −2.75 µm.

3.3.9 Image processing

The motion of the individual particles in the frames was tracked and corrected using UCSF motioncor2. Then these particles were used for determination of the contrast transfer function (CTF) parameters with Gctf. Then micrographs with resolution better than 4Å were selected using phyton. The initial dataset from the grids containing $30S_{Era\text{-}depleted}$, 30S+Era and 30S+Era+YjeQ mixture after particle extraction contained 908,772, 1,826,243 and 1,015,287 particles respectively (‘dirty’ dataset). These images were subjected to 2D and 3D classification (Class3D 1st iteration), which resulted in a ‘clean’ dataset comprised of 511247, 444,879 and 696,802 particles. The ‘clean’ dataset was run through a second cycle of 3D classification (Class3D 2nd iteration) using the entire signal in the particle images. This classification produced one 3D class representing the $30S_{Era\text{-}depleted}$. For 30S+Era and 30S+Era+YjeQ complex, Class3D produced two classes (Subclass I and Subclass II). Each class was separately refined using a binary mask with a soft edge. This approach produced the best map for all three structures.

In a parallel approach, the ‘clean’ dataset was subjected to focused classification with subtraction of the residual signal using Relion (Scheres, 2012) following an approach previously described (Bai et al., 2015a, b). To this end, we applied a low pass filter to the atomic model of the 30S (PDB 2AVY) (Guo et al., 2011) after we remove the head domain and lower part of the body. This procedure produced a density map that was used to create a soft-edge mask for the focused classification and also for the signal subtraction in the experimental particles. The newly created stacks of particles after signal subtraction and the mask were used as input for the focused classification run. During the classification step, we kept all orientations fixed at the values determined in the refinement of the consensus maps. The classification produced two distinct classes in 30S Era depleted particles that were refined independently using a binary mask with a soft edge. One of the classes represented the 30S particles from the Era depleted strain at an early stage of maturation. The other class represented the immature 30S subunit at the later stage of maturation.

3.4 Results

3.4.1 The Era depleted strains exhibit a slow-growth phenotype and altered ribosome profile

Era depleted *E. coli* strain was previously generated in our laboratory (Thurlow et al., 2016a). Briefly, an *era* gene was inserted into the bacterial chromosome under the control of the *araBAD* promoter. Subsequently, the endogenous *era* gene was replaced with an apramycin cassette.

The growth conditions for Era-depleted strain in liquid LB media were previously characterized in our laboratory at 37°C and 15 °C (Thurlow, 2016). In the presence of arabinose at 37°C, a slow growth phenotype was observed with the growth curve exhibiting an extended lag phase and reaching saturation at a lower optical density compared to the parental strain. In the absence of arabinose, the growth was severely reduced unlike the parental strain.

Similar analysis of growth phenotype at 15°C in the presence and absence of arabinose demonstrated complete inhibition of growth in the absence of the inducer. Thus, the Era depleted strain exhibits cold sensitive phenotype, a well-known hallmark of ribosome assembly defects in bacteria (Connolly and Culver, 2009; Stokes et al., 2014).

To determine whether this phenotype holds true for the Era-depleted strain on a solid LB media, we compared the growth of the Era depleted and parental strains at 37°C. The slow growth phenotype of the Era depleted strain in the presence of arabinose was also evident (Figure 3.1). As expected, in absence of arabinose, no growth was observed for the Era depleted strain. However, the parental strain grew normally in the presence and absence of arabinose.

Previous works from our lab and different groups have shown that ribosome assembly in wild type bacterial cells is extremely efficient and assembly intermediates do not accumulate (Lindahl, 1975). Therefore, the majority of 30S and 50S subunits are associated to form 70S ribosomes with just few free 30S and 50S subunits. However, the Era depleted strain exhibited

accumulation of free 30S and 50S subunits under depletion conditions (Thurlow, 2016). In the Era-depleted strains, 67% of the 30S particles were not associated with 50S subunits, whereas in wild type cells only 18% of the 30S subunits were not bound to the 50S subunits (Thurlow, 2016).

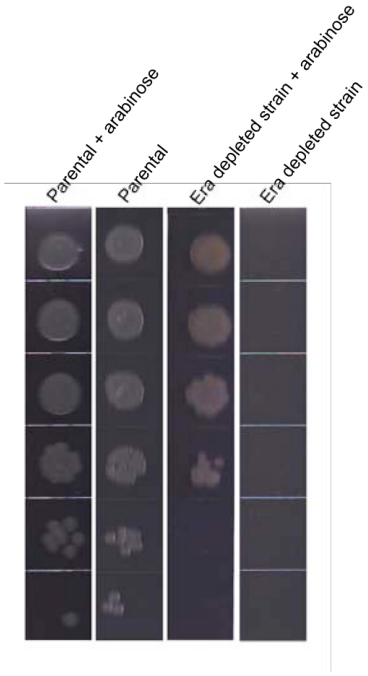

Figure 3.1: Characterization of Era-depleted strain. Dilution plating experiment of saturated cultures of parental and Era-depleted strain in solid media. Cultures were diluted in 10-fold increments, spotted on LB agar plates, and incubated at 37 ºC. The profiles for the parental and the Era-depleted strains grown in the presence of 1% arabinose (+ arabinose) and in the absence of arabinose are shown.

3.4.2 Immature 30S subunits with incomplete protein complement accumulate in the Era depleted strain

Next, we used Quantitative Mass Spectrometry (qMS) to determine the protein complement of the immature ribosomal particles that accumulate in the Era depletion strain. In this technique, ribosomal particles from the Era depleted cells were fractionated and purified on a sucrose gradient first. The purified particles were then spiked with ^{15}N-labeled 70S ribosomes. Samples were then digested with trypsin and peptide abundances were analyzed by qMS using a

targeted multiple reaction monitoring (MRM-HR) approach (Davis et al., 2016). To determine the reproducibility of our measurements, the immature subunits were analyzed in duplicate.

This analysis revealed that $30S_{Era\text{-}depleted}$ particles were depleted of the r-proteins bS21, bS1, uS5, uS3 and uS2. These effects are the strongest on bS1, uS2 and bS21, with milder effects on uS3 and uS5 (Figure 3.2A). The Nomura assembly map (Nomura et al., 1969) establishes that the r-proteins bind to the 16S rRNA in a hierarchical manner. According to the assembly map, the depleted r-proteins enter the assembling ribosomal particle at the late stage of maturation. Therefore, these data suggest Era depleted particles represent the late stages of maturation of the 30S subunit.

Given the low occupancy levels of bS1, uS2 and bS21 in the 30S particles, we analyzed their abundance in the cell. To this end, we grew wild type and $30S_{Era\text{-}depleted}$ strains in ^{14}N-labeled media under Era depletion conditions. We then spiked these cell lysates with ^{15}N-labeled cell lysate and measured the whole cell protein levels using qMS (Figure 3.2B). We observed subtle depletion of bS21 and bS1 and partial depletion of uS5 and uS19. In addition, we observed overexpression of uS3, uS12, bS18 and bS20 proteins, and also overexpression of uS4, uS7, uS9, uS11 and uS14 to a lesser extent. There was also a more subtle effect on the level of the 50S subunit r-proteins. Our results demonstrated the overexpression of bL28, uL13 and uL2 at a greater extent and less extent in uL14, uL18, uL22 and bL35, and underrepresentation of uL6, uL10, uL11 and uL29. Furthermore, our analysis of 70 particles spiked with 70S indicated the normal level of the r-proteins in the fully assembled ribosomes (Figure 3.2C).

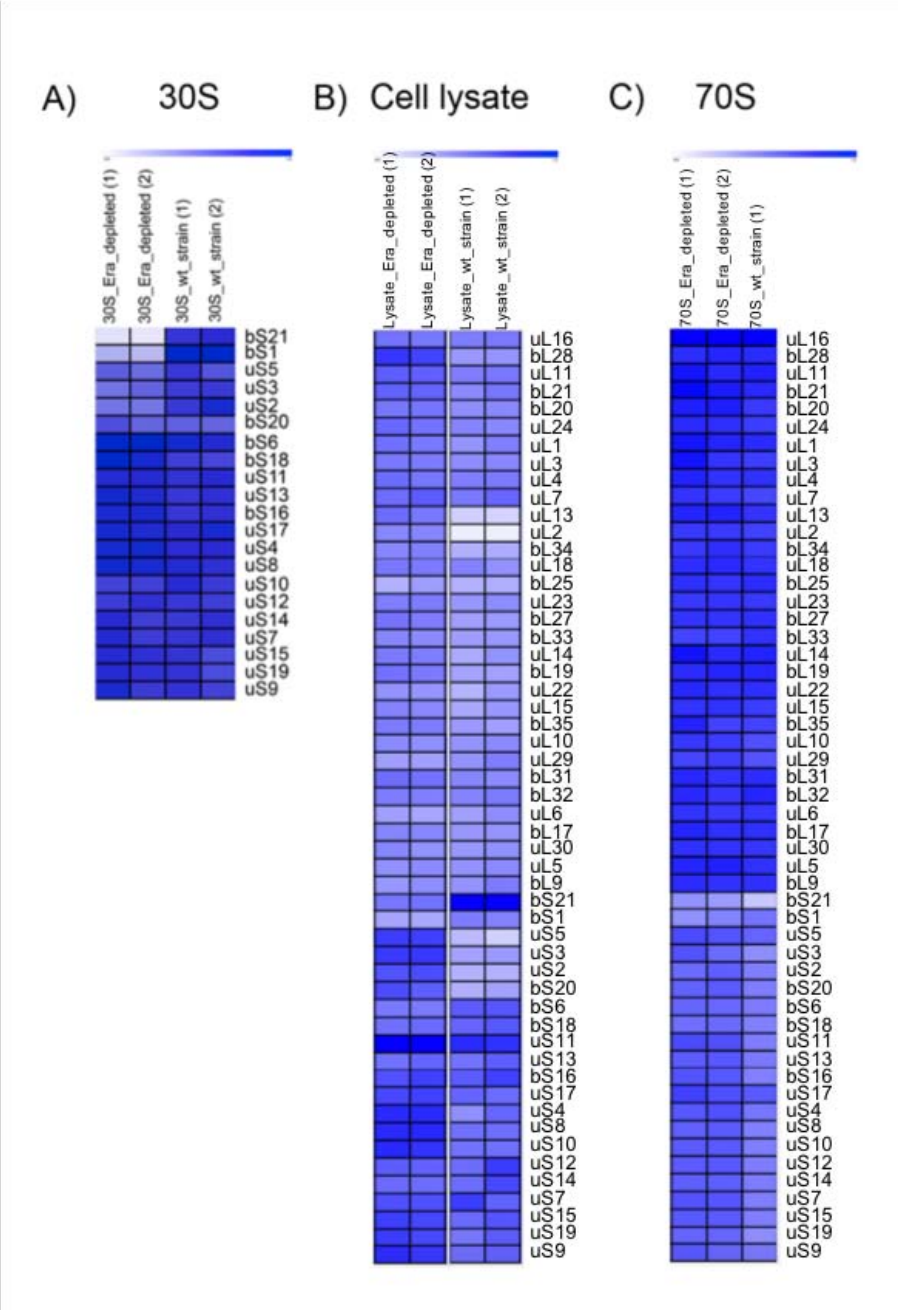

Figure 3.2: Ribosomal protein occupancy in ribosomal particles and cell lysates measured by qMS. Protein abundance is calculated as the $^{14}N/^{15}N$ ratio for each protein. Each sample was done in replicates indicated with (1) and (2). Occupancy from 0 to 1 scales from white to blue. A) Ribosomal proteins occupancy of the 30S subunits purified from Era depleted and parental strains. B) ^{14}N-labeled whole cell lysates were spiked with ^{15}N-labeled 70S particles. $^{14}N/^{15}N$ relative abundance calculated from extracted ion chromatograms is normalized to that of protein uS4 and, to highlight strain specific differences, finally normalized relative to the wild-type lysate, C) Ribosomal proteins occupancy of the r-proteins in 70S ribosomes purified from Era depleted and parental strains.

3.4.3 Structural analysis of the $30S_{Era\text{-}depleted}$ particle accumulating in the Era depleted strain assembly suggests the role of Era as a local organizer

We subjected the intermediate that accumulates upon depletion of Era to cryo-EM analysis. Image classification revealed one large subpopulation, which corresponds to premature 30S subunits at the late stage of maturation. We refined this structure to 3.8Å resolution, which enabled the unambiguous assignment of all the rRNA helices and r-proteins in this immature 30S particle.

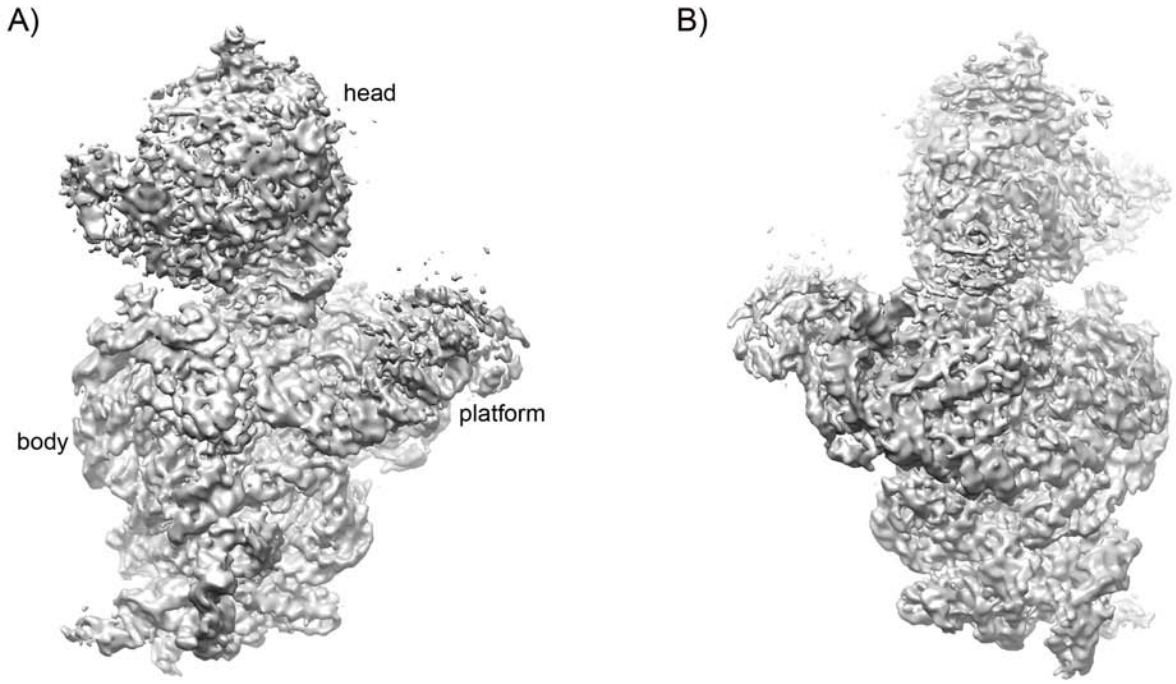

Figure 3.3: Cryo-EM structure of the Era-depleted 30S particles. This data revealed there is one intermediate class that accumulated upon depletion of Era. A) front and (B) back views of the cryo-EM map of the $30S_{Era\text{-}depleted}$ particles. Important landmarks of the 30S subunit are indicated.

The local resolution analysis allows us to see how the resolution varies in different areas

of the structure. The local resolution map indicated that the core region of the particle reached 3.5Å resolution, while the head and region at the decoding center and platform are less resolved due to flexibility and/or incomplete assembly in these regions (Figure 3.4). In addition, the solvent side of the 30S subunit demonstrates well-defined density, and most of the domains in the interface side are also folded. Remarkably, the body of the particle is predominately mature and closely resembles the fully assembled 30S subunit. It is clear that this immature particle has most of the domains already folded, indicating it is a late assembly intermediate.

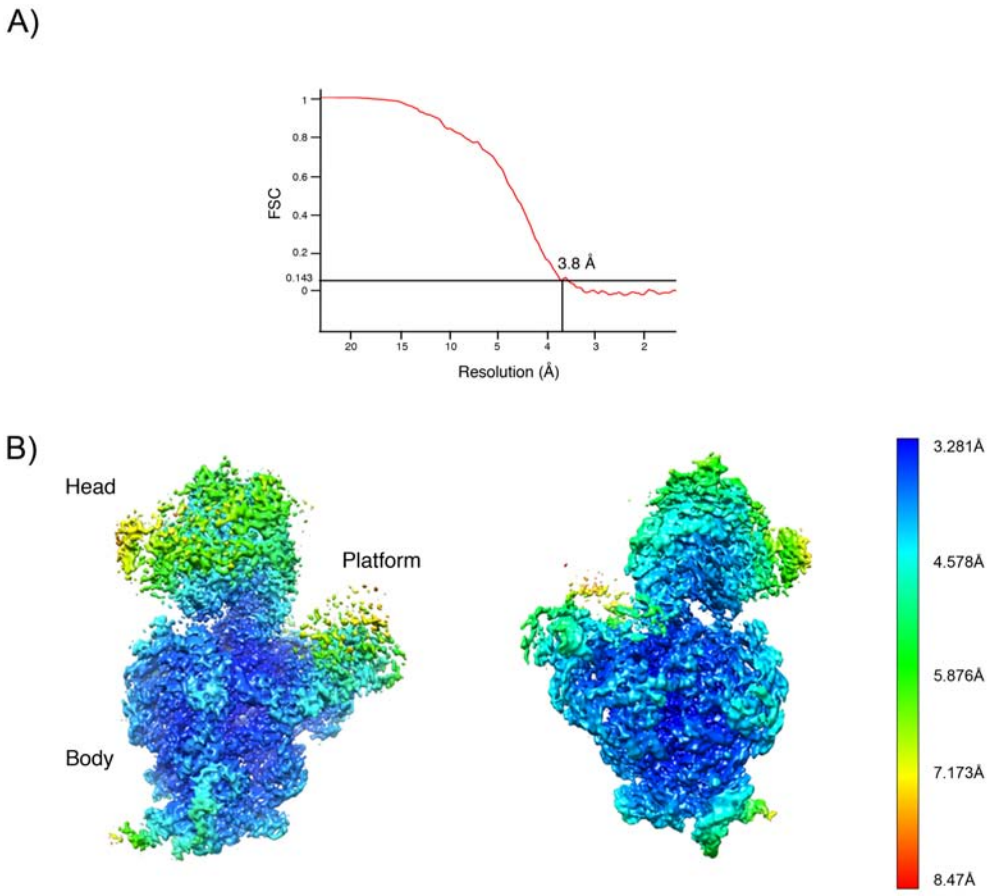

Figure 3.4: Resolution analysis of the 30S Era-depleted structure. A) Fourier Shell Correlation (FSC) plot for the $30S_{Era\text{-}depleted}$ particles structure, B) Local resolution analysis of the $30S_{Era\text{-}depleted}$ structure performed with relion.

However, comparison of this major class with the structure of the mature 30S subunit demonstrated missing density at the decoding center and platform of the 30S subunit. More specifically, the 5' and 3' major domain of rRNA showed the same structure as the mature 30S subunit. However, the central domain contained missing density for helix 23 and helix 24 at the platform. In addition, the 3' minor domain had missing density for helix 44 and helix 45 at the decoding center (Figure 3.5A).

Analysis of r-proteins reveals that the map exhibits clear density for all primary and secondary proteins. However, further analysis of tertiary r-proteins revealed that uS7 (Figure 3.5A, right panel), which is anchored from the head and uS11 anchored from the decoding center are missing. Moreover, analysis of the 30S subunit solvent side revealed partial or broken density for the r-proteins uS2, uS3, and bS21 (Figure 3.5B), consistent with qMS (Figure 3.2).

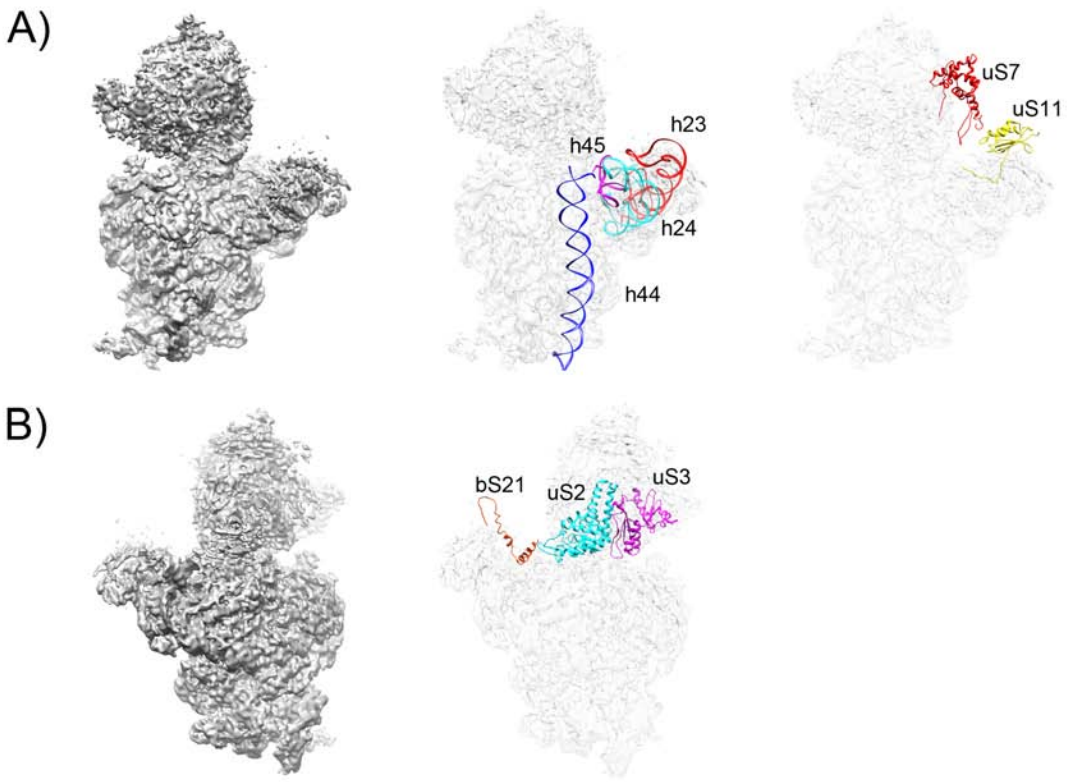

Figure 3.5: Structural analysis of the Era-depleted particles highlighting differences with the mature 30S subunit. A) Front view of the surface rendering representation of the cryo-EM map of the $30S_{Era\text{-}depleted}$ particles (left panel). Middle and right panels display a shadow of the same view of the same cryo-EM map, over layered with specific structural elements from the atomic model of the 30S subunit (PDB ID 2AVY.pdb) that were missing in the $30S_{Era\text{-}depleted}$ particles. These motifs included helices 23 (red), 24(cyan), 44 (dark blue) and 45(magenta) of the 16S rRNA and r-proteins uS7 (red color) and uS11 (yellow color), B) Back view of the surface rendering representation of the cryo-EM map of the $30S_{Era\text{-}depleted}$ particles (left panel). Middle panel displays a shadow of the same view of the same cryo-EM map, over layered with specific structural elements from the atomic model of the 30S subunit (PDB ID 2AVY.pdb) that were missing in the $30S_{Era\text{-}depleted}$ particles. These motifs included uS2 (cyan color), uS3 (purple color), and uS21 (orange color).

To further analyze the possibility of having more than one class with a different conformation or missing different density, we performed focused classification with signal subtraction on the platform domain of the immature particle. This focused classification approach resulted in two classes with structural flexibility within the platform. One of the classes revealed the particles at the earlier stage of maturation (class I) versus the other one representing

particles at a slightly later stage of maturation (class II) with more density at the central domain of the 30S subunit (Figure 3.6).

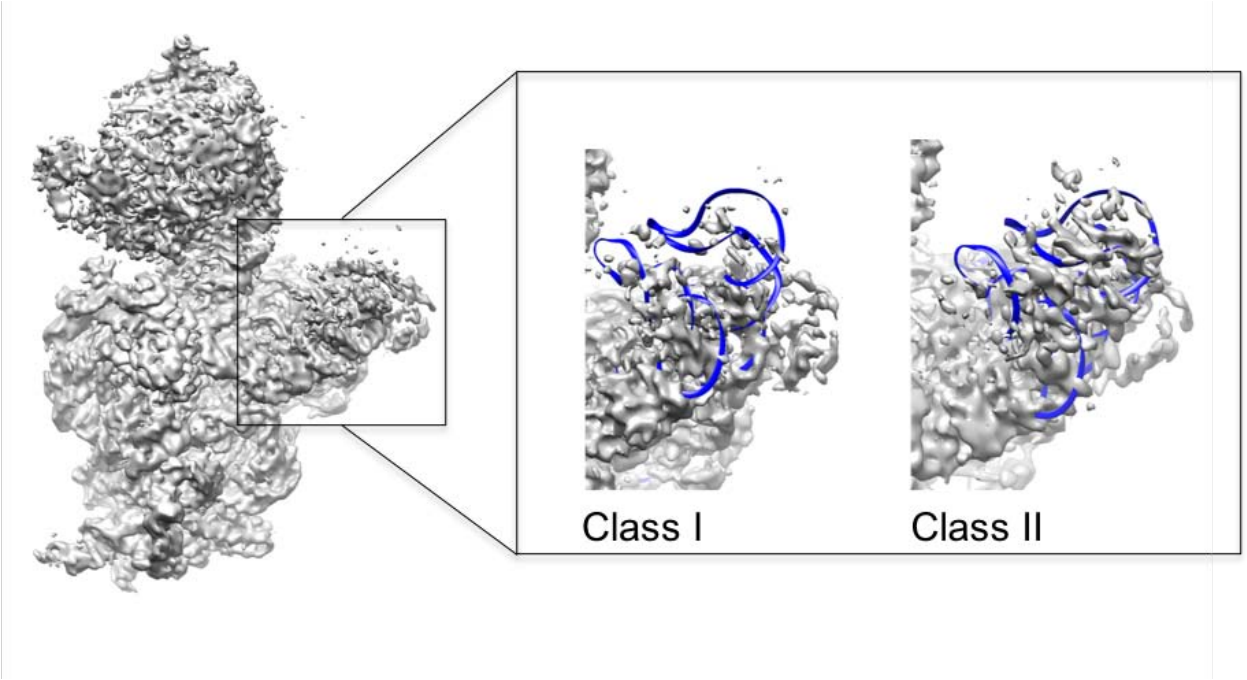

Figure 3.6: Structural details of the platform region of the Era depleted particles. Cryo-EM structures of the $30S_{Era\text{-}depleted}$ particles obtained from focused classification. Ribbon representation of the helix 23 and 24 were fitted to the cryo-EM maps. Class I and Class II differ in the amount of density present in these two rRNA helices. represents cryo-EM structure of the 30S Era depleted particles with less missing density in the platform.

These findings suggest that Era may have a role as a local chaperon to facilitate the proper folding of the platform region of the 30S subunit. In addition, Era may assist in recruiting a number of r-proteins located at the platform region of the 30S subunit.

3.4.4 Era binding rejuvenate the mature 30S subunit

One of the r-proteins, bS1, is essential in *E. coli* and is able to interact with both the ribosome and mRNA (Subramanian, 1983). The cryo-EM structure of the 30S subunit in the presence of bS1 reveals that it binds at the cavity between head and platform of the 30S subunit. This structure demonstrates that there is an interaction between bS1 and 11 nucleotides of the 5'

region of mRNA, upstream of the Shine-Dalgarno (SD) sequence (Sengupta et al., 2001). Also, crosslinking experiments of bS1 with RNA, positioned bS1 in the same region as observed by immunoelectron microscopy (Goelz and Steitz, 1977). Comparing the binding site of bS1 with the low resolution structure obtained previously from the complex of the 30S with Era, reveals that bS1 and Era have overlapping binding position. In addition, binding assays and MST experiments revealed that Era binds to the mature 30S subunit with an affinity of ~ 7.3μM (Thurlow et al., 2016a).

Thus, we used cryo-EM to identify the interactions between Era and the mature 30S subunit at atomic resolution. We obtained two major classes, subclass one (subclass I) at 4.2Å resolution, which represents 30S subunit in its immature state, with missing density at the 3' minor domain of the 30S subunit (Figure 3.7A). The other class that we obtained (subclass II) at 4.5Å resolution reveals 30S subunit in its more mature state compare to subclass I, since it demonstrates more density at the platform (Figure 3.7B). In subclass II, there is still a missing density at the decoding center. However, helix 44 in the 3' minor domain started to fold. However, we did not observe any density correspond to Era in the cavity between head and platform, which was observed in a previous study (Sharma et al., 2005). These findings suggest that Era rejuvenate the mature 30S subunit upon binding.

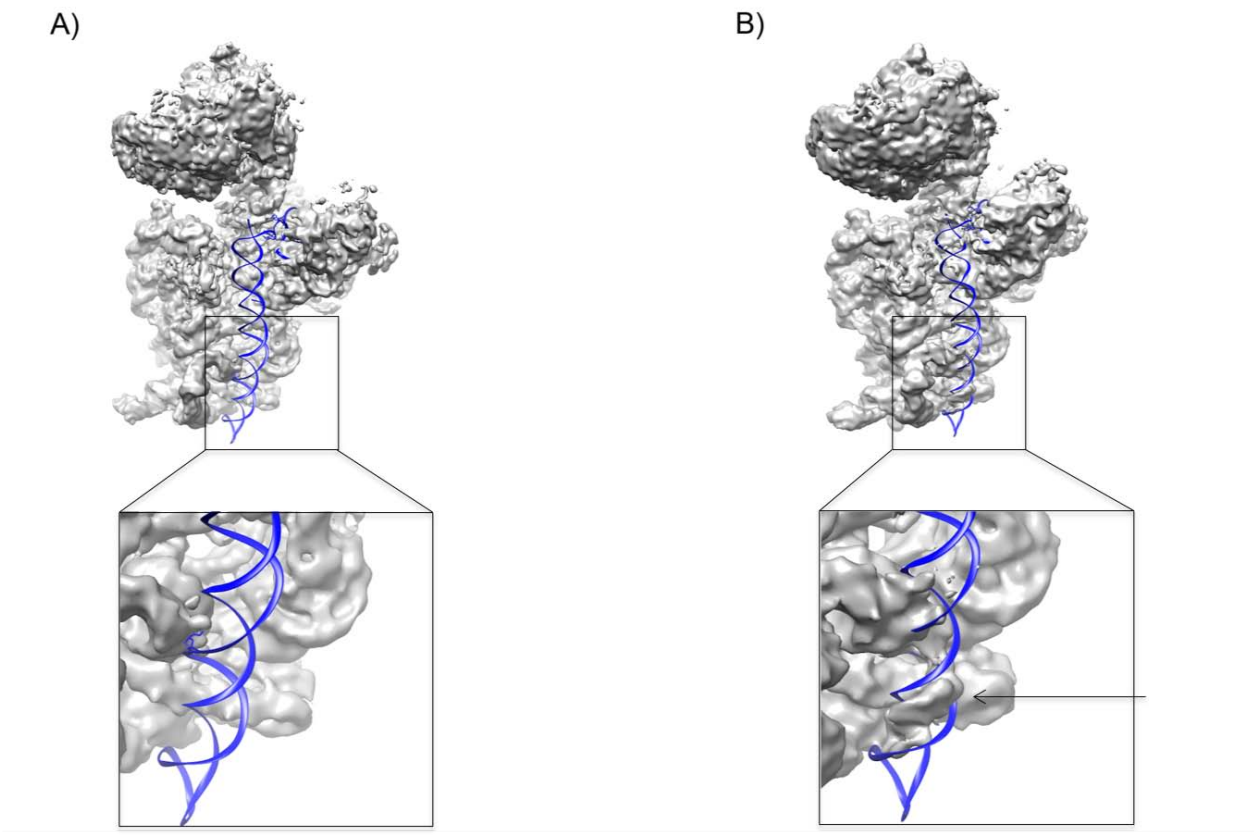

Figure 3.7: Cryo-EM structure of the 30S+Era particles. This data revealed there are two classes, A) the panel show the surface rendering representation of the cryo-EM map obtained for the 30S+Era complex (subclass I). Helix 44 from the atomic model of the 30S subunit (PDB ID 2AVY.pdb) was fitted into the cryo-EM map and is show in a ribbon representation, B) the panel show the surface rendering representation of the cryo-EM map obtained for the 30S+Era complex (subclass II). Helix 44 from the atomic model of the 30S subunit (PDB ID 2AVY.pdb) was fitted into the cryo-EM map and is show in a ribbon representation.

The local resolution analysis of the 30S+Era cryo-EM map indicated that in both subclasses I and II, the core region of the particle reached 3.7Å resolution, while the head and platform are less resolved due to flexibility in these regions (Figure 3.8).

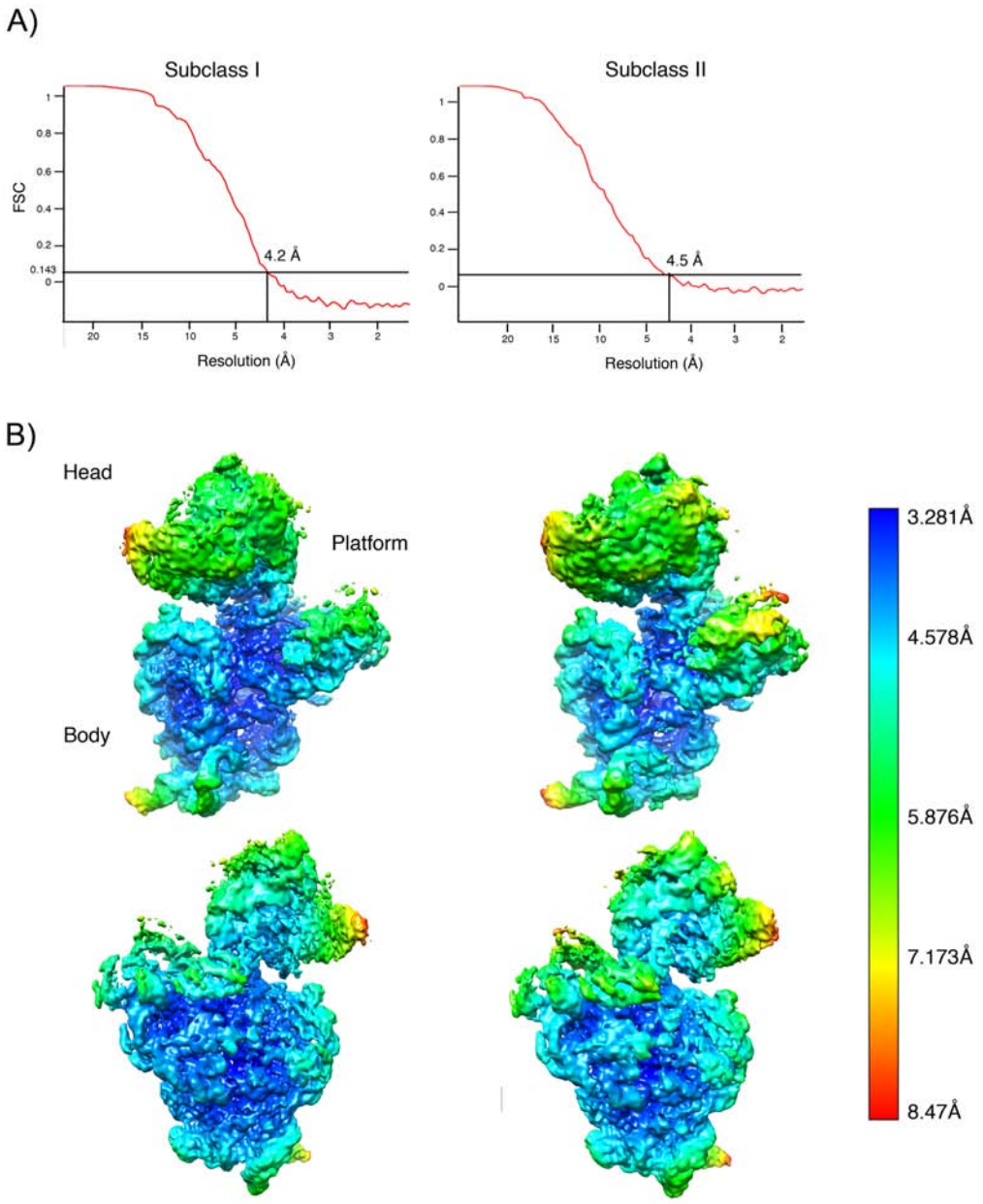

Figure 3.8: Resolution analysis of the 30S+Era cryo-EM map. A) This panel shows the Fourier Shell Correlation (FSC) plots for the subclass I and subclass II structures. B) Local resolution analysis of the two structures performed with relion.

3.4.5 Era induces a conformational change in the 30S subunit that prevents YjeQ from binding:

Comprehensive understanding of ribosome biogenesis requires detailed knowledge of the functional interplays that may exist amongst assembly factors. Work from our laboratory and other groups indicate that Era and YjeQ assist in the maturation of the functional core of the 30S

subunit (Leong et al., 2013; Sharma et al., 2005). In addition, genetic evidence demonstrates that overexpression of Era suppresses the slow growth of cells lacking YjeQ (Campbell and Brown, 2008). These findings suggest that both factors may be working in conjunction rather than independently. However, it is unknown how the functional interplay between Era and YjeQ is implemented. Therefore, to analyze the binding of Era and YjeQ to the mature 30S subunit, we used MST. Previously, the affinity of YjeQ to the mature 30S subunit was measured by MST and determined with the K_d value of 66nM (Thurlow et al., 2016a). MST experiments revealed that the K_d of YjeQ to the mature 30S subunit in the presence of GMPPNP and two different concentrations of Era, 10X and 20X are 1.24 μM ± 0.65 nM and 2.33 μM ± 1.21 μM respectively (Figure3.8).

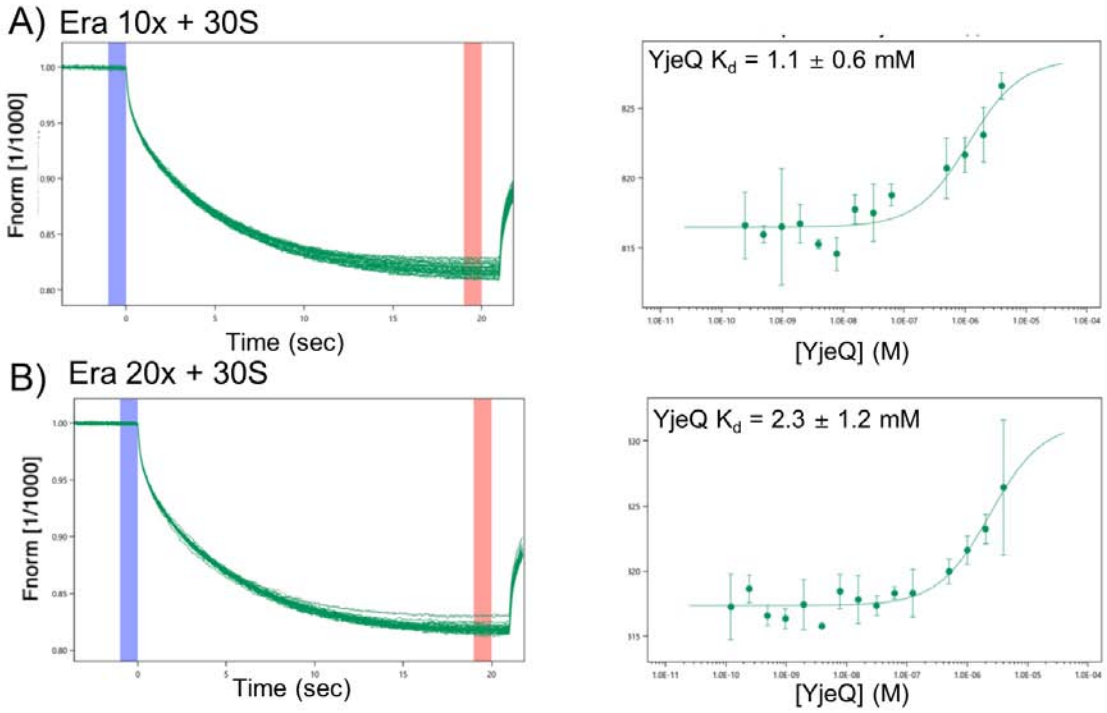

Figure 3.9: Binding of Era and YjeQ to the mature 30S subunit. Measurement of the binding affinity of YjeQ with the mature 30S ribosome subunit pre-incubated with 10-fold molar excess of Era (A) and mature 30S ribosome subunit pre-incubated with 20-fold molar excess of Era (B) in the presence of GMP-PNP. In these experiments the concentration of the fluorescently labeled ribosomal particles complexed with unlabeled Era was constant, while the concentration of

unlabeled YjeQ was varied. After a short incubation the samples were loaded into MST glass capillaries, and the thermophoretic mobility of the labeled ribosomal particles bound to unlabeled Era (left panels) was measured using the Monolith.NT.115 instrument (NanoTemper). Measured changes in the MST response were used to produce curves that plotted the Fnorm (‰) = F_1/F_0 versus YjeQ concentrations in logarithmic scale. The F_0 (blue) and F_1 (red) regions of the fluorescence time traces used to calculate Fnorm (‰) are indicated in the left panels. The Fnorm (‰) curves were fit using the law of mass action to yield a Kd value (right panels).

These experiments demonstrated that the presence of Era in excess reduces the affinity of YjeQ to the mature 30S subunits. To understand the mechanism by which Era reduces the binding affinity of YjeQ, we set up assembly reaction containing mature 30S subunit as well as molar excess of YjeQ and Era. Subsequently, we attempted to solve the structure of this tertiary complex to near atomic resolution using cryo-EM.

Classification of particles revealed two predominant subpopulations for the 30S subunit in the presence of YjeQ and Era (Figure 3.10). These two structures were solved at 3.5Å and 4Å resolution. We called these two classes subclass I and subclass II, respectively. Subclass I (Figure 3.10A) showed a broken density corresponding to Era in the cavity between head and platform. However, subclass II (Figure 3.10B) did not showed any extra density that could correspond to Era protein.

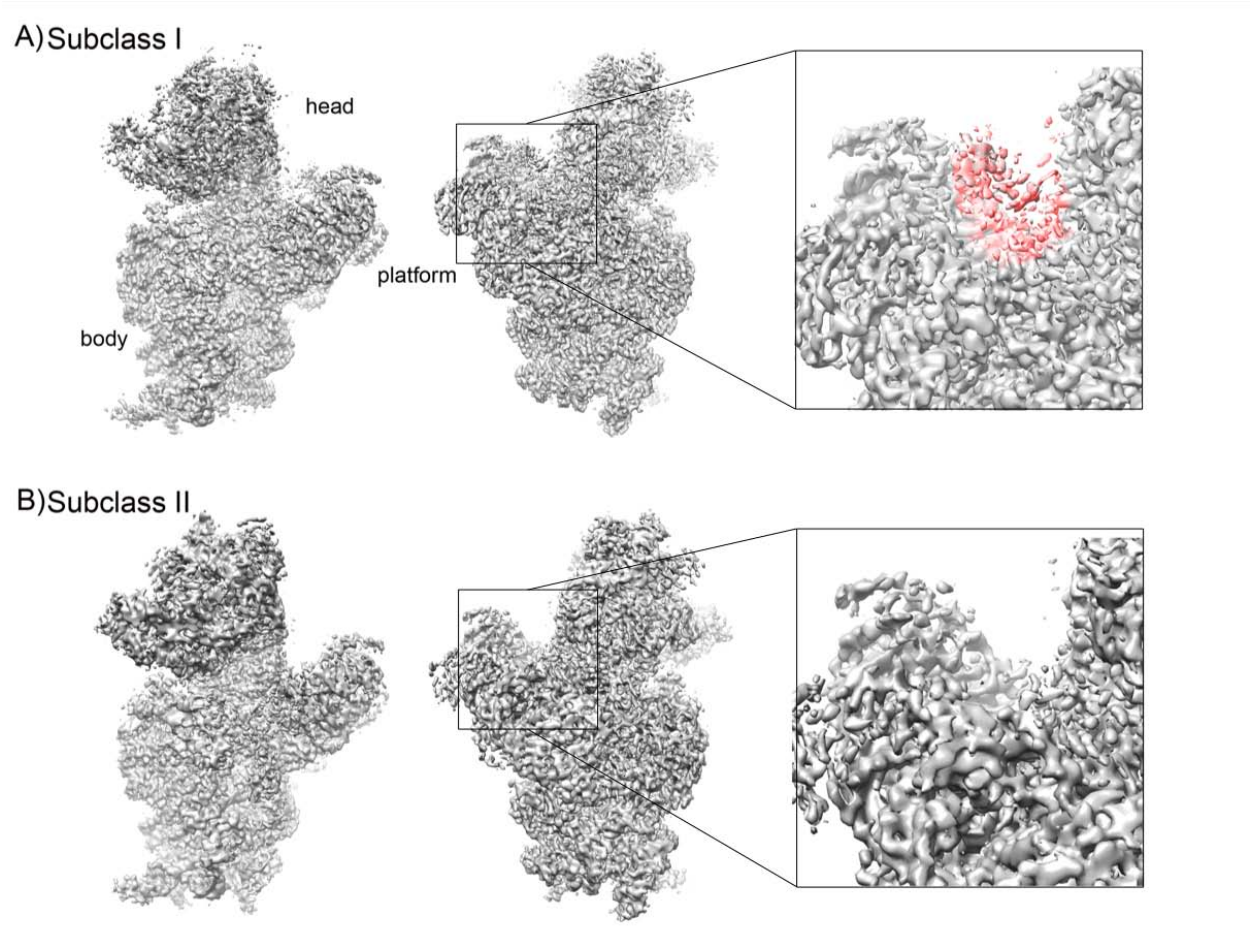

Figure 3.10: Cryo-EM structure of the 30S subunit in complex with YjeQ and Era. Front view of the surface rendering representation of the cryo-EM maps of the 30S+YjeQ+Era (left panels) and back view (middle panels). Right panels show a zoomed view of the framed area. A) Subclass I revealed immature 30S subunit with partial density for Era in the cavity between head and platform indicated in red and B) subclass II represented mature 30S subunit with no density corresponds to Era and YjeQ.

The cryo-EM map of the 30S+YjeQ+Era complex was refined to a mean resolution of 3.5 Å and 4Å (Figure 3.11A). Local resolution analysis revealed that both maps exhibited isotropic resolution with the body region refining to resolution values around the mean value. However, head and platform regions of the map refined to resolution values lower than the mean resolution (Figure 3.11B).

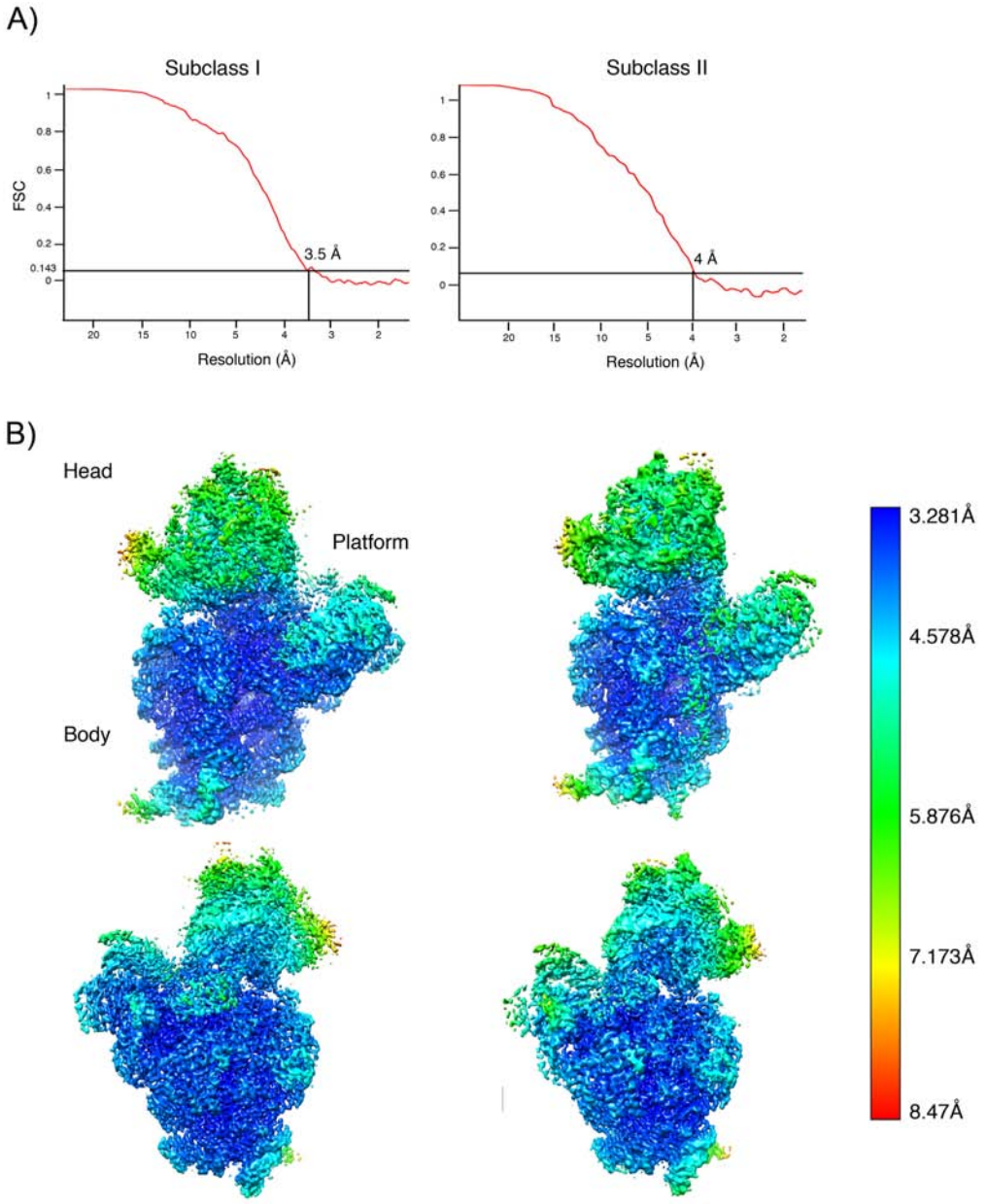

Figure 3.11: Resolution analysis of the 30S+Era+YjeQ cryo-EM map. A) This panel shows the Fourier Shell Correlation (FSC) plots for the subclass I and subclass II structures. A FSC value of 0.143 was used to report the resolution. B) Local resolution analysis of the two structures performed with relion.

Subclass I revealed an extra density at the cavity between the head and platform of the 30S subunit. Previously, a low resolution structure of the 30S subunit in complex with Era

showed (Sharma et al., 2005) that Era binds to the 30S subunit in this same region of the 30S subunit. Therefore, we believed this density represents Era. However, we did not observe any density for YjeQ in the decoding region of the 30S subunit (Figure 3.12A). More specifically, most of the 5' domain and central domain of rRNA was folded and adopted the mature conformation, except helix 44 and helix 45 of the 3' minor domain for which we did not observe any density. In addition, there is missing density for some portions of helix 33 at the 3' major domain of 16S rRNA. Moreover, the density for all of the primary and secondary r-proteins is present and the r-proteins in the body and platform already folded. However, there was no existing density that could be assigned to uS7 and uS13, which are anchored from the head of the 30S subunit (Figure 3.12).

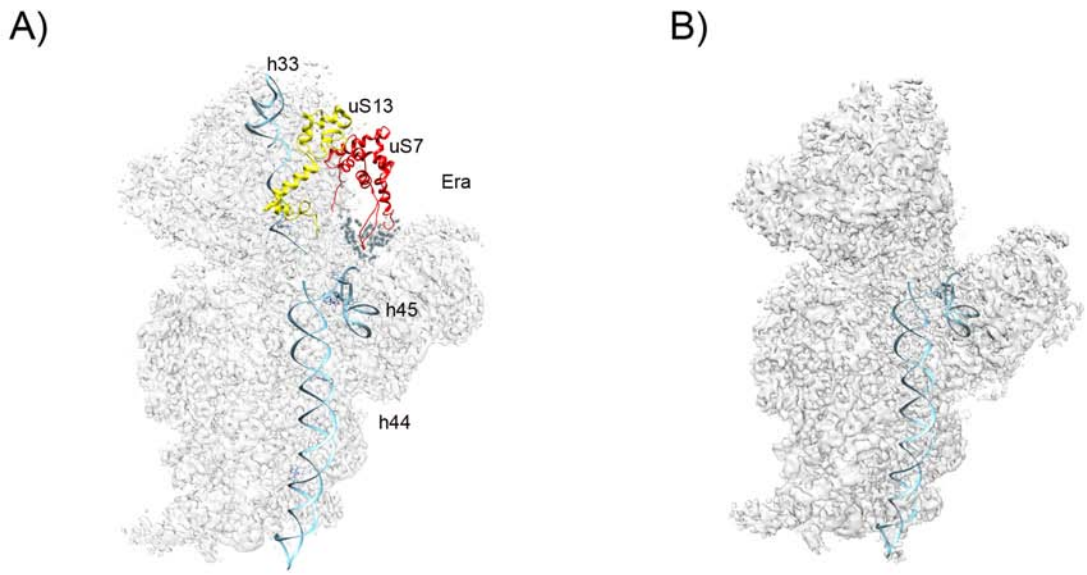

Figure 3.12: Cryo-EM structural analysis of the 30S subunit in complex with YjeQ and Era. Front view of the surface rendering representation of the cryo-EM maps of the 30S+YjeQ+Era. A) Subclass I with specific structural elements from the atomic model of the 30S subunit (PDB ID 2AVY.pdb) that were missing density at helix 44 and helix 45, and portion of helix 33 and uS7 (red color) and uS13 (yellow color), B) Subclass II with specific structural elements from the atomic model of the 30S subunit (PDB ID 2AVY.pdb) that were helix 44 and helix 45, with all domains are present and folded.

The extra density between the head and platform in subclass I represents only a partial density for Era. There is no sufficient extra density to fit the KH and GTPase domain of the factor. To analyze further the density for Era, we performed focused classification on the region partially covered by Era. However, we still observed the same broken density for Era. This result suggests Era binds to the 30S subunit in a flexible manner. It may bind with its KH RNA binding domain; however, it is not able to bring the GTPase domain in close contact with the 30S subunit. Analysis of the structure of the subclass I particle demonstrated that this class closely resembles the structure of an immature 30S particles at the late stages of maturation. These results suggest that, binding of Era causes conformational changes in the 30S subunit reverting it to an immature state, which YjeQ no longer recognizes.

Subclass II did not show any extra density corresponding to either Era or YjeQ (Figure 3.12B). The overall conformation of 16S rRNA in this structure is very close to the mature 30S subunit. The 5' domain, central domain and 3' domain of the 16S rRNA are completely folded. All of the r-proteins in the body and platform were present. However, there was no density for uS2 located at the solvent side of the 30S subunit. In addition, there was a missing density for uS7 and uS13, two r-proteins located in the head domain of the 30S subunit.

In addition, during the early stage of classification, we observed an additional class with no density for the head of the 30S subunit (Figure 3.13). Due to 5' to 3' transcription of rRNA and binding of r-proteins and the fact that the head and then decoding center are the last two domains that mature, we assumed this class represented the earliest stage in the maturation process.

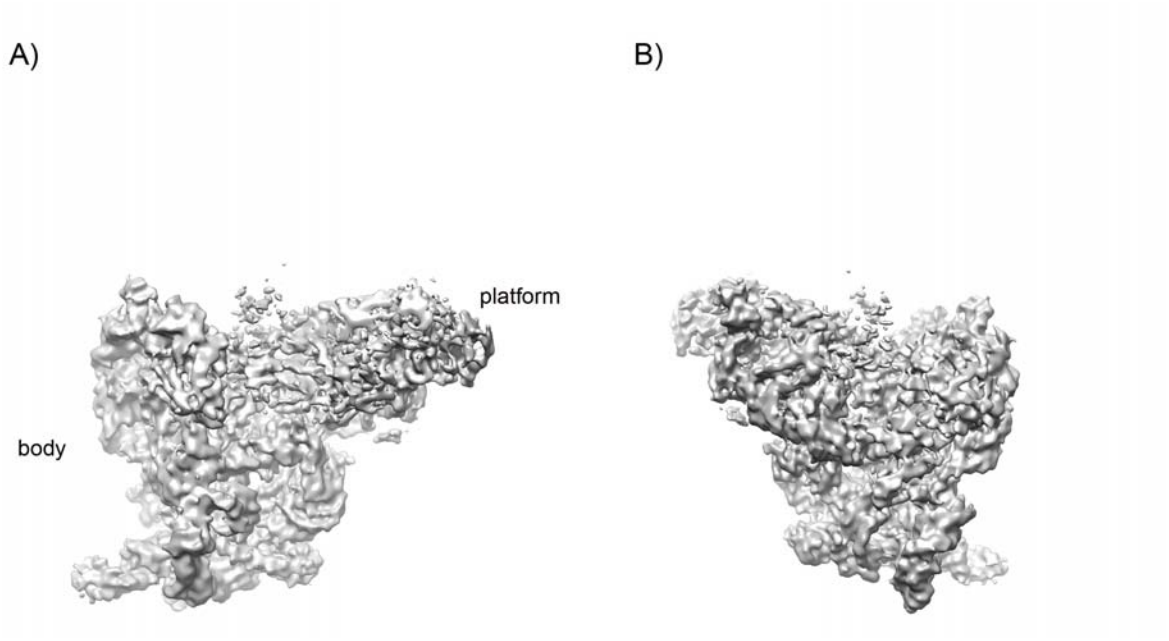

Figure 3.13: Cryo-EM structure of one class of the 30S subunit in complex with YjeQ and Era. This data revealed there is one class that missing head. A) front and (B) back views of the cryo-EM map of the 30S+YjeQ+Era. Important landmarks of the 30S subunit are indicated.

All these results suggested that Era is assisting the folding of the platform domain in the

30S subunit, where it acts as a local RNA chaperone dedicated to fold h23 and h24. In addition, Era may also assist the entry of r-proteins that locate around the platform domain (uS2, uS3, bS21, uS7 and uS11). Era may mediate the entry of these r-proteins directly or indirectly.

3.5 Discussion

In this paper, we demonstrated that depletion of Era in bacterial cells causes accumulation of an immature 30S subunit exhibiting missing densities in the central domain region and 3' minor domain (helix 44). In our previous publication (Razi et al., 2017b), we observed that binding of YjeQ stabilizes helix 44 in its mature conformation and thus allowing the 30S subunit to associate with the mature 50S subunit. Although, it was not shown that the central domain of the 30S subunit is required directly for its association with the 50S subunit, the lack of a properly folded helix 44 in this assembly intermediates also prevent their association with the 50S subunits and subsequent protein translation initiation.

In addition to a missing density in the central domain of the Era depleted particles, in our solved structure of the 30S subunit in complex with Era we observed a partial density for Era in the cavity between head and platform. This binding position for Era is consistent with the previous literature (Sharma et al., 2005; Tu et al., 2011; Tu et al., 2009). These findings suggest that Era may have a role as a local chaperon that binds to the central domain of the assembling 30S subunit and facilitate the folding of this region of the rRNA.

Another possible role of Era is that it may mediate the recruitment of other assembly factors or even RNases involved in processing the rRNA. Era may perform this role by direct interaction with these factors or indirectly by inducing a conformational change in the assembling subunit that allow these factors to bind. This hypothesis is consistent with previous literature implicating the role of some GTPases in recruitment of RNAases or assembly factors in

eukaryotic ribosome biogenesis. This function was observed in the Bms1 GTPase factor in yeast, which has a role in recruiting Rcl1 factor to the immature 40S subunit (Karbstein and Doudna, 2006). Rcl1 perform endonucleolytic processing of pre-rRNA during ribosome maturation. However, this function hasn't been described in bacteria ribosome biogenesis up to date.

Interestingly, qMS also revealed that bS1 r-protein is absent in the 30S Era depleted particles, which has an overlapping binding position with Era. This suggests the possibility Era may bind to the immature 30S subunit and work as a placeholder for this ribosomal protein. Subsequent release of Era would create the site binding for uS1. The same function was shown in eukaryotes (*Saccharomyces cerevisiae*), assembly factor Mrt4. Binding of factor Mrt4 to the pre-60S subunit blocks the binding of r-protein P0 (Boehringer et al., 2012; Datta et al., 2007; Rodriguez-Mateos et al., 2009; Xu et al., 2008).

Moreover, it has been shown that Era is an essential factor for cell survival (Anderson et al., 1996; Hansen et al., 1998; Inada et al., 1989; March et al., 1988; Minkovsky et al., 2002). However, there is no evidence to indicate whether Era is an essential factor in ribosome biogenesis. Previous work testing the effect of Era on the kinetics of incorporation of r-proteins during the assembly of the 30S subunit *in vitro* found that Era accelerates the binding rates of r-proteins uS5, uS9, uS11 and uS12. There was also a subtler increase in the kinetics of incorporation of uS7, uS10, uS13, uS14 and uS19 (Bunner et al., 2010). However, the qMS analysis presented earlier here revealed that all the r-proteins with modified incorporation kinetics were present in the 30S Era depleted particles at full occupancy, suggesting that Era is not essential in incorporating most of the remaining r-proteins (except S2, S3, S5 and S21). These results combined indicate that the incorporation of these r-proteins is not what makes this factor essential.

Generally, due to the 5' to 3' directionality of rRNA transcription, the early-binding proteins interact with the 5' domain (body) of the rRNA, mid-binding proteins with the central domain (platform) and late-binding proteins with the 3' domain (head) (de Narvaez and Schaup, 1979; Lindahl, 1975). Also, based on pulse-chase mass spectroscopy analysis of the 30S subunit by the Williamson group (Talkington et al., 2005), proteins bind faster to the 5' domain compared to the central and 3' domain of 16S rRNA (Chen and Williamson, 2013; Culver and Noller, 1999; Grondek and Culver, 2004; Holmes and Culver, 2005). These findings suggest that first the body of the 30S subunit is folded and then the platform followed by the head. However, we observed that in the 30S Era depleted particles the head domain is already folded, while the platform is still in an immature state. This suggests that under Era depletion conditions, the assembly of the 30S subunit is rerouted.

Genetic and biochemical studies suggest that there is a functional interplay between assembly factors in assisting the maturation of the 30S subunit (Bylund et al., 1998; Campbell and Brown, 2008; Goto et al., 2011; Inoue et al., 2003; Inoue et al., 2006). Biochemical analysis has been shown that YjeQ enhances the release of RbfA at the late stage of maturation (Goto et al., 2011; Jeganathan et al., 2015). Moreover, genetic studies reveal that impaired ribosome assembly resulted by deletion of *yjeQ* can be suppressed by overexpression of Era (Campbell and Brown, 2008).

Therefore, to further analyze the possible functional interplay between Era and YjeQ, we solved the cryo-EM structure of the mature 30S subunit in complex with both factors. In this structure, we did not observe any density for helix 44 and helix 45 at the 3' minor domain. Also, we found that Era prevents binding of YjeQ by reverting the structure of the 30S subunit to an immature state not recognized by YjeQ. These results suggest that Era and YjeQ perform their function in a sequential manner, rather than simultaneously. The model derived from these

experiments proposes that Era acts first to facilitate the folding of the platform motifs. Subsequently, when Era is released, YjeQ binds and facilitates the folding of the decoding center and check the proofreading ability of the subunit before it is released to the pool of actively translating ribosomes.

An unsolved aspect of our structural analysis of the 30S subunit in complex with Era+GMPNP in *E. coli* is that this factor appears as a fragmented density in the cryo-EM map. Focused classification analysis of these maps did not improve the definition of the density for Era suggesting that the factor is bound to the subunit in a flexible manner. However, the cryo-EM structure of 30S+Era from *Thermus Thermophilus* in the absence of nucleotide obtained by the Sharma group showed a defined density for Era in the cavity between head and platform (Sharma et al., 2005). Our cryo-EM structure was obtained using Era protein and 30S subunits purified from *E. coli* whereas the Sharma group used Era from *T. Thermophilus*. This organism lives in extreme condition and then perhaps Era under 37 ºC binds with enhance affinity to the 30S subunit to assist in subunit assembly. The second difference between these two structures is the nucleotide that we used. We solved our structure in the presence of GMPNP, and the complex was assembled in the absence of nucleotide in the other study (Sharma et al., 2005). However, crystallography studies of Era and RNA fragments of the 3' end of the 16S rRNA demonstrated that in the absence of nucleotide, Era domains adopt the open conformation in which the nucleotide binding site is accessible, but the RNA binding site in the KH domain is occluded and thus Era is not able to bind to the 30S subunit. Therefore, it is puzzling that in our cryo-EM structure, we did not observe a fully defined density for Era even though our experimental condition were more favorable for a tight binding of Era to the 30S subunit. A possibility is that we are not actually looking at the true substrate for Era. Previous work reveals that none of the nonessential assembly factors bind to the intermediate accumulated upon

deletion of these factors, such as YjeQ and RimM (Thurlow et al., 2016a). In addition, our structural analysis of the 30S subunit in complex with Era demonstrated that Era reverts back the structure of the mature 30S subunit to the immature. These data suggest that Era may have a role in the context of immature particles. Therefore, it is possible that in *E. coli* tight binding of Era may only happen to the immature 30S particles and not to the mature 30S subunit. Perhaps, attempting the cryo-EM reconstruction of Era in complex with the $30S_{Era\text{-}depleted}$ particles would allow to define the domain arrangement of the factor when bound to the ribosomal subunit at high resolution.

Therefore, although the function of the assembly factors is not well understood, the presented data suggest that Era may play important roles during the assembly process of the 30S subunit including assisting the binding of ribosomal proteins around the platform domain of the 30S subunit, regulation of processing and folding of rRNA in this motif and blocking the premature binding of the 30S subunit to the 50S subunit.

3.6 Acknowledgments

We are grateful to Dr. Mike Strauss for assisting us to collect dataset. We acknowledge Dr. Bui at the Anatomy and Cell Biology Department in McGill University for granting us access to his server for processing the data. We also thank FEMR at McGill, Dr. Vali, Dr. Sears and Jeannie Mui. This work was supported by grants from the National Science and Engineering Research Council of Canada [RGPIN288327-07 to J.O.] and Canadian Institutes of Health Research [PJT-153044 to J.O.].

Chapter 4: Discussion

The goal of this thesis is to understand the precise mechanism on how YjeQ and Era perform their function in the maturation of the 30S subunit. In this thesis we characterized the structure of the 30S subunit in complex with YjeQ using cryo-EM. Also, we described the 30S assembly intermediate that accumulated upon depletion of Era, in addition to exploring the structure of the mature 30S subunit in complex with Era. Finally, we investigated the functional interplay between these two assembly factors, YjeQ and Era.

4.1 The evolving function of YjeQ

Numerous biochemical and genetic studies in the last decade have suggested that YjeQ is an assembly factor that assists the late stages of assembly of the 30S subunit (Daigle et al., 2002; Himeno et al., 2004). Deletion of YjeQ causes slow growth phenotype of cells and accumulation of immature 30S subunits (Guo et al., 2011; Jomaa et al., 2011a). Existing evidence suggests that YjeQ is an important factor for the assembly of the functional core of the subunit (Jomaa et al., 2011a; Jomaa et al., 2011b; Kimura et al., 2008). Surprisingly, recent work (Thurlow et al., 2016a) measuring the binding affinity of YjeQ to the mature 30S subunit and to immature ribosomal particles that accumulate in *yjeQ* null cells revealed that YjeQ binds the mature 30S subunit with high affinity. Instead, the binding affinity of the YjeQ to the immature particles suggests that binding does not occur at what is considered physiological concentrations (Thurlow et al., 2016a). These findings transformed the current thinking regarding YjeQ and suggested that YjeQ, in addition to its role in assembly, also has a role in the context of the mature 30S subunit.

To gain new key insights regarding the function of YjeQ, we obtained the structure of the 30S+YjeQ complex at ~5Å described in chapter 2. The presented cryo-EM structure of the 30S+YjeQ complex shows that through extensive interactions involving the OB-fold and zinc finger domain, YjeQ anchor both ends of the protein to three out of the four domains of the 30S subunit (body, head and platform). These interactions are important for the functionality of YjeQ

as described by earlier mutational studies indicating that deletion of the first N-terminal 20 amino acids of YjeQ decreases significantly the binding of YjeQ to the 30S subunit. Removal of the entire OB-fold domain completely suppresses any association with the ribosomal particle (Daigle and Brown, 2004). Similarly, partial or complete removal of the C-terminal zinc finger domain also abolishes YjeQ binding (Jeganathan et al., 2015).

Previous structural work has suggested a general checkpoint role for YjeQ by sterically blocking the binding of initiation factors to the 30S subunit or its association with the large 50S subunit (Guo et al., 2011). Involvement of assembly factors in quality control mechanisms has been extensively studied in eukaryotic cells. There are examples where assembly factors bind to the subunits and block binding of initiation factors or tRNA to the subunit (Strunk et al., 2011). Moreover, there are also factors that mimic the steps of the translation cycle in assembling ribosomes. For instance, there are seven factors (Tsr1, Rio2, Dim1, Nob1, Pno1 and Enp1/Ltv1) that bind to the 40S subunit interface in yeast and block every step in the translation initiation (Strunk et al., 2012). However, the cryo-EM structure presented here provides for the first time evidence of a bacterial assembly factor testing a specific translation mechanism of the 30S ribosomal subunit before the particle is release to the pool of actively translating ribosomes.

A key step to allow the 30S subunit to enter the pool of actively translating ribosomes is the release of these factors. Previous studies have been suggested that YjeQ promotes the removal of RbfA from the mature 30S subunit (Goto et al., 2011). We also demonstrated that RbfA binds weakly to the mature 30S subunit and subsequent binding of YjeQ to the mature 30S subunit results in releasing of RbfA in a GTP dependent manner (Jeganathan et al., 2015). However, the mechanism of RbfA removal by YjeQ could not be concluded. In our published work in chapter 2, we proposed a model that YjeQ is able to remove RbfA from the mature 30S subunit. In this model, we found that binding of YjeQ to the 30S subunit has a significant

stabilizing effect in the upper region of helix 44. This is the same rRNA motif that appears severely disrupted upon RbfA binding. Therefore, it is likely that binding of YjeQ to the 30S subunit forces helix 44 back into the normal decoding position and triggers the release of RbfA. In addition, *E. coli* YjeQ presents an N-terminal region comprised of 34 amino acids before the OB-fold domain starts. In the cryo-EM map this N-terminal region is visible and forms an extended α-helix that is inserted as a finger into the neck region in the area that has been described as the binding site for RbfA (Datta et al., 2007). We concluded from the analysis of this region of the cryo-EM map that likely the combined stabilizing effect of YjeQ in the conformation of helix 44 with the introduction of the N-terminal α-helix in the binding site of RbfA creates the necessary conditions to force the removal of this factor from the mature 30S subunit. The mechanism of release of RbfA by YjeQ has not been described by any other groups. Interestingly, most species do not have this N-terminal extension and then perhaps cannot remove RbfA following the described mechanism in *E.coli*.

Moreover, it has been shown that the GTPase activity of YjeQ is stimulated over 160-fold in the presence of mature 30S subunits. Also, the tightest binding of YjeQ to the mature 30S subunit occurs in the presence of GMP-PNP. However, this affinity decreases in the presence of GTP and mainly GDP (Daigle and Brown, 2004; Jeganathan et al., 2015; Thurlow et al., 2016b). That suggests YjeQ may bind to the 30S subunit in its GTP state and perform its function. Subsequent hydrolysis of GTP induces conformational changes that YjeQ is not able to bind to the 30S subunit longer. Therefore, GTP hydrolysis can be a release mechanism of the YjeQ from the 30S subunit. However, there is no evidence demonstrating the precise mechanism on how YjeQ gets release from the 30S subunit.

Our presented cryo-EM structure of the 30S+YjeQ complex shows placing the GTPase domain in direct contact with the upper part of helix 44. According to the structure of the free

30S and the 30S+YjeQ complex described in Chapter 2, this area of helix 44 constitutes the ribosomal motif undergoing the largest conformational change upon YjeQ binding. Consequently, in the 30S+YjeQ complex, the GTPase domain of YjeQ is ideally placed to monitor the largest conformational changes that the 30S subunit undergoes. However, we were not able to observe in our structure the precise role of switch I and II in GTPase activity of YjeQ. On the other hand, a cryo-EM structure of the 30S+YjeQ from the Connell group obtained around the time our structure was published exhibited a well ordered GTP binding pocket with visible switch 1 and 2 regions in cryo-EM structure (Lopez-Alonso et al., 2017). They demonstrated that interaction between YjeQ and 30S repositions the OB fold and the Zinc finger domain such that the β-hairpins β6/β7 and β12/β13 and the α6 helix help reorder the core of the GTPase domain. These arrangements help ordering of switch I and II such that Gly269, Thr 250 and Se221 can now interact with the γ-phosphate of GDPNPN (analogue of GTP) nucleotide due to the closed conformation of the core GTPase domain. Furthermore, due to the visibility of switch I region, they observed its interactions with helices 24, 44, 45 and could propose a mechanism for the stimulation of the YjeQ GTPase activity by the mature 30S subunit. Proper positioning of helix 45 during YjeQ and 30S interaction allows G1517 to reposition the catalytic residue His248 such that it can now access the active site water molecule to attack the γ-phosphate of GDPNPN. With this model they discovered that the mechanism for YjeQ GTPase activation is different from other GTPases where the catalytic histidine residue is present on the switch II.

Therefore, this data suggests that the role of the GTPase activity of YjeQ is mainly to act as a switch to facilitate the release of the protein factor from the 30S subunit once YjeQ has performed its functions.

In addition, the Connell group demonstrated that some of the tertiary binding r-proteins (uS2, uS3, bS21, uS7 and uS12) are missing from their solved structure of the 30S+YjeQ. However, our structure of the 30S+YjeQ has a complete r-proteins complement (Razi et al., 2017b). Their hypothesis is that YjeQ induces conformational changes in the 30S subunit and may destabilize the incorporation of these r-proteins. However, we noticed that the Connell group purified the 30S subunit with high salt wash (1M) and perhaps that resulted in dissociation of these r-proteins from the 30S subunit (Mulder et al., 2010).

4.2 Era depleted *Escherichia coli strain*, an old tool with regained potential due to recent advances in cryo-EM

Over the past decades it was a tremendous effort to study the mechanism of 30S biogenesis. The Williamson lab determines the rates of association of all ribosomal proteins to 16S rRNA by pulse-chase quantified by mass spectrometry (PC-QMS) (Talkington et al., 2005). In this study, they demonstrated the distinct activation energies during biogenesis. Thus, they suggest that there are multiple global rate-limiting steps in ribosome biogenesis.

In addition, the Woodson group used hydroxyl radical footprinting to follow the folding of the 16S rRNA and its binding with r-proteins during 30S subunit assembly (Adilakshmi et al., 2006). They determined the rates of RNA folding for the various 16S rRNA domains and characterized multiple folding pathways, establishing that multiple parallel folding pathways are possible during 30S maturation.

Studying the immature 30S particles accumulating in Δ*yjeQ* (Jomaa et al., 2011a), Δ*rimM* (Guo et al., 2013; Leong et al., 2013) and Δ*yjeQ*Δ*rbfA* bacterial strains have proven to be a powerful tool for investigating the function of these assembly factors in the maturation of the 30S subunit. Previous biochemical and structural analyses of immature particles from Δ*yjeQ*, Δ*rimM* and Δ*yjeQ*Δ*rbfA* strains reveal that the accumulated immature particles represent late

stages of maturation with a distortion at the decoding center. The similarity in their structural defects and protein composition suggests that these non-essential assembly factors are involved in the maturation of the decoding center of the 30S subunit and their function be overlapping.

Until now all these genetic studies of assembly intermediates on the 30S subunit were characterized at low resolution. Solving structures of macromolecular complexes at high resolution (3-4Å) was not possible for cryo-EM. However, recent breakthroughs in hardware and software have now empowered this technique to also obtain structures at comparable resolution. Direct detector devices (DDDs) have finally replaced photographic film and Charge-couple devices (CCD cameras) for imaging radiation sensitive specimens. These new detectors have substantially better performance than previously used media. Consequently, 3D structures can be obtained at high resolution. Indeed, maps at better than 3Å resolution have been calculated for ribosomes from different organisms (Bai et al., 2013; Brown et al., 2014; Shalev-Benami et al., 2017). In addition, previously a major limitation in studying the assembly intermediates that accumulate in the *yjeQ* or *rimM* deletion strains was the small number of images comprising the collected datasets, preventing a comprehensive analysis of all conformational states adopted by these intermediates. However, today we have microscopes like Titan Krios that can generate massive datasets of millions of particle images. These microscopes are able to collect a large number of particles that we can analyze. Thus, we used these new capabilities of resolution and high throughput cryo-EM to solve and characterize the structure of the assembly intermediates that accumulate under Era depleted conditions. By extensive analysis of all these particles, we concluded that this depletion strain mainly accumulates one assembly intermediate. Perhaps, this intermediate could be a "convergency node" that during assembling of the 30S subunits, all particles need to pass through this stage. At this stage, Era is needed to assist in the folding of the motifs and prevent them from trapping into local energy minima. Thus, Era, which is an essential

assembly factor for cell survival, may function as a “rescue factor” ensuring the continuous maturation process.

References

Adilakshmi, T., Bellur, D.L., and Woodson, S.A. (2008). Concurrent nucleation of 16S folding and induced fit in 30S ribosome assembly. Nature *455*, 1268-1272.

Adilakshmi, T., Lease, R.A., and Woodson, S.A. (2006). Hydroxyl radical footprinting in vivo: mapping macromolecular structures with synchrotron radiation. Nucleic Acids Res *34*, e64.

Al Refaii, A., and Alix, J.H. (2009). Ribosome biogenesis is temperature-dependent and delayed in Escherichia coli lacking the chaperones DnaK or DnaJ. Mol Microbiol *71*, 748-762.
Amunts, A., Brown, A., Toots, J., Scheres, S.H.W., and Ramakrishnan, V. (2015). Ribosome. The structure of the human mitochondrial ribosome. Science *348*, 95-98.

Anand, B., Verma, S.K., and Prakash, B. (2006). Structural stabilization of GTP-binding domains in circularly permuted GTPases: implications for RNA binding. Nucleic Acids Res *34*, 2196-2205.

Anderson, P.E., Matsunaga, J., Simons, E.L., and Simons, R.W. (1996). Structure and regulation of the Salmonella typhimurium rnc-era-recO operon. Biochimie *78*, 1025-1034.

Baba, T., Ara, T., Hasegawa, M., Takai, Y., Okumura, Y., Baba, M., Datsenko, K.A., Tomita, M., Wanner, B.L., and Mori, H. (2006). Construction of Escherichia coli K-12 in-frame, single-gene knockout mutants: the Keio collection. Mol Syst Biol *2*, 2006 0008.

Bai, X.C., Fernandez, I.S., McMullan, G., and Scheres, S.H. (2013). Ribosome structures to near-atomic resolution from thirty thousand cryo-EM particles. eLife *2*, e00461.

Bai, X.C., Rajendra, E., Yang, G., Shi, Y., and Scheres, S.H. (2015a). Sampling the conformational space of the catalytic subunit of human gamma-secretase. eLife *4*.

Bai, X.C., Rajendra, E., Yang, G., Shi, Y., and Scheres, S.H. (2015b). Sampling the conformational space of the catalytic subunit of human gamma-secretase. eLife *4*, e11182.

Ban, N., Beckmann, R., Cate, J.H., Dinman, J.D., Dragon, F., Ellis, S.R., Lafontaine, D.L., Lindahl, L., Liljas, A., Lipton, J.M.*, et al.* (2014). A new system for naming ribosomal proteins. Curr Opin Struct Biol *24*, 165-169.

Ben-Shem, A., Garreau de Loubresse, N., Melnikov, S., Jenner, L., Yusupova, G., and Yusupov, M. (2011). The structure of the eukaryotic ribosome at 3.0 A resolution. Science *334*, 1524-1529.

Boehringer, D., O'Farrell, H.C., Rife, J.P., and Ban, N. (2012). Structural insights into methyltransferase KsgA function in 30S ribosomal subunit biogenesis. J Biol Chem *287*, 10453-10459.

Boriack-Sjodin, P.A., Margarit, S.M., Bar-Sagi, D., and Kuriyan, J. (1998). The structural basis of the activation of Ras by Sos. Nature *394*, 337-343.

Britton, R.A. (2009). Role of GTPases in bacterial ribosome assembly. Annu Rev Microbiol *63*, 155-176.

Britton, R.A., Powell, B.S., Court, D.L., and Lupski, J.R. (1997). Characterization of mutations affecting the Escherichia coli essential GTPase era that suppress two temperature-sensitive dnaG alleles. J Bacteriol *179*, 4575-4582.

Britton, R.A., Powell, B.S., Dasgupta, S., Sun, Q., Margolin, W., Lupski, J.R., and Court, D.L. (1998). Cell cycle arrest in Era GTPase mutants: a potential growth rate-regulated checkpoint in Escherichia coli. Mol Microbiol *27*, 739-750.

Brown, A., Amunts, A., Bai, X.C., Sugimoto, Y., Edwards, P.C., Murshudov, G., Scheres, S.H.W., and Ramakrishnan, V. (2014). Structure of the large ribosomal subunit from human mitochondria. Science *346*, 718-722.

Brown, S.D., and Jun, S. (2015). Complete Genome Sequence of Escherichia coli NCM3722. Genome Announc *3*.

Bunner, A.E., Beck, A.H., and Williamson, J.R. (2010). Kinetic cooperativity in Escherichia coli 30S ribosomal subunit reconstitution reveals additional complexity in the assembly landscape. Proc Natl Acad Sci U S A *107*, 5417-5422.

Bylund, G.O., Wipemo, L.C., Lundberg, L.A., and Wikstrom, P.M. (1998). RimM and RbfA are essential for efficient processing of 16S rRNA in Escherichia coli. J Bacteriol *180*, 73-82.

Byrgazov, K., Grishkovskaya, I., Arenz, S., Coudevylle, N., Temmel, H., Wilson, D.N., Djinovic-Carugo, K., and Moll, I. (2015). Structural basis for the interaction of protein S1 with the Escherichia coli ribosome. Nucleic Acids Res *43*, 661-673.

Caldon, C.E., Yoong, P., and March, P.E. (2001). Evolution of a molecular switch: universal bacterial GTPases regulate ribosome function. Mol Microbiol *41*, 289-297.

Campbell, T.L., and Brown, E.D. (2008). Genetic interaction screens with ordered overexpression and deletion clone sets implicate the Escherichia coli GTPase YjeQ in late ribosome biogenesis. J Bacteriol *190*, 2537-2545.

Carter, A.P., Clemons, W.M., Brodersen, D.E., Morgan-Warren, R.J., Wimberly, B.T., and Ramakrishnan, V. (2000). Functional insights from the structure of the 30S ribosomal subunit and its interactions with antibiotics. Nature *407*, 340-348.

Carter, A.P., Clemons, W.M., Jr., Brodersen, D.E., Morgan-Warren, R.J., Hartsch, T., Wimberly, B.T., and Ramakrishnan, V. (2001). Crystal structure of an initiation factor bound to the 30S ribosomal subunit. Science *291*, 498-501.

Chen, S.S., and Williamson, J.R. (2013). Characterization of the ribosome biogenesis landscape in E. coli using quantitative mass spectrometry. J Mol Biol *425*, 767-779.

Chen, X., Court, D.L., and Ji, X. (1999). Crystal structure of ERA: a GTPase-dependent cell cycle regulator containing an RNA binding motif. Proc Natl Acad Sci U S A *96*, 8396-8401.

Comartin, D.J., and Brown, E.D. (2006). Non-ribosomal factors in ribosome subunit assembly are emerging targets for new antibacterial drugs. Curr Opin Pharmacol *6*, 453-458.

Connolly, K., and Culver, G. (2009). Deconstructing ribosome construction. Trends Biochem Sci *34*, 256-263.

Culver, G.M. (2003). Assembly of the 30S ribosomal subunit. Biopolymers *68*, 234-249.

Culver, G.M., and Noller, H.F. (1999). Efficient reconstitution of functional Escherichia coli 30S ribosomal subunits from a complete set of recombinant small subunit ribosomal proteins. RNA *5*, 832-843.

Daigle, D.M., and Brown, E.D. (2004). Studies of the interaction of Escherichia coli YjeQ with the ribosome in vitro. J Bacteriol *186*, 1381-1387.

Daigle, D.M., Rossi, L., Berghuis, A.M., Aravind, L., Koonin, E.V., and Brown, E.D. (2002). YjeQ, an essential, conserved, uncharacterized protein from Escherichia coli, is an unusual GTPase with circularly permuted G-motifs and marked burst kinetics. Biochemistry *41*, 11109-11117.

Datta, P.P., Wilson, D.N., Kawazoe, M., Swami, N.K., Kaminishi, T., Sharma, M.R., Booth, T.M., Takemoto, C., Fucini, P., Yokoyama, S.*, et al.* (2007). Structural aspects of RbfA action during small ribosomal subunit assembly. Mol Cell *28*, 434-445.

Dauphin, F., and Hamel, E. (1992). Identification of multiple muscarinic binding site subtypes in cat and human cerebral vasculature. J Pharmacol Exp Ther *260*, 660-667.

Davis, J.H., Tan, Y.Z., Carragher, B., Potter, C.S., Lyumkis, D., and Williamson, J.R. (2016). Modular Assembly of the Bacterial Large Ribosomal Subunit. Cell *167*, 1610-1622 e1615.

Davis, R.E., Shao, J., Dally, E.L., Zhao, Y., Gasparich, G.E., Gaynor, B.J., Athey, J.C., Harrison, N.A., and Donofrio, N. (2015). Complete Genome Sequence of Spiroplasma kunkelii Strain CR2-3x, Causal Agent of Corn Stunt Disease in Zea mays L. Genome Announc *3*.

de Narvaez, C.C., and Schaup, H.W. (1979). In vivo transcriptionally coupled assembly of Escherichia coli ribosomal subunits. J Mol Biol *134*, 1-22.

Deutsch, E.W., Mendoza, L., Shteynberg, D., Farrah, T., Lam, H., Tasman, N., Sun, Z., Nilsson, E., Pratt, B., Prazen, B.*, et al.* (2010). A guided tour of the Trans-Proteomic Pipeline. Proteomics *10*, 1150-1159.

Dunkle, J.A., and Cate, J.H. (2013). An Introduction to the Structure and Function of the Ribosome. EcoSal Plus *5*.

Earnest, T.M., Lai, J., Chen, K., Hallock, M.J., Williamson, J.R., and Luthey-Schulten, Z. (2015). Toward a Whole-Cell Model of Ribosome Biogenesis: Kinetic Modeling of SSU Assembly. Biophys J *109*, 1117-1135.

El Hage, A., Sbai, M., and Alix, J.H. (2001). The chaperonin GroEL and other heat-shock proteins, besides DnaK, participate in ribosome biogenesis in Escherichia coli. Mol Gen Genet *264*, 796-808.

Emsley, P., Lohkamp, B., Scott, W.G., and Cowtan, K. (2010). Features and development of Coot. Acta Crystallogr D Biol Crystallogr *66*, 486-501.

Eng, J.K., Jahan, T.A., and Hoopmann, M.R. (2013). Comet: an open-source MS/MS sequence database search tool. Proteomics *13*, 22-24.

Escher, C., Reiter, L., MacLean, B., Ossola, R., Herzog, F., Chilton, J., MacCoss, M.J., and Rinner, O. (2012). Using iRT, a normalized retention time for more targeted measurement of peptides. Proteomics *12*, 1111-1121.

Frank, J. (2003). Electron microscopy of functional ribosome complexes. Biopolymers *68*, 223-233.

Gao, H., Sengupta, J., Valle, M., Korostelev, A., Eswar, N., Stagg, S.M., Van Roey, P., Agrawal, R.K., Harvey, S.C., Sali, A.*, et al.* (2003). Study of the structural dynamics of the E coli 70S ribosome using real-space refinement. Cell *113*, 789-801.

Gilbert, R.J., Fucini, P., Connell, S., Fuller, S.D., Nierhaus, K.H., Robinson, C.V., Dobson, C.M., and Stuart, D.I. (2004). Three-dimensional structures of translating ribosomes by Cryo-EM. Mol Cell *14*, 57-66.

Goelz, S., and Steitz, J.A. (1977). Escherichia coli ribosomal protein S1 recognizes two sites in bacteriophage Qbeta RNA. J Biol Chem *252*, 5177-5179.

Gollop, N., and March, P.E. (1991a). A GTP-binding protein (Era) has an essential role in growth rate and cell cycle control in Escherichia coli. J Bacteriol *173*, 2265-2270.

Gollop, N., and March, P.E. (1991b). Localization of the membrane binding sites of Era in Escherichia coli. Res Microbiol *142*, 301-307.

Goto, S., Kato, S., Kimura, T., Muto, A., and Himeno, H. (2011). RsgA releases RbfA from 30S ribosome during a late stage of ribosome biosynthesis. EMBO J *30*, 104-114.

Green, R., and Noller, H.F. (1997). Ribosomes and translation. Annu Rev Biochem *66*, 679-716.

Grondek, J.F., and Culver, G.M. (2004). Assembly of the 30S ribosomal subunit: positioning ribosomal protein S13 in the S7 assembly branch. RNA *10*, 1861-1866.

Guo, Q., Goto, S., Chen, Y., Feng, B., Xu, Y., Muto, A., Himeno, H., Deng, H., Lei, J., and Gao, N. (2013). Dissecting the in vivo assembly of the 30S ribosomal subunit reveals the role of RimM and general features of the assembly process. Nucleic Acids Res *41*, 2609-2620.

Guo, Q., Yuan, Y., Xu, Y., Feng, B., Liu, L., Chen, K., Sun, M., Yang, Z., Lei, J., and Gao, N. (2011). Structural basis for the function of a small GTPase RsgA on the 30S ribosomal subunit maturation revealed by cryoelectron microscopy. Proc Natl Acad Sci U S A *108*, 13100-13105.

Hang, J.Q., Meier, T.I., and Zhao, G. (2001). Analysis of the interaction of 16S rRNA and cytoplasmic membrane with the C-terminal part of the Streptococcus pneumoniae Era GTPase. Eur J Biochem *268*, 5570-5577.

Hang, J.Q., and Zhao, G. (2003). Characterization of the 16S rRNA- and membrane-binding domains of Streptococcus pneumoniae Era GTPase: structural and functional implications. Eur J Biochem *270*, 4164-4172.

Hansen, J.E., Sato, M., Lacis, A., Ruedy, R., Tegen, I., and Matthews, E. (1998). Climate forcings in the industrial era. Proc Natl Acad Sci U S A *95*, 12753-12758.

Himeno, H., Hanawa-Suetsugu, K., Kimura, T., Takagi, K., Sugiyama, W., Shirata, S., Mikami, T., Odagiri, F., Osanai, Y., Watanabe, D.*, et al.* (2004). A novel GTPase activated by the small subunit of ribosome. Nucleic Acids Res *32*, 5303-5309.

Holmes, K.L., and Culver, G.M. (2005). Analysis of conformational changes in 16 S rRNA during the course of 30 S subunit assembly. J Mol Biol *354*, 340-357.

Hosokawa, K., Fujimura, R.K., and Nomura, M. (1966). Reconstitution of functionally active ribosomes from inactive subparticles and proteins. Proc Natl Acad Sci U S A *55*, 198-204.

Inada, T., Kawakami, K., Chen, S.M., Takiff, H.E., Court, D.L., and Nakamura, Y. (1989). Temperature-sensitive lethal mutant of era, a G protein in Escherichia coli. J Bacteriol *171*, 5017-5024.

Inoue, K., Alsina, J., Chen, J., and Inouye, M. (2003). Suppression of defective ribosome assembly in a rbfA deletion mutant by overexpression of Era, an essential GTPase in Escherichia coli. Mol Microbiol *48*, 1005-1016.

Inoue, K., Chen, J., Tan, Q., and Inouye, M. (2006). Era and RbfA have overlapping function in ribosome biogenesis in Escherichia coli. J Mol Microbiol Biotechnol *11*, 41-52.

Jankowsky, E., Gross, C.H., Shuman, S., and Pyle, A.M. (2001). Active disruption of an RNA-protein interaction by a DExH/D RNA helicase. Science *291*, 121-125.

Jeganathan, A., Razi, A., Thurlow, B., and Ortega, J. (2015). The C-terminal helix in the YjeQ zinc-finger domain catalyzes the release of RbfA during 30S ribosome subunit assembly. RNA *21*, 1203-1216.

Ji, X. (2016). Structural insights into cell cycle control by essential GTPase Era. Postepy Biochem *62*, 335-342.

Jomaa, A., Jain, N., Davis, J.H., Williamson, J.R., Britton, R.A., and Ortega, J. (2013). Functional domains of the 50S subunit mature late in the assembly process. Nucleic Acids Res.

Jomaa, A., Jain, N., Davis, J.H., Williamson, J.R., Britton, R.A., and Ortega, J. (2014). Functional domains of the 50S subunit mature late in the assembly process. Nucleic Acids Res *42*, 3419-3435.

Jomaa, A., Stewart, G., Martin-Benito, J., Zielke, R., Campbell, T.L., Maddock, J.R., Brown, E.D., and Ortega, J. (2011a). Understanding ribosome assembly: the structure of in vivo assembled immature 30S subunits revealed by cryo-electron microscopy. RNA *17*, 697-709.

Jomaa, A., Stewart, G., Mears, J.A., Kireeva, I., Brown, E.D., and Ortega, J. (2011b). Cryo-electron microscopy structure of the 30S subunit in complex with the YjeQ biogenesis factor. RNA *17*, 2026-2038.

Jomaa, A., Stewart, G., Mears, J.A., Kireeva, I., Brown, E.D., and Ortega, J. (2011c). Cryo-electron microscopy structure of the 30S subunit in complex with the YjeQ biogenesis factor. RNA *17*, 2026-2038.

Karbstein, K. (2007). Role of GTPases in ribosome assembly. Biopolymers *87*, 1-11.

Karbstein, K. (2013). Quality control mechanisms during ribosome maturation. Trends Cell Biol *23*, 242-250.

Karbstein, K., and Doudna, J.A. (2006). GTP-dependent formation of a ribonucleoprotein subcomplex required for ribosome biogenesis. J Mol Biol *356*, 432-443.

Keller, A., and Shteynberg, D. (2011). Software pipeline and data analysis for MS/MS proteomics: the trans-proteomic pipeline. Methods Mol Biol *694*, 169-189.

Kimura, T., Takagi, K., Hirata, Y., Hase, Y., Muto, A., and Himeno, H. (2008). Ribosome-small-subunit-dependent GTPase interacts with tRNA-binding sites on the ribosome. J Mol Biol *381*, 467-477.

King, T.C., Sirdeskmukh, R., and Schlessinger, D. (1986). Nucleolytic processing of ribonucleic acid transcripts in procaryotes. Microbiol Rev *50*, 428-451.

Kucukelbir, A., Sigworth, F.J., and Tagare, H.D. (2014). Quantifying the local resolution of cryo-EM density maps. Nat Methods *11*, 63-65.

Kuhlbrandt, W. (2014). Biochemistry. The resolution revolution. Science *343*, 1443-1444.

Lam, L., Arthur, J., and Semsarian, C. (2007). Proteome map of the normal murine ventricular myocardium. Proteomics *7*, 3629-3633.

Leipe, D.D., Wolf, Y.I., Koonin, E.V., and Aravind, L. (2002). Classification and evolution of P-loop GTPases and related ATPases. J Mol Biol *317*, 41-72.

Leong, V., Kent, M., Jomaa, A., and Ortega, J. (2013). Escherichia coli rimM and yjeQ null strains accumulate immature 30S subunits of similar structure and protein complement. RNA *19*, 789-802.

Lerner, C.G., and Inouye, M. (1991). Pleiotropic changes resulting from depletion of Era, an essential GTP-binding protein in Escherichia coli. Mol Microbiol *5*, 951-957.

Lerner, C.G., Sood, P., Ahnn, J., and Inouye, M. (1992). Cold-sensitive growth and decreased GTP-hydrolytic activity from substitution of Pro17 for Val in Era, an essential Escherichia coli GTPase. FEMS Microbiol Lett *74*, 137-142.

Levdikov, V.M., Blagova, E.V., Brannigan, J.A., Cladiere, L., Antson, A.A., Isupov, M.N., Seror, S.J., and Wilkinson, A.J. (2004). The crystal structure of YloQ, a circularly permuted GTPase essential for Bacillus subtilis viability. J Mol Biol *340*, 767-782.

Li, X., Mooney, P., Zheng, S., Booth, C.R., Braunfeld, M.B., Gubbens, S., Agard, D.A., and Cheng, Y. (2013). Electron counting and beam-induced motion correction enable near-atomic-resolution single-particle cryo-EM. Nat Methods *10*, 584-590.

Li, Z., Pandit, S., and Deutscher, M.P. (1999a). Maturation of 23S ribosomal RNA requires the exoribonuclease RNase T. RNA *5*, 139-146.

Li, Z., Pandit, S., and Deutscher, M.P. (1999b). RNase G (CafA protein) and RNase E are both required for the 5' maturation of 16S ribosomal RNA. EMBO J *18*, 2878-2885.

Lindahl, L. (1975). Intermediates and time kinetics of the in vivo assembly of Escherichia coli ribosomes. J Mol Biol *92*, 15-37.

Lopez-Alonso, J.P., Kaminishi, T., Kikuchi, T., Hirata, Y., Iturrioz, I., Dhimole, N., Schedlbauer, A., Hase, Y., Goto, S., Kurita, D.*, et al.* (2017). RsgA couples the maturation state of the 30S ribosomal decoding center to activation of its GTPase pocket. Nucleic Acids Res *45*, 6945-6959.

March, P.E., Lerner, C.G., Ahnn, J., Cui, X., and Inouye, M. (1988). The Escherichia coli Ras-like protein (Era) has GTPase activity and is essential for cell growth. Oncogene *2*, 539-544.

Meier, T.I., Peery, R.B., McAllister, K.A., and Zhao, G. (2000). Era GTPase of Escherichia coli: binding to 16S rRNA and modulation of GTPase activity by RNA and carbohydrates. Microbiology *146 (Pt 5)*, 1071-1083.

Mindell, J.A., and Grigorieff, N. (2003). Accurate determination of local defocus and specimen tilt in electron microscopy. J Struct Biol *142*, 334-347.

Minkovsky, N., Zarimani, A., Chary, V.K., Johnstone, B.H., Powell, B.S., Torrance, P.D., Court, D.L., Simons, R.W., and Piggot, P.J. (2002). Bex, the Bacillus subtilis homolog of the essential Escherichia coli GTPase Era, is required for normal cell division and spore formation. J Bacteriol *184*, 6389-6394.

Misra, T.K., and Apirion, D. (1979). RNase E, an RNA processing enzyme from Escherichia coli. J Biol Chem *254*, 11154-11159.

Mizushima, S., and Nomura, M. (1970). Assembly mapping of 30S ribosomal proteins from E. coli. Nature *226*, 1214.

Mulder, A.M., Yoshioka, C., Beck, A.H., Bunner, A.E., Milligan, R.A., Potter, C.S., Carragher, B., and Williamson, J.R. (2010). Visualizing ribosome biogenesis: parallel assembly pathways for the 30S subunit. Science *330*, 673-677.

Nesterchuk, M.V., Sergiev, P.V., and Dontsova, O.A. (2011). Posttranslational Modifications of Ribosomal Proteins in Escherichia coli. Acta Naturae *3*, 22-33.

Nichols, C.E., Johnson, C., Lamb, H.K., Lockyer, M., Charles, I.G., Hawkins, A.R., and Stammers, D.K. (2007). Structure of the ribosomal interacting GTPase YjeQ from the enterobacterial species Salmonella typhimurium. Acta Crystallogr Sect F Struct Biol Cryst Commun *63*, 922-928.

Nissen, P., Hansen, J., Ban, N., Moore, P.B., and Steitz, T.A. (2000). The structural basis of ribosome activity in peptide bond synthesis. Science *289*, 920-930.

Nomura, M. (1969). Ribosomes. Sci Am *221*, 28-35.

Nomura, M. (1970). Bacterial Ribosome. Bacteriol Rev *34*, 228-277.

Nomura, M., and Traub, P. (1968). Structure and function of Escherichia coli ribosomes. 3. Stoichiometry and rate of the reconstitution of ribosomes from subribosomal particles and split proteins. J Mol Biol *34*, 609-619.

Nomura, M., Traub, P., Guthrie, C., and Nashimoto, H. (1969). The assembly of ribosomes. J Cell Physiol *74*, Suppl 1:241+.

Obmolova, G., Ban, C., Hsieh, P., and Yang, W. (2000). Crystal structures of mismatch repair protein MutS and its complex with a substrate DNA. Nature *407*, 703-710.

Ogle, J.M., Brodersen, D.E., Clemons, W.M., Jr., Tarry, M.J., Carter, A.P., and Ramakrishnan, V. (2001). Recognition of cognate transfer RNA by the 30S ribosomal subunit. Science *292*, 897-902.

Pettersen, E.F., Goddard, T.D., Huang, C.C., Couch, G.S., Greenblatt, D.M., Meng, E.C., and Ferrin, T.E. (2004). UCSF Chimera--a visualization system for exploratory research and analysis. J Comput Chem *25*, 1605-1612.

Ramakrishnan, V. (2002). Ribosome structure and the mechanism of translation. Cell *108*, 557-572.

Rasmussen, B., Noller, H.F., Daubresse, G., Oliva, B., Misulovin, Z., Rothstein, D.M., Ellestad, G.A., Gluzman, Y., Tally, F.P., and Chopra, I. (1991). Molecular basis of tetracycline action: identification of analogs whose primary target is not the bacterial ribosome. Antimicrob Agents Chemother *35*, 2306-2311.

Razi, A., Britton, R.A., and Ortega, J. (2017a). The impact of recent improvements in cryo-electron microscopy technology on the understanding of bacterial ribosome assembly. Nucleic Acids Res *45*, 1027-1040.

Razi, A., Guarne, A., and Ortega, J. (2017b). The cryo-EM structure of YjeQ bound to the 30S subunit suggests a fidelity checkpoint function for this protein in ribosome assembly. Proc Natl Acad Sci U S A *114*, E3396-E3403.

Rodriguez-Mateos, M., Garcia-Gomez, J.J., Francisco-Velilla, R., Remacha, M., de la Cruz, J., and Ballesta, J.P. (2009). Role and dynamics of the ribosomal protein P0 and its related trans-acting factor Mrt4 during ribosome assembly in Saccharomyces cerevisiae. Nucleic Acids Res *37*, 7519-7532.

Rosenthal, P.B., and Henderson, R. (2003). Optimal determination of particle orientation, absolute hand, and contrast loss in single-particle electron cryomicroscopy. J Mol Biol *333*, 721-745.

Roy, A., Kucukural, A., and Zhang, Y. (2010). I-TASSER: a unified platform for automated protein structure and function prediction. Nat Protoc *5*, 725-738.

Rubinstein, J.L., and Brubaker, M.A. (2015). Alignment of cryo-EM movies of individual particles by optimization of image translations. J Struct Biol *192*, 188-195.

Sayed, A., Matsuyama, S., and Inouye, M. (1999). Era, an essential Escherichia coli small G-protein, binds to the 30S ribosomal subunit. Biochem Biophys Res Commun *264*, 51-54.

Scheres, S.H. (2012). RELION: implementation of a Bayesian approach to cryo-EM structure determination. J Struct Biol *180*, 519-530.

Schluenzen, F., Tocilj, A., Zarivach, R., Harms, J., Gluehmann, M., Janell, D., Bashan, A., Bartels, H., Agmon, I., Franceschi, F*., et al.* (2000). Structure of functionally activated small ribosomal subunit at 3.3 angstroms resolution. Cell *102*, 615-623.

Schuwirth, B.S., Borovinskaya, M.A., Hau, C.W., Zhang, W., Vila-Sanjurjo, A., Holton, J.M., and Cate, J.H. (2005). Structures of the bacterial ribosome at 3.5 A resolution. Science *310*, 827-834.

Sengupta, J., Agrawal, R.K., and Frank, J. (2001). Visualization of protein S1 within the 30S ribosomal subunit and its interaction with messenger RNA. Proc Natl Acad Sci U S A *98*, 11991-11996.

Shajani, Z., Sykes, M.T., and Williamson, J.R. (2011). Assembly of bacterial ribosomes. Annu Rev Biochem *80*, 501-526.

Shalev-Benami, M., Zhang, Y., Rozenberg, H., Nobe, Y., Taoka, M., Matzov, D., Zimmerman, E., Bashan, A., Isobe, T., Jaffe, C.L*., et al.* (2017). Atomic resolution snapshot of Leishmania ribosome inhibition by the aminoglycoside paromomycin. Nat Commun *8*, 1589.

Sharma, M.R., Barat, C., Wilson, D.N., Booth, T.M., Kawazoe, M., Hori-Takemoto, C., Shirouzu, M., Yokoyama, S., Fucini, P., and Agrawal, R.K. (2005). Interaction of Era with the 30S ribosomal subunit implications for 30S subunit assembly. Mol Cell *18*, 319-329.

Shin, D.H., Lou, Y., Jancarik, J., Yokota, H., Kim, R., and Kim, S.H. (2004). Crystal structure of YjeQ from Thermotoga maritima contains a circularly permuted GTPase domain. Proc Natl Acad Sci U S A *101*, 13198-13203.

Shine, J., and Dalgarno, L. (1974). The 3'-terminal sequence of Escherichia coli 16S ribosomal RNA: complementarity to nonsense triplets and ribosome binding sites. Proc Natl Acad Sci U S A *71*, 1342-1346.

Sirdeshmukh, R., and Schlessinger, D. (1985). Ordered processing of Escherichia coli 23S rRNA in vitro. Nucleic Acids Res *13*, 5041-5054.

Smith, M.T., and Rubinstein, J.L. (2014). Structural biology. Beyond blob-ology. Science *345*, 617-619.

Stewart, D., Chao, A., Kodner, I., Birnbaum, E., Fleshman, J., and Dietz, D. (2009). Subtotal colectomy for toxic and fulminant colitis in the era of immunosuppressive therapy. Colorectal Dis *11*, 184-190.

Stokes, J.M., Davis, J.H., Mangat, C.S., Williamson, J.R., and Brown, E.D. (2014). Discovery of a small molecule that inhibits bacterial ribosome biogenesis. eLife *3*, e03574.

Stokes, J.M., Selin, C., Cardona, S.T., and Brown, E.D. (2015). Chemical inhibition of bacterial ribosome biogenesis shows efficacy in a worm infection model. Antimicrob Agents Chemother *59*, 2918-2920.

Strunk, B.S., Loucks, C.R., Su, M., Vashisth, H., Cheng, S., Schilling, J., Brooks, C.L., 3rd, Karbstein, K., and Skiniotis, G. (2011). Ribosome assembly factors prevent premature translation initiation by 40S assembly intermediates. Science *333*, 1449-1453.

Strunk, B.S., Novak, M.N., Young, C.L., and Karbstein, K. (2012). A translation-like cycle is a quality control checkpoint for maturing 40S ribosome subunits. Cell *150*, 111-121.

Sturn, A., Quackenbush, J., and Trajanoski, Z. (2002). Genesis: cluster analysis of microarray data. Bioinformatics *18*, 207-208.

Subramanian, A.R. (1983). Structure and functions of ribosomal protein S1. Prog Nucleic Acid Res Mol Biol *28*, 101-142.

Sullivan, S.M., Mishra, R., Neubig, R.R., and Maddock, J.R. (2000). Analysis of guanine nucleotide binding and exchange kinetics of the Escherichia coli GTPase Era. J Bacteriol *182*, 3460-3466.

Sulthana, S., and Deutscher, M.P. (2013). Multiple exoribonucleases catalyze maturation of the 3' terminus of 16S ribosomal RNA (rRNA). J Biol Chem *288*, 12574-12579.

Sykes, M.T., and Williamson, J.R. (2009). A Complex Assembly Landscape for the 30S Ribosomal Subunit. Annu Rev Biophys *38*, 197-215.

Talkington, M.W., Siuzdak, G., and Williamson, J.R. (2005). An assembly landscape for the 30S ribosomal subunit. Nature *438*, 628-632.

Thurlow, B. (2016). THE ROLE OF ASSEMBLY FACTORS IN 30S SUBUNIT BIOGENESIS (McMaster University).

Thurlow, B., Davis, J.H., Leong, V., Moraes, T.F., Williamson, J.R., and Ortega, J. (2016a). Binding properties of YjeQ (RsgA), RbfA, RimM and Era to assembly intermediates of the 30S subunit. Nucleic Acids Res *44*, 9918-9932.

Thurlow, B., Davis, J.H., Leong, V., T, F.M., Williamson, J.R., and Ortega, J. (2016b). Binding properties of YjeQ (RsgA), RbfA, RimM and Era to assembly intermediates of the 30S subunit. Nucleic Acids Res.

Trabuco, L.G., Villa, E., Mitra, K., Frank, J., and Schulten, K. (2008). Flexible fitting of atomic structures into electron microscopy maps using molecular dynamics. Structure *16*, 673-683.

Traub, P., and Nomura, M. (1968a). Structure and function of E. coli ribosomes. V. Reconstitution of functionally active 30S ribosomal particles from RNA and proteins. Proc Natl Acad Sci U S A *59*, 777-784.

Traub, P., and Nomura, M. (1968b). Structure and function of Escherichia coli ribosomes. I. Partial fractionation of the functionally active ribosomal proteins and reconstitution of artificial subribosomal particles. J Mol Biol *34*, 575-593.

Traub, P., and Nomura, M. (1969). Studies on the assembly of ribosomes in vitro. Cold Spring Harb Symp Quant Biol *34*, 63-67.

Tu, C., Zhou, X., Tarasov, S.G., Tropea, J.E., Austin, B.P., Waugh, D.S., Court, D.L., and Ji, X. (2011). The Era GTPase recognizes the GAUCACCUCC sequence and binds helix 45 near the 3' end of 16S rRNA. Proc Natl Acad Sci U S A *108*, 10156-10161.

Tu, C., Zhou, X., Tropea, J.E., Austin, B.P., Waugh, D.S., Court, D.L., and Ji, X. (2009). Structure of ERA in complex with the 3' end of 16S rRNA: implications for ribosome biogenesis. Proc Natl Acad Sci U S A *106*, 14843-14848.

Wilson, D.N., and Nierhaus, K.H. (2007). The weird and wonderful world of bacterial ribosome regulation. Crit Rev Biochem Mol Biol *42*, 187-219.

Wimberly, B.T., Brodersen, D.E., Clemons, W.M., Jr., Morgan-Warren, R.J., Carter, A.P., Vonrhein, C., Hartsch, T., and Ramakrishnan, V. (2000). Structure of the 30S ribosomal subunit. Nature *407*, 327-339.

Woodson, S.A. (2008). RNA folding and ribosome assembly. Curr Opin Chem Biol *12*, 667-673.

Woodson, S.A. (2011). RNA folding pathways and the self-assembly of ribosomes. Accounts of chemical research *44*, 1312-1319.

Xu, Z., O'Farrell, H.C., Rife, J.P., and Culver, G.M. (2008). A conserved rRNA methyltransferase regulates ribosome biogenesis. Nat Struct Mol Biol *15*, 534-536.

Yang, Z., Guo, Q., Goto, S., Chen, Y., Li, N., Yan, K., Zhang, Y., Muto, A., Deng, H., Himeno, H.*, et al.* (2014). Structural insights into the assembly of the 30S ribosomal subunit in vivo: functional role of S5 and location of the 17S rRNA precursor sequence. Protein & cell *5*, 394-407.

Yoshizawa, S., Fourmy, D., and Puglisi, J.D. (1999). Recognition of the codon-anticodon helix by ribosomal RNA. Science *285*, 1722-1725.

Yusupov, M.M., Yusupova, G.Z., Baucom, A., Lieberman, K., Earnest, T.N., Cate, J.H., and Noller, H.F. (2001). Crystal structure of the ribosome at 5.5 A resolution. Science *292*, 883-896.

Zhao, G., Meier, T.I., Peery, R.B., Matsushima, P., and Skatrud, P.L. (1999). Biochemical and molecular analyses of the C-terminal domain of Era GTPase from Streptococcus pneumoniae. Microbiology *145 (Pt 4)*, 791-800.

List of the attached papers in appendix

1. Ribosomal proteins: Their role in the assembly, structure and function of the ribosome

Aida Razi and Joaquin Ortega

eLS, 2017 September; 10.1002/978047001590 **(attached)**.

2. Final touches and quality control on the assembly of the eukaryotic ribosome

Aida Razi and Joaquin Ortega

EMBO J., 2017; 36(7):834-836 **(attached)**.

3. The Impact of recent improvements in cryo-electron microscopy technology on the understanding of bacterial ribosome assembly.

Aida Razi, Robert A. Britton and Joaquin Ortega

Nucleic Acid Research, 2016 November; 45(3):1027-1040 **(attached)**.

4. YphC and YsxC GTPases assist the maturation of the central protuberance, GTPase associated region and functional core of the 50S ribosomal subunit.

Xiaodan Ni, Joseph H. Davis, Nikhil Jain, Aida Razi, Samir Benlekbir, Andrew G. McArthur, John L. Rubinstein, Robert A. Britton, James R. Williamson, and Joaquin Ortega

Nucleic Acids Research, 2016 July; 44:8442-55 **(attached)**.

5. YjeQ zinc finger domain monitors the conformation of the decoding center and catalyzes the release of RbfA during 30S ribosome subunit assembly.

Ajitha Jeganathan, Aida Razi, Brett Thurlow and Joaquin Ortega

RNA*, 2015;* 21: 1203-1216 **(attached)**.

Appendix

Ribosomal Proteins: Their Role in the Assembly, Structure and Function of the Ribosome

Aida Razi, *Department of Anatomy and Cell Biology, McGill University, Montreal, Quebec, Canada*

Joaquin Ortega, *Department of Anatomy and Cell Biology, McGill University, Montreal, Quebec, Canada*

Based in part on the previous version of this eLS article 'Ribosomal Proteins: Structure and Evolution' (2001) by Brigitte Wittmann-Liebold and Hanns-Rüdiger Graack.

Introductory article

Article Contents

Online posting date: 15th September 2017

The ribosome is the macromolecular assembly dedicated to translating the genetic information into proteins. Ribosomes are made of several RNA molecules and between 50 and 80 proteins. The role played by these proteins has been the focus of investigations for over five decades. Initially, proteins were thought to be the only functional component of the ribosome, whereas the rRNA was considered merely a scaffold. This view has evolved and now is clear that both the RNA and protein components of the ribosome are functionally important. The r-proteins play a role in the assembly process of the ribosome and are also essential for the structure and function of the ribosome. Their importance in the physiology of the ribosome is revealed by the fact that mutations in ribosomal proteins lead to ribosomopathies, a group of diseases that include developmental, haematological, metabolic and cardiovascular disorders, as well as cancers.

Introduction

Ribosomes are essential enzymes that synthesize all proteins in the cell. All ribosomes consist of two subunits, a large and a small one, each containing rRNA and several dozens of ribosomal proteins (r-proteins). Our understanding of the contributions of the r-proteins to the structure and function of the ribosome has evolved over the years, as new insights into the processes of ribosome assembly and protein synthesis were discovered. Functional models of the ribosome in the 1970s initially suggested that r-proteins are the functional component of the ribosome and the rRNA is merely a scaffold keeping the r-proteins in optimal position for function. However, the subsequent decade brought clear evidence that the rRNA is involved in ribosomal function. An example is the interactions of the Shine–Dalgarno with the messenger RNA (mRNA) during initiation of protein synthesis or the fact that the decoding centre and peptidyl transferase centre (PTC) is exclusively made of rRNA. These discoveries changed the previous view and created in the 1980s a new prevailing model suggesting that the r-proteins constitute the scaffold that stabilises the structure of the rRNA for optimal function. Further research in the last 20 years has made clear that the ribosome functions following a model that lies somewhere in between these two extremes. It is now accepted that r-proteins are much more than a simple 'RNA glue' (Wilson and Nierhaus, 2005) and they have several specific functions. **See also: Ribosomal Proteins: Role in Ribosomal Functions**; **Ribosomes and Ribosomal Proteins: More Than Just 'Housekeeping'**

Several examples have been identified of r-proteins that directly participate in key aspects of the ribosome functionality, including decoding fidelity, binding of elongation factors or controlling the access of the nascent peptide chain into the channel. It is clear now that a prerequisite for optimal functioning of the ribosome requires an extensive interplay between r-proteins and rRNA. Even though not all the r-proteins are essential (about one third are dispensable), the current view is that both r-proteins and rRNA are equally important for the assembly and function of the ribosome.

eLS subject area: Biochemistry

How to cite:
Razi, Aida and Ortega, Joaquin (September 2017) Ribosomal Proteins: Their Role in the Assembly, Structure and Function of the Ribosome. In: eLS. John Wiley & Sons, Ltd: Chichester.
DOI: 10.1002/9780470015902.a0000535.pub2

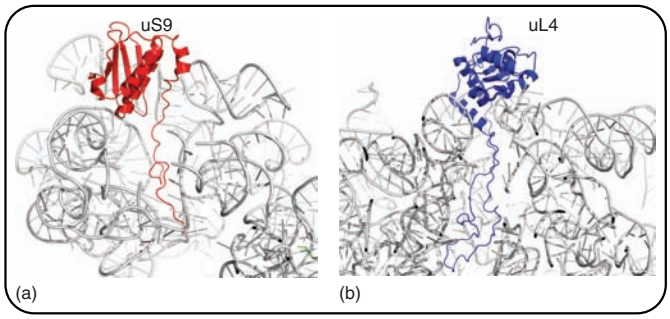

Figure 1 **Ribosomal proteins exhibit globular domains and long extensions.** Proteins in the ribosome typically contain one or more globular domains that locate in the surface of the ribosome and long extensions that reach far into the internal parts of the ribosome. r-Protein uS9 (a) and uL4 (b) from *Bacillus subtilis* showing this frequent topology. Reprinted from Sohmen *et al.* (2015) © Nature Communications distributed under the terms of the Creative Commons Attribution License (http://creativecommons.org/licenses/by/4.0/).

Most of the r-proteins are located around the periphery of the ribosome structure and few of them are located at the interaction surface between the two subunits. Proteins in the ribosome typically contain one or more globular domains with similar folds found in other non-r-proteins. This includes, for example, β-barrels or α-helices packed against a β-sheet and often similar domains found in different r-proteins interact with RNA in different ways (Wimberly *et al.*, 2000). Nearly all r-proteins contain long extensions in addition to their globular domains. These can be helical, long β-hairpins or unstructured loops. These extensions make intimate contacts with the rRNA and reach far into the internal parts of the ribosome (**Figure 1**). They are rich in basic residues, which allow them to neutralise the charge repulsion of the RNA backbone. Importantly, these extensions allow r-proteins to contact several RNA elements simultaneously, which is probably important for the stabilization of the overall structure of the ribosomal subunits and to implement allosteries existing between r-proteins and rRNA.

In this article, we first described how the ribosome field has recently adopted a new nomenclature system to name the r-proteins in the eukaryotic and prokaryotic ribosome. Next, we explain the different protein complement exhibited by the ribosome in bacteria, yeast and human mitochondria and our current understanding of the function of r-proteins in both the assembly process of the ribosome and protein translation. Mutations in r-proteins lead to a slow growth phenotype in bacteria and a group of diseases in eukaryotes generically known as ribosomopathies. These severe phenotypes reveal that r-proteins play important roles. We also described how ribosomal proteins have represented an extremely useful tool for the study of protein evolution.

Current Nomenclature of Ribosomal Proteins

Since the 1960s that ribosome investigations began, several conventions for naming r-proteins became embedded in the literature. Each laboratory working in the r-proteins from *Escherichia coli* devised its own naming system making very difficult to make sense of the published data. The problem became larger when other groups started to assign names to archaeal and eukaryotic ribosomal proteins. Some of these names were the same as those used in the bacterial ribosome. However, at the time names were assigned, the sequences of the r-proteins had not been determined and the same names were used for different r-proteins. Compounding the problem, groups working in yeast ribosomal proteins developed several naming systems.

Fortunately, in 2014 the field came together and adopted a new convention for naming r-proteins (**Tables 1 and 2**) (Ban *et al.*, 2014) that is now broadly adopted. The r-proteins in *E. coli* were the first to be identified and sequenced. Consequently, their archaeal and eukaryotic homologues were assigned *E. coli* names. The r-proteins found in the three domains of life (bacterial, archaea and eukaryotes) are given the prefix 'u' for 'universal' followed by the bacterial names first adopted in 1971 (Wittmann *et al.*, 1971). In the 1971 convention, r-proteins from the small subunit have the form of SX, where X is a number, and r-proteins from the larger subunit are designated LY, where Y is also a number. Bacterial proteins without a eukaryotic homologue are designated using the prefix 'b'. Finally, eukaryotic proteins without a bacterial homologue have the letter 'e' before the protein name.

Structure of the Ribosome in Different Organisms

In all living organisms, the ribosome consists of two functional subunits: a smaller subunit (**Figure 2a**) responsible for base pairing between the mRNA codon and the aminoacyl-transfer ribonucleic acid (tRNA) anticodon at the decoding centre; and a larger subunit (**Figure 2b**) responsible for peptide bond formation at the peptidyl transferase centre. Although ribosomes carry the same function in all living organisms, they are different in size and level of complexity. The overall shape of the ribosomes was first observed in negatively stained electron microscopy

Table 1 New nomenclature for r-proteins from the small ribosomal subunit

New name	Bacteria name	Yeast name	Human name
bS1	S1	–	–
eS1	–	S1	S3A
uS2	S2	S0	SA
uS3	S3	S3	S3
uS4	S4	S9	S9
eS4	–	S4	S4
uS5	S5	S2	S2
bS6	S6	–	–
eS6	–	S6	S6
uS7	S7	S5	S5
eS7	–	S7	S7
uS8	S8	S22	S15A
eS8	–	S8	S8
uS9	S9	S16	S16
uS10	S10	S20	S20
eS10	–	S10	S10
uS11	S11	S14	S14
uS12	S12	S23	S23
eS12	–	S12	S12
uS13	S13	S18	S18
uS14	S14	S29	S29
uS15	S15	S13	S13
bS16	S16	–	–
uS17	S17	–	–
eS17	–	S17	S17
bS18	S18	–	–
uS19	–	S19	S19
bS20	S20	–	–
bS21	S21	–	–
bTHX	THX	–	–
eS21	–	S21	S21
eS24	–	S24	S24
eS25	–	S25	S25
eS26	–	S26	S26
eS27	–	S27	S27
eS28	–	S28	S28
eS30	–	S30	S30
eS31	–	S31	S27A
RACK1	–	Asc1	RACK1

b, bacterial; e, eukaryotic; u, universal.

images (Vasiliev, 1974; Lake, 1976). Cryo-electron microscopy (cryo-EM) and single particle analysis rendered the first 3D structures of ribosomes (Frank, 1997). However, it was only when the X-ray structures of the individual bacterial ribosomal subunits (Ban *et al.*, 2000; Wimberly *et al.*, 2000; Harms *et al.*, 2001) and the entire ribosome (Yusupov *et al.*, 2001; Schuwirth *et al.*, 2005) began to emerge that accurate atomic models of the bacterial ribosome became available. Remarkable recent advances in direct electron detectors for cryo-EM (Desai *et al.*, 2017) and crystallography (Ben-Shem *et al.*, 2011) over the last decade have provided also atomic resolution models of the eukaryotic ribosome (**Figure 3**). **See also: Single Particle EM**

Table 2 Nomenclature for r-proteins from the large ribosomal subunit

New name	Bacteria name	Yeast name	Human name
uL1	L1	L1	L10A
uL2	L2	L2	L8
uL3	L3	L3	L3
uL4	L4	L4	L4
uL5	L5	L11	L11
uL6	L6	L9	L9
eL6	–	L6	L6
eL8	–	L8	L7A
bL9	L9	–	–
uL10	L10	P0	P0
uL11	L11	L12	L12
bL12	L7/L12	–	–
uL13	L13	L16	L13A
eL13	–	L13	L13
uL14	L14	L23	L23
eL14	–	L14	L14
uL15	L15	L28	L27A
eL15	–	L15	L15
uL16	L16	L10	L10
bL17	L17	–	–
uL18	L18	L5	L5
eL18	–	L18	L18
bL19	L19	–	–
eL19	–	L19	L19
bL20	L20	–	–
eL20	–	L20	L18A
bL21	L21	–	–
eL21	–	L21	L21
uL22	L22	L17	L17
eL22	–	L22	L22
uL23	L23	L25	L23A
uL24	L24	L26	L26
eL24	–	L24	L24
bL25	L25	–	–
bL27	L27	–	–
eL27	–	L27	L27
bL28	L28	–	–
eL28	–	–	L28
uL29	L29	L35	L35
eL29	–	L29	L29
uL30	L30	L7	L7
eL30	–	L30	L30
bL31	L31	–	–
eL31	–	L31	L31
bL32	L32	–	–
eL32	–	L32	L32
bL33	L33	–	–
eL33	–	L33	L35A
bL34	L34	–	–
eL34	–	L34	L34
bL35	L35	–	–
bL36	L36	–	–
eL36	–	L36	L36

(*continued overleaf*)

Table 2 (*continued*)

New name	Bacteria name	Yeast name	Human name
eL37	–	L37	L37
eL38	–	L38	L38
eL39	–	L39	L39
eL40	–	L40	L40
eL41	–	L41	L41
eL42	–	L42	L36A
eL43	–	L43	L37A
P1/P2	–	P1/P2	P1/P2

b, bacterial; e, eukaryotic; u, universal.

The bacterial ribosome is a 70S assembly with a molecular mass of 2.3 MDa and comprised of the small 30S and large 50S subunits (**Figures 2 and 4a**). The 30S subunit is made of 16S rRNA and 21 r-proteins named from S1 to S21 (with a prefix u or b; see below) (**Table 3**) (Ban *et al.*, 2014). The 16S rRNA folds into four domains that constitute the key landmarks of the 30S subunit: body (5′ domain), platform (central domain), head (3′ major domain) and helix 44 (3′ minor domain) (**Figure 2a**) (Wimberly *et al.*, 2000). The four domains fold around the decoding centre that constitutes the functional core of the 30S subunit. The 50S subunit is made of the 5S and 23S rRNAs and 34 r-proteins designated from L1 to L36 (with u or b prefix) (**Table 3**) (Ban *et al.*, 2014). The view frequently referred to as the 'crown view' of the 50S subunit looks like a halved pear, where the bottom is the 'body' and the top is called 'central protuberance'. The two lateral protuberances are the L1 and L7/L12 stalks. The front side of the 50S particle is a flat surface through which the particle interfaces with the 30S subunit. The back of the particle is round and faces the solvent (**Figure 2b**). The 23S rRNA forms most of the body of the 50S subunit and the 5S rRNA is an important component of the central protuberance. The six different domains identified in the secondary structure of the 23S rRNA and the one domain in the 5S rRNA do not fold into independent domains,

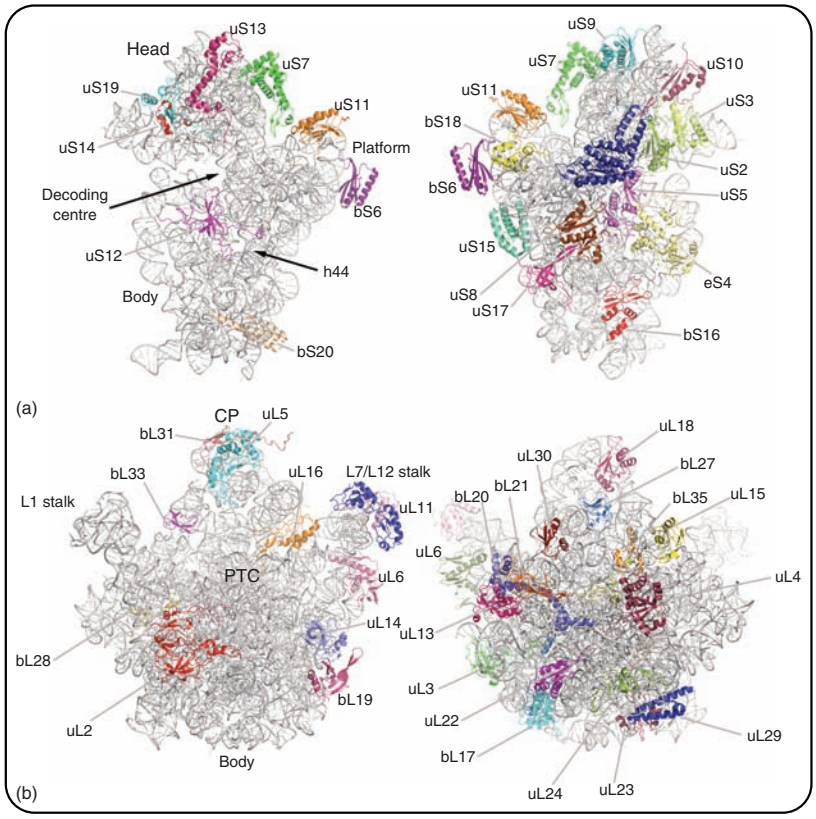

Figure 2 **Structure and main landmarks of the bacterial ribosomal subunits.** (a) Front (left) and back (right) views of the structure of the 30S subunit. Labels indicate the main landmarks of the ribosomal subunit and the r-proteins. Panel (b) shows the 'crown view' (left) and solvent (right) view of the 50S subunit of *Bacillus subtilis*, respectively. Reprinted from Sohmen *et al.* (2015) © Nature Communications distributed under the terms of the Creative Commons Attribution License (http://creativecommons.org/licenses/by/4.0/)

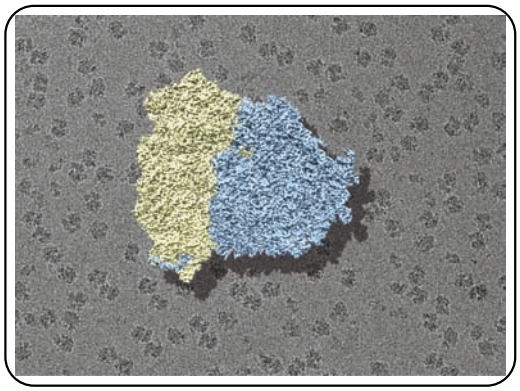

Figure 3 Structure of the human 80S ribosome obtained by cryo-electron microscopy. Cryo-electron microscopy of the human 80S ribosome. The 40S subunit is shown in yellow and the 60S subunit is coloured in cyan. The background picture is an electron micrograph obtained by cryo-electron microscopy using a Gatan K2 direct electron detector. Reprinted by permission from Macmillan Publishers Ltd: Nature (Khatter H, Myasnikov AG, Natchiar SK, Klaholz BP. Structure of the human 80S ribosome 520, 640–645), copyright (2015).

as it is the case for the 30S subunit with the 16S rRNA. Instead, the seven domains of the two rRNA molecules fold into a compact intertwined structure (Ban *et al.*, 2000). In the 70S ribosome, there are several intersubunit contacts, or bridges, that hold the two ribosomal subunits together. Most of these contacts break or rearrange during the translation cycle (**Figure 4a**) (Yusupov *et al.*, 2001; Schuwirth *et al.*, 2005). **See also: Bacterial Ribosomes**

In eukaryotes, the ribosome is made of the 40S and 60S subunits, which upon association form the 80S particle (**Figure 4b,c**). The size of the eukaryotic 80S ribosome ranges from 3.3 MDa in lower eukaryotes to 4.3 MDa in higher eukaryotes. The eukaryotic ribosome shares a common structural core with the bacterial ribosome. This core is comprised of 15 r-proteins in the small subunit, 19 in the large subunit and 4400 bases in the rRNA. Most of these bases in the rRNA are in the functional cores of the two subunits. Most of the r-proteins in this core contain additional extensions and insertions. In addition to the core r-proteins, the 80S ribosome contains eukaryote-specific proteins. Except for the stalk proteins (P r-proteins) that are present in four or six copies, each r-protein is present as a single copy, similarly to the bacterial ribosome. The rRNA molecule in the 40S subunit is called 18S rRNA. The 60S subunit is formed by three different rRNA molecules (25S rRNA, 5.8 rRNA and 5S rRNA), instead of the two found in bacteria (**Table 3**). All the eukaryotic rRNA molecules contain additional bases that are not found in the bacterial ribosome. The eukaryotic 40S and 60S subunits share also structural similarity with the bacterial small and large subunits, respectively. The 40S subunit has similar landmarks to that of the 30S subunit, including the body, head, platform and helix 44. The 60S subunit is also comprised of the body, central protuberance and two stalks (L1 and P-stalks). **See also: Ribosomal Proteins in Eukaryotes**

The structure of the 80S ribosome from *Saccharomyces cerevisiae* was determined by X-ray crystallography in 2011 (Ben-Shem *et al.*, 2011), providing an atomic resolution description of its 79 proteins and 5500 rRNA bases (**Figure 4b**). Forty-five of the r-proteins in this ribosome are eukaryote specific (**Table 3**). Many of them have unusual folds and contain remarkably long tails and loops extending from the globular domains of the r-proteins. Interestingly, most of these extensions are located in the surface of the ribosome and not buried between rRNA, as it is the case for the bacterial ribosome (**Figure 1**). Each intersubunit bridge that has been described in the bacterial 70S ribosome has a counterpart in the 80S ribosome. However, the 80S ribosome features additional eukaryotic specific bridges. In contrast to bacteria where RNA–RNA contacts are predominant, r-proteins are the main element participating in establishing the intersubunit contacts in the yeast ribosome.

In humans, the 80S ribosome (**Figure 4c**) has a molecular weight of 4.3 MDa and contains the same four rRNA molecules found in the yeast ribosome plus 80 r-proteins (33 in the 40S subunit and 47 in the 60S subunit). This is one additional protein (eL28) compared to the yeast ribosome (**Table 3**).

In the last 2 years, the structure of the highly divergent ribosomes of human (**Figure 4d**) (Amunts *et al.*, 2015) and yeast

Table 3 Components of the ribosome in different organisms

Bacteria (*E. coli*)	Lower eukaryotes (*S. cerevisiae*)	Higher eukaryotes (*H. sapiens*)	Yeast mitochondrial (*S. cerevisiae*)	Human mitochondrial (*H. sapiens*)
2.3 MDa	3.3 MDa	4.3 MDa	3.3 MDa	2.8 MDa
54 proteins	79 proteins	80 proteins	75 proteins	80 proteins
3 rRNA	4 rRNA	4 rRNA	2 rRNA	2 rRNA
Large subunit (50S)	**Large subunit (60S)**	**Large subunit (60S)**	**Large subunit (60S)**	**Large subunit (60S)**
33 proteins	46 proteins	47 proteins	39 proteins	50 proteins
23 rRNA – 2904 bases	5.8S rRNA – 158 bases	5.8S rRNA – 156 bases	21S rRNA – 3296 bases	16S mt-rRNA – 1559 bases
5S rRNA – 121 bases	25S rRNA – 3396 bases	28S rRNA – 5034 bases		
	5S rRNA – 121 bases	5S rRNA – 121 bases		mt-tRNA^{Val} 73 bases
Small subunit (30S)	**Small subunit (40S)**	**Small subunit (40S)**	**Small Subunit (40S)**	**Small Subunit (40S)**
21 proteins	33 proteins	33 proteins	34 proteins	30 proteins
16S rRNA – 1542 bases	18S rRNA – 1800 bases	18S rRNA – 1870 bases	15S rRNA – 1649 bases	12S mt-rRNA – 954 bases

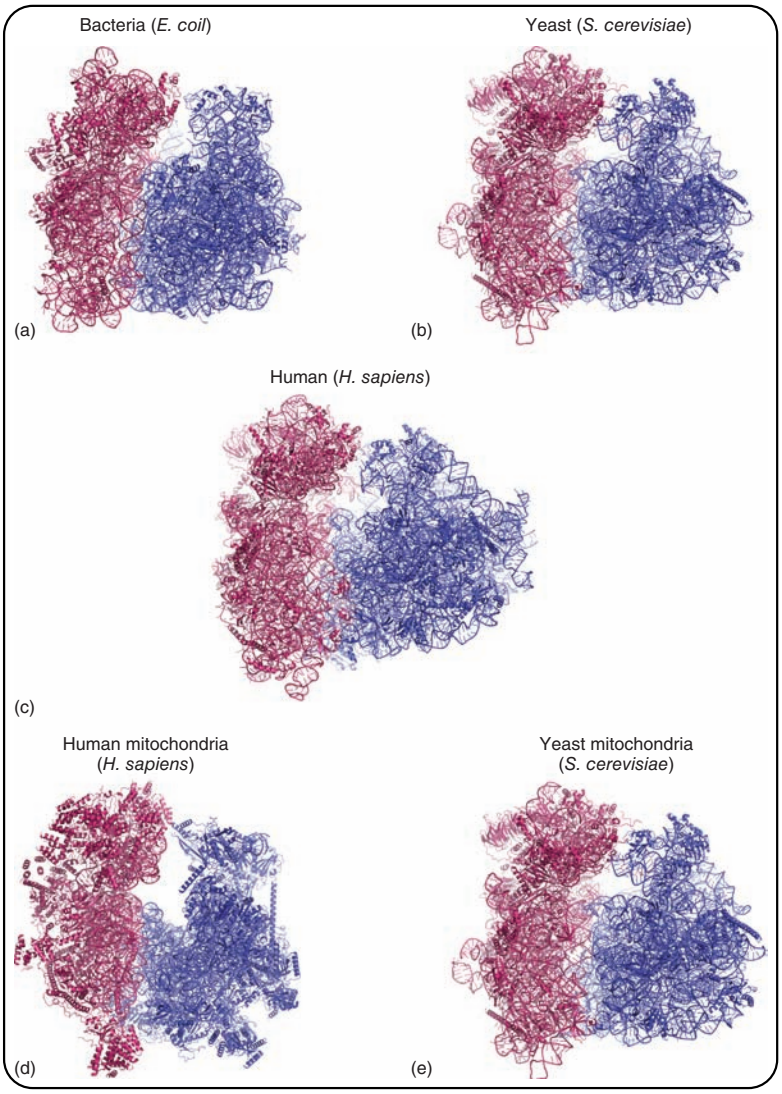

Figure 4 **Gallery of ribosomal structures.** A side-by-side comparison of the structures of the bacteria (*E. coli*) (PDB ID: 4v4q) (a), yeast (*S. cerevisiae*) (PDB ID: 4v88) (b) and human (PDB ID: 4ug0) (c) ribosomes. Panel (d) and (e) show the structures of the mitochondrial ribosome from human (PDB ID: 3j9m) and yeast (PDB ID: 5mrf), respectively.

(**Figure 4e**) (Desai *et al.*, 2017) mitochondria (mitoribosomes) have been obtained using cryo-EM.

The structure of the human mitochondrial ribosome reveals that this assembly is comprised of 80 r-proteins (30 r-proteins in the small subunit and 50 in the large subunit) that are extensively interconnected (**Table 3**). Thirty-six of the r-proteins are specific to mitochondria and the r-proteins with homologues in bacteria have substantial extensions. The increase in protein mass causes the mitochondrial ribosome to have a distinct morphology. It contains three rRNA molecules as the bacterial ribosome. The 12S mt-rRNA is the RNA component in the small subunit and the 16S mt-rRNA and mt-tRNA^{Val} are the two molecules in the large subunit (**Table 3**). The mt-rRNA in this ribosome is about half the size of that in bacteria. The sequences that are common to the bacterial rRNA adopt similar conformations, except for helix 44 in the small subunit. This helix is a universal element

forming part of the decoding centre and it is also used to form essential intersubunit bridges. In bacteria, the lower part of helix 44 is rigid and anchors through interactions with bS20. However, in the human mitochondrial ribosome, the lower part of the helix is highly flexible.

The yeast mitochondrial ribosome is somehow different from its human counterpart. It is a 75-component assembly, but with less extensive rRNA contractions. It contains two rRNA molecules (21S rRNA in the large subunit and 15S rRNA in the small subunit) and a mt-tRNA. The small subunit contains 34 r-proteins from which 14 are mitochondria specific. The protein complement in the large subunit is comprised of 39 r-proteins with 13 of them unique to mitochondria (**Table 3**).

Overall, all these structures reveal that bacterial and eukaryotic ribosomes share a conserved core and suggest that ribosomes from different domains of life evolved from a common ancestor by addition of r-proteins and RNA sequences that confer extra functionalities to these ribosomes.

Overview on the Function of Ribosomal Proteins

The number of r-proteins forming part of the ribosome structure ranges from 54 in bacteria to 80 in humans (**Table 3**), but despite the presence of so many r-proteins the ribosome is functionally a ribozyme. Although the participation of the r-proteins in the peptide bond formation was entertained in the mid-1970s, it was found subsequently that the peptidyl transferase activity of the ribosome was extremely resistant to procedures that extract, denature and digest proteins (Noller *et al.*, 1992). The structure of the 50S ribosomal subunit (Ban *et al.*, 2000) showing that there are no protein elements within 17 Å of the catalytic site for the peptidyl transferase centre put finally to rest the possibility of r-protein participating in the catalysis of peptide bond formation.

Then, if the ribosome is a ribozyme that functions as a RNA-based catalyst to promote peptide bond formation, what are the roles of the r-proteins? Foundational work by Nomura (Mizushima and Nomura, 1970) and Nierhaus (Roth and Nierhaus, 1980) earlier revealed a clear role of r-proteins in driving folding of the rRNA and, thus, in ribosome biogenesis. However, there have been a more limited number of studies successfully identifying specific roles of r-proteins in the context of mature ribosomal particles. The r-proteins have been also believed to possess ribosome-independent functions since their discovery. Significant progress has been made over the past decade in identifying many examples of r-proteins with a function beyond the ribosome. For example, there are more than a dozen of eukaryotic r-proteins that have been found to activate the tumour suppressor p53 pathway and play a role in tumorigenesis. Ribosome-free r-proteins can act as either oncoproteins or tumour suppressors. Beyond these roles, other r-proteins have been shown to participate in the innate immune response (Zhou *et al.*, 2015).

Function of the Ribosomal Proteins in the Assembly of the Ribosome

The role of r-proteins in ribosomal assembly assisting the folding of the rRNA is now well established. Vintage experiments by Nomura and (Traub and Nomura, 1969) and Nierhaus (Roth and Nierhaus, 1980) defined the hierarchy of binding of the r-proteins to the bacterial 30S and 50S subunits, respectively. The r-proteins are designated as primary (bind directly to the rRNA), secondary (binding is dependent on primary binding r-proteins) or tertiary (binding is dependent on secondary binding r-proteins).

Work from the Woodson laboratory and others (Woodson, 2011) showed that in the absence of r-proteins, the rRNA rapidly folds into secondary and tertiary structures resembling those found in the ribosomal subunits. However, as the rRNA folds, it easily becomes kinetically trapped in local energy minima of its folding landscape. The presence of r-proteins during folding prevents the rRNA to fall into these energetic traps and also expands the structural space accessible to rRNA stabilising complex RNA folds that are inaccessible to pure RNA (**Figure 5**). Binding of r-proteins simultaneously during folding guides the rRNA folding and keeps it in a pathway leading to the correct structure. These studies also revealed that r-proteins assist rRNA folding by an induced fit mechanism in which both the r-protein and rRNA undergo structural changes. The r-protein initially interacts forming a labile complex with the rRNA that strengthens as assembly and co-folding proceeds. RNA structure probing experiments from the Noller, Woodson and Weeks laboratories have also provided evidence that much of the native rRNA secondary structure in the ribosomal particles is formed in a protein-independent manner, whereas native tertiary rRNA contacts are often stabilised through protein-binding events (Adilakshmi *et al.*, 2008).

Even though the folding of the rRNA is driven by interaction with r-proteins, the assembly of the ribosomal subunits *in vivo* is highly flexible. Folding can occur through multiple accessible pathways, assuring complete assembly still occurs even when a r-protein is limiting. This was elegantly demonstrated recently by the Williamson lab by using a genetic system to starved cells of the essential r-protein bL17 (Davis *et al.*, 2016). Depletion of this protein caused the accumulation of 13 distinct assembly intermediates, structure of which was determined to be 4–5 Å using cryo-EM and quantitative mass spectrometry. These structures revealed that the protein-driven folding of the rRNA can be rerouted through different pathways as needed as well as the complexity of the folding landscape of the rRNA during assembly.

Function of the Ribosomal Proteins in the Ribosome Structure and Function

It has been more challenging to identify individual functions for r-proteins during translation. This is because of the highly cooperative nature of the interactions between rRNA and r-proteins and between r-proteins themselves. This cooperativity

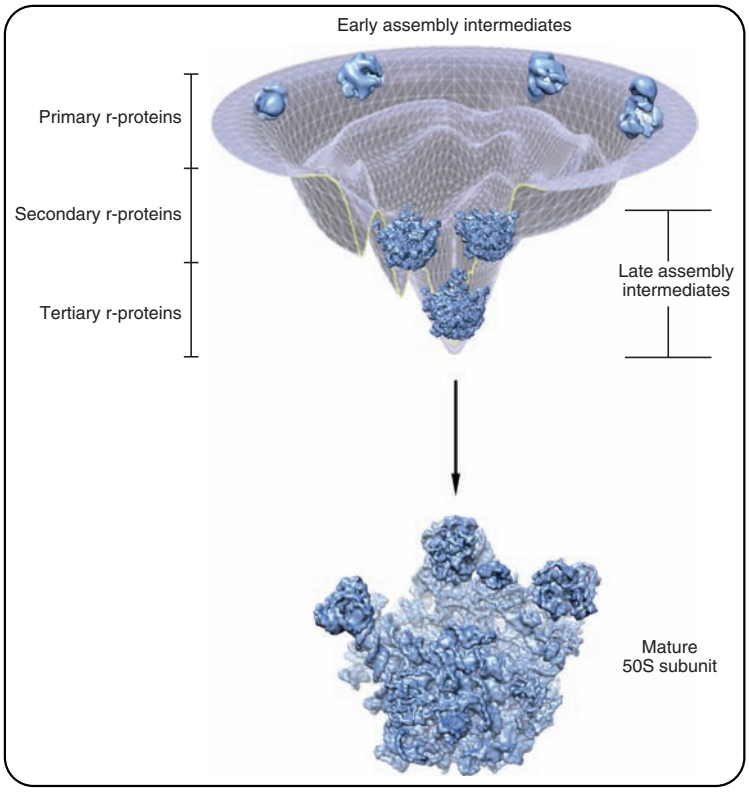

Figure 5 **Ribosomal proteins assist the folding of the rRNA during ribosomal assembly.** A hypothetical folding landscape for the 50S ribosomal subunit. At the top of the energy funnel, the rRNA starts to fold. Binding of r-proteins, simultaneously during folding, guides the rRNA folding and keeps it in a pathway leading to the correct structure. The r-proteins are designated as primary when they bind directly to rRNA, secondary when binding is dependent on primary r-proteins or tertiary for those when binding depends on secondary r-proteins. The structure at the bottom represents the 50S subunit after reaching the mature state.

became apparent early on in experiments performed in the late 1970s, while characterising suppressor strains of *E. coli* to a specific streptomycin-dependent mutant. Surprisingly, strains reverting to an independent phenotype showed mutations in any of the 50 r-proteins (Dabbs, 1978). Allosteric regulations have been also found between r-proteins located as distant as opposite sides of the ribosome. In addition, some r-proteins (or parts of them) are highly flexible and their precise placement in the ribosome structure is still not fully established and this fact has hindered efforts in their functional elucidation. At least 22 r-proteins in *Bacillus subtilis* have been found to be nonessential when deleted individually (Akanuma *et al.*, 2012). This raises the question of whether these r-proteins contribute any function during translation or even why they have been preserved during evolution.

Nevertheless, several studies from the last two decades have been successful in identifying individual r-proteins playing a significant role in the functionality of the ribosome. In this section, we describe a few of these examples. In bacteria, bS1 is an r-protein weakly bound to the ribosome that also interacts with mRNA. It has been proposed that bS1 actively participates in translation initiation possibly by interacting with the mRNA and directing it to the ribosome, thereby assisting subsequent mRNA interactions with the anti-Shine-Delgarno sequence in the 3′ end of the 16SrRNA (Suryanarayana and Subramanian, 1983). Also in bacteria, a few r-proteins influence significantly the accuracy of the decoding process and ultimately the fidelity by which the ribosome translates the sequence of the mRNA into a protein. uS12 is one of these proteins, and both mutations or the complete absence of this protein increases the accuracy of the ribosome. These findings suggest that S12 increases the rate of translation at the cost of accuracy. Conversely, mutations in uS4 and uS5 genes cause a severe reduction in translation accuracy. One last bacterial example is bL7/L12 r-proteins, which form one of the two stalks of the 50S subunit. These proteins are involved in the binding of elongation factors EF-Tu and EF-G as well as the initiation factor IF-2 and the release factor RF-2 (Agrawal *et al.*, 1998).

The roles of eukaryotic r-proteins in the functioning of the translation machinery have been studied in less detail than those in bacteria. However, there are recent studies combining structural, biochemical and genetic approaches suggesting implication of many eukaryotic r-proteins in binding participating molecules of the translation machinery. Interestingly, most of the r-proteins in bacteria for which a function has been identied have a eukaryotic counterpart, initially implying these proteins have the same function in eukaryotes. However, existing examples made clear that evolutionary conservation does not necessarily mean the same functional roles (Graifer and Karpova, 2015). For example, uS4 in bacteria participates in the entry of the mRNA molecule, while location of its eukaryotic counterpart in the 40S subunit excludes this function (Rabl *et al.*, 2011). Consequently, the assignment of specific functions to eukaryotic r-proteins typically requires additional new data. Overall, their roles remain much less well understood mainly because methods for *in vitro* reconstitution of eukaryotic ribosomes are not available yet. This limitation makes it difficult to study the role of individual r-proteins by analysis of reconstituted ribosomes missing a r-protein or with this r-protein carrying specific mutations. In this regard, yeast genetics has been a useful tool to produce ribosomes *in vivo* lacking r-proteins or containing specific mutations on them and identify the function of individual r-proteins (Ghosh *et al.*, 2014). Similarly, cross-linking studies revealing intimate contacts of r-proteins with various ligands of the eukaryotic ribosomes, mRNA and translation factors (Demeshkina *et al.*, 2003; Graifer *et al.*, 2004) and the recent atomic and near atomic resolution structures of eukaryotic ribosomes obtained by X-ray crystallography (Lomakin and Steitz, 2013) or cryo-EM (**Figure 4**) (Voorhees *et al.*, 2014) have also been effective sources for identifying functions of r-proteins in the translation process. These approaches have revealed that r-proteins in eukaryotes are implicated in numerous interactions with the translational machinery and many of the r-proteins have several functions (Graifer and Karpova, 2015).

What Makes a True Ribosomal Protein?

The r-proteins are not the only proteins interacting with the rRNA as it folds during subunit assembly. Two other large groups of proteins also become associated with the ribosome at specific stages along the assembly pathway: placeholder proteins and assembly factors. **See also: Factor-Mediated Ribosome Assembly in Bacteria**; **Bacterial Ribosomes: Assembly**

Placeholder factors are a distinct group of trans-acting factors. In the classical view first proposed by S. J. Baserga (Dunbar *et al.*, 2000), proteins in this group are r-protein paralogues that share extensive identity and similarity to them (Espinar-Marchena *et al.*, 2017). They are not components of the mature ribosome and are unable to functionally replace their r-protein counterpart. However, they all have a role in ribosome assembly. Placeholder factors delay the incorporation of r-proteins by binding to the same rRNA structures in the assembling ribosomal subunits that the r-proteins bind typically with higher affinity. By this strategy, placeholder factors prevent premature recruitment to the nascent preribosomal particles of the respective r-protein counterpart, catalysing important events that only the placeholder factors can exert or prevent the rRNA to fold into kinetically trapped intermediates that impede downstream maturation steps. The best characterised example is that of the r-protein uL10 and its paralogue Mrt4 in *S. cerevisiae*. These two proteins compete for the same binding site in the rRNA, but they are never present at the same time in the pre-60S particles or mature 60S subunits.

Assembly factors, on the other hand, are a plethora of proteins that facilitate not only the binding of r-proteins. Overall, they constitute a platform to regulate and implement rRNA modifications and processing, as well as for quality control of the ribosomal particles that are produced. In eukaryotes, these factors also mediate the intranuclear transport and exit of the preribosomal particles to the cytoplasm, as well as carriage of the r-proteins synthesised in the cytoplasm to the nucleus for association with the preribosomal particles. Bacteria represents the organism using the lowest number of factors with only about 20 reported to participate in the ribosome assembly process (Wilson and Nierhaus, 2007; Shajani *et al.*, 2011). In archaea, about 40 protein trans-acting factors have been described (Ebersberger *et al.*, 2014). However, in eukaryotes, the ribosome assembly process is assisted by more than 300 trans-acting factors in yeast (Woolford and Baserga, 2013) and in humans over 600 factors have been shown so far to be required for the biogenesis of the ribosomes (Tafforeau *et al.*, 2013).

The fact that placeholder proteins and some of the assembly factors play a role in the stabilisation of transient conformations and overall folding of the rRNA brings an interesting functional analogy between these two groups of proteins and *bona fide* r-proteins. Future research may show that mechanistically placeholder proteins, assembly factors and r-proteins may work very similarly in assisting rRNA folding, but the question remaining is whether these factors and r-proteins are coming from a common ancestor. There is currently no evidence supporting this hypothesis. However, what is clear is that differently from r-proteins, placeholder proteins and assembly factors have evolved to fall off from the ribosome once they have completed their function because their binding site either overlap with current r-proteins or with important subunit bridges, essential for the association with the 50S subunit. Consequently, what it makes a true r-protein is the fact that once they bind they remain bound to the ribosomal particle and become an integral part of the functional mature ribosome.

Ribosomal Proteins Are a Window to the Past

The hypothesis of the 'RNA world' (Gilbert, 1986) predicts that life started in a simpler form than the DNA–RNA–protein tripartite system observed today. In living organisms, typically DNA constitutes the information carrier and the chemical reactions supporting life are catalysed by proteins. The information stored in the DNA is translated into proteins during translation, a process dependent on RNA. In the 'RNA world', enzymes were comprised of RNA capable of autocatalytic replication, and thus,

this molecule was both capable of bearing the information and performing catalysis. Due to the limited catalytic repertoire of RNA, RNA primordial enzymes must have formed complexes with polypeptides that would have conferred the RNA with necessary reactive capabilities. These polypeptides would have been in the form of small peptides initially but evolved later into longer peptides. These peptides were likely unable to initially maintain their structure, but as their complexity increased over time they became able to fold into stable structures independently from the RNA scaffold and originating the cellular proteins as we know them today.

The ribosome is so central in sustaining life in all cells that evolution has only caused a limited divergence of its features and molecular structures. Most of the primordial RNA–peptide complexes populating the 'RNA world' were lost over geological timescales. However, the ribosome is a 'living fossil' (Lupas and Alva, 2017) and constitutes a survivor of the primordial 'RNA world' allowing to retrace the evolutionary steps that led to the folded proteins of today. In the oldest part of the ribosome, the PTC located at its core, r-proteins are largely lacking any secondary structure. Further from the centre, the r-proteins have an increased content of secondary structure and at the periphery, they present folds that resemble those seen in cytosolic-independent proteins. However, r-proteins at the surface of the ribosome still do not have hydrophobic cores that typically drive the folding of independent proteins. The lack of these cores makes r-proteins still dependent on the RNA for folding. It is tempting to imagine that the protein families observed today as having emerged from RNA–peptide complexes similar to the ribosome after they achieved sufficient complexity to fold independently, rather than through interactions with the RNA scaffold.

The ribosome is the last survivor of the 'RNA world' and offers a chance to study the enzymes supporting life more than 3.5 billion years ago and how cellular proteins became functionally independent enzymes.

Ribosomal Proteins and Disease

Growth and cellular proliferation are highly dependent on proper ribosome function and assembly. Dysregulation of any of these two processes due to mutations in r-proteins causes not only the cells but the entire individual to exhibit severe phenotypes. Several mutations described in r-proteins cause a complete loss of function, and these mutations are typically embryonic lethal (Marygold *et al.*, 2007; Terzian and Box, 2013). However, the bulk of the described mutations in r-proteins cause only a partial loss of function and lead to a group of diseases generically called ribosomopathies.

A common characteristic in most ribosomopathies induced by mutations in r-proteins is that typically they result in tissue-specific phenotypes rather than systemically spread miss function. This is unexpected, as proper ribosome function is essential to sustain growth and proliferation in all cells. Several arguments have been put forward to explain the tissue-specific phenotypes exhibited by ribosomopathies. It is plausible that certain r-protein mutations may be deleterious only in specialised ribosomes dedicated to the translation of a class of mRNA. If this class of mRNA is only present or essential for cells in a tissue, it could explain the tissue-specific phenotypes exhibited by ribosomopathies. Certain cells may also contain specific mRNAs with sequences that are difficult to translate. These cells may be more sensitive to partial loss of function of an r-protein as these mutations may compromise translation of the difficult-to-translate mRNAs, but not other mRNA molecules.

Similarly, it is difficult to understand how loss of ribosomal function, which leads to slow cellular growth and cell death, is typically followed with development of cancer, a disease characterised by the appearance of cells exhibiting uncontrolled cell division and proliferation (Armistead and Triggs-Raine, 2014). To explain how ribosomopathies cause a hyperproliferative disease, investigators have proposed that it is the suppressor mutations that appear to compensate for reduced ribosome biogenesis may be what lead to dysregulation of cell division and cancer. These secondary mutations may perturb regulation of oncogenes and tumour suppressors promoting cellular transformation. It is also possible that loss of function of r-proteins compromises the immune system and, thus, the ability of these patients to clear cancerous cells that appear spontaneously (de la Cruz *et al.*, 2015).

There has been an increasing interest in further elucidating the role or r-proteins in the ribosomopathies. These diseases include a large variety of both hypo- and hyperproliferative disorders, which manifest as development disorders in organogenesis, haematological disorders or cancers, as well as cardiovascular and metabolic disorders (Narla and Ebert, 2010; Teng *et al.*, 2013). A detailed description of these diseases and the r-protein defects associated with them is beyond the scope of this article. There are multiple excellent reviews on this topic, and we refer the reader to them (Freed *et al.*, 2010; Narla and Ebert, 2010; Teng *et al.*, 2013; de Las Heras-Rubio *et al.*, 2014).

Conclusions and Perspectives

It has now become clear that the three core mechanisms of protein synthesis, including decoding, catalysis of peptide bond formation and the translocation of mRNA and tRNA, are performed by rRNA. However, it is also apparent that the r-proteins play essential roles in the functionality of the ribosome. Fast and efficient folding of the rRNA during ribosome assembly is driven by r-proteins, but many of the roles of r-proteins in the function, structure and allosteric communication between parts of the ribosome are still elusive. Current work in many groups using new approaches in biochemistry, genetics and structural biology ensures rapid progress in elucidating many of the still unknown functions of r-proteins. These new discoveries are of practical importance as they are paving the way to use the r-proteins as new targets for the development of new and more potent antimicrobials and cancer therapies.

Acknowledgements

We apologize to all our colleagues whose work has not being discussed or cited in this article due to space limitations.

Funding

This work was supported by grants from the National Science and Engineering Research Council of Canada (RGPIN288327-07) and Canadian Institutes of Health Research (PJT-153044) to J.O.

Competing Financial Interest

The authors declare no competing financial interests. The funders had no role in study design, data collection and analysis, decision to publish or preparation of the manuscript.

Glossary

70S The eukaryotic ribosome is also called 70S ribosome, referring to their sedimentation coefficients in Svedberg units.

80S The eukaryotic ribosome is also called 80S ribosome, referring to their sedimentation coefficients in Svedberg units.

Evolution Change in the heritable characteristics of biological populations over successive generations.

Placeholder protein Protein that share extensive identity and similarity to the ribosomal proteins but they are unable to functionally replace their r-protein counterpart.

Ribosomal protein Proteins that are considered intrinsic part of the ribosomal structure.

Ribosome assembly factor Proteins factors that assist the process of assembly of the ribosomes both in eukaryotic and prokaryotes.

Ribosome Macromolecular assembly that synthesizes every protein in the cell.

References

Adilakshmi T, Bellur DL and Woodson SA (2008) Concurrent nucleation of 16S folding and induced fit in 30S ribosome assembly. *Nature* **455**: 1268–1272.

Agrawal RK, Penczek P, Grassucci RA and Frank J (1998) Visualization of elongation factor G on the *Escherichia coli* 70S ribosome: the mechanism of translocation. *Proceedings of the National Academy of Sciences of the United States of America* **95**: 6134–6138.

Akanuma G, Nanamiya H, Natori Y, *et al.* (2012) Inactivation of ribosomal protein genes in *Bacillus subtilis* reveals importance of each ribosomal protein for cell proliferation and cell differentiation. *Journal of Bacteriology* **194**: 6282–6291.

Amunts A, Brown A, Toots J, Scheres SH and Ramakrishnan V (2015) Ribosome. The structure of the human mitochondrial ribosome. *Science* **348**: 95–98.

Armistead J and Triggs-Raine B (2014) Diverse diseases from a ubiquitous process: the ribosomopathy paradox. *FEBS Letters* **588**: 1491–1500.

Ban N, Nissen P, Hansen J, Moore PB and Steitz TA (2000) The complete atomic structure of the large ribosomal subunit at 2.4 Å resolution. *Science* **289**: 905–920.

Ban N, Beckmann R, Cate JH, *et al.* (2014) A new system for naming ribosomal proteins. *Current Opinion in Structural Biology* **24**: 165–169.

Ben-Shem A, Garreau de Loubresse N, Melnikov S, *et al.* (2011) The structure of the eukaryotic ribosome at 3.0 Å resolution. *Science* **334**: 1524–1529.

Dabbs ER (1978) Mutational alterations in 50 proteins of the *Escherichia coli* ribosome. *Molecular and General Genetics* **165**: 73–78.

Davis JH, Tan YZ, Carragher B, *et al.* (2016) Modular assembly of the bacterial large ribosomal subunit. *Cell* **167**: 1610–1622, e1615.

de la Cruz J, Karbstein K and Woolford JL Jr, (2015) Functions of ribosomal proteins in assembly of eukaryotic ribosomes in vivo. *Annual Review of Biochemistry* **84**: 93–129.

de Las Heras-Rubio A, Perucho L, Paciucci R, Vilardell J and LLeonart ME (2014) Ribosomal proteins as novel players in tumorigenesis. *Cancer Metastasis Reviews* **33**: 115–141.

Demeshkina NA, Laletina ES, Meshchaninova MI, *et al.* (2003) The mRNA codon environment at the P and E sites of human ribosomes deduced from photo crosslinking with pUUUGUU. *Molekuliarnaia Biologiia (Mosk)* **37**: 147–155.

Desai N, Brown A, Amunts A and Ramakrishnan V (2017) The structure of the yeast mitochondrial ribosome. *Science* **355**: 528–531.

Dunbar DA, Dragon F, Lee SJ and Baserga SJ (2000) A nucleolar protein related to ribosomal protein L7 is required for an early step in large ribosomal subunit biogenesis. *Proceedings of the National Academy of Sciences of the United States of America* **97**: 13027–13032.

Ebersberger I, Simm S, Leisegang MS, *et al.* (2014) The evolution of the ribosome biogenesis pathway from a yeast perspective. *Nucleic Acids Research* **42**: 1509–1523.

Espinar-Marchena F, Babiano R and de la Cruz J (2017) Placeholder factors in ribosome biogenesis: please, pave my way. *Microbial Cell* **4** (5): 144–168.

Frank J (1997) The ribosome at higher resolution—the donut takes shape. *Current Opinion in Structural Biology* **7**: 266–272.

Freed EF, Bleichert F, Dutca LM and Baserga SJ (2010) When ribosomes go bad: diseases of ribosome biogenesis. *Molecular Biosystems* **6**: 481–493.

Ghosh A, Jindal S, Bentley AA, Hinnebusch AG and Komar AA (2014) Rps5-Rps16 communication is essential for efficient translation initiation in yeast *S. cerevisiae*. *Nucleic Acids Research* **42**: 8537–8555.

Gilbert W (1986) Origin of life: the RNA world. *Nature* **319**: 618.

Graifer D, Molotkov M, Styazhkina V, *et al.* (2004) Variable and conserved elements of human ribosomes surrounding the mRNA at the decoding and upstream sites. *Nucleic Acids Research* **32**: 3282–3293.

Graifer D and Karpova G (2015) Roles of ribosomal proteins in the functioning of translational machinery of eukaryotes. *Biochimie* **109**: 1–17.

Harms J, Schluenzen F, Zarivach R, *et al.* (2001) High resolution structure of the large ribosomal subunit from a mesophilic eubacterium. *Cell* **107**: 679–688.

Khatter H, Myasnikov AG, Natchiar SK, Klaholz BP (2015) Structure of the human 80S ribosome. *Nature* **520**: 640–645

Lake JA (1976) Ribosome structure determined by electron microscopy of *Escherichia coli* small subunits, large subunits and monomeric ribosomes. *Journal of Molecular Biology* **105**: 131–139.

Lomakin IB and Steitz TA (2013) The initiation of mammalian protein synthesis and mRNA scanning mechanism. *Nature* **500**: 307–311.

Lupas AN and Alva V (2017) Ribosomal proteins as documents of the transition from unstructured (poly)peptides to folded proteins. *Journal of Structural Biology* **198** (2): 74–81.

Marygold SJ, Roote J, Reuter G, *et al.* (2007) The ribosomal protein genes and Minute loci of Drosophila melanogaster. *Genome Biology* **8**: R216.

Mizushima S and Nomura M (1970) Assembly mapping of 30S ribosomal proteins from *E. coli*. *Nature* **226**: 1214.

Narla A and Ebert BL (2010) Ribosomopathies: human disorders of ribosome dysfunction. *Blood* **115**: 3196–3205.

Noller HF, Hoffarth V and Zimniak L (1992) Unusual resistance of peptidyl transferase to protein extraction procedures. *Science* **256**: 1416–1419.

Rabl J, Leibundgut M, Ataide SF, Haag A and Ban N (2011) Crystal structure of the eukaryotic 40S ribosomal subunit in complex with initiation factor 1. *Science* **331**: 730–736.

Roth HE and Nierhaus KH (1980) Assembly map of the 50-S subunit from *Escherichia coli* ribosomes, covering the proteins present in the first reconstitution intermediate particle. *European Journal of Biochemistry* **103**: 95–98.

Schuwirth BS, Borovinskaya MA, Hau CW, *et al.* (2005) Structures of the bacterial ribosome at 3.5 Å resolution. *Science* **310**: 827–834.

Shajani Z, Sykes MT and Williamson JR (2011) Assembly of bacterial ribosomes. *Annual Review of Biochemistry* **80**: 501–526.

Sohmen D, Chiba S, Shimokawa-Chiba N, *et al.* (2015) Structure of the Bacillus subtilis 70S ribosome reveals the basis for species-specific stalling. *Nature Communications* **6**: 6941. DOI: http://doi.org/10.1038/ncomms7941

Suryanarayana T and Subramanian AR (1983) An essential function of ribosomal protein S1 in messenger ribonucleic acid translation. *Biochemistry* **22**: 2715–2719.

Tafforeau L, Zorbas C, Langhendries JL, *et al.* (2013) The complexity of human ribosome biogenesis revealed by systematic nucleolar screening of Pre-rRNA processing factors. *Molecular Cell* **51**: 539–551.

Teng T, Thomas G and Mercer CA (2013) Growth control and ribosomopathies. *Current Opinion in Genetics and Development* **23**: 63–71.

Terzian T and Box N (2013) Genetics of ribosomal proteins: "curiouser and curiouser". *PLoS Genetics* **9**: e1003300.

Traub P and Nomura M (1969) Studies on the assembly of ribosomes in vitro. *Cold Spring Harbor Symposia on Quantitative Biology* **34**: 63–67.

Vasiliev VD (1974) Morphology of the ribosomal 30S subparticle according to electron microscopic data. *Acta Biologica et Medica Germanica* **33**: 779–793.

Voorhees RM, Fernandez IS, Scheres SH and Hegde RS (2014) Structure of the mammalian ribosome-Sec61 complex to 3.4 Å resolution. *Cell* **157**: 1632–1643.

Wilson DN and Nierhaus KH (2005) Ribosomal proteins in the spotlight. *Critical Reviews in Biochemistry and Molecular Biology* **40**: 243–267.

Wilson DN and Nierhaus KH (2007) The weird and wonderful world of bacterial ribosome regulation. *Critical Reviews in Biochemistry and Molecular Biology* **42**: 187–219.

Wimberly BT, Brodersen DE, Clemons WM Jr,, *et al.* (2000) Structure of the 30S ribosomal subunit. *Nature* **407**: 327–339.

Wittmann HG, Stofflet G, Hindennach I, *et al.* (1971) Correlation of 30S ribosomal proteins of *Escherichia coli* isolated in different laboratories. *Molecular and General Genetics* **111**: 327–333.

Woodson SA (2011) RNA folding pathways and the self-assembly of ribosomes. *Accounts of Chemical Research* **44**: 1312–1319.

Woolford JL Jr, and Baserga SJ (2013) Ribosome biogenesis in the yeast *Saccharomyces cerevisiae*. *Genetics* **195**: 643–681.

Yusupov MM, Yusupova GZ, Baucom A, *et al.* (2001) Crystal structure of the ribosome at 5.5 Å resolution. *Science* **292**: 883–896.

Zhou X, Liao WJ, Liao JM, Liao P and Lu H (2015) Ribosomal proteins: functions beyond the ribosome. *Journal of Molecular Cell Biology* **7**: 92–104.

Further Reading

Goudarzi KM and Lindstrom MS (2016) Role of ribosomal protein mutations in tumor development (Review). *International Journal of Oncology* **48**: 1313–1324.

Kim TH, Leslie P and Zhang Y (2014) Ribosomal proteins as unrevealed caretakers for cellular stress and genomic instability. *Oncotarget* **5**: 860–871.

Razi A, Britton RA and Ortega J (2016) The impact of recent improvements in cryo-electron microscopy technology on the understanding of bacterial ribosome assembly. *Nucleic Acids Research* **45** (3): 1027–1040

Wang W, Nag S, Zhang X, *et al.* (2015) Ribosomal proteins and human diseases: pathogenesis, molecular mechanisms, and therapeutic implications. *Medicinal Research Reviews* **35**: 225–285.

News & Views

THE EMBO JOURNAL

Final touches and quality control on the assembly of the eukaryotic ribosome

Aida Razi & Joaquin Ortega

One of the most fundamental processes of life is protein synthesis by the ribosome. Although much is known about the function and structure of this macromolecular complex, our understanding on its assembly is still vague. In this issue of *The EMBO Journal*, Malyutin *et al* (2017) provide a detailed picture of one of the latest assembly stages of the yeast 60S ribosomal subunit. The cryo-EM map of the 60S-Nmd3-Lsg1-Tif6 complex sheds new light on the function of Nmd3, Lsg1 and Tif6—and their release mechanisms—right before the 60S subunit joins the pool of actively translating ribosomes.

See also: **AG Malyutin *et al*** (April 2017) and **C Ma *et al*** (March 2017)

The eukaryotic ribosome consists of four ribosomal RNA molecules (rRNA) and ~80 ribosomal proteins (r-proteins). These components are organized into the 40S small and 60S large subunits that associate forming the 80S ribosome. Ribosome assembly starts in the nucleus and is completed in the cytoplasm, with immature particles exported from the nucleus to the cytoplasm during this process. Assembly of the eukaryotic ribosome involves more than 200 biogenesis factors that support folding, processing and modifications of the rRNA, enable nuclear export of the assembling ribosomal particles or functionally test the active sites of the subunits (Karbstein, 2013; Woolford & Baserga, 2013; Greber, 2016). The general mechanisms by which these factors perform their functions remain poorly understood.

Pioneering work from the Hurt and Beckman's laboratories (Bradatsch *et al*, 2012) provided the first moderate resolution (11.9 Å) cryo-EM reconstruction of a pre-60S particle revealing how multiple assembly factors bind immature ribosomal particles. The recent introduction of direct electron detectors in cryo-electron microscopy (cryo-EM) is transforming our understanding of the role of assembly factors (Razi *et al*, 2017). We are now able to capture high-resolution snapshots of the assembly process that shows multiple maturation factors simultaneously bound to pre-ribosomal particles. In this issue, Malyutin *et al* (2017) present the cryo-EM structure of the 60S subunit in complex with Nmd3, Lsg1 and Tif6 (Fig 1), providing a 3D view of one of the latest stages of 60S maturation.

Assembly factor Nmd3 associates with the pre-60S particle in the nucleus and participates in the nuclear export process along with a myriad of transiently interacting factors. Most of these factors are released prior to nuclear export. However, Nmd3 remains associated with the ribosomal particle until late during cytoplasmic maturation, where it is ultimately released in a process assisted by the GTPase Lsg1 (Hedges *et al*, 2005). Tif6 is a ribosome anti-association factor that is released at the end of the maturation process assisted by the Efl1 GTPase and protein Sdo1. The reconstitution of the 60S-Nmd3-Lsg1-Tif6 complex by Malyutin *et al* (2017) was done *in vitro* using purified components and mature 60S subunits, and it likely captures the complete subunit right before the release of Nmd3 and Tif6 in the cytoplasm of yeast cells.

The cryo-EM map reveals that Nmd3 spans the joining face of the 60S subunit from the uL1 protein on the L1 stalk, covers the E and P sites and ends up contacting Tif6, which is bound at the sarcin-ricin loop (SRL). The cryo-EM map is of sufficient resolution to build an atomic model of all three domains of Nmd3. The N-terminal domain of Nmd3 contacts Tif6, the second domain adopts a fold similar to that of r-protein eL22 and occupies the P site, while the third domain contacts the L1 stalk, which is seen to adopt a closed conformation. Density for GTPase Lsg1 is also apparent in the cryo-EM map. This protein binds at the intersubunit surface of the 60S subunit contacting helix 69, essential for association with the smaller subunit. A striking finding of the structure is that binding of Lsg1 induces a shift of rRNA helix 69 that causes guanosine 2261 to flip out towards residues near switch I in the GTPase domain of Lsg1, possibly triggering GTP hydrolysis. This observation suggests that helix 69 could act as a general activator of GTPases involved in large subunit biogenesis. The structure also suggests a role for Nmd3 in promoting the loading of uL16, a step that causes drastic conformational changes leading to the formation of the mature subunit.

The cryo-EM map of the 60S-Nmd3-Lsg1-Tif6 complex provides new examples of how assembly factors act as checkpoint proteins in the mature subunits. It reveals that the domain of Nmd3 bound to the E site adopts a topology remarkably similar to eIF5A, a protein factor necessary for the rescue of ribosomes stalled on polyproline-containing sequences. One of the domains of Nmd3

Department of Biochemistry and Biomedical Sciences and M. G. DeGroote Institute for Infectious Diseases Research, McMaster University, Hamilton, ON, Canada.
E-mail: ortegaj@mcmaster.ca
DOI 10.15252/embj.201796722 | Published online 13 March 2017

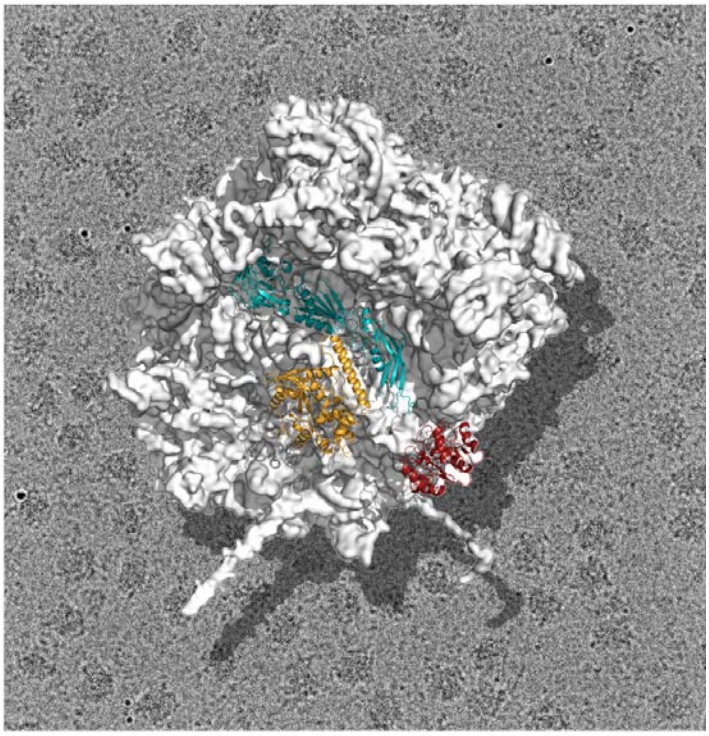

Figure 1. Yeast 60S subunit bound to assembly factors.
Cryo-EM structure of the yeast 60S subunit in complex with assembly factors Nmd3 (teal), Lsg1 (gold) and Tif6 (red). This structure provides a 3D view of one of the latest stages of 60S maturation capturing the complete subunit right before the release of Nmd3, Lsg1 and Tif6 in the cytoplasm of yeast cells. This final step allows the 60S subunit to join the pool of actively translating ribosomes.

also occupies the P site, thus adding to the list of assembly factors that perform quality control checks and test the functionality and conformation of specific ribosome sites.

Finally, this study deepens our understanding of how late-stage assembly factors are released right before the active 60S subunit joins the pool of translating ribosomes. Cryo-EM analysis of several partial sub-complexes undertaken in this study, in addition to the full 60S-Nmd3-Lsg1-Tif6 complex, allowed the authors to propose a sequence of events leading to the release of Nmd3, Lsg1 and Tif6. They suggest that breakage of the interaction between Nmd3 and Tif6 constitutes the initial event that destabilizes the complex. The L1 stalk is then free to move from a closed to an open conformation, thereby pulling out Nmd3 from the P and E sites. The absence of direct contacts between Lsg1 and Nmd3 suggests that another factor, possibly Efl1, may be responsible for disengaging Nmd3 from Tif6 and initiate the release. Subsequent entry of Sdo1, recruited by Efl1, releases Tif6.

In a related publication (Ma *et al*, 2017), the Woolford and Gao's groups reported the cryo-EM structure of a pre-60S particle purified with epitope-tagged Nmd3. They found that these particles are depleted for r-proteins uL16, uL10, uL11, eL40 and eL41 and are bound to the Nmd3, Lsg1, Tif6 and Reh1 assembly factors. The structure reported in that study likely typifies the maturation stage of the 60S subunit just prior to that shown in the Malyutin *et al* (2017) article. Therefore, it brings additional insights on the maturation events occurring at these late stages. A noticeable difference between the two structures is that the density for Lsg1 appears fragmented in the pre-60S particle. The N-terminal region of Nmd3 is also not well ordered, suggesting that Nmd3 and Lsg1 bind in a flexible manner. These observations are consistent with these pre-60S particles representing a late cytoplasmic stage just prior to the incorporation of uL16. This stage of maturation is earlier than that described in the structure of the *in vitro* reconstituted 60S-Nmd3-Lsg1-Tif6 complex and suggests a different order of release for Nmd3 and Tif6 from that proposed in Malyutin *et al* (2017). The structure by Ma *et al* (2017) implies that Tif6 is the last remaining factor released from the maturing particle and that Nmd3 release precedes this event. Additional structures and genetic analysis will need to be done to resolve these conflicting models.

Overall, the structures presented by Malyutin *et al* (2017) and Ma *et al* (2017) provide two important snapshots of a cellular pathway essential to sustain life. We see cryo-EM with the incorporation of direct electron detectors as a technique of great promise that is currently transforming our understanding of the ribosome biogenesis process and the role played by assembly factors. Studies in the last decade linking defects in ribosome assembly with cancer development make these studies of general importance and have the potential to translate into clinical benefits.

References

Bradatsch B, Leidig C, Granneman S, Gnadig M, Tollervey D, Bottcher B, Beckmann R, Hurt E (2012) Structure of the pre-60S ribosomal subunit with nuclear export factor Arx1 bound at the exit tunnel. *Nat Struct Mol Biol* 19: 1234 – 1241

Greber BJ (2016) Mechanistic insight into eukaryotic 60S ribosomal subunit biogenesis by cryo-electron microscopy. *RNA* 22: 1643 – 1662

Hedges J, West M, Johnson AW (2005) Release of the export adapter, Nmd3p, from the 60S ribosomal subunit requires Rpl10p and the cytoplasmic GTPase Lsg1p. *EMBO J* 24: 567 – 579

Karbstein K (2013) Quality control mechanisms during ribosome maturation. *Trends Cell Biol* 23: 242 – 250

Ma C, Wu S, Li N, Chen Y, Yan K, Li Z, Zheng L, Lei J, Woolford JL Jr, Gao N (2017) Structural snapshot of cytoplasmic pre-60S ribosomal

particles bound by Nmd3, Lsg1, Tif6 and Reh1. *Nat Struct Mol Biol* 24: 214 – 220

Malyutin AG, Musalgaonkar S, Patchett S, Frank J, Johnson AW (2017) Nmd3 is a structural mimic of eIF5A, and activates the cpGTPase Lsg1 during 60S ribosome biogenesis. *EMBO J* 36: 854 – 868

Razi A, Britton RA, Ortega J (2017) The impact of recent improvements in cryo-electron microscopy technology on the understanding of bacterial ribosome assembly. *Nucleic Acids Res* 45: 1027 – 1040

Woolford JL Jr, Baserga SJ (2013) Ribosome biogenesis in the yeast *Saccharomyces cerevisiae*. *Genetics* 195: 643 – 681

Published online 8 December 2016

Nucleic Acids Research, 2017, Vol. 45, No. 3 ***1027–1040***
doi: 10.1093/nar/gkw1231

SURVEY AND SUMMARY

The impact of recent improvements in cryo-electron microscopy technology on the understanding of bacterial ribosome assembly

Aida Razi[1], Robert A. Britton[2] and Joaquin Ortega[1,*]

[1]Department of Biochemistry and Biomedical Sciences and M. G. DeGroote Institute for Infectious Diseases Research, McMaster University, Hamilton, Ontario L8S 4K1, Canada and [2]Department of Molecular Virology and Microbiology and Center for Metagenomics and Microbiome Research, Baylor College of Medicine, Houston, TX 77030, USA

Received August 30, 2016; Revised November 20, 2016; Editorial Decision November 22, 2016; Accepted November 25, 2016

ABSTRACT

Cryo-electron microscopy (cryo-EM) had played a central role in the study of ribosome structure and the process of translation in bacteria since the development of this technique in the mid 1980s. Until recently cryo-EM structures were limited to ∼10 Å in the best cases. However, the recent advent of direct electron detectors has greatly improved the resolution of cryo-EM structures to the point where atomic resolution is now achievable. This improved resolution will allow cryo-EM to make groundbreaking contributions in essential aspects of ribosome biology, including the assembly process. In this review, we summarize important insights that cryo-EM, in combination with chemical and genetic approaches, has already brought to our current understanding of the ribosomal assembly process in bacteria using previous detector technology. More importantly, we discuss how the higher resolution structures now attainable with direct electron detectors can be leveraged to propose precise testable models regarding this process. These structures will provide an effective platform to develop new antibiotics that target this fundamental cellular process.

INTRODUCTION

X-ray crystallography and cryo-electron microscopy (cryo-EM) have been key techniques used to understand the structure and function of the bacterial ribosome. In the year 2000, the groups of Venki Ramakrishnan, Tom Steitz and Ada Yonath published atomic resolution structures of the 30S and 50S ribosomal subunits (1–3). This historical landmark culminated a long quest aimed at solving the structure of the ribosome that started in the 1970s in Harry Noller's laboratory when the secondary structure of the 16S and 23S rRNA was elucidated. In the time span between these two historical landmarks, many groups contributed to slowly define the topography of the bacterial ribosome. To name a few, significant progress was obtained by the Stöffler's group (4,5) using immune electron microscopy to define the spatial arrangement of the ribosomal proteins (r-proteins). Cross-linking approaches in the Brimacombe's group (6–8) allowed to reveal r-protein-rRNA and r-protein contacts. Peter Moore and Don Engelman used neutron scattering to determine the relative positions of the r-proteins in the 30S subunit (9) and comparative sequence analysis was also instrumental to infer the higher order structures adopted by the 5S, 16S and 23S rRNAs (10–15).

All along, but especially after the development of the specimen vitrification process by Dubochet *et al.* (16) in 1984, cryo-EM has contributed significantly to the joint effort of determining the structure of the ribosome. Initially, low-resolution cryo-EM maps of the ribosome, mainly from Frank's group (17), provided the envelopes to dock high-resolution structures of individual r-proteins and fragments of RNA that several groups were busy solving. Around the 1990s, it was believed that this divide and conquer approach would eventually render the atomic resolution structure of the 70S ribosome (18). However, in the latter half for the 1990s solid progress in ribosome crystallization and concurrent improvements in synchrotron radiation sources led to the structural determination of ribosomal subunits at atomic resolution from entire particles.

*To whom correspondence should be addressed. Tel: +1 905 525 9140 (Ext 22703); Fax: +1 905 522 9033; Email: ortegaj@mcmaster.ca

The contributions of cryo-EM to ribosome biology are not only limited to structure. An important part of our understanding of the protein synthesis process is also derived from cryo-EM. An important challenge in this effort has always been that the ribosome is a molecule in constant motion and that fluctuates between different states during the process of protein translation (19–21). Most of these states constitute transient structures that are difficult to trap in a crystalline form, and consequently challenging to be solved by X-ray crystallography. However, mixtures of complexes populating the ribosome work cycle and coexisting in the same sample are not a limiting factor for cryo-EM. Image classification approaches (22–25) have long been used to separate particle subpopulations and build 3D reconstructions for each conformer in the mixture.

Until recently, the drawback of this approach was that the resolution of the resulting reconstructions was limited to ∼8 Å resolution in the best cases (26,27). Atomic resolution models were only attainable when all the individual components of the complex were known to atomic resolution and it was possible to dock them unambiguously into the limited resolution cryo-EM maps (28). Recent advances in direct electron detector cameras (direct detectors) have dramatically changed the resolution limit that is now attainable by cryo-EM (29–31). These detectors have opened a much easier way to gather atomic resolution information on translating ribosome intermediates that are extremely challenging to crystallize. The avalanche of ribosome structures in the 3–4 Å resolution range that have recently been produced from these new detectors (32–36) demonstrate that it is currently possible to retrieve the entire inventory of states co-existing during the work cycle of the ribosome and gain a complete portrait of the protein synthesis process in three dimensions.

These recently published structures of mature ribosomes provide little insight into ribosome biogenesis. The next frontier in the ribosome field is to understand the assembly process. Ribosomal subunit assembly has been the subject of >50 years of investigation that began with seminal studies by the Nomura (37–41) and Nierhaus (42–44) laboratories in the late 1960s and early 1970s to map the reconstitution of the 30S and 50S subunits *in vitro*. Structural interest in this field has resurfaced in the last several years, sparked by the publication of several cryo-EM structures of ribosome assembly intermediates (Figure 1A) (45–51) and complexes of ribosomal subunits with protein assembly factors (Figure 1B) (52–55). All these structures were produced from electron micrographs collected either on photographic film or standard charge-couple device (CCD) cameras. Consequently, the obtained resolution in these structures was ∼10 Å or lower. The advent of direct electron detectors now offers the possibility to study these assembly intermediates and complexes at atomic resolution, which will most likely transform our understanding of the ribosome assembly process.

In this review, we briefly describe how in light of recent progress in direct electron detector devices, cryo-EM represents now an ideal tool to study the process of assembly of the ribosome. We also summarize the main contributions that cryo-EM so far has brought in combination with chemical and genetic approaches to our understanding of this

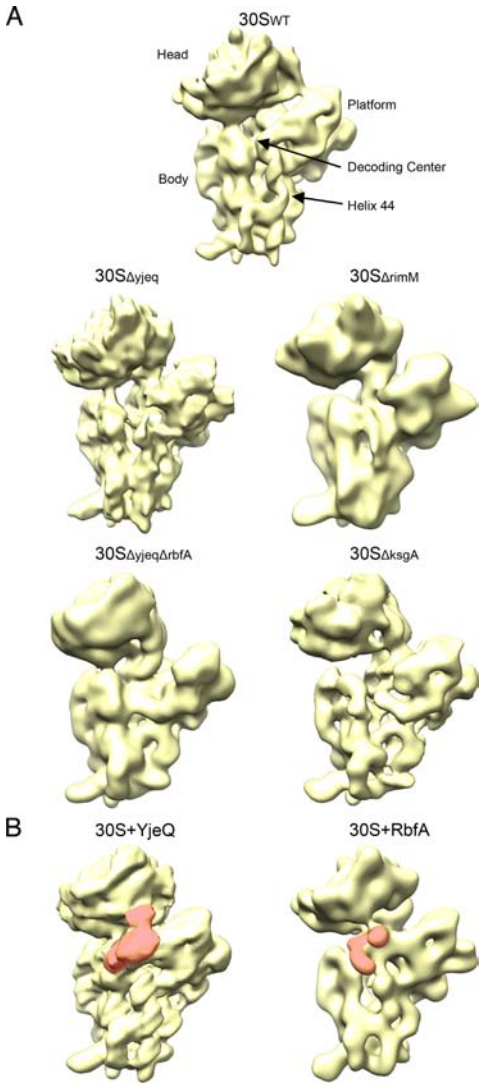

Figure 1. Cryo-EM structure of 30S subunit assembly intermediates and complexes of the 30S subunit with assembly factors. (**A**) Gallery of cryo-EM structures of immature 30S subunit that accumulate in *Escherichia coli* strains lacking one or multiple assembly factors. The assembly factor that has been knocked out in the strain is indicated in the label. A density map of the mature 30S subunit is at the top of the panel for comparison purposes. This structure was obtained by applying a 20 Å low pass filter to the atomic structure of the 30S subunit (PDB ID: 2AVY). All these structures were obtained at resolutions ranging from 11 to 17 Å resolution and from images recorded on a CCD camera or film. (**B**) Cryo-EM structures of the 30S subunit in complex with either YjeQ or RbfA. These structures were obtained at 10 and 12 Å resolution, respectively. Images for the 30S + YjeQ complex were recorded in a CCD camera and the images for the complex with RbfA were recorded on film.

process in bacteria. Finally, we discuss the potential that the new direct electron detectors will provide into how ribosome assembly occurs.

OVERVIEW OF THE RIBOSOME ASSEMBLY PROCESS IN BACTERIA

The bacterial 70S ribosome is a ribonucleoprotein complex composed of a large 50S and small 30S subunit. The 30S subunit is responsible for the decoding of the mRNA and consists of the 16S rRNA molecule and 21 r-proteins named from S1 to S21 (with a u or b prefix) (56). The 50S subunit contains the active center where peptide bond formation is catalyzed and it is made of two RNA molecules, the 23S and 5S rRNAs and 34 r-proteins designated from L1 to L36 (with a u or b prefix) (56). The three rRNA molecules form the core of the particles, whereas r-proteins mainly sit on the surface of the structure.

Bacterial ribosome assembly commences with the transcription of rRNA as a single precursor transcript containing the three rRNAs for the two subunits (along with one or two tRNA molecules) (57). RNase III performs the primary processing that separates the three rRNAs. The resulting fragments are called precursor rRNAs and contain additional nucleotides at both their 5′ and 3′ ends called precursor sequences (57). The coordinated action of multiple RNases removes the precursor sequences to generate the mature rRNA molecules. After transcription, the rRNA molecules undergo covalent modifications and form local secondary structures that are rapidly recognized and bound by r-proteins. Vintage studies by Nomura (37,38,40,58), Nierhaus (59,60) and more recent experiments from the Williamson and Woodson laboratories (61,62) have defined the hierarchy of binding of r-proteins and the forces shaping rRNA and r-protein interactions during subunit assembly. The binding of r-proteins is designated as primary (directly to the rRNA), secondary (dependent on primary r-proteins) or tertiary (dependent on secondary r-proteins). Evidence to date suggests that r-protein binding to the rRNA drives folding that stabilizes local RNA structure and induces conformational changes to create new binding sites for secondary proteins (63,64). Likewise, these studies suggest that, at least *in vitro*, ribosome assembly appears to occur via multiple parallel pathways without significant rate-limiting steps, outlining a process of large complexity and built-in redundancy to ensure efficient assembly even under unfavorable conditions (62,65).

Mainly through genetic approaches and through the slow assembly of ribosomes *in vitro*, the field came to realize that in cells the assembly process is extremely efficient because of being assisted by many assembly factors. These factors included enzymes responsible for the processing and covalent modifications of the rRNA and ribosomal proteins, rRNA chaperones, GTPases and helicases (66–69). However, for most of the factors their precise functions in ribosome biogenesis are still uncharacterized (70).

CRYO-ELECTRON MICROSCOPY AS AN IDEAL TOOL FOR STUDYING RIBOSOME BIOGENESIS

Similarly, to the protein translation process, all aspects of the ribosome assembly process involve dynamic events. The assembling ribosome is a complex in constant change. New r-proteins are incorporated and its rRNA is being covalently modified and processed as it fluctuates between different conformations. The complexity and dynamics inherent to the ribosome represents a major limiting factor for the crystallization of ribosome assembly intermediates and thus, their study using X-ray crystallography (71). In cryo-EM, the assembling ribosomes are embedded in a thin layer of vitreous ice and remain in a fully hydrated state (16,72). Ribosomal particles are not forced into any crystal lattice or subjected to steric constrains, therefore, in principle cryo-EM allows for the visualization of the entire dynamic course of the assembly process. One limitation to keep in mind is that because multiple copies of assembling ribosomes that have the same structure must be averaged to produce the 3D structure, the assembly states that are more easily observed are those that represent long-lived intermediates or local minima conformations within the free-energy landscape of the ribosome assembly process.

All the existing chemical or genetic approaches presently used (see below) to capture assembly intermediates in bacteria invariably produce a heterogeneous mixture of complexes that must be sorted out. In the last decade several image-processing packages for cryo-EM images (73–75) have implemented maximum-likelihood (ML) classification approaches (22) to sort out the particle images into structurally homogeneous subsets. This methodology has been proven to be very robust for classifying noisy cryo-EM images. Once the different subpopulations have been identified and separated, individual 3D reconstructions at atomic resolution can be generated for each of the individual assembly intermediates.

Until recently cryo-EM images from the electron microscope were recorded in photographic film. Subsequently, the field transitioned to the use of CCD cameras. These cameras allowed for the development of automation during data collection and offered the possibility to produce more and significantly larger data sets that allowed for higher resolution 3D structures and to study structurally heterogeneous assemblies (76,77). However, the attenuation of the signal and blurring of the image resulting from the indirect detection of the electrons in these devices often resulted in structures that were limited to ∼10–15 Å resolution (Figure 2A). The recent development of direct detectors has transformed cryo-EM into a much more powerful technique. These devices record electrons directly with little or no noise. Images collected in these detectors contain much higher contrast and have better preservation of the high-resolution signal (Figure 2B) (29,78). Images obtained in a detector are capable to produce 3D structures to much higher resolution (Figure 2B) (<3 Å in many cases) that those obtained from CCD cameras (Figure 2A). Direct detectors also have extremely fast image read-outs, which produce 'movies' instead of single snapshots. Movies produced by these detectors allow compensating for 'beam-induced motion'. This is the movement that the particles in the specimen experience because of the energy deposited by the electron beam while the image is being collected, resulting in blurring and resolution degradation (79,80). Collecting multi-frame movies instead of single snapshots allows for an effective tracking and correction of this movement efficiently restoring the

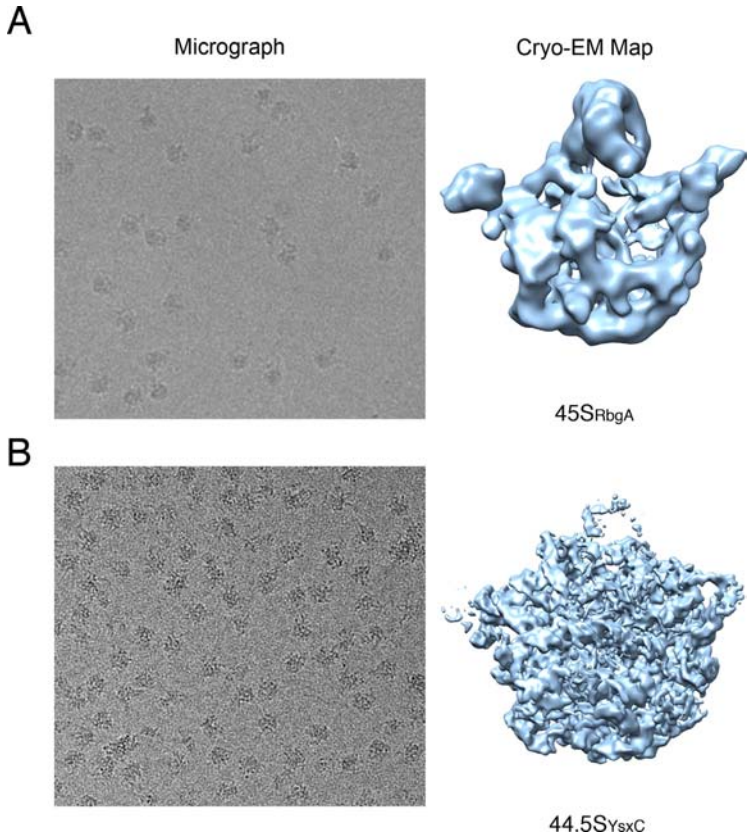

Figure 2. Direct detectors produce images with better preservation of the high-resolution information. (**A**) Cryo-electron micrograph (left panel) obtained in a CCD camera showing immature $45S_{RbgA}$ ribosomal particles obtained from a depletion strain of *Bacillus subtilis* lacking the RbgA protein. The right panel shows a 3D reconstruction of the $45S_{RbgA}$ particle obtained from CCD images similar to that displayed on the left panel. This 3D structure was refined to 13 Å resolution. (**B**) Cryo-electron micrograph (left panel) of a similar immature ribosomal particle ($44.5S_{YsxC}$ particle) obtained in a direct electron detector. These particles were purified from a depletion strain of *B. subtilis* lacking the YsxC protein. The contrast and structural details in this image are significantly higher than in the equivalent micrograph from a CCD shown in panel (**A**). Direct detector images similar to that shown in this panel, produced a 3D structure at ∼5 Å resolution.

high resolution in the images (30,81,82) (Figure 3). Overall, direct detectors represent a quantum leap for the capability of cryo-EM to deliver atomic resolution (27) and recently published ribosome structures (34,83–85) constitute outstanding examples of what is now possible using cryo-EM. These structures illustrate the current potential of cryo-EM to gather atomic resolution structural information of the ribosome assembly process.

Therefore, because of major improvements in both software and hardware, cryo-EM can now deliver atomic resolution structures. These advances make cryo-EM an ideal tool for the structural understanding of dynamic processes such as the assembly of the ribosome. Cryo-EM is definitively posed to bring a flood of new biological insights into this complex biological process in the upcoming years.

CHEMICAL AND GENETIC APPROACHES TO CAPTURE *IN VIVO* ASSEMBLED RIBOSOMAL SUBUNIT INTERMEDIATES FOR STRUCTURAL STUDIES

The Williamson lab was among the first groups to analyze bacterial immature ribosomal particles using electron microscopy (86). In this pioneer study, 30S subunits were assembled *in vitro* from purified 16S rRNA and ribosomal proteins. As the assembly reaction was allowed to proceed, aliquots were removed and imaged by negative staining electron microscopy. Using this approach, it was possible to observe many 30S particles at different stages of the maturation process. More importantly, this analysis showed that image classification approaches were effective in sorting out the multiple subpopulations of intermediates existing at the various time points without the need for biochemical pu-

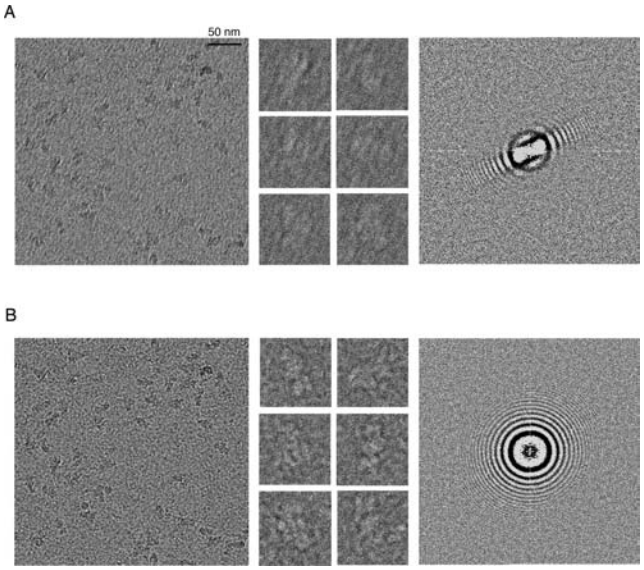

Figure 3. Restoration of high-resolution information by beam-induced correction. (**A**) Micrograph showing 30S ribosomal subunits obtained by merging the 30 frames from a movie obtained in a Gatan K2 direct electron detector without previous beam-induced motion correction. The micrograph (left) and particles (center) extracted from this micrograph are clearly drifted. The disappearance of the 'Thon rings' in the power spectra from the micrograph reveals the loss of high-resolution information due to drifting. The power spectra are obtained by calculating the Fourier Transform of the micrograph. (**B**) Performing beam-induced motion correction of the movie frames prior to generating the merged image recovers the high-resolution information in the micrograph (right panel). This is demonstrated by analysis of the power spectra of the corrected micrograph that shows clearly defined 'Thon rings'. Both the micrograph and extracted particles also do not show any sign of drifting after the beam-induced motion correction was applied.

rification. These results also provided specific structural evidence for the existence of parallel assembly pathways *in vitro*. However, the question remaining was whether the observed structures recapitulate the assembly intermediates existing *in vivo*.

A significant challenge faced to structurally study the ribosome assembly process *in vivo* is that bacteria are highly efficient in assembling ribosomes and the process occurs in a timescale of just a few minutes. Consequently, ribosome assembly intermediates do not naturally accumulate in significant amounts in bacterial cells (87). To date, structural biologists have leveraged mainly two types of approaches to trigger accumulation of assembly intermediates: chemical and genetic.

The essence of the chemical approach consists of using a small-molecule inhibitor to disable or slow down a specific step in the ribosome assembly process, leading to the accumulation of immature subunits that can be purified and characterized (Figure 4A). Using small-molecule inhibitors as probes for studying a complex biological process has advantages. For example, the chemical compound can be added or removed easily from the cell system and the inhibition effect appears in a time scale of minutes (88).

This type of approach was instrumental in the dissection of the protein synthesis process. This was possible because there is a plethora of chemical probes (antibiotics and other small molecule inhibitors) that affect this process (89,90) and they were used extensively to capture ribosomes in numerous conformational states during protein translation.

Unfortunately, presently there is a scarcity of chemical probes that could be used to study the assembly process of the ribosome. Some of the antibiotics inhibiting translation cause accumulation of 30S and 50S ribosomal subunit precursors (91). However, to date, only lamotrigine, a drug that is also used as an anticonvulsant, has been confirmed as a specific inhibitor of bacterial ribosome biogenesis by targeting a still uncharacterized function of the translation initiation factor IF2 in ribosome assembly. This effect only takes place at cold temperatures but not at 37°C (92). In eukaryotes, only three other compounds have been shown to inhibit specific factors in ribosome assembly in eukaryotes (93–95). These examples clearly shed light on the potential of small molecule inhibitors as probes to study ribosome assembly and to uncover the role of new assembly factors. Therefore, even though chemical approaches in combination with cryo-EM hold tremendous promise and offer unique advantages for the study of the ribosome assembly process, current progress is hampered for the limited number of available probes. Nevertheless, the moment is ripe for a collaborative effort to identify specific chemical inhibitors of ribosome assembly that will be of great use as probes (92).

Instead, genetic approaches have been extensively used to investigate the role of assembly factors in ribosome biogenesis. The main approach has consisted in creating single

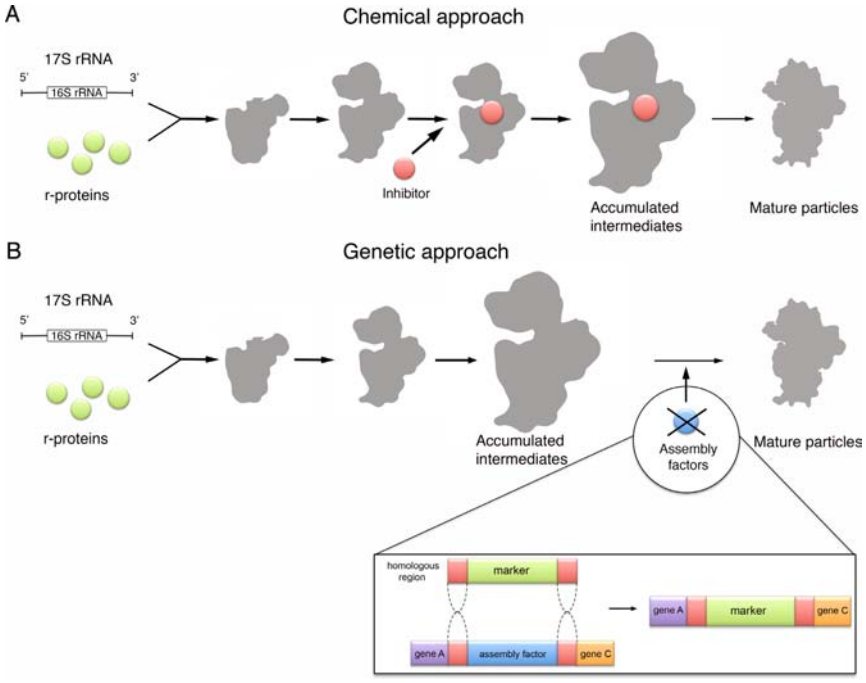

Figure 4. Chemical and genetic approaches to capture *in vivo* assembled ribosomal subunit intermediates. (**A**) The diagram represents the assembly line of the 30S subunit. Chemical approaches use small-molecule inhibitors to block a specific step in the ribosome assembly process, which leads to the accumulation of immature subunits. These particles can be purified and characterized using biochemical or structural methods including cryo-EM. (**B**) In genetic approaches single-gene deletion strains are created by homologous recombination where the open-reading frame coding region of the gene for an assembly factor is replaced with a marker cassette. Absence of a particular assembly factor causes a slowdown of the specific assembly steps assisted by this factor, which eventually leads to accumulation of assembly intermediates that are possible to purify for subsequent analysis.

(or double) deletion strains for one of the assembly factors to disable or slow down the ribosome biogenesis process. These strains accumulate immature subunits in sufficient amounts to be isolated and characterized (Figure 4B).

The foundation of this experimental approach is that the ribosomal particles that accumulate upon single deletion of one of these protein factors are informative on the maturation reaction catalyzed by this enzyme. An important premise for this statement is that the ribosomal particles that accumulate constitute the actual substrate for the factor (45–51). However, it is not trivial to confirm this assumption because genetic perturbations cause a steady-state in which, the actual particles that accumulate may have evolved and do not necessarily constitute the actual substrate for the assembly factor. Instead, they may represent particles that have transitioned into a local energy minimum that are thermodynamically stable and off pathway. Ideally, these particles should also be able to mature into functional subunits to rule out that they are not simply dead-end assembly products (Figure 5). It is only recently that a couple of studies (see section 6 below) (96,97) have asked which of these potential scenarios concur in single deletion strains used to capture assembly intermediates.

Despite these caveats, biochemical and structural studies of particles accumulating in single gene deletion strains of assembly factors have provided a great deal of information regarding the function of a group of assembly factors, mainly those involved at the late stages of maturation (45–51). In the next section, we summarize these studies and the significance of their findings.

WHAT HAVE WE LEARNED FROM STRUCTURAL STUDIES OF RIBOSOME ASSEMBLY INTERMEDIATES PURIFIED FROM DELETION STRAINS?

Several studies have been published in the last few years where single deletion (or depletion) strains of assembly factors were used to trigger accumulation of assembly intermediates for purification and analysis by cryo-EM. Structural characterization of several late 30S assembly intermediates that accumulate in *Escherichia coli* cells lacking either YjeQ (RsgA) (45), RimM (46,49), KsgA (48) or both YjeQ and RbfA (50) assembly factors revealed that the immature 30S particles that accumulate in these null strains are at the late stages of the maturation process (Figure 1A). Most of the structural motifs of these ribosomal subunits resemble

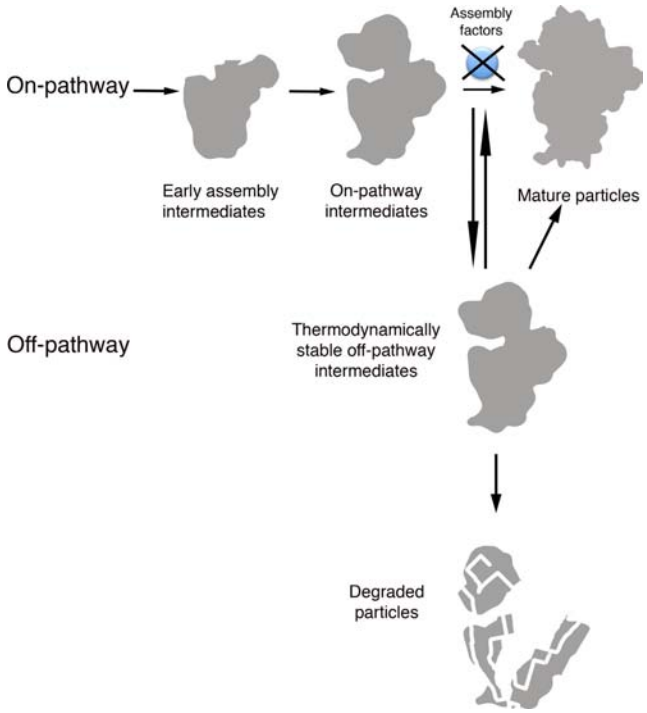

Figure 5. Diagram describing the nature of the immature ribosomal particles accumulating in bacterial cells depleted from assembly factors. In the presence of assembly factors, ribosomal assembly progresses normally to produce mature 30S subunits. In the absence of one or multiple assembly factors, it is possible that the assembly intermediate, which represents the actual substrate for the factor remains as such and accumulates (on-pathway intermediate). It is also plausible that the true on-pathway intermediate may be thermodynamically unstable and end up evolving into a more energetically favorable state. This particle then progresses into the immature particles that are observed accumulating in the null strains and eventually into the mature 30S subunits. A fraction of the particles could also be targeted for degradation.

those of the mature 30S subunit, however they all present a severe distortion at the decoding center that renders these ribosomal particles unable to associate with the 50S subunit and engage in translation. These observations, along with cryo-EM structures of either YjeQ, RbfA and Era (another 30S assembly factor) in complex with mature 30S subunits (Figure 1B) (52–55) postulated that these assembly factors bind immature 30S particles at or near the decoding center to assist in the folding of this functional core.

These studies highlight significant differences regarding the late stages of maturation of the prokaryotic small ribosomal subunit with respect to that in eukaryotes. During the late stages of 40S maturation in yeast there are seven stably bound assembly factors: Tsr1, Rio2 and Dim1 bind to the subunit interface, Pno1 and Nob1 to the platform and Enp1 and Ltv1 to the mRNA opening channel. Together, these factors provide a multi-pronged approach to preventing premature translation initiation (98,99). This is necessary because pre-40S particles can bind mRNAs, translation initiation factors and 60S subunits that are present in the cytoplasm at high concentrations. Therefore, these seven assembly factors cooperate to inhibit each step in the translation initiation pathway.

In bacteria, assembling 30S subunits at the late stages of maturation are also exposed to high concentrations of tRNAs, mRNAs, translation factors and large ribosomal subunits that are present in the cytoplasm. When YjeQ (52,53) and RbfA (55) are bound, they are positioned to block binding of the translation initiation factors IF1 and IF3 (Figure 1B). Similarly, Era binds the anti-Shine Dalgarno sequence at the 3′ end of 16S rRNA (54), thus likely preventing mRNA recruitment (Figure 1B). However, in the 30S subunit ligand blocking is also achieved by the structure of the rRNA itself. The cryo-EM structures of the immature $30S_{\Delta rimM}$ and $30S_{\Delta yjeQ}$ subunits (45,46,49) revealed that the upper domain of helix 44 is dislodged (Figure 1A). Thus, inter-subunit bridges cannot be formed, and the decoding site helix sterically blocks joining with the 50S subunit. Furthermore, the rearrangements of helix 44 distort the decoding site, which is then unable to provide the minor groove interactions critical for productive recognition of aminoacylated tRNA and translation initiation. It is also unclear

whether YjeQ, RbfA, RimM and Era test the functionality of nascent ribosomal subunits by mimicking elements of the translational cycle, as it is the case for some of the eukaryotic assembly factors assisting the maturation of the small ribosomal subunit (98). Therefore, based on what cryo-EM has revealed, several significant differences seem to exist in the way prokaryotic and eukaryotic cells prevent ribosomal subunits from being engaged in translation before their maturation has been completed.

Similar work has also been done with assembly factors involved in the biogenesis of the 50S subunit, including RbgA (47,51), YphC or YsxC (96). These factors are all essential GTPases (100–103). Using *Bacillus subtilis* strains in which one of these three proteins was under the control of an inducible promoter, it was possible to purify incomplete 50S particles that accumulated in the cells under depletion conditions for these factors. Characterization of the immature particles by cryo-EM (Figure 6A) and other techniques, including quantitative mass spectrometry (qMS), revealed that these factors primarily play a role mainly at the late stages of maturation of the 50S subunit. Their role is related to the maturation of the central protuberance and peptidyl transferase center of the 50S subunit (47,51,96).

Overall, analysis of these assembly intermediates revealed that the functional cores of the 30S and 50S ribosomal subunit are the last structural motif to adopt a mature conformation.

Most of these assembly factors acting at these late stages of the process bind to the maturing functional site of the subunits to likely assist their folding. Their coordinated actions also prevent immature particles from prematurely engaging in protein synthesis. The mechanistic insights on how each assembly factor assists in this process and their precise functions remain largely unknown.

Even though most of these structures were obtained before the direct detectors were available and the resolution of these structures is moderate (>10 Å) (Figure 1), these studies clearly illustrate the potential of cryo-EM to visualize in three dimensions the ribosome assembly process.

LIMITATIONS OF USING RIBOSOME ASSEMBLY INTERMEDIATES ACCUMULATING IN DELETION STRAINS FOR CRYO-EM STUDIES

An important question underlying the use of assembly intermediates accumulating in single deletion (or depletion) strains as samples for cryo-EM structural studies on ribosome assembly is whether these particles can progress to a mature subunit that can associate and form functional 70S ribosomes. In addition, it is also essential to understand the nature of these particles and whether they constitute on-pathway assembly intermediates and true substrate for the assembly factors (Figure 5).

The first study addressing the question of competency for maturation of these immature particles chose to analyze an incomplete 50S particle ($45S_{RgbA}$) (51) purified from a *B. subtilis* strain in which the essential assembly factor RbgA had been depleted (100). Pulse-labeling experiments followed by quantitative mass spectrometry (qMS) demonstrated that the $45S_{RgbA}$ particles that accumulate in the cells under RbgA depletion conditions are competent for maturation and progress into functional 70S particles. This initial finding provided reassurance that at least some of the particles that accumulate in these depletion strains do not represent a dead-end product of the reaction and thus, they are likely informative about the function of assembly factors (Figure 5).

More recently, a second study (97) performed pulse-chase experiments to test whether the $30S_{\Delta yjeQ}$ and $30S_{\Delta rimM}$ particles, accumulating in single deletion strains of the YjeQ and RimM assembly factors progress to mature 30S subunits. In these experiments, a discrete population of 17S rRNA that accumulated in the Δ*yjeQ*, Δ*rimM* and wild type strains was labeled by adding ^{3}H (tritium)-uracil to the growing culture and the 17S/16S rRNA ratio was used as a proxy to estimate the proportion of immature 30S subunits that progressed to mature 30S subunits. The obtained results were consistent with the progression of at least a substantial proportion (∼50%) of the $30S_{\Delta yjeQ}$ and $30S_{\Delta rimM}$ particles into mature 30S subunits (Figure 5).

Surprisingly, the same study (97) found that affinity binding of assembly factors YjeQ, Era, RbfA and RimM to the $30S_{\Delta yjeQ}$ and $30S_{\Delta rimM}$ immature particles is weak and that binding would not occur at physiological concentrations. In alignment with these results, mass spectrometry analysis revealed that *in vivo* the occupancy level of these factors in these immature 30S particles is below 10% and that the concentration of factors does not increase when immature particles accumulate in cells. These results suggest that in the absence of these factors, the immature particles evolve into a thermodynamically stable intermediate that exhibits low affinity for the assembly factors (Figure 5). It also implies that the true substrates of YjeQ, RbfA, RimM and Era are immature particles that precede the ribosomal particles accumulating in the knockouts strains.

This conclusion aligns well with a presumed role of these factors in chaperoning the folding of rRNA. It seems likely that these assembly factors may play a role in stabilizing specific rRNA motifs at or near the decoding center in certain conformations (52–55,104). In the absence of any of these factors, the conformation of the rRNA motifs that these factors should bind may transition into a local energy minimum that is thermodynamically more stable. The proposed model from this study (97) is that in the single deletion strains the on-pathway intermediate that constitute the real substrate for each factor progresses to a downstream assembly intermediate that exhibits low affinity to the factors. Indeed, recent studies (45,46,49,50) found that the $30S_{\Delta yjeQ}$ and $30S_{\Delta rimM}$ particles accumulating in the Δ*rimM* and Δ*yjeQ* null strains are structurally similar. Therefore, it seems that in the knockout strains the different on-pathway intermediates that are recognized by the specific assembly factors may be progressing into a structurally similar local energy minimum intermediate (Figure 5).

A similar study (96) investigated the nature of assembly intermediates in the 50S subunit in *B. subtilis* strains depleted from RbgA, YphC and YsxC. In this study, it was found that these assembly factors bind specifically to the immature particles that the depletion strains accumulate. This result is different from what it was found for the 30S subunit assembly intermediates that accumulate in the absence of YjeQ and RimM (97). These results suggest that the 50S

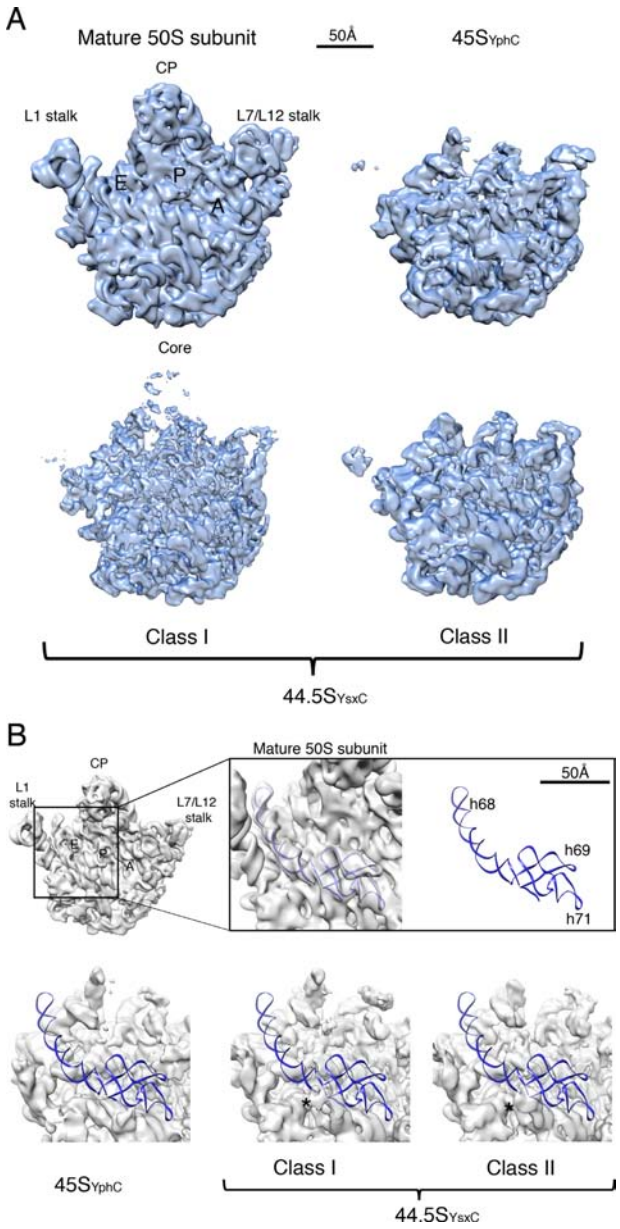

Figure 6. Cryo-EM structures of ribosome assembly intermediates obtained using direct electron detector cameras. (**A**) Gallery of cryo-EM structures from assembly intermediates of the 50S subunit from *B. subtilis*. These intermediates accumulate in the cells of *B. subtilis* strains depleted for assembly factors YhpC ($45S_{YphC}$) and YsxC ($44.5S_{YsxC}$). (**B**) The cryo-EM structures obtained with a direct detector are at sufficient resolution to allow identification of individual rRNA helices still remaining in an immature state. This panel shows rRNA helices in the P and E site of the 50S subunit that are not adopting the mature conformation. A corresponding density for these helices is not observed in the density map. The atomic model of the *B. subtilis* 50S subunit (PDB ID: 3j9W) was docked onto the cryo-EM map to indicate the conformation of these rRNA helices in the mature 50S subunit. This figure is a modified version of that in the publication from Ni *et al*. (96).

immature particles constitute either the actual on-pathway substrates or their conformations have not diverged significantly and they are still recognized by the factors (Figure 5). Therefore, the structural differences existing in these immature particles compared to the mature 50S subunit are likely more informative of the function of the assembly factors than those inferred from the 30S assembly intermediates. These two studies (96,97) also indicate interesting differences in the thermodynamic stability of the assembly intermediates of the 30S and 50S subunits.

The fact that assembly factors acting at late stages seem to be playing a role in the stabilization of transient RNA conformations introduces an interesting functional analogy between assembly factors and *bona fide* r-proteins. Should further research provide mechanistic details of the role of the assembly factors as an RNA chaperone, it may suggest that the function for the assembly factors is not substantially different than the function played by r-proteins. An intriguing difference between the two groups of proteins is that *bona fide* r-proteins remain bound to the ribosomal particle, but assembly factors fall off or are removed once their chaperone function has been completed. The fact that their binding site overlaps with important intersubunit bridges that are essential for the association with the 50S subunit (52–55,104) makes necessary their release and it may have driven this functional divergence.

Overall, *in vivo* assembled immature particles accumulated through genetic approaches present several limitations when used for cryo-EM studies to infer about the function of assembly factors. However, particles characterized up to date have still provided a great deal of functional insights about assembly factors and the late stages of assembly.

OVERCOMING EXISTING LIMITATIONS FOR THE STUDY OF THE RIBOSOME ASSEMBLY PROCESS IN BACTERIA

All assembly intermediates that have been structurally characterized by cryo-EM so far have been purified from single deletion strains or depleted strains lacking individual assembly factors. In addition, most of these structures were obtained from electron micrographs captured either on film or in a CCD and thus, they were only obtained to moderate resolution. Consequently, our current understanding of the function of assembly factors and how these functions are performed in three dimensions is most likely vague at best.

Recent developments in hardware and software for cryo-EM has made possible to obtain the first structures of assembly intermediates in bacteria at a level of detail approaching atomic resolution. An example of the use of these new advancements is a recent publication (96) presenting the structure at ∼5 Å resolution of two 50S immature particles obtained upon depletion of YphC and YsxC, two essential assembly factors (Figure 6A). Different from previous moderate-resolution (∼10–15 Å) cryo-EM studies (45–47,49–51), the structures obtained from direct detectors allow visualization of individual rRNA helices in the intermediate particles that are still in an immature conformation (Figure 6B). Consequently, these structures are generating testable models regarding the function of protein factors in assembly.

With the technology to obtain atomic resolution structures using cryo-EM of immature ribosomal particles now available, developing methods that have the capability to introduce immediate perturbations in the assembly process and allow rapid capture of these intermediates are much needed to move the field forward. Certainly, chemical approaches and the use of small inhibitor molecules against assembly factors (Figure 4A) hold great promise and are uniquely suited to contribute to our structurally understanding of the sequence of events that leads to assembly of the mature subunits with high temporal precision. The ability of small molecules to target specific functions and to produce perturbations with basically no-lag phase allows for a much simpler interpretation of the structures and the information they convey regarding the function of the targeted factors. Similarly small molecule inhibitors of rRNA-ribosomal protein interactions or rRNA folding events also have great potential for isolation of other structurally valuable intermediates (88). Unfortunately, they do not represent at this moment a realistic option due to the scarcity of effective small molecules available to inhibit specific steps of the ribosome assembly process in bacteria (88).

On the other side, the intrinsic thermodynamic instability of the assembly intermediates that accumulate in cells using current genetic approaches (96,97) requires modifying and extending these methods to be able to achieve purification of the on-pathway assembly intermediates that constitute the true substrate for particular assembly factors. Having these purification methods in place will allow obtaining snapshots of the entire spectrum of states existing in the cell during the ribosome biogenesis process by cryo-EM. However, to what extent the protocols for extraction, purification, and cryo-EM specimen preparation will allow us to obtain an unbiased description of these intermediates states is also an open question that needs to be addressed with considerable urgency.

Recent structural work using direct electron detectors for the structural analysis of ribosome assembly intermediates in yeast (105) is providing examples for potential approaches that could be applied in bacteria and they would likely capture the on-pathway assembly intermediates representing the true substrate of particular assembly factors. In this publication nucleoplasmic pre-60S ribosomal particles were purified by tandem affinity purification after introducing a TAP tag (Figure 7A) in the assembly factor Nog2, which associates with nucleoplasmic pre-60S ribosomal particles. The structure of the purified Nog2 particles was solved to ∼3 Å resolution using cryo-EM and showed over 20 different assembly factors bound mainly to an arc region extending from the central protuberance to the polypeptide tunnel exit and the domain called internal transcribed space 2. Guided by chemical cross-linking of proteins coupled with mass spectrometry, it was possible to build the atomic model for 19 of the assembly factors bound to the assembly intermediate.

Considering that in this work the TAP-Nog2 factor was expressed at close to physiological concentrations and that in the tandem affinity purification the tagged factor recovered under native conditions along with associated partners, it is quite likely that this remarkable structure has a close resemblance to the on-pathway assembly intermediate that

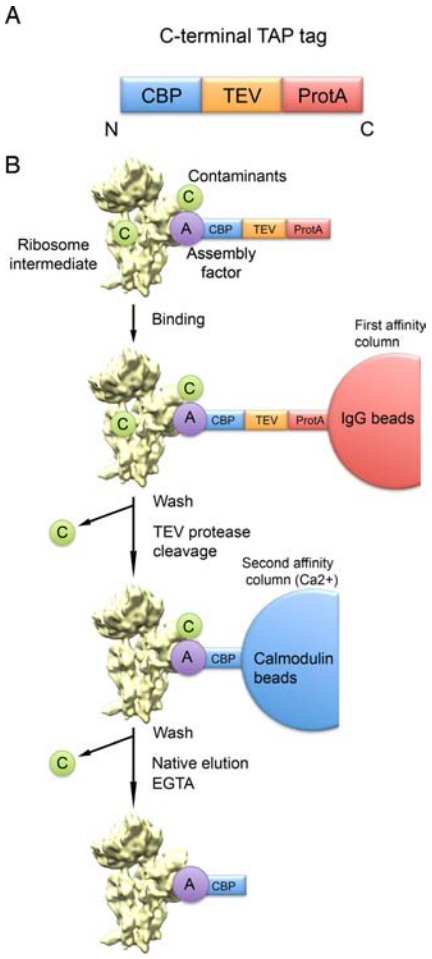

Figure 7. Tandem affinity purification (TAP) as a method for purification of ribosome assembly intermediates. (**A**) Schematic of the C-terminal tag used for TAP. The tag consists of protein A (ProtA) and a calmodulin binding peptide (CBP) separated by a Tobacco Etch Virus (TEV) protease cleavage site. (**B**) Overview of the TAP strategy for purification of ribosome assembly intermediates. This method requires the fusion of the TAP tag to the C-terminal end of the target protein (assembly factor) and introduction of this construct into the host cell. Upon induction the tagged assembly factor will interact with the assembly intermediate (true substrate) in the cells. Cell extracts are prepared and passed through two affinity purification steps. In the first step, ProtA binds tightly to an IgG matrix carrying along the assembly factor in complex with the immature subunit. However, contaminants are washed away. Elution from this column is attained by cleaving the construct with TEV protease. The eluted complex is then loaded in a second column containing calmodulin beads, which have high affinity for the CBP module on the TAP tag (CBP). Additional washes allow for further removal of contaminating proteins. Final elution is achieved under mild conditions with EGTA. All buffer conditions used during this procedure are mild. Therefore, the obtained purified assembly factor in complex with the immature ribosomal particle is eluted under native conditions.

constitutes the true substrate of these assembly factors and that bacterial studies have endeavored to capture, so far with much more limited success.

Tandem affinity purification (Figure 7) was initially developed in yeast, but has been subsequently employed successfully in the analysis of protein–protein interactions and protein complexes in other organisms including mammals, plants, *Drosophila* and more importantly for the work discussed here, also in bacteria. At this point, only a limited number of examples exist in the usage of tandem affinity purification for characterization of protein complexes in bacteria. A few instances include, Gully *et al*. that first used this approach to isolate native protein complexes (106) and Shereda *et al*. (107) that employed this method to purify the RecQ complex and identified three new heterologous proteins that associate with this complex. The most relevant example for the prospects of using tandem affinity purification for the study of ribosome biogenesis in bacteria was work from the same laboratory (108) that discovered the formation of a specific ribonucleoprotein complex between SrmB, a DEAD-box protein, and ribosomal proteins uL4, uL24 and the 5′ region of the 23S rRNA. All of these examples provide exciting prospects for the use of this purification method for capturing on-pathway assembly intermediates that constitute the true substrate of particular assembly factors.

The incorporation of tags in the rRNA has been a recent successful approach for the purification of *in vivo* assembled immature ribosomal particles in bacteria. Gupta *et al*. (109) devised a strategy for purification of pre-16S rRNA-containing assembly intermediates of the 30S subunit. In this approach, an MS2 bacteriophage RNA stem–loop was placed at different positions in the 5′ or 3′ precursor sequences of the 17S rRNA and used for affinity purification using beads pre-bound with MS2 fusion protein. The different location of the MS2 tag led to the purification of three intermediates, each one of them containing different length of the 5′ or 3′ precursor sequences.

Exploring the conformation of the precursor 16S rRNA in these intermediates using chemical probing revealed, similar to the cryo-EM studies from single deletion strains of assembly factors (45,46,48,49) that these particles are at the late stages of maturation and all lack mature functional sites. Similarly, they were also depleted of some of late binding r-proteins that enter late in the assembly; in particular uS2, uS3 and bS21 were severely underrepresented in all of these intermediates. An important conclusion of this work is that the 17S rRNA acts as a major scaffold for 30S subunit biogenesis, which occurs following multiple assembly pathways. More importantly, this MS2-tag based purification method also offers a number of *in vivo* snapshots of assembling 30S subunits, however they have yet to be characterized by cryo-EM. Only then, it will be possible to determine their potential to contribute to our understanding of the late stages of maturation of the 30S subunit and the structural aspects related to the processing of the precursor sequences of the 17S rRNA.

Finally, a recent review paper (88) has also proposed the idea of using small molecule inhibitors as affinity purification tags for low abundance ribosomal intermediates. Once effective small molecule inhibitors of the ribosome matura-

tion process become available, this approach will certainly represent an exciting alternative to the tandem affinity purification method described above for purification of on-pathway immature particles indicated above. The small size of molecular inhibitors makes them less likely to introduce structural artifacts upon perturbations in assembly.

FUTURE PERSPECTIVES AND CONCLUSION

Since the development of the vitrification process by Dubochet and colleagues (16) in 1984, cryo-EM has been an essential contributor to the structure and function of the ribosome. The recent developments in hardware and software and new emerging methods to capture on-pathway ribosome assembly intermediates in complex with assembly factors are currently positioning cryo-EM to make tremendous contributions to the understanding of the ribosome assembly process in bacteria. Undoubtedly, the rich structural information contained in the structures that cryo-EM will produce in the upcoming years using these new developments will provide an extremely valuable framework for the dissection of the molecular roles and function of assembly factors involved in the maturation of the two ribosomal subunits. Furthermore, these structures will provide an effective platform to develop new antibiotics against this fundamental cellular process and pave the way to use these assembly factors as antimicrobial targets. Finally, the fact that some of the bacterial GTPases functioning as assembly factors have eukaryotic counterparts (69) ensures that some of the new insights brought by cryo-EM about the assembly process in bacteria will also provide new therapeutic opportunities for cancer.

ACKNOWLEDGEMENTS

We are grateful to our collaborators in the field of ribosome biogenesis including Drs. James Williamson, Eric Brown and Joseph Davis for invigorating discussion over the years. We also thank Dr. Brett Thurlow for insightful comments on this manuscript. We are also in debt to Dr. John Rubinstein for generously giving us access to the electron microscopy facility at the Hospital for Sick Children in Toronto.

FUNDING

National Science and Engineering Research Council of Canada [RGPIN288327-07]; Canadian Institutes of Health Research (CIHR) [MOP-82930 to J.O.]; National Institutes of Health [1R01GM110248 to R.A.B.]. Funding for open access charge: CIHR.
Conflict of interest statement. None declared.

REFERENCES

1. Schluenzen,F., Tocilj,A., Zarivach,R., Harms,J., Gluehmann,M., Janell,D., Bashan,A., Bartels,H., Agmon,I., Franceschi,F. *et al.* (2000) Structure of functionally activated small ribosomal subunit at 3.3 angstroms resolution. *Cell*, **102**, 615–623.
2. Wimberly,B.T., Brodersen,D.E., Clemons,W.M. Jr, Morgan-Warren,R.J., Carter,A.P., Vonrhein,C., Hartsch,T. and Ramakrishnan,V. (2000) Structure of the 30S ribosomal subunit. *Nature*, **407**, 327–339.
3. Ban,N., Nissen,P., Hansen,J., Moore,P.B. and Steitz,T.A. (2000) The complete atomic structure of the large ribosomal subunit at 2.4 A resolution. *Science*, **289**, 905–920.
4. Tischendorf,G.W., Zeichhardt,H. and Stoffler,G. (1974) Location of proteins S5, S13 and S14 on the surface of the 30S ribosomal subunit from Escherichia coli as determined by immune electron microscopy. *Mol. Gen. Genet.*, **134**, 209–223.
5. Tischendorf,G.W., Zeichhardt,H. and Stoffler,G. (1974) Determination of the location of proteins L14, L17, L18, L19, L22, L23 on the surface of the 50S ribosomal subunit of Escherichia coli by immune electron microscopy. *Mol. Gen. Genet.*, **134**, 187–208.
6. Branlant,C., Krol,A., Sriwidada,J. and Brimacombe,R. (1976) RNA sequences associated with proteins L1, L9, and L5, L18, L25, in ribonucleoprotein fragments isolated from the 50-S subunit of Escherichia coli ribosomes. *Eur. J. Biochem.*, **70**, 483–492.
7. Brimacombe,R., Nierhaus,K.H., Garrett,R.A. and Wittmann,H.G. (1976) The ribosome of Escherichia coli. *Prog. Nucleic Acid Res. Mol. Biol.*, **18**, 323–325.
8. Rinke,J., Yuki,A. and Brimacombe,R. (1976) Studies on the environment of protein S7 within the 30-S subunit Escherichia coli ribosomes. *Eur. J. Biochem.*, **64**, 77–89.
9. Capel,M.S., Engelman,D.M., Freeborn,B.R., Kjeldgaard,M., Langer,J.A., Ramakrishnan,V., Schindler,D.G., Schneider,D.K., Schoenborn,B.P., Sillers,I.Y. *et al.* (1987) A complete mapping of the proteins in the small ribosomal subunit of Escherichia coli. *Science*, **238**, 1403–1406.
10. Fox,G.E. and Woese,C.R. (1975) The architecture of 5S rRNA and its relation to function. *J. Mol. Evol.*, **6**, 61–76.
11. Noller,H.F. and Woese,C.R. (1981) Secondary structure of 16S ribosomal RNA. *Science*, **212**, 403–411.
12. Woese,C.R., Gutell,R., Gupta,R. and Noller,H.F. (1983) Detailed analysis of the higher-order structure of 16S-like ribosomal ribonucleic acids. *Microbiol. Rev.*, **47**, 621–669.
13. Woese,C.R., Winker,S. and Gutell,R.R. (1990) Architecture of ribosomal RNA: constraints on the sequence of "tetra-loops". *Proc. Natl. Acad. Sci. U.S.A.*, **87**, 8467–8471.
14. Gutell,R.R. and Woese,C.R. (1990) Higher order structural elements in ribosomal RNAs: pseudo-knots and the use of noncanonical pairs. *Proc. Natl. Acad. Sci. U.S.A.*, **87**, 663–667.
15. Gutell,R.R., Weiser,B., Woese,C.R. and Noller,H.F. (1985) Comparative anatomy of 16-S-like ribosomal RNA. *Prog. Nucleic Acid Res. Mol. Biol.*, **32**, 155–216.
16. Dubochet,J., Adrian,M., Chang,J.J., Homo,J.C., Lepault,J., McDowall,A.W. and Schultz,P. (1988) Cryo-electron microscopy of vitrified specimens. *Q. Rev. Biophys.*, **21**, 129–228.
17. Frank,J. (1995) Approaches to large-scale structures. *Curr. Opin. Struct. Biol.*, **5**, 194–201.
18. Williamson,J.R. (2009) The ribosome at atomic resolution. *Cell*, **139**, 1041–1043.
19. Munro,J.B., Sanbonmatsu,K.Y., Spahn,C.M. and Blanchard,S.C. (2009) Navigating the ribosome's metastable energy landscape. *Trends Biochem. Sci.*, **34**, 390–400.
20. Frank,J. and Gonzalez,R.L. Jr (2010) Structure and dynamics of a processive Brownian motor: the translating ribosome. *Annu. Rev. Biochem.*, **79**, 381–412.
21. Mitra,K. and Frank,J. (2006) Ribosome dynamics: insights from atomic structure modeling into cryo-electron microscopy maps. *Annu. Rev. Biophys. Biomol. Struct.*, **35**, 299–317.
22. Sigworth,F.J. (1998) A maximum-likelihood approach to single-particle image refinement. *J. Struct. Biol.*, **122**, 328–339.
23. Scheres,S.H., Nunez-Ramirez,R., Gomez-Llorente,Y., San Martin,C., Eggermont,P.P. and Carazo,J.M. (2007) Modeling experimental image formation for likelihood-based classification of electron microscopy data. *Structure*, **15**, 1167–1177.
24. Scheres,S.H., Valle,M. and Carazo,J.M. (2005) Fast maximum-likelihood refinement of electron microscopy images. *Bioinformatics*, **21**(Suppl. 2), ii243–ii244.
25. Scheres,S.H., Valle,M., Nunez,R., Sorzano,C.O., Marabini,R., Herman,G.T. and Carazo,J.M. (2005) Maximum-likelihood multi-reference refinement for electron microscopy images. *J. Mol. Biol.*, **348**, 139–149.
26. Henderson,R. (2004) Realizing the potential of electron cryo-microscopy. *Q. Rev. Biophys.*, **37**, 3–13.

27. Henderson,R. (2015) Overview and future of single particle electron cryomicroscopy. *Arch. Biochem. Biophys.*, **581**, 19–24.
28. Baker,T.S. and Johnson,J.E. (1996) Low resolution meets high: towards a resolution continuum from cells to atoms. *Curr. Opin. Struct. Biol.*, **6**, 585–594.
29. Grigorieff,N. (2013) Direct detection pays off for electron cryo-microscopy. *eLife*, **2**, e00573.
30. Li,X., Mooney,P., Zheng,S., Booth,C.R., Braunfeld,M.B., Gubbens,S., Agard,D.A. and Cheng,Y. (2013) Electron counting and beam-induced motion correction enable near-atomic-resolution single-particle cryo-EM. *Nat. Methods*, **10**, 584–590.
31. Ruskin,R.S., Yu,Z. and Grigorieff,N. (2013) Quantitative characterization of electron detectors for transmission electron microscopy. *J. Struct. Biol.*, **184**, 385–393.
32. Voorhees,R.M., Fernandez,I.S., Scheres,S.H. and Hegde,R.S. (2014) Structure of the mammalian ribosome-Sec 61 complex to 3.4 A resolution. *Cell*, **157**, 1632–1643.
33. Wong,W., Bai,X.C., Brown,A., Fernandez,I.S., Hanssen,E., Condron,M., Tan,Y.H., Baum,J. and Scheres,S.H. (2014) Cryo-EM structure of the Plasmodium falciparum 80S ribosome bound to the anti-protozoan drug emetine. *eLife*, **3**, doi:10.7554/eLife.03080.
34. Fischer,N., Neumann,P., Konevega,A.L., Bock,L.V., Ficner,R., Rodnina,M.V. and Stark,H. (2015) Structure of the E. coli ribosome-EF-Tu complex at <3 A resolution by Cs-corrected cryo-EM. *Nature*, **520**, 567–570.
35. Greber,B.J., Boehringer,D., Leibundgut,M., Bieri,P., Leitner,A., Schmitz,N., Aebersold,R. and Ban,N. (2014) The complete structure of the large subunit of the mammalian mitochondrial ribosome. *Nature*, **515**, 283–286.
36. Khatter,H., Myasnikov,A.G., Natchiar,S.K. and Klaholz,B.P. (2015) Structure of the human 80S ribosome. *Nature*, **520**, 640–645.
37. Traub,P. and Nomura,M. (1968) Structure and function of Escherichia coli ribosomes. I. Partial fractionation of the functionally active ribosomal proteins and reconstitution of artificial subribosomal particles. *J. Mol. Biol.*, **34**, 575–593.
38. Traub,P. and Nomura,M. (1968) Structure and function of E. coli ribosomes. V. Reconstitution of functionally active 30S ribosomal particles from RNA and proteins. *Proc. Natl. Acad. Sci. U.S.A.*, **59**, 777–784.
39. Traub,P. and Nomura,M. (1969) Structure and function of Escherichia coli ribosomes. VI. Mechanism of assembly of 30 s ribosomes studied in vitro. *J. Mol. Biol.*, **40**, 391–413.
40. Traub,P. and Nomura,M. (1969) Studies on the assembly of ribosomes in vitro. *Cold Spring Harb. Symp. Quant. Biol.*, **34**, 63–67.
41. Traub,P., Soll,D. and Nomura,M. (1968) Structure and function of Escherichia coli ribosomes. II. Translational fidelity and efficiency in protein synthesis of a protein-deficient subribosomal particle. *J. Mol. Biol.*, **34**, 595–608.
42. Dietrich,S., Schrandt,I. and Nierhaus,K.H. (1974) Interdependence of E. coli ribosomal proteins at the peptidyltransferase centre. *FEBS Lett.*, **47**, 136–139.
43. Nierhaus,K.H. and Dohme,F. (1974) Total reconstitution of functionally active 50S ribosomal subunits from Escherichia coli. *Proc. Natl. Acad. Sci. U.S.A.*, **71**, 4713–4717.
44. Nierhaus,K.H. and Dohme,F. (1979) Total reconstitution of 50 S subunits from Escherichia coli ribosomes. *Methods Enzymol.*, **59**, 443–449.
45. Jomaa,A., Stewart,G., Martin-Benito,J., Zielke,R., Campbell,T.L., Maddock,J.R., Brown,E.D. and Ortega,J. (2011) Understanding ribosome assembly: the structure of in vivo assembled immature 30S subunits revealed by cryo-electron microscopy. *RNA*, **17**, 697–709.
46. Leong,V., Kent,M., Jomaa,A. and Ortega,J. (2013) Escherichia coli rimM and yjeQ null strains accumulate immature 30S subunits of similar structure and protein complement. *RNA*, **19**, 789–802.
47. Li,N., Chen,Y., Guo,Q., Zhang,Y., Yuan,Y., Ma,C., Deng,H., Lei,J. and Gao,N. (2013) Cryo-EM structures of the late-stage assembly intermediates of the bacterial 50S ribosomal subunit. *Nucleic Acids Res.*, **41**, 7073–7083.
48. Boehringer,D., O'Farrell,H.C., Rife,J.P. and Ban,N. (2012) Structural insights into methyltransferase KsgA function in 30S ribosomal subunit biogenesis. *J. Biol. Chem.*, **287**, 10453–10459.
49. Guo,Q., Goto,S., Chen,Y., Feng,B., Xu,Y., Muto,A., Himeno,H., Deng,H., Lei,J. and Gao,N. (2013) Dissecting the in vivo assembly of the 30S ribosomal subunit reveals the role of RimM and general features of the assembly process. *Nucleic Acids Res.*, **41**, 2609–2620.
50. Yang,Z., Guo,Q., Goto,S., Chen,Y., Li,N., Yan,K., Zhang,Y., Muto,A., Deng,H., Himeno,H. *et al.* (2014) Structural insights into the assembly of the 30S ribosomal subunit in vivo: functional role of S5 and location of the 17S rRNA precursor sequence. *Protein Cell*, **5**, 394–407.
51. Jomaa,A., Jain,N., Davis,J.H., Williamson,J.R., Britton,R.A. and Ortega,J. (2014) Functional domains of the 50S subunit mature late in the assembly process. *Nucleic Acids Res.*, **42**, 3419–3435.
52. Jomaa,A., Stewart,G., Mears,J.A., Kireeva,I., Brown,E.D. and Ortega,J. (2011) Cryo-electron microscopy structure of the 30S subunit in complex with the YjeQ biogenesis factor. *RNA*, **17**, 2026–2038.
53. Guo,Q., Yuan,Y., Xu,Y., Feng,B., Liu,L., Chen,K., Sun,M., Yang,Z., Lei,J. and Gao,N. (2011) Structural basis for the function of a small GTPase RsgA on the 30S ribosomal subunit maturation revealed by cryoelectron microscopy. *Proc. Natl. Acad. Sci. U.S.A.*, **108**, 13100–13105.
54. Sharma,M.R., Barat,C., Wilson,D.N., Booth,T.M., Kawazoe,M., Hori-Takemoto,C., Shirouzu,M., Yokoyama,S., Fucini,P. and Agrawal,R.K. (2005) Interaction of Era with the 30S ribosomal subunit implications for 30S subunit assembly. *Mol. Cell*, **18**, 319–329.
55. Datta,P.P., Wilson,D.N., Kawazoe,M., Swami,N.K., Kaminishi,T., Sharma,M.R., Booth,T.M., Takemoto,C., Fucini,P., Yokoyama,S. *et al.* (2007) Structural aspects of RbfA action during small ribosomal subunit assembly. *Mol. Cell*, **28**, 434–445.
56. Ban,N., Beckmann,R., Cate,J.H., Dinman,J.D., Dragon,F., Ellis,S.R., Lafontaine,D.L., Lindahl,L., Liljas,A., Lipton,J.M. *et al.* (2014) A new system for naming ribosomal proteins. *Curr. Opin. Struct. Biol.*, **24**, 165–169.
57. Srivastava,A.K. and Schlessinger,D. (1990) Mechanism and regulation of bacterial ribosomal RNA processing. *Annu. Rev. Microbiol.*, **44**, 105–129.
58. Hosokawa,K., Fujimura,R.K. and Nomura,M. (1966) Reconstitution of functionally active ribosomes from inactive subparticles and proteins. *Proc. Natl. Acad. Sci. U.S.A.*, **55**, 198–204.
59. Rohl,R. and Nierhaus,K.H. (1982) Assembly map of the large subunit (50S) of Escherichia coli ribosomes. *Proc. Natl. Acad. Sci. U.S.A.*, **79**, 729–733.
60. Herold,M. and Nierhaus,K.H. (1987) Incorporation of six additional proteins to complete the assembly map of the 50 S subunit from Escherichia coli ribosomes. *J. Biol. Chem.*, **262**, 8826–8833.
61. Adilakshmi,T., Bellur,D.L. and Woodson,S.A. (2008) Concurrent nucleation of 16S folding and induced fit in 30S ribosome assembly. *Nature*, **455**, 1268–1272.
62. Talkington,M.W., Siuzdak,G. and Williamson,J.R. (2005) An assembly landscape for the 30S ribosomal subunit. *Nature*, **438**, 628–632.
63. Woodson,S.A. (2008) RNA folding and ribosome assembly. *Curr. Opin. Chem. Biol.*, **12**, 667–673.
64. Woodson,S.A. (2011) RNA folding pathways and the self-assembly of ribosomes. *Acc. Chem. Res.*, **44**, 1312–1319.
65. Kim,H., Abeysirigunawarden,S.C., Chen,K., Mayerle,M., Ragunathan,K., Luthey-Schulten,Z., Ha,T. and Woodson,S.A. (2014) Protein-guided RNA dynamics during early ribosome assembly. *Nature*, **506**, 334–338.
66. Connolly,K. and Culver,G. (2009) Deconstructing ribosome construction. *Trends Biochem. Sci.*, **34**, 256–263.
67. Shajani,Z., Sykes,M.T. and Williamson,J.R. (2011) Assembly of bacterial ribosomes. *Annu. Rev. Biochem.*, **80**, 501–526.
68. Wilson,D.N. and Nierhaus,K.H. (2007) The weird and wonderful world of bacterial ribosome regulation. *Crit. Rev. Biochem. Mol. Biol.*, **42**, 187–219.
69. Britton,R.A. (2009) Role of GTPases in bacterial ribosome assembly. *Annu. Rev. Microbiol.*, **63**, 155–176.
70. Brown,E.D. (2005) Conserved P-loop GTPases of unknown function in bacteria: an emerging and vital ensemble in bacterial physiology. *Biochem. Cell Biol.*, **83**, 738–746.
71. Orlova,E.V. (2000) Structural analysis of non-crystalline macromolecules: the ribosome. *Acta Crystallogr. D Biol. Crystallogr.*, **56**, 1253–1258.

72. Orlova,E.V. and Saibil,H.R. (2011) Structural analysis of macromolecular assemblies by electron microscopy. *Chem. Rev.*, **111**, 7710–7748.
73. Scheres,S.H., Nunez-Ramirez,R., Sorzano,C.O., Carazo,J.M. and Marabini,R. (2008) Image processing for electron microscopy single-particle analysis using XMIPP. *Nat. Protoc.*, **3**, 977–990.
74. Scheres,S.H. (2012) RELION: implementation of a Bayesian approach to cryo-EM structure determination. *J. Struct. Biol.*, **180**, 519–530.
75. Lyumkis,D., Brilot,A.F., Theobald,D.L. and Grigorieff,N. (2013) Likelihood-based classification of cryo-EM images using FREALIGN. *J. Struct. Biol.*, **183**, 377–388.
76. Bammes,B.E., Rochat,R.H., Jakana,J. and Chiu,W. (2011) Practical performance evaluation of a 10k x 10k CCD for electron cryo-microscopy. *J. Struct. Biol.*, **175**, 384–393.
77. Booth,C.R., Jakana,J. and Chiu,W. (2006) Assessing the capabilities of a 4kx4k CCD camera for electron cryo-microscopy at 300kV. *J. Struct. Biol.*, **156**, 556–563.
78. Bammes,B.E., Rochat,R.H., Jakana,J., Chen,D.H. and Chiu,W. (2012) Direct electron detection yields cryo-EM reconstructions at resolutions beyond 3/4 Nyquist frequency. *J. Struct. Biol.*, **177**, 589–601.
79. Glaeser,R.M. and Hall,R.J. (2011) Reaching the information limit in cryo-EM of biological macromolecules: experimental aspects. *Biophys. J.*, **100**, 2331–2337.
80. Glaeser,R.M., McMullan,G., Faruqi,A.R. and Henderson,R. (2011) Images of paraffin monolayer crystals with perfect contrast: minimization of beam-induced specimen motion. *Ultramicroscopy*, **111**, 90–100.
81. Rubinstein,J.L. and Brubaker,M.A. (2015) Alignment of cryo-EM movies of individual particles by optimization of image translations. *J. Struct. Biol.*, **192**, 188–195.
82. Brilot,A.F., Chen,J.Z., Cheng,A., Pan,J., Harrison,S.C., Potter,C.S., Carragher,B., Henderson,R. and Grigorieff,N. (2012) Beam-induced motion of vitrified specimen on holey carbon film. *J. Struct. Biol.*, **177**, 630–637.
83. Sohmen,D., Chiba,S., Shimokawa-Chiba,N., Innis,C.A., Berninghausen,O., Beckmann,R., Ito,K. and Wilson,D.N. (2015) Structure of the Bacillus subtilis 70S ribosome reveals the basis for species-specific stalling. *Nat. Commun.*, **6**, 6941.
84. Amunts,A., Brown,A., Bai,X.C., Llacer,J.L., Hussain,T., Emsley,P., Long,F., Murshudov,G., Scheres,S.H. and Ramakrishnan,V. (2014) Structure of the yeast mitochondrial large ribosomal subunit. *Science*, **343**, 1485–1489.
85. Bai,X.C., Fernandez,I.S., McMullan,G. and Scheres,S.H. (2013) Ribosome structures to near-atomic resolution from thirty thousand cryo-EM particles. *eLife*, **2**, e00461.
86. Mulder,A.M., Yoshioka,C., Beck,A.H., Bunner,A.E., Milligan,R.A., Potter,C.S., Carragher,B. and Williamson,J.R. (2010) Visualizing ribosome biogenesis: parallel assembly pathways for the 30S subunit. *Science*, **330**, 673–677.
87. Lindahl,L. (1975) Intermediates and time kinetics of the in vivo assembly of Escherichia coli ribosomes. *J. Mol. Biol.*, **92**, 15–37.
88. Stokes,J.M. and Brown,E.D. (2015) Chemical modulators of ribosome biogenesis as biological probes. *Nat. Chem. Biol.*, **11**, 924–932.
89. Wilson,D.N. (2009) The A-Z of bacterial translation inhibitors. *Crit. Rev. Biochem. Mol. Biol.*, **44**, 393–433.
90. Wilson,D.N. (2014) Ribosome-targeting antibiotics and mechanisms of bacterial resistance. *Nat. Rev. Microbiol.*, **12**, 35–48.
91. Champney,W.S. (2006) The other target for ribosomal antibiotics: inhibition of bacterial ribosomal subunit formation. *Infect. Disord. Drug Targets*, **6**, 377–390.
92. Stokes,J.M., Davis,J.H., Mangat,C.S., Williamson,J.R. and Brown,E.D. (2014) Discovery of a small molecule that inhibits bacterial ribosome biogenesis. *eLife*, **3**, e03574.
93. Loibl,M., Klein,I., Prattes,M., Schmidt,C., Kappel,L., Zisser,G., Gungl,A., Krieger,E., Pertschy,B. and Bergler,H. (2014) The drug diazaborine blocks ribosome biogenesis by inhibiting the AAA-ATPase Drg1. *J. Biol. Chem.*, **289**, 3913–3922.
94. Drygin,D., Lin,A., Bliesath,J., Ho,C.B., O'Brien,S.E., Proffitt,C., Omori,M., Haddach,M., Schwaebe,M.K., Siddiqui-Jain,A. *et al.* (2011) Targeting RNA polymerase I with an oral small molecule CX-5461 inhibits ribosomal RNA synthesis and solid tumor growth. *Cancer Res.*, **71**, 1418–1430.
95. Drygin,D., Siddiqui-Jain,A., O'Brien,S., Schwaebe,M., Lin,A., Bliesath,J., Ho,C.B., Proffitt,C., Trent,K., Whitten,J.P. *et al.* (2009) Anticancer activity of CX-3543: a direct inhibitor of rRNA biogenesis. *Cancer Res.*, **69**, 7653–7661.
96. Ni,X., Davis,J.H., Jain,N., Razi,A., Benlekbir,S., McArthur,A.G., Rubinstein,J.L., Britton,R.A., Williamson,J.R. and Ortega,J. (2016) YphC and YsxC GTPases assist the maturation of the central protuberance, GTPase associated region and functional core of the 50S ribosomal subunit. *Nucleic Acids Res.*, **44**, 8442–8455.
97. Thurlow,B., Davis,J.H., Leong,V., Moraes,T.F., Williamson,J.R. and Ortega,J. (2016) Binding properties of YjeQ (RsgA), RbfA, RimM and Era to assembly intermediates of the 30S subunit. *Nucleic Acids Res.*, **44**, 9918–9932.
98. Strunk,B.S., Novak,M.N., Young,C.L. and Karbstein,K. (2012) A translation-like cycle is a quality control checkpoint for maturing 40S ribosome subunits. *Cell*, **150**, 111–121.
99. Karbstein,K. (2013) Quality control mechanisms during ribosome maturation. *Trends Cell Biol.*, **23**, 242–250.
100. Uicker,W.C., Schaefer,L. and Britton,R.A. (2006) The essential GTPase RbgA (YlqF) is required for 50S ribosome assembly in Bacillus subtilis. *Mol. Microbiol.*, **59**, 528–540.
101. Uicker,W.C., Schaefer,L., Koenigsknecht,M. and Britton,R.A. (2007) The essential GTPase YqeH is required for proper ribosome assembly in Bacillus subtilis. *J. Bacteriol.*, **189**, 2926–2929.
102. Matsuo,Y., Morimoto,T., Kuwano,M., Loh,P.C., Oshima,T. and Ogasawara,N. (2006) The GTP-binding protein YlqF participates in the late step of 50 S ribosomal subunit assembly in Bacillus subtilis. *J. Biol. Chem.*, **281**, 8110–8117.
103. Schaefer,L., Uicker,W.C., Wicker-Planquart,C., Foucher,A.E., Jault,J.M. and Britton,R.A. (2006) Multiple GTPases participate in the assembly of the large ribosomal subunit in Bacillus subtilis. *J. Bacteriol.*, **188**, 8252–8258.
104. Lovgren,J.M., Bylund,G.O., Srivastava,M.K., Lundberg,L.A., Persson,O.P., Wingsle,G. and Wikstrom,P.M. (2004) The PRC-barrel domain of the ribosome maturation protein RimM mediates binding to ribosomal protein S19 in the 30S ribosomal subunits. *RNA*, **10**, 1798–1812.
105. Wu,S., Tutuncuoglu,B., Yan,K., Brown,H., Zhang,Y., Tan,D., Gamalinda,M., Yuan,Y., Li,Z., Jakovljevic,J. *et al.* (2016) Diverse roles of assembly factors revealed by structures of late nuclear pre-60S ribosomes. *Nature*, **534**, 133–137.
106. Gully,D., Moinier,D., Loiseau,L. and Bouveret,E. (2003) New partners of acyl carrier protein detected in Escherichia coli by tandem affinity purification. *FEBS Lett.*, **548**, 90–96.
107. Shereda,R.D., Bernstein,D.A. and Keck,J.L. (2007) A central role for SSB in Escherichia coli RecQ DNA helicase function. *J. Biol. Chem.*, **282**, 19247–19258.
108. Trubetskoy,D., Proux,F., Allemand,F., Dreyfus,M. and Iost,I. (2009) SrmB, a DEAD-box helicase involved in Escherichia coli ribosome assembly, is specifically targeted to 23S rRNA in vivo. *Nucleic Acids Res.*, **37**, 6540–6549.
109. Gupta,N. and Culver,G.M. (2014) Multiple in vivo pathways for Escherichia coli small ribosomal subunit assembly occur on one pre-rRNA. *Nat. Struct. Mol. Biol.*, **21**, 937–943.

8442–8455 *Nucleic Acids Research, 2016, Vol. 44, No. 17* *Published online 2 August 2016*
doi: 10.1093/nar/gkw678

YphC and YsxC GTPases assist the maturation of the central protuberance, GTPase associated region and functional core of the 50S ribosomal subunit

Xiaodan Ni[1,2], Joseph H. Davis[3,4], Nikhil Jain[5,6], Aida Razi[1,2], Samir Benlekbir[7], Andrew G. McArthur[1,2], John L. Rubinstein[7,8,9], Robert A. Britton[5,6], James R. Williamson[3,4] and Joaquin Ortega[1,2,*]

[1]Department of Biochemistry and Biomedical Sciences, McMaster University, Hamilton, Ontario L8S4K1, Canada, [2]M.G. DeGroote Institute for Infectious Diseases Research, McMaster University, Hamilton, Ontario L8S4K1, Canada, [3]Department of Molecular Biology, The Scripps Research Institute, La Jolla, CA 92037, USA, [4]Department of Chemistry and The Skaggs Institute for Chemical Biology, The Scripps Research Institute, La Jolla, CA 92037, USA, [5]Department of Molecular Virology and Microbiology, Baylor College of Medicine, Houston, TX 77030, USA, [6]Center for Metagenomics and Microbiome Research, Baylor College of Medicine, Houston, TX 77030, USA, [7]Molecular Structure and Function Program, The Hospital for Sick Children,Toronto, Ontario M5G 0A4, Canada, [8]Department of Biochemistry, University of Toronto, Toronto, Ontario M5S 1A8, Canada and [9]Department of Medical Biophysics, University of Toronto, Toronto, Ontario M5G 1L7, Canada

Received April 12, 2016; Revised July 20, 2016; Accepted July 21, 2016

ABSTRACT

YphC and YsxC are GTPases in *Bacillus subtilis* that facilitate the assembly of the 50S ribosomal subunit, however their roles in this process are still uncharacterized. To explore their function, we used strains in which the only copy of the *yphC* or *ysxC* genes were under the control of an inducible promoter. Under depletion conditions, they accumulated incomplete ribosomal subunits that we named 45S$_{YphC}$ and 44.5S$_{YsxC}$ particles. Quantitative mass spectrometry analysis and the 5–6 Å resolution cryo-EM maps of the 45S$_{YphC}$ and 44.5S$_{YsxC}$ particles revealed that the two GTPases participate in the maturation of the central protuberance, GTPase associated region and key RNA helices in the A, P and E functional sites of the 50S subunit. We observed that YphC and YsxC bind specifically to the two immature particles, suggesting that they represent either on-pathway intermediates or that their structure has not significantly diverged from that of the actual substrate. These results describe the nature of these immature particles, a widely used tool to study the assembly process of the ribosome. They also provide the first insights into the function of YphC and YsxC in 50S subunit assembly and are consistent with this process occurring through multiple parallel pathways, as it has been described for the 30S subunit.

INTRODUCTION

A challenge in studying ribosome assembly in bacteria is that cells do not accumulate assembly intermediates. Early studies (1–3) relied on pulse labeling and polyacrylamide gels to study the small amounts of incomplete ribosomal particles that accumulate in normal cells. These experiments identified several 30S and 50S intermediates that overall accounted for only a 2–5% of the total rRNA present in exponentially growing bacteria.

More recently, a few groups have explored the use of small molecule screenings to find chemical inhibitors of specific steps in the ribosome assembly process (4). Small molecules have been extremely effective as precision tools to dissect the translation process performed by the mature ribosome. Many of these small molecules are used as antibiotics and researchers have also used them to capture the conformational changes that mature ribosomes undergo as they decode the mRNA sequence and synthesize the polypeptide chain. However, there are only a handful of chemical probes that inhibit ribosome biogenesis in yeast and mammals (5–9) and only one in bacteria (10). With so few inhibitors available to probe such a complex process, to date ribosome biogenesis has been studied almost exclusively by genetic and biochemical approaches.

A genetic approach that has been popular (11–14) consists of using single gene deletion strains for trans-acting

*To whom correspondence should be addressed. Tel: +1 905 525 9140 (Ext. 22703); Fax: +1 905 522 9033; Email: ortegaj@mcmaster.ca

factors that assist the assembly process of the ribosome. In these strains, the ribosome biogenesis process slows down significantly and it is then possible to isolate and characterize the immature subunits that are the product of the perturbation. Analysis of these particles has provided some of the initial insights into how protein factors assist the assembly process of the ribosomal subunits. For example, characterization of several 30S assembly intermediates that accumulate in *Escherichia coli* cells lacking either YjeQ (11), RimM (12,13) or RbfA (14,15) led to the conclusion that these assembly factors act at the late stages of assembly assisting the maturation of the decoding center of the 30S subunit.

Genetic approaches have also been a prominent experimental tool to establish the function of assembly factors assisting the maturation of the 50S subunit. Of particular interest are three GTPases: RbgA (also known as YlqF), YphC and YsxC. These proteins are essential for growth in *Bacillus subtilis*. Initially, genetic approaches established that the three GTPases act late in the assembly process of the 50S subunit (16–18). More recently (19,20) using a *B. subtilis* strain in which RbgA was under the control of an inducible promoter, it was possible to purify incomplete 50S particles ($45S_{RbgA}$) that accumulated in the cells under depletion conditions for this factor. Characterization of the $45S_{RbgA}$ particles by quantitative mass spectrometry (qMS), cryo-electron microscopy (cryo-EM) and chemical footprinting revealed that RbgA plays a critical role in the maturation of the central protuberance and peptidyl transferase center of the 50S subunit. Importantly, pulse-labeling experiments determined that the $45S_{RbgA}$ particles that accumulate in the cells under RbgA depletion conditions are competent for maturation and progress into functional 70S particles. This finding was important as it provided reassurance that the $45S_{RbgA}$ particles do not represent a dead-end product of the reaction and thus, they render physiologically relevant information about the function of RbgA.

Despite these advances, the mechanistic insights of how RbgA assists the maturation of the functional core of the 50S subunit or the exact functions of the other two GTPases (YphC and YsxC) remain largely unknown. Similarly to RbgA, cells depleted in YphC or YsxC also accumulate incomplete 50S subunits, named $45S_{YphC}$ and $44.5S_{YsxC}$ particles, respectively (17). Therefore, we undertook the analysis of these particles to reveal the function of YphC and YsxC in the assembly of the large ribosomal subunit.

Quantitative mass spectrometry (qMS) analysis revealed that the $45S_{YphC}$ and $44.5S_{YsxC}$ particles lacked several late-binding r-proteins indicating that they represent, as for the $45S_{RbgA}$ particles, late assembly intermediates of the 50S subunit. Cryo-EM reconstructions showed that these particles exhibited significant structural differences with the mature 50S subunit in important functional sites, including the A, P and E sites, central protuberance and GTPase associated region suggesting that YphC and YsxC, together with RbgA, play key roles in the maturation of these regions.

To further investigate the nature of the immature $45S_{RbgA}$, $45S_{YphC}$ and $44.5S_{YsxC}$ particles and determine whether they constitute the actual substrates for the GTPases, we tested the binding of each factor to the immature particles. We found that RbgA, YphC and YsxC can individually bind to each of the immature particles as well as to the mature 50S subunit. This binding is specific as it triggers a stimulation of the intrinsic GTPase activity of the assembly factors. However, a hierarchy of binding similar to that found for bona fide r-proteins was not apparent for the binding of these factors. This finding is consistent with recent kinetic work revealing that assembly of the ribosome occurs through multiple parallel pathways, which introduce the necessary flexibility and redundancy to make ribosome assembly an extremely robust and efficient process. The immature particles also supported binding of multiple assembly factors simultaneously. These results suggest that the assembly intermediates that accumulate in the absence of RbgA, YphC or YsxC are thermodynamically stable. They either constitute the actual substrates for the assembly factors or their conformations have not diverged significantly from that present in the actual substrate, so that RbgA, YphC or YsxC still bind to them.

MATERIALS AND METHODS

Purification of mature 50S subunits and immature $45S_{YphC}$, $45S_{RbgA}$ and $44.5S_{YsxC}$ particles

The mature 50S subunits and immature $45S_{YphC}$, $44.5S_{YsxC}$ and $45S_{RbgA}$ particles were purified from IF2-depleted (RB419), YphC-depleted (RB290), YsxC-depleted (RB260) and RbgA-depleted (RB301) *B. subtilis* strains, respectively. Generation of these strains has been previously described (17,21). The mature 50S subunit and immature $45S_{RbgA}$ particles were purified as described previously (19). The $44.5S_{YsxC}$ and $45S_{YphC}$ particles were purified by the same procedure used with the $45S_{RbgA}$ particles.

Protein overexpression clones

The pET21b-*ylqF* plasmid used to overexpress RbgA was expressed with a C-terminal His_6-tag was generated as described previously (16). The pET15b-*yphC* and pET15b-*ysxC* plasmids used to overexpress YphC and YsxC with a N-terminal His_6 tag cleavable by thrombin protease were produced as follows. The sequence of the *yphC* gene (NCBI reference sequence: NC_000964.3) and *ysxC* gene (NCBI reference sequence: NC_016047.1) were optimized for overexpression in *E. coli* cells using the GeneOptimizer software® and subsequently synthesized (Life Technologies; Thermo Fisher Scientific) with a NdeI and a BamHI site in the 5′ and 3′ ends of the gene, respectively. The genes were cloned into the carrier pMA-RQ (ampR) plasmid using the *SfiI* and *SfiI* cloning sites and subsequently subcloned into the final expression vector pET15b using the NdeI and a BamHI restriction sites. The final constructs were verified by sequencing (MOBIX, McMaster University).

Protein overexpression and purification

YphC and YsxC were overexpressed as N-terminal His_6-tag proteins by transforming *E. coli* BL21 (DE3) with pET15b-*yphC* and pET15b-*ysxC* plasmids, respectively. For both proteins, one liter of LB medium containing 100 μg/ml ampicillin was inoculated with 10 ml of saturated overnight

culture and cells were grown to OD_{600} = 0.6 by incubation at 37°C and shaking at 225 rpm in an Excella E24 incubator (New Brunswick). Expression was induced by the addition of 1mM isopropyl β-D-1-thiogalactopyranoside (IPTG). Cells were then induced for 3 h at 37°C and harvested by centrifugation at 3700*g* for 15 min. Cell pellets were washed with 1 × phosphate-buffered saline (PBS) buffer (137 mM NaCl, 2.7 mM KCl, 8.1 mM Na_2HPO_4 at pH 7.4) and re-suspended in 20 ml of binding buffer containing 50 mM $NaPO_4$ pH 8 and 0.3 M NaCl containing a protease inhibitor cocktail (Complete Protease Inhibitor Cocktail Tablets. Roche). The cell suspension was passed through a French press at 20 000 lb/in^2 pressure three consecutive times and the lysate was spun at 30 000*g* for 45 min to clear cell debris, then filtered with a 0.45 μm filter and loaded into a HiTrap Metal Chelating Column (GE Healthcare Life Sciences) previously equilibrated with binding buffer. Nonspecifically bound proteins were washed with buffer containing 20 mM $NaPO_4$ pH 7.5, 0.5M NaCl and 60 mM imidazole. Elution of YphC and YsxC was done by increasing the concentration of imidazole to 250 mM. Purity of the fractions was assayed by SDS-PAGE and fractions containing each respective protein were collected, pooled together and dialyzed overnight against 20 mM $NaPO_4$ pH 7.5 and 5% glycerol. Dialyzed protein preparations were centrifuged at 12 000*g* for 10 min in an Eppendorf Mini-spin centrifuge to remove any precipitated protein. The N-terminal His_6-tags of YphC and YsxC were removed by digestion with thrombin (Sigma) that was added in the amount of 25 U/ml to the pooled fractions containing the target proteins during dialysis. The reaction mixtures were then loaded onto a Hi-Trap Q HP anion exchange column (GE Healthcare Life Sciences) for YphC protein and Hi-Trap SP HP column (GE Healthcare Life Sciences) for YsxC protein. The columns were pre-equilibrated with Buffer A (20 mM $NaPO_4$ pH 7.5, 5% glycerol). A linear gradient of NaCl concentration from 0 mM and 1 M was used to wash and elute the protein. YphC and YsxC were eluted at a concentration of 350 and 500 mM NaCl, respectively. Protein-containing fractions were verified by SDS-PAGE, concentrated, and NaCl was removed by exchanging the buffer to desalting buffer (50 mM Tris–HCl (pH 7.5), 750 mM KCl, 5 mM $MgCl_2$, 20 mM imidazole, 2 mM DTT and 10% glycerol) using a 10 kDa-cutoff centrifuged concentrator (Amicon). In the final step of concentration the buffer was exchanged to storage buffer (50 mM Tris–HCl at pH 7.5, 750 mM KCl, 5 mM $MgCl_2$, 2 mM DTT and 10% glycerol) also using a 10 kDa-cutoff centrifuged concentrator (Amicon). Pure proteins were frozen in liquid nitrogen and stored at −80°C.

RbgA was overexpressed as a C-terminal His_6-tag protein by transforming *E. coli* BL21 (DE3) with the pET21b-*ylqF* plasmid. The overexpression and purification protocol for RbgA was identical to that used for YphC and YsxC. However, RbgA only required a HiTrap Metal Chelating Column (GE Healthcare Life Sciences) to be purified. There were also the following differences in the buffers used for the purification: the binding buffer used in this case contained 20 mM $NaPO_4$ pH 7.5, 0.5 M NaCl and 20 mM imidazole. The washing buffer for the HiTrap Metal Chelating Column was 20 mM $NaPO_4$ pH 7.5, 0.5 M NaCl and 60 mM imidazole. The protein eluted at a concentration of 250 mM imidazole. The fractions containing RbgA were pooled and dialyzed against buffer containing 20 mM $NaPO_4$ pH 7.5 and 5% glycerol. The C-terminal His_6-tag in RbgA was not removable.

Binding assays

Binding assays were done using a previously published protocol but with modifications (22). In particular, Nanosep Omega centrifugal devices (PALL) (100 kDa cut-off) were prepared by blocking for non-specific binding of proteins by incubating the filter membrane with 500 μl of 1% [w/v] bovine serum albumin (BSA) for 90 min. Filters were then washed by rinsing with 500 μl of RNase free water and then removing any residual blocking solution by adding 500 μl of RNase free water and spinning at 12 000*g* for 10 min. Binding reactions were prepared by incubating 200 pmoles of each assembly factor with 40 pmol of mature or immature ribosomal particles in a 100 μl reaction in Binding Buffer (10 mM Tris–HCl at pH 7.5, 7 mM magnesium acetate, 150 mM NH_4Cl and 1 mM DTT). GTP, GDP and GMPPNP was added in the reactions as indicated at a final concentration of 1 mM. Reactions were incubated at 37°C for 30 min followed by centrifugation in the 100 kDa centrifugal devices at 12 000*g* for 10 min to separate ribosomal particles and bound factors that were retained by the filter from unbound proteins in the flow-through (FT) fraction. The flow-through was collected and the filter was gently washed twice with 100 μl of Binding Buffer followed by a 5 min spin at 12 000*g*. Finally, the ribosomal particles and bound proteins retained by the filter were vigorously resuspended in 100 μl of Binding Buffer and collected as the bound fraction (B). To resolve the flow-through and bound fractions, 30 μl of sample were mixed with 6× SDS-PAGE loading buffer and loaded into a 4–12% Criterion™ XT Bis–Tris gel (Bio-Rad). Samples were run in XT MOPS buffer (Bio-Rad). Gels were stained with Coomassie Brilliant Blue and visualized using a ChemiDoc MP system (Bio-Rad).

Quantitative mass spectrometry

Samples were purified as described above with either 500 mM (high salt) or 150 mM (low salt) NH_4Cl present during the sucrose cushion centrifugation. For the low salt samples, 10 pmol of each sample (50S, $45S_{RbgA}$, $45S_{YphC}$ or $44.5S_{YxsC}$) was spiked with 10 pmol of 70S particles purified from wild-type cells grown in ^{15}N-labeled media as described previously (19). Samples were then precipitated, reduced, alkylated, and digested to tryptic peptides according to Jomaa *et al.* (19). Peptides were injected onto a C18 nanoflex column (Eksigent), and eluted using a 120 min 5–45% convex acetonitrile gradient.

Data was initially collected in a data-dependent acquisition mode with a cycle consisting of a 200 ms MS^1 scan followed by 30 100 ms MS^2 scans, selecting precursors exceeding 125 counts per second. Precursors were excluded for 12 s after their being selected twice. Datasets were searched against the *B. subtilis* proteome using Mascot. Search results were combined to generate a spectral library using Skyline (23).

Data was also collected in a data-independent SWATH acquisition mode (24), using a 250 ms MS^1 scan followed by 32 MS^2 scans ranging 400–1200 Th, each 25 Th in width. Using the spectral library noted above, product ion chromatograms from the SWATH acquisition were extracted for ^{14}N and ^{15}N species using Skyline. Peptides and transitions were filtered to eliminate spectral interference and poorly ionized precursors. $^{14}N/^{15}N$ abundance ratios were calculated for each transition. Protein abundance was calculated as the median value of this ratio, normalized to the median value observed for protein L20, which was expected to be bound stoichiometrically.

Samples undergoing the high salt wash were spiked with a mixture of ^{14}N- and ^{15}N-labeled 70s particles as described (25), and peptide abundances were determined from MS^1 data obtained on an Agilent G1969A ESI-TOF mass spectrometer according to Gulati *et al.* (25). Protein abundance was again calculated as the median $^{14}N/^{15}N$ ratio, normalized to that of protein L20.

GTPase assays

To measure intrinsic GTPase activity, RbgA and YsxC were incubated at a concentration of 2 μM with a range of GTP concentrations (0–1 mM). YphC in equivalent reactions was added to a concentration of 200 nM. The background of the assay itself was measured by running control reactions with no enzyme at each GTP concentration. These background values were subtracted from the total GTPase activity exhibited by the reactions containing the assembly factor at each GTP concentration. To determine the stimulation of RbgA, YsxC and YphC GTPase activity by the ribosomal particles, we assembled reactions containing 50 nM concentration of assembly factor and an equal concentration of either mature 50S subunits or one of the immature particles. All assays were performed by first calculating the background GTPase activity from each ribosomal particle (50S subunit, $45S_{YphC}$, $44.5S_{YsxC}$ and $45S_{RbgA}$ particles) at 50 nM incubated from 0 to 1 mM of GTP. This background subtraction ensured accuracy in the calculations by removing all background phosphate production not due to the assembly factors themselves.

All reactions were incubated at 37°C for 30 min before measuring the released free phosphate by the malachite green assay (BioAssays Systems). The assay showed a linear behaviour for this incubation time. Reactions were performed in the reaction buffer (50 mM Tris–HCl (pH 7.5), 200 mM KCl, 10 mM $MgCl_2$ and 1 mM DTT) and terminated by the addition of malachite green reagent. Released phosphate was detected by monitoring the color formation at 620 nm using a 96-well plate reader (Tecan Sunrise). The apparent K_M and k_{cat} values were calculated by fitting the data to the Michaelis-Menten equation with non-linear regression using the GraphPad Prism software. All these assays were performed at least in triplicate and with at minimum of two different preparations of the assembly factors and ribosomal particles.

Cryo-electron microscopy and image processing

Purified ribosomal particles ($45S_{YphC}$, $44.5S_{YsxC}$) were diluted to a concentration of 40–50 nM in buffer E (10 mM Tris–HCl at pH 7.5, 10 mM magnesium acetate, 60 mM NH_4Cl and 3 mM 2-mercaptoethanol). Approximately 3.6 μl of the diluted sample was applied in the holey carbon grids (c-flat CF-2/2-2C-T) with an additional layer of continuous thin carbon (5–10 nm). Before the sample was applied, grids were glow discharged in air at 5 mA for 15 s. Vitrification of samples was performed in a Vitrobot (FEI) by blotting the grids twice, 15 s each time and with an offset of −1.5 before they were plunged into liquid ethane.

Grids were loaded in a Gatan 626 single tilt cryo-holder and introduced into a FEI Tecnai F20 electron microscope operated at 200 kV and equipped with a Gatan K2 Summit direct detector device camera. This detector was used in counting movie mode with five electrons per pixel per second for 15 seconds exposures and 0.5 s/frame. This method produced movies consisting of 30 frames with an exposure rate of ∼1 $e^-/Å^2$. Movies were collected with a defocus range of 1–2.5 μm and a nominal magnification of 25 000×, which produced images with a calibrated pixel size of 1.45 Å.

The 30 frames in each movie were aligned using the program alignframesleastsquares_list (26) and averaged into one single micrograph with the shiftframes_list program (26). These programs are available from (https://sites.google.com/site/rubinsteingroup/home). These micrographs were used to estimate the parameters of the contrast transfer function using CTFFIND3 (27) and also to determine the coordinates for particles in the frames of the movies. This last step was performed using the autopicking procedure in Relion (28). The coordinates obtained were used to extract candidate particle images from the 30 unaligned frames in the movie. The motion of the individual particles in the frames was tracked and corrected using alignparts_lmbfgs algorithm (26). This procedure produced one stack of particle images fully corrected from beam-induced motion from the first 20 frames of each movie. Therefore, the total accumulated dose to produce these particles images was 20 $e^-/Å^2$. The initial number of particle images in the data sets for the $45S_{YphC}$ and $44.5S_{YsxC}$ structures was 105 302 and 91 724, respectively. These particle data sets were subjected to two- and three-dimensional classification with Relion (28). In the case of the $45S_{YphC}$ particle three-dimensional classes were built from 101 264 particle images and the 45 369 particles assigned to one class were used to build the final consensus 3D map. A similar approach was followed with the $44.5S_{YsxC}$ structure where three-dimensional classes were produced from 87 684 particle images. The final three-dimensional consensus map for the class I conformation was built from the 36 033 particle images that were assigned to one of the 3D classes obtained in the 3D classification and the consensus class II map was produced from the 46 430 particle images from another of the 3D classes.

Subsequently, the data sets producing the consensus structures were subjected to focus classification with subtraction of the residual signal using Relion (28) following an approach previously described (29). The mask for focus classification on the central protuberance, helix 38, GTPase associated region and A, P and E functional sites was generated by converting the atomic model of the 50S subunit (PDB ID 3j9w) into a density map after the following mo-

tifs were removed from the atomic model: 5S rRNA, helices from the 23S rRNA including h80-88 (nt 2280–2420), h38 (nt 890–980), h42-44 (nt 1080–1160), h89-93 (nt 2480–2630), h68-71 (nt 1870–2000), h76-78 (2140-2200), and ribosomal proteins uL16, bL27, uL6, bL33, bL35, bL28, bL36, bL31, uL18, uL5, uL30, uL15, uL10 and uL11. This density map was used to create a soft-edged mask and to also subtract the signal of the mature motifs in the experimental particles. The newly created stacks of particles after signal subtraction and the mask were used as input for the focus classification run. During the classification step, we kept all orientations fixed at the values determined in the refinement of the consensus maps. Each data set rendered three distinct classes that were subjected to a separate 3D auto-refinement using the cryo-EM structure of the 50S subunit from *B. subtilis* (PDB ID 3j9w) low pass filtered to 50 Å.

Prior to visualization, sharpening of the cryo-EM maps was done by applying a negative *B*-factor estimated using automated procedures (30). Relion processes were calculated using the SciNet cluster (31) and a VMWare-based Ubuntu linux server with 32 processors / 256 GB RAM within the McMaster Service Lab and Repository (MSLR) computing cluster. We used the program ResMap (32) to estimate the local resolution of the structures. The UCSF Chimera program (33) was used for the visualization of cryo-EM maps and render figures. To identify the rRNA helices in the $45S_{YphC}$ and $44.5S_{YsxC}$ structures that were different from the mature 50S subunit the atomic model of the *B. subtilis* 50S subunit (PDB ID 3J9W) was docked into the cryo-EM maps first as a rigid body using Chimera and then the fitting was optimized by Molecular Dynamics Flexible Fitting (MDFF) (34).

RESULTS

The $45S_{YphC}$, $44.5S_{YsxC}$ particles represent late assembly intermediates

Depletion of YphC or YsxC in *B. subtilis* cells results in the accumulation of altered large ribosomal subunits (17) that we called $45S_{YphC}$ and $44.5S_{YsxC}$ (Supplementary Figure S1). To purify these particles, we used strains with a single copy of the *yphC* or *ysxC* genes under the control of an IPTG-inducible promoter (17). In the presence of the inducer, lysates from these strains fractionated by sucrose density gradient ultracentrifugation produced ribosome profiles that were indistinguishable from those of wild type cells (17). However, the absence of IPTG produced a drastic reduction in the level of 70S and the accumulation of $45S_{YphC}$ and $44.5S_{YsxC}$ particles that we purified (Supplementary Figure S1). In addition, we also purified mature 50S subunits (Supplementary Figure S1) and $45S_{RbgA}$ particles as we previously described (19).

To determine the protein complement of the three immature particles ($45S_{YphC}$, $44.5S_{YsxC}$ and $44.5S_{RbgA}$) and the mature 50S subunit all cells were grown in ^{14}N-labeled media. The purified particles from these cells were then mixed with a reference spike containing a fixed concentration of ^{15}N-labeled 70S ribosomes and we measured their protein levels relative to this spike using qMS. This analysis showed that r-proteins uL16, bL28 and bL35 (r-protein nomenclature according to Ban *et al.* (35)) were severely depleted (occupancy < 0.25), and that bL27, bL33 and bL36 were significantly depleted (occupancy > 0.25) from all three 45S particles (Figure 1A; orange and purple, respectively). No peptides were found for bL34 in our analysis for any of the samples, thus the occupancy level for this r-protein remained uncharacterized. The mature 50S subunits exhibited a full complement and no signs of depletion for any of these r-proteins. This control experiment confirmed that the buffers used for particle purification and mass spectrometry analysis were not the cause of any of the depletions observed for the other six r-proteins. To determine the effect of NH_4Cl on r-protein association, these assays were performed in duplicate with particles purified either under low (150 mM) or high (500 mM) salt conditions. Interestingly, purification under high salt conditions led to similar occupancy profiles, with depleted proteins exhibiting even lower abundance (Figure 1B).

uL16, bL27, bL28, bL33, bL35 and bL36 are all r-proteins that bind late in 50S subunit reconstitution experiments (36–40). Therefore, we concluded from this analysis that the $45S_{YphC}$, $44.5S_{YsxC}$ particles, similar to the $45S_{RbgA}$ particles, represent late assembly intermediates.

The immature particles accumulating in the YphC and YsxC-depleted cells exhibit multiple conformations

Perhaps the most remarkable finding of the qMS analysis was the fact that the depletion pattern of the $45S_{YphC}$, $44.5S_{YsxC}$ and $45S_{RbgA}$ particles is identical. This result led us to investigate the structural similarity between the three particles and whether the function of YphC and YsxC could be inferred from the structures of the $45S_{YphC}$ and $44.5S_{YsxC}$.

To this end, purified $45S_{YphC}$ and $44.5S_{YsxC}$ particles were imaged by cryo-EM (Supplementary Figure S2; top panels) with a direct detector device camera allowing for full-correction of the beam-induced motion that the ribosomal particles experienced during the image acquisition process (Supplementary Figure S2; bottom panels). Three-dimensional classification of the $45S_{YphC}$ data set using the entire signal in the particle images revealed one distinct three-dimensional class. However, the $44.5S_{YsxC}$ particles exhibited two three-dimensional classes (Figure 2A and B). The percentages of the images assigned to class I and II were 44% and 56%, respectively. The most striking structural differences between the three maps representing the immature particles and the mature 50S subunit structure were in the A, P and E sites. The central protuberance and region nearby the bL7/L12 stalk also differed substantially from the mature subunit (Figure 2A) suggesting that this motif and the functional sites of the subunit are still in an immature state. However, the core of the subunit resembled closely the conformation of the mature 50S subunit (Supplementary Figure S3).

Consistently with the qMS data (Figure 1), the six r-proteins that were found severely depleted in the immature particles (uL16, bL27, bL28, bL33, bL35 and bL36) were all also missing from the cryo-EM maps of the $45S_{YphC}$ and $44.5S_{YsxC}$ particles. These r-proteins are located at the base

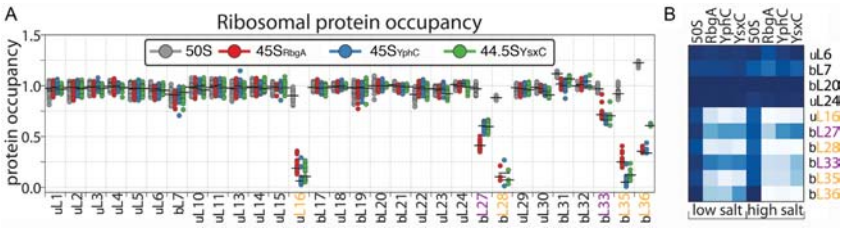

Figure 1. Ribosomal protein occupancy measured by qMS. (**A**) Ribosomal protein occupancy in 50S (gray), $45S_{RbgA}$ (red), $45S_{YphC}$ (blue) and $44.5S_{YsxC}$ (green) particles purified in the presence of 150 mM NH_4Cl. MRM-like transitions were extracted for each product ion from the SWATH datasets (see methods) and $^{14}N/^{15}N$ abundance ratios were calculated and normalized to the median value determined for protein L20. Circles denote individual MRM-transition measurements, lines signify the median $^{14}N/^{15}N$ abundance ratio measured for each protein. (**B**) Protein occupancy for a subset of ribosomal proteins measured in particles purified in the presence of either 150 mM (low salt; left) or 500 mM (high salt; right) NH_4Cl. Occupancy from 0 to 1 scales from white to blue.

of the central protuberance (Figure 2C). In addition, there were six other r-proteins that were present at ∼100% occupancy according to qMS (Figure 1), however density corresponding to these proteins was partially or completely missing from the cryo-EM maps (Figure 2A). These r-proteins were uL6, uL10, uL11 in the bL7/L12 stalk and uL5, bL31 and uL18 in the central protuberance (Figure 2D).

The cryo-EM maps obtained for these classes had a mean resolution of 6.5 Å ($45S_{YphC}$), 5.8 Å ($44.5S_{YsxC}$, class I) and 6.2 Å ($44.5S_{YsxC}$, class II) (Supplementary Figure S4A) with local resolution calculations indicating that the resolution of the core of the immature particles is higher than these values (Supplementary Figures S4B and S4C). This is consistent with the features of the cryo-EM maps in these regions showing clear separation of α-helices and β-sheets in the r-proteins (Supplementary Figure S5A) and the pitch of the rRNA helices (Supplementary Figure S5B). Instead, regions of the cryo-EM maps still in an immature state (central protuberance and functional sites) (Supplementary Figure S4B and S4C) refined to resolutions values lower than the mean resolution of the cryo-EM maps. The non-homogenous resolution likely reflects the stable conformation of the core of these particles, already in the mature conformation, and the relatively flexible nature of the central protuberance and functional sites, which are yet to reach the mature conformation. These maps constitute the highest-resolution structures available to date for a bacterial immature ribosomal particle.

Overall, we found that depletion of YphC or YsxC led to the accumulation of particles that have areas of the central protuberance, L7/12 stalk and functional sites still in an immature conformation. Therefore, we concluded that YphC or YsxC are involved in the maturation of these functional sites, which occur at the late stages of assembly of the 50S subunit. This function is similar to that suggested for RbgA (19,20).

Essential helices in the A, P and E sites of the 50S subunit adopt an immature state in the $45S_{YphC}$ and $44.5S_{YsxC}$ particles

The resolution at which the maps for the $45S_{YphC}$ and $44.5S_{YsxC}$ particles were obtained using the direct detector camera was sufficient to identify clearly the individual rRNA helices that differed from those of the mature 50S subunit in these structures.

The first and most important group of helices that were different in the $45S_{YphC}$ and $44.5S_{YsxC}$ immature particles were those involved in the binding of the tRNA in the A, P and E sites. Densities for helix 89 and for helices 91–93, which are part of the A and P sites were not observed in the cryo-EM maps (Figure 3A and Supplementary Figure S6). Similarly, helix 71 in the P site and the long helix 68, a major structural component of the E site, also did not exhibit a correspondent density (Figure 3B and Supplementary Figure S6). Interestingly, these helices were completely absent in the cryo-EM maps suggesting that they are still flexible and adopt multiple conformations within the population of individual particles.

Helix 69 is another functionally important motif located in the P site and in the immature particles also diverges structurally from the mature 50S subunit (Figure 3B). This helix mediates the essential B2a intersubunit bridge, where helix 69 contacts the decoding site of the 30S subunit. A density for helix 69 is apparent in the $44.5S_{YsxC}$ class I and class II maps, however this helix was bent outward from the mature position by ∼30° (Figure 3B, lower panels, asterisks). This non-native conformation of the helix likely prevents the premature association of the immature particles with the 30S subunit.

Overall, the structural divergence found in the A, P and E sites in the $45S_{YphC}$ and $44.5S_{YsxC}$ particles with respect to the mature 50S subunits most likely prevents these particles from becoming prematurely engage in translation. The obtained structures suggest they are likely to be defective in tRNA binding and in their ability to associate to the 30S subunit. Furthermore, these maps demonstrate that the $45S_{YphC}$ and $44.5S_{YsxC}$ particles have not structurally reached the mature state.

Maturation dependencies between the central protuberance, helix 38 and the GTPase associated region

In addition to the RNA helices forming the A, P and E sites, the $45S_{YphC}$ and $44.5S_{YsxC}$ particles also presented structural differences with the mature subunit in three other important functional domains. These regions were the central

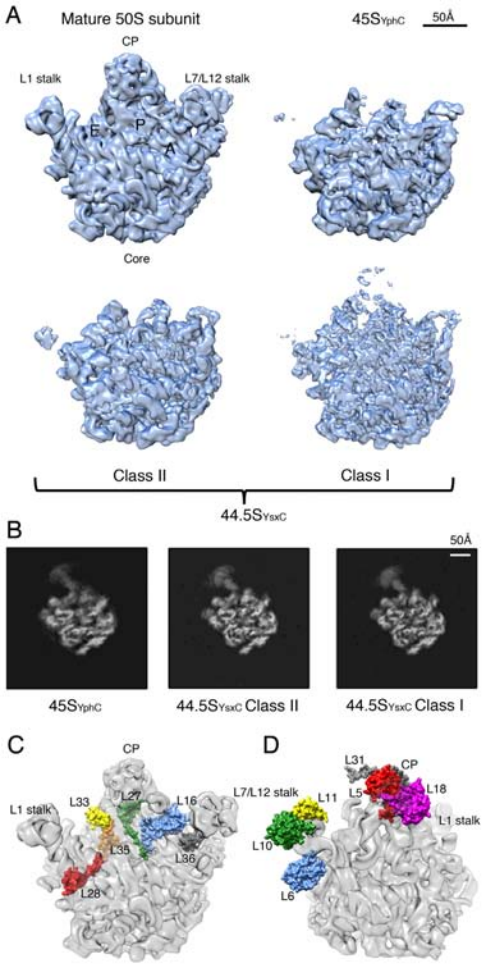

Figure 2. Cryo-EM maps of the $45S_{YphC}$ and $44.5S_{YsxC}$ ribosomal particles. (**A**) Surface rendered views of the maps show that the $45S_{YphC}$ particle was present in one conformational state, whereas the $44.5S_{YsxC}$ particles exhibited two. The map for the mature 50S subunit was obtained from the 3.9 Å resolution cryo-EM structure of the 50S subunit from *B. subtilis* (PDB ID: 3j9w) by applying a low-pass filter at comparable resolution. Landmarks in the 50S subunit are labeled in the mature subunit. CP stands for central protuberance. (**B**) Cross-sections through the three-dimensional map of the $45S_{YphC}$ particle and the two conformational states of the $44.5S_{YsxC}$ particle. (**C**) Location in the 50S subunit mature structure of the ribosomal proteins that were found severely depleted or absent in the $45S_{YphC}$ and $44.5S_{YsxC}$ particles. (**D**) The six ribosomal proteins displayed in the structure of the 50S subunit were found to be present at ∼100% occupancy by qMS, but a corresponding density for these proteins was not observed in the $45S_{YphC}$ and $44.5S_{YsxC}$ maps.

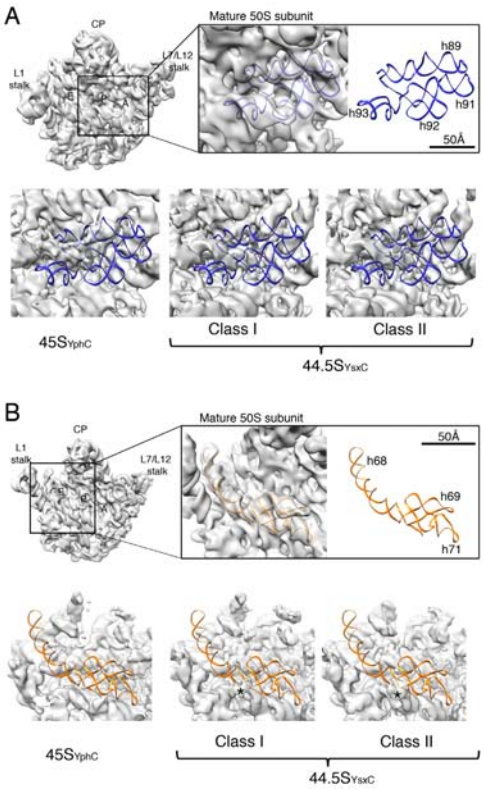

Figure 3. Structure of the functional core of the $45S_{YphC}$ and $44.5S_{YsxC}$ immature particles. (**A**) Zoomed view of helices 89–93 in the A site of the 50S subunit. A ribbon representation of these helices (PDB ID: 3j9w) was fitted into the map of the mature 50S subunit (top panel) and the $45S_{YphC}$ and $44.5S_{YsxC}$ immature particles (bottom panel). (**B**) This panel shows the structural details of the P and E sites in the immature particles and how they compare with the mature 50S subunit. The indicated helices differ structurally from the mature structure.

protuberance, helix 38 and the GTPase associated region (Supplementary Figure S6).

The central protuberance appeared at a different assembly stage in the obtained $45S_{YphC}$ and $44.5S_{YsxC}$ structures. However, none of the maps exhibited a fully assembled central protuberance (Figure 2A). This motif is comprised of helices 80–88 from domain V in the 23S rRNA (Supplementary Figure S6). These helices form the bulk of the central protuberance, whereas the 5S rRNA forms its back. In the maps obtained for the $45S_{YphC}$ and $44.5S_{YsxC}$ class II particles, densities for both helices 80–88 and 5S rRNA were missing. However, in the map of the $44.5S_{YsxC}$ class I, some disconnected densities were apparent for these regions. Similarly, the amount of density representing helix 38 and helices 42–44 comprising the GTPase associated region were

also featuring variable amounts of density among the obtained structures (Figure 2A).

To better understand the conformational changes that these important functional domains undergo during the late stages of assembly, we performed focus classification with the three sets of particle images that generated the $45S_{YphC}$, $44.5S_{YsxC}$ class I and $44.5S_{YsxC}$ class II consensus cryo-EM maps. To this end, we kept the signal in the particle images corresponding to the central protuberance, helix 38, GTPase associated region and helices forming the A, P and E functional sites during the 3D classification. In addition, the signal from all ribosomal motifs that had already reached the mature state was masked out and subtracted from the particle images (29). Each data set rendered three distinct classes with a resolution range of 8–10 Å for $44.5S_{YsxC}$ particle (Supplementary Figure S7) and 9–14 Å for the $45S_{YphC}$ particle (Supplementary Figure S8). These maps still allowed for unequivocal identification of rRNA helices (Figure 4).

Comparison of the three structures identified from the data set producing the consensus $44.5S_{YsxC}$ class I structure revealed that the rRNA helices forming the A, P and E site were consistently not present in any of the maps. However, the other immature regions including the central protuberance, helix 38 and the GTPase associated region (helix 42–44) presented variations (Figure 4A and B). The first class ($44.5S_{YsxC}$ class Ia) did not show density for any of these regions. The second class ($44.5S_{YsxC}$ class Ib) had density present for helix 42 and most of helices 43–44. It also displayed density for the proximal part of helix 38, although the direction of this helix deviated by ∼30° from the mature conformation. There was also no density for helices 80–88 or 5S rRNA indicating that the central protuberance is still in an immature state. Finally, the third class showed a fully formed central protuberance and helix 38 and the GTPase associated region was also close to the mature state (Figure 4B).

The data set generating the consensus $44.5S_{YsxC}$ class II structure also produced three structures (Figure 4C). Two of them ($44.5S_{YsxC}$ class IIa and $44.5S_{YsxC}$ class IIb) were identical to the $44.5S_{YsxC}$ class Ia and $44.5S_{YsxC}$ class Ib described above. The third structure ($44.5S_{YsxC}$ class IIc) presented densities similar to the mature structures for helix 38 (proximal region) and helices 42–44 corresponding to the GTPase associated region. In addition, it also featured fragmented densities in the central protuberance corresponding to helices 80–88 and 5S rRNA. This structure likely represents an immature particle in the process of folding the central protuberance. The RNA helices in the A, P and E site were consistently in an immature state in these three maps.

Finally, the data set producing the consensus $45S_{YphC}$ map also produced three structures (Figure 4D). The first structure was similar to $44.5S_{YsxC}$ class Ia and had no density for the central protuberance and helix 38. It only showed incipient densities for the GTPase associated region. The second structure was again equivalent to the $44.5S_{YsxC}$ class Ib with most of the density for the GTPase associated region present and helix 38 density deviated by ∼30° from the mature conformation. The third map presented density for the three regions and in a conformation

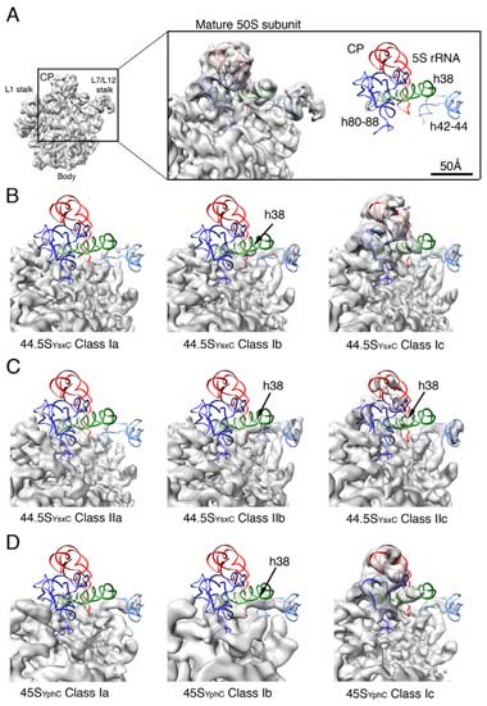

Figure 4. Structure of the central protuberance and GTPase associated region of the $45S_{YphC}$ and $44.5S_{YsxC}$ immature particles. Closed-up views of the central protuberance, helix 38 and the GTPase associated region (helix 42–44) in the cryo-EM maps of the multiple classes obtained from focus classification for the $45S_{YphC}$ (**B**) and (**C**) and $44.5S_{YsxC}$ data sets (**D**). Panel (**A**) shows this region in the mature 50S subunit (PDB ID: 3j9w) and the three bottom panels (B), (C) and (D) in the immature particles. A ribbon representation of helices 80–88, helix 38 and helices 42–44 of the 23S rRNA and 5S rRNA were fitted to the cryo-EM maps. The density representing helix 38 in some of the classes obtained for the $44.5S_{YsxC}$ and $45S_{YphC}$ particles is indicated with a black arrow. The frontal view of the 50S subunit (left) is for orientation purposes and the framed area correspond to the zoomed views in the rest of the panel.

close to the mature state. However, similar to all the other structures it showed fully immature A, P and E sites.

These structural data suggest that the GTPase associated region, helix 38, central protuberance and A, P and E functional sites fold sequentially and in a coordinated manner. It starts with folding of helix 42 and is followed by the other two helices that are part of the GTPase associated region (helix 43–44) adopting the mature conformation. Simultaneously, helix 38 starts extending, however it initially attaches to the particle with an angle different from the mature structure (Movie 1). Subsequently, folding of helices 80–88 and 5S rRNA forming the central protuberance drags helix 38 toward his mature position (Movies 2 and 3). The very last regions to mature are the A, P and E site. The densities corresponding to the RNA helices forming these sites were consistently missing in all the cryo-EM maps obtained

for the $45S_{YphC}$ and $44.5S_{YsxC}$ structure and discrete steps during their maturation were not visualized.

YphC, YsxC and RbgA directly interact with both the mature and immature ribosomal particles

The structural similarities of the $45S_{YphC}$ and $44.5S_{YsxC}$ particles prompted us to test whether YphC and YsxC have the ability to bind to the two assembly intermediates or conversely, whether they only recognize the immature particle that appears upon their depletion. We noticed that the two immature particles analyzed structurally here resemble to that of the $45S_{RbgA}$ particle (19,20). Thus, we also purified $45S_{RbgA}$ particles and the RbgA protein and tested the binding of YphC, YsxC and RbgA to all three immature particles and to mature 50S subunits.

We first used a filtration assays to test the binding of YphC, YsxC and RbgA to the mature 50S subunit and to the three immature ribosomal particles (Figure 5). In these assays, a mixture of the assembly factor with the ribosomal particle was incubated at 37°C for 1 h in the presence of 1 mM GMPPNP. Subsequently, reactions were centrifuged in a centrifugal concentrating device, which retains assembly factor when bound to the ribosome particles and free ribosomal subunits (bound fraction), but passes through the membrane when not bound to ribosomes or free ribosomal subunits (unbound fraction). Both fractions were subsequently analyzed by SDS-PAGE.

We found that none of the three proteins were retained by the filter in the absence of ribosomes, but when combined with the ribosomal particles YsxC exhibited similar binding to both the mature and immature particles (Figure 5C). YphC and RbgA also associated with the immature and mature particles and although the quantitative nature of these assays is limited, we could observe a larger fraction of the protein in the bound fraction for reactions containing the immature particles than for reactions containing the mature 50S subunit (Figure 5A and B). In addition, the filtration assays suggested that a strict hierarchy of binding for these factors or to the ribosomal subunits does not exist.

To determine the effect of the nucleotide on the binding affinity of RbgA, YphC and YsxC to the ribosomal particles, identical reactions were tested in the presence of 1mM GTP or 1mM GDP (Supplementary Figure S9). In the case of RbgA and YphC we found that the binding observed in the presence of these two nucleotides was weaker than in the presence of GMPPNP (Supplementary Figure S9A and S9B). Instead, YsxC showed similar binding to the ribosomal particles with the three nucleotides (Supplementary Figure S9C). These binding results for RbgA are in full agreement with previous literature (16,41,42).

Next, we tested whether the ribosomal particles could simultaneous bind multiple assembly factors. To this end, we performed filtration assays (Figure 5D) where we incubated the ribosomal particles with 5-fold molar excess of each one of the assembly factors and in the presence of 1 mM GMPPNP. These assays revealed that several assembly factors were retained with each of the immature particles and the mature 50S subunit in approximately stoichiometric amounts. This experiment suggested that simultaneous

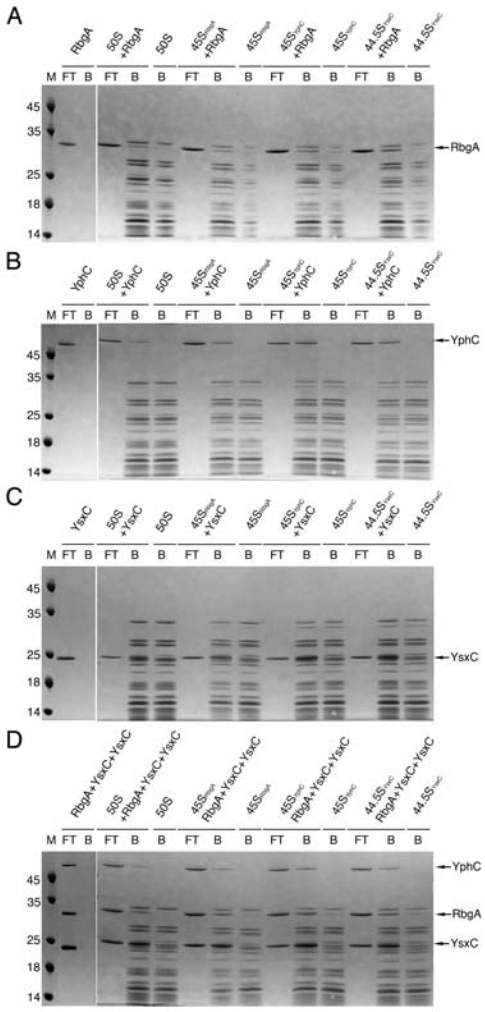

Figure 5. Binding of RbgA, YphC and YsxC to the mature 50S subunit and the $45S_{YphC}$ and $44.5S_{YsxC}$ immature particles. (**A**) Filtration assays testing binding of RbgA to the mature 50S subunit and the $45S_{YphC}$ and $44.5S_{YsxC}$ immature particles. A Coomassie blue stained 4–12% bis–tris polyacrylamide gel shows the content of the flow-through (FT) and bound (**B**) fractions of the filtration assay. Reactions contained RbgA alone or a mixture of ribosomal particles with a five-fold molar excess of RbgA. The molecular weight (M) is in kDa. Similar assay as described in the two panels below showing a similar filtration assay to test the binding of YphC (**B**) or YsxC (**C**) to the mature 50S subunit and the $45S_{YphC}$ and $44.5S_{YsxC}$ immature particles. (**D**) Filtration assay testing binding of multiple assembly factors to the ribosomal particles. In this assay a five-fold molar excess of each factor with respect to the ribosomal particle was added to the assembly reaction.

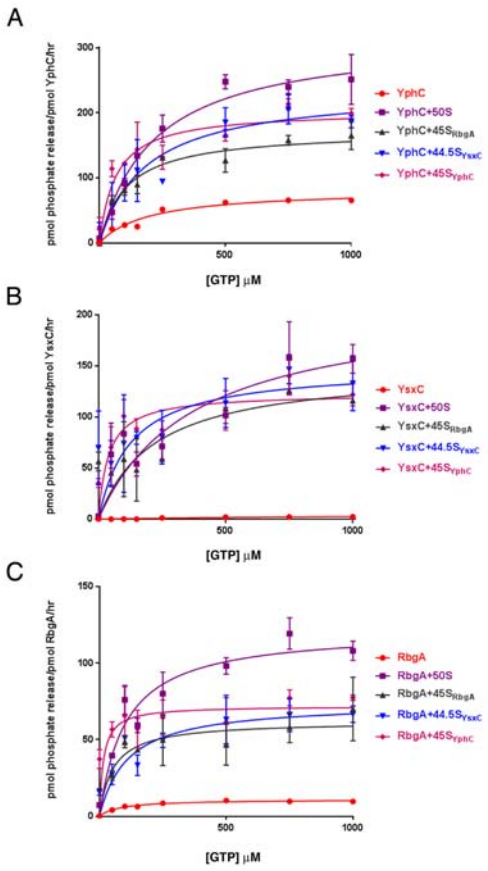

Figure 6. Stimulation of the GTPase activity of YphC, YsxC and RbgA by the mature 50S subunit and immature 45S$_{YphC}$, 45S$_{RbgA}$ and 44.5S$_{YsxC}$ particles. (**A**) The GTP hydrolysis rates of YphC in the presence and absence of the mature and immature ribosomal particles were measured at different concentrations of GTP to determine kinetic parameters. Equivalent experiment with YsxC (**B**) and RbgA (**C**) to determine the kinetic parameters of these enzymes.

binding of more than one of the assembly factors to the mature 50S and immature particles is possible.

RbgA, like most other GTPases exhibits low intrinsic GTPase activity. However, this activity increases upon a specific interaction with the 50S subunit (41,42). We hypothesized that YphC and YsxC may exhibit a similar behavior and measured their GTPase activity in the absence and presence of ribosomal particles to test whether the binding observed in the filtration assays was specific. RbgA was also included in these experiments as a control.

We started by performing a steady-state kinetic analysis of the YphC, YsxC and RbgA intrinsic GTPase activity (Figure 6 and Table 1). The three proteins had low affinity for GTP exhibiting an apparent K_M for this nucleotide in the micromolar range. They also showed a low intrinsic GTP hydrolysis rate. YsxC and RbgA exhibited a k_{cat} of ∼5 and 10 h^{-1}, respectively (Figure 6B and C and Table 1). YphC contains two GTPase domains and it showed a higher rate with a k_{cat} of ∼82 h^{-1} (Figure 6A and Table 1.) These basal levels of GTPase activity were comparable to the k_{cat} reported for RbgA (42) and EngA (43), the ortholog of YphC in *Escherichia coli*.

We then tested the GTPase activity of YphC, YsxC and RbgA in the presence of the mature 50S subunit and the three immature particles (45S$_{YphC}$, 44.5S$_{YsxC}$ and 45S$_{RbgA}$) (Figure 6 and Table 1). The GTPase activity exhibited by each ribosomal particle by itself at each GTP concentration was subtracted. These experiments showed that for the three GTPases a significantly higher stimulation of the catalytic rate of the enzyme against GTP (increase in k_{cat} Table 1) occurred in the presence of the mature 50S subunit. The three immature particles also stimulated the catalytic rate but always to a lesser extent. Overall, the YsxC catalytic rate showed a much higher stimulation (∼26–38-fold) in the presence of the ribosomal particles than in the case of YphC and RbgA (∼2–11-fold).

Interaction with the ribosomal particles also had an effect in the apparent K_M of the enzymes for GTP (Table 1). YphC and RbgA followed a similar pattern exhibiting a small increase in the apparent K_M value in the presence of 50S subunits but a decrease with the immature particles (with the only exception of RbgA in the presence of 44.5S$_{YsxC}$ particle). Instead, YsxC showed a decrease in the apparent K_M value with both mature and immature particles. An interesting observation was that for the three GTPases, the biggest decrease in the apparent K_M value was always observed in the presence of the 44.5S$_{YphC}$ particle. Consequently, we observed an increase in the enzyme efficiency (increase in k_{cat}/apparent K_M Table 1) for all the reactions performed in the presence of ribosomal particles compared to those reactions with the assembly intermediates by themselves. The highest increases in enzyme efficiency were always shown by the reactions of the three GTPases containing the 44.5S$_{YphC}$ particle.

Overall, these results suggest that each one of the GTPases (YphC, YsxC and RbgA) have the ability to bind in a specific manner to both the mature 50S subunit and the three immature ribosomal particles. This finding is consistent with the last steps of assembly of the 50S subunit following multiple parallel pathways of assembly. The observed binding promiscuity of the YphC, YsxC and RbgA GTPases and the fact that a specific binding hierarchy does not exist likely allows for the last steps of maturation of the 50S subunit to occur without following a precise sequence.

DISCUSSION

Inferring the function of YphC and YsxC from the analysis of ribosome assembly intermediates

Recent work (19,20) has described that the RbgA GTPase is involved in the maturation of the central protuberance, tRNA binding sites and GTPase associating region. Here, we describe that two additional GTPases, YphC and YsxC

Table 1. Kinetic parameters of YphC, YsxC and RbgA in the presence and absence of the mature 50S subunit and immature $45S_{YphC}$, $45S_{RbgA}$ and $44.5S_{YsxC}$ particles

	Apparent K_M (μM)	k_{cat} (h^{-1})	k_{cat}/apparent K_M (μM^{-1} h^{-1})	Increase in apparent K_M	Increase in k_{cat}	Increase in k_{cat}/apparent K_M
YphC	199 ± 31.4	82.2 ± 4.3	0.41	1	1	1
YphC+50S	217.4 ± 39.2	317.9 ± 19.2	1.4	1.1	3.9	3.5
YphC+45SYphC	64.5 ± 18.9	203.3 ± 13.1	3.1	0.3	2.5	7.7
YphC+45SRbgA	108.3 ± 21.2	172.4 ± 9.3	1.5	0.5	2.1	3.9
YphC+44.5SYsxC	185.3 ± 57.4	236.5 ± 24.6	1.2	0.9	2.9	3.1
YsxC	1268 ± 116.6	5.5 ± 3.3	0.004	1	1	1
YsxC +50S	377.1 ± 166.7	212.3 ± 40.9	0.5	0.3	38.1	128.1
YsxC +45SYphC	39.5 ± 18.4	123 ± 9.6	3.1	0.03	22.1	707.9
YsxC +45SRbgA	219.6 ± 174.6	147.6 ± 45.5	0.6	0.2	26.5	153
YsxC +44.5SYsxC	126.3 ± 72.5	149 ± 25.3	1.1	0.1	26.7	268.5
RbgA	82.8 ± 9.4	10.9 ± 0.3	0.1	1	1	1
RbgA +50S	102.8 ± 24.4	121.7 ± 6.9	1.2	1.2	11.1	8.9
RbgA +45SYphC	15.5 ± 16	72 ± 7.5	4.6	0.2	6.6	35
RbgA +45SRbgA	53.4 ± 21.6	61.9 ± 5.2	1.2	0.6	5.6	8.8
RbgA +44.5SYsxC	110.5 ± 36.7	74.2 ± 6.3	0.7	1.3	6.8	5.1

also contribute in the maturation of these essential ribosomal motifs.

Interestingly, we found that the $45S_{YphC}$ and $44.5S_{YsxC}$ particles that accumulate in *B. subtilis* strains upon depletion of YphC and YsxC are structurally similar to each other and also resemble the $45S_{RbgA}$ particles that result from the depletion of RbgA (19,20). From the analysis of the immature regions in the cryo-EM maps, it is still difficult to pinpoint specific roles for RbgA, YphC and YsxC during the assembly of the 50S subunit.

Identification of structurally divergent intermediates would have been the expected outcome if each one of the factors performs a distinct function not related to the function of other factors. Instead, we found that the cryo-EM maps of the $45S_{YphC}$, $44.5S_{YsxC}$ and $45S_{RbgA}$ particles were similar. One possibility consistent with this result is that RbgA, YphC and YsxC work in conjunction during the maturation of the central protuberance, helix 38, GTPase associated region and A, P and E functional sites and thus, removing any of the factors leads to accumulation of the same intermediate. However, similar intermediate structures would also be expected if depletion of each one of these factors blocks the assembly at a different step and leads to the accumulation of a different thermodynamically unstable intermediate that evolves into a similar energetically stable conformation. Consequently, a related and relevant question is whether these particles are on-pathway and whether they represent the actual substrate for the assembly factors.

We recently demonstrated that the $45S_{RbgA}$ particles are competent for maturation and are eventually incorporated into 70S ribosomes (19). In addition, the work presented here reveals that the $45S_{YphC}$, $44.5S_{YsxC}$ and $45S_{RbgA}$ particles specifically bind YphC, YsxC and RbgA suggesting that they either constitute actual on-pathway intermediates or their conformations have not diverged significantly from the actual substrate recognized by the assembly factors. Therefore, the structural differences existing in these immature particles compared to the mature 50S subunit should be informative of the function of the assembly factors.

High resolution cryo-EM structures provides precise testable models about YphC and YsxC function

The presented structures were obtained using a direct electron detector and were refined to a resolution of 5–6 Å. They constitute to our knowledge the highest resolution cryo-EM structures available for a bacterial ribosome intermediate. Therefore, different from previous moderate-resolution cryo-EM studies on other assembly intermediates (11–13,15,19,20), these structures allow defining individual rRNA helices in the $45S_{YphC}$ and $44.5S_{YsxC}$ particles that are still adopting an immature conformation. Consequently, these structures are making possible to propose precise testable models regarding the function of YphC and YsxC in assembly. For example, Li *et al.* (20) assigned RbgA a role as an rRNA chaperone with the essential role of positioning helix 38 during 50S subunit maturation. The structures presented here indicate that helix 38 is able to adopt its mature conformation in the absence of YphC or YsxC (Movies 1–3). Similarly, our results also indicate that YphC and YsxC are not essential for the assembly of the central protuberance and GTPase associated center. However, the RNA helices forming the A, P and E site consistently appear in an immature state in the $45S_{YphC}$, $44.5S_{YsxC}$ structures (Figure 3), thus suggesting that the essential role of YphC and YsxC may be more related to the remodeling of the RNA helices in the functional core of the particle. Consistent with this proposed function, a recent high-resolution structure of EngA, the *Escherichia coli* homologue of YphC, in complex with the mature 50S subunit (44) revealed that this factor binds deeply into the tRNA passage at the P and E site. Interestingly, binding of EngA results in significant rearrangements of the same rRNA helices (helix 68–71) that we found still in an immature state in the $45S_{YphC}$, $44.5S_{YsxC}$ particles.

The high resolution obtained in the cryo-EM maps also provides a structural explanation to deficiencies found in the protein complement of these particles. For example, the cryo-EM maps for the $44.5S_{YsxC}$ class Ib, $44.5S_{YsxC}$ class IIb and the $45S_{YphC}$ class Ib particles, the position of helix 38 completely blocks the binding site of uL16. Only when the central protuberance is formed, helix 38 is dragged closed

to its mature position making the uL16 binding site accessible and providing a justification for the almost complete absence of uL16 found in the 44.5S$_{YsxC}$ and 45S$_{YphC}$ particles. The abnormal positioning of helix 38 and steric blockage of the uL16 binding site is a structural feature of the 44.5S$_{YsxC}$ and 45S$_{YphC}$ particles shared with the cryo-EM map of the 45S$_{RbgA}$ particles that was described recently (19,20).

Certain features of the cryo-EM maps of the 45S$_{YphC}$ and 44.5S$_{YsxC}$ particles are in full agreement with the assembly of the ribosomal particle following multiple parallel pathways of assembly (45–48). In particular, we found that there were not densities in these maps representing the RNA helices comprising the A, P and E sites at the site for the mature 50S subunit or nearby (Figure 3). This finding suggests that these rRNA motifs probably adopt a large number of conformations that are those populating the multiple assembly pathways undergoing in the cell. In addition, as described for the 45S$_{RbgA}$ particles (19,20) these structures are also consistent with the folding of the 23S rRNA not proceeding in 5′-3′ fashions, as domains II, IV and V are still in an immature state. However, all other domains including I, III and VI already reached the mature stage (Supplementary Figure S6). This is in contrast to the assembly of the 16S rRNA forming the 30S subunit where the rRNA folding follows and strict 5′-3′ transcriptional order (49).

Cryo-EM allows for direct visualization of the ribosomal assembly process

The 45S$_{YphC}$ and 44.5S$_{YsxC}$ cryo-EM maps also describe the discrete stages leading to the coordinated assembly of functional important sites for the 50S subunit, including the GTPase associated center, helix 38 and central protuberance (Movies 1–3). It starts with the helix 42 reaching its mature conformation and followed by the folding of helix 43–44, which are the other two helices comprising the GTPase associated region. At this moment helix 38 start to grow, however it initially attaches to the ribosomal particle with a different angle. As helices 80–88 and 5S rRNA forming the central protuberance start to fold simultaneously, helix 38 is dragged towards its mature position. Two of the conformations observed for the central protuberance (classes I and II of the 44.5S$_{YsxC}$ particle) had also much resemblance with two of the conformational classes that have been described for the 45S$_{RbgA}$ immature particle (19,20). These results suggest that although the assembly of the central protuberance follow multiple parallel pathways, the conformational variability existing among the population of assembling particles may not be as diverse as it has been observed for the RNA motifs comprising A, P and E sites where discrete conformations were not observed.

These structures also suggest that the assembly of the central protuberance in the bacterial ribosome occurs differently than in the eukaryotic ribosome. A recent study (50) revealed the existence of an energetically favored intermediate of the 60S ribosomal subunit with a drastically rearranged topology of the central protuberance. Compared to its mature position, the 5S rRNA, an integral part of the central protuberance exhibits an essentially unchanged fold but the entire molecule is rotated by 180°. This non-native conformation is stabilized by assembly factors Rsa4 and Nog1. In subsequent maturation steps, the 5S rRNA rotates to its native position and for this movement it is predicted that one of the assembly factors will have to provide a substantial power stroke. During the late stages of assembly of the bacterial 50S subunit studied here, we did not observed assembly intermediates exhibiting a central protuberance with a rearranged topology.

CONCLUSION

Overall, these results provide the first insights into the function of YphC and YsxC at the late stages of assembly of the 50S subunit. Ribosome assembly intermediates generated through depletion and knock-out bacterial strains constitute today an important tool for studying the function of assembly factors. Therefore, the key questions answered here regarding the nature of these intermediates and their ability to inform on the reactions catalyzed by assembly factors constitute an important step forward toward our understanding of the ribosome assembly process.

ACCESION NUMBERS

The 44.5S$_{YsxC}$ class I and class II cryo-EM maps have been assigned the EMDB IDs 8274 and 8275, respectively. The EMDB ID for the 45S$_{YphC}$ cryo-EM map is 8276.

SUPPLEMENTARY DATA

Supplementary Data are available at NAR Online.

ACKNOWLEDGEMENTS

We are grateful to Dr Brandon Aubie for technical assistance with the MSLR computing cluster. We acknowledge the Hospital for Sick Children in Toronto for allowing us access to the Electron Microscopy Facility. Canadian Institutes of Health Research provided the funds for open access charges.

FUNDING

National Science and Engineering Research Council of Canada [RGPIN288327-07]; Canadian Institutes of Health Research [MOP-82930 to J.O.]; Canadian Institutes of Health Research [MOP-81294]; Canada Research Chair funding (to J.L.R.); National Institutes of Health [R01GM110248 to to R.A.B. and J.R.W.]; The McMaster Service Lab and Repository (MSLR) computing cluster was, in part, funded by a grant from the Canadian Foundation for Innovation (to A.G.M.). A.G.M. holds a Cisco Research Chair in Bioinformatics, supported by Cisco Systems Canada, Inc.; Jane Coffin Childs Postdoctoral fellowship and a grant from the National Institute of Aging [1K99AG050749-01 to J.H.D.]. Funding for open access charge: Canadian Institutes of Health Research.
Conflict of interest statement. None.

REFERENCES

1. Lindahl,L. (1973) Two new ribosomal precursor particles in E. coli. *Nat. New Biol.*, **243**, 170–172.

2. Lindahl,L. (1975) Intermediates and time kinetics of the in vivo assembly of Escherichia coli ribosomes. *J. Mol. Biol.*, **92**, 15–37.
3. Hayes,F. and Hayes,D.H. (1971) Biosynthesis of ribosomes in E. coli. I. Properties of ribosomal precursor particles and their RNA components. *Biochimie*, **53**, 369–382.
4. Stokes,J.M. and Brown,E.D. (2015) Chemical modulators of ribosome biogenesis as biological probes. *Nat. Chem. Biol.*, **11**, 924–932.
5. Loibl,M., Klein,I., Prattes,M., Schmidt,C., Kappel,L., Zisser,G., Gungl,A., Krieger,E., Pertschy,B. and Bergler,H. (2014) The drug diazaborine blocks ribosome biogenesis by inhibiting the AAA-ATPase Drg1. *J. Biol. Chem.*, **289**, 3913–3922.
6. Pertschy,B., Zisser,G., Schein,H., Koffel,R., Rauch,G., Grillitsch,K., Morgenstern,C., Durchschlag,M., Hogenauer,G. and Bergler,H. (2004) Diazaborine treatment of yeast cells inhibits maturation of the 60S ribosomal subunit. *Mol. Cell. Biol.*, **24**, 6476–6487.
7. Drygin,D., Lin,A., Bliesath,J., Ho,C.B., O'Brien,S.E., Proffitt,C., Omori,M., Haddach,M., Schwaebe,M.K., Siddiqui-Jain,A. *et al.* (2011) Targeting RNA polymerase I with an oral small molecule CX-5461 inhibits ribosomal RNA synthesis and solid tumor growth. *Cancer Res.*, **71**, 1418–1430.
8. Drygin,D., Siddiqui-Jain,A., O'Brien,S., Schwaebe,M., Lin,A., Bliesath,J., Ho,C.B., Proffitt,C., Trent,K., Whitten,J.P. *et al.* (2009) Anticancer activity of CX-3543: a direct inhibitor of rRNA biogenesis. *Cancer Res.*, **69**, 7653–7661.
9. Deisenroth,C. and Zhang,Y. (2010) Ribosome biogenesis surveillance: probing the ribosomal protein-Mdm2-p53 pathway. *Oncogene*, **29**, 4253–4260.
10. Stokes,J.M., Davis,J.H., Mangat,C.S., Williamson,J.R. and Brown,E.D. (2014) Discovery of a small molecule that inhibits bacterial ribosome biogenesis. *eLife*, **3**, e03574.
11. Jomaa,A., Stewart,G., Martin-Benito,J., Zielke,R., Campbell,T.L., Maddock,J.R., Brown,E.D. and Ortega,J. (2011) Understanding ribosome assembly: the structure of in vivo assembled immature 30S subunits revealed by cryo-electron microscopy. *RNA*, **17**, 697–709.
12. Leong,V., Kent,M., Jomaa,A. and Ortega,J. (2013) Escherichia coli rimM and yjeQ null strains accumulate immature 30S subunits of similar structure and protein complement. *RNA*, **19**, 789–802.
13. Guo,Q., Goto,S., Chen,Y., Feng,B., Xu,Y., Muto,A., Himeno,H., Deng,H., Lei,J. and Gao,N. (2013) Dissecting the in vivo assembly of the 30S ribosomal subunit reveals the role of RimM and general features of the assembly process. *Nucleic Acids Res.*, **41**, 2609–2620.
14. Clatterbuck Soper,S.F., Dator,R.P., Limbach,P.A. and Woodson,S.A. (2013) In vivo X-ray footprinting of pre-30S ribosomes reveals chaperone-dependent remodeling of late assembly intermediates. *Mol. Cell*, **52**, 506–516.
15. Yang,Z., Guo,Q., Goto,S., Chen,Y., Li,N., Yan,K., Zhang,Y., Muto,A., Deng,H., Himeno,H. *et al.* (2014) Structural insights into the assembly of the 30S ribosomal subunit in vivo: functional role of S5 and location of the 17S rRNA precursor sequence. *Protein Cell*, **5**, 394–407.
16. Uicker,W.C., Schaefer,L. and Britton,R.A. (2006) The essential GTPase RbgA (YlqF) is required for 50S ribosome assembly in Bacillus subtilis. *Mol. Microbiol.*, **59**, 528–540.
17. Schaefer,L., Uicker,W.C., Wicker-Planquart,C., Foucher,A.E., Jault,J.M. and Britton,R.A. (2006) Multiple GTPases participate in the assembly of the large ribosomal subunit in Bacillus subtilis. *J. Bacteriol.*, **188**, 8252–8258.
18. Hwang,J. and Inouye,M. (2006) The tandem GTPase, Der, is essential for the biogenesis of 50S ribosomal subunits in Escherichia coli. *Mol. Microbiol.*, **61**, 1660–1672.
19. Jomaa,A., Jain,N., Davis,J.H., Williamson,J.R., Britton,R.A. and Ortega,J. (2014) Functional domains of the 50S subunit mature late in the assembly process. *Nucleic Acids Res.*, **42**, 3419–3435.
20. Li,N., Chen,Y., Guo,Q., Zhang,Y., Yuan,Y., Ma,C., Deng,H., Lei,J. and Gao,N. (2013) Cryo-EM structures of the late-stage assembly intermediates of the bacterial 50S ribosomal subunit. *Nucleic Acids Res.*, **41**, 7073–7083.
21. Uicker,W.C., Schaefer,L., Koenigsknecht,M. and Britton,R.A. (2007) The essential GTPase YqeH is required for proper ribosome assembly in Bacillus subtilis. *J. Bacteriol.*, **189**, 2926–2929.
22. Jeganathan,A., Razi,A., Thurlow,B. and Ortega,J. (2015) The C-terminal helix in the YjeQ zinc-finger domain catalyzes the release of RbfA during 30S ribosome subunit assembly. *RNA*, **21**, 1203–1216.
23. MacLean,B., Tomazela,D.M., Shulman,N., Chambers,M., Finney,G.L., Frewen,B., Kern,R., Tabb,D.L., Liebler,D.C. and MacCoss,M.J. (2010) Skyline: an open source document editor for creating and analyzing targeted proteomics experiments. *Bioinformatics*, **26**, 966–968.
24. Gillet,L.C., Navarro,P., Tate,S., Rost,H., Selevsek,N., Reiter,L., Bonner,R. and Aebersold,R. (2012) Targeted data extraction of the MS/MS spectra generated by data-independent acquisition: a new concept for consistent and accurate proteome analysis. *Mol. Cell. Proteomics*, **11**, doi:10.1074/mcp.O111.016717.
25. Gulati,M., Jain,N., Davis,J.H., Williamson,J.R. and Britton,R.A. (2014) Functional interaction between ribosomal protein L6 and RbgA during ribosome assembly. *PLoS Genet.*, **10**, e1004694.
26. Rubinstein,J.L. and Brubaker,M.A. (2015) Alignment of cryo-EM movies of individual particles by optimization of image translations. *J. Struct. Biol.*, **192**, 188–195.
27. Mindell,J.A. and Grigorieff,N. (2003) Accurate determination of local defocus and specimen tilt in electron microscopy. *J. Struct. Biol.*, **142**, 334–347.
28. Scheres,S.H. (2012) RELION: implementation of a Bayesian approach to cryo-EM structure determination. *J. Struct. Biol.*, **180**, 519–530.
29. Bai,X.C., Rajendra,E., Yang,G., Shi,Y. and Scheres,S.H. (2015) Sampling the conformational space of the catalytic subunit of human gamma-secretase. *eLife*, **4**, e11182.
30. Rosenthal,P.B. and Henderson,R. (2003) Optimal determination of particle orientation, absolute hand, and contrast loss in single-particle electron cryomicroscopy. *J. Mol. Biol.*, **333**, 721–745.
31. Loken,C., Gruner,D., Groer,L., Peltier,R., Bunn,N., Craig,M., Henriques,T., Dempsey,J., Yu,C.-H., Chen,J. *et al.* (2010) SciNet: Lessons Learned from Building a Power-efficient Top-20 System and Data Centre. *J. Phys.*, **256**, 012026.
32. Kucukelbir,A., Sigworth,F.J. and Tagare,H.D. (2014) Quantifying the local resolution of cryo-EM density maps. *Nat. Methods*, **11**, 63–65.
33. Pettersen,E.F., Goddard,T.D., Huang,C.C., Couch,G.S., Greenblatt,D.M., Meng,E.C. and Ferrin,T.E. (2004) UCSF Chimera–a visualization system for exploratory research and analysis. *J. Comput. Chem.*, **25**, 1605–1612.
34. Trabuco,L.G., Villa,E., Mitra,K., Frank,J. and Schulten,K. (2008) Flexible fitting of atomic structures into electron microscopy maps using molecular dynamics. *Structure*, **16**, 673–683.
35. Ban,N., Beckmann,R., Cate,J.H., Dinman,J.D., Dragon,F., Ellis,S.R., Lafontaine,D.L., Lindahl,L., Liljas,A., Lipton,J.M. *et al.* (2014) A new system for naming ribosomal proteins. *Curr. Opin. Struct. Biol.*, **24**, 165–169.
36. Rohl,R. and Nierhaus,K.H. (1982) Assembly map of the large subunit (50S) of Escherichia coli ribosomes. *Proc. Natl. Acad. Sci. U.S.A.*, **79**, 729–733.
37. Herold,M. and Nierhaus,K.H. (1987) Incorporation of six additional proteins to complete the assembly map of the 50 S subunit from Escherichia coli ribosomes. *J. Biol. Chem.*, **262**, 8826–8833.
38. Chen,S.S. and Williamson,J.R. (2013) Characterization of the ribosome biogenesis landscape in E. coli using quantitative mass spectrometry. *J. Mol. Biol.*, **425**, 767–779.
39. Nomura,M. and Erdmann,V.A. (1970) Reconstitution of 50S ribosomal subunits from dissociated molecular components. *Nature*, **228**, 744–748.
40. Fahnestock,S., Erdmann,V. and Nomura,M. (1973) Reconstitution of 50S ribosomal subunits from protein-free ribonucleic acid. *Biochemistry*, **12**, 220–224.
41. Matsuo,Y., Morimoto,T., Kuwano,M., Loh,P.C., Oshima,T. and Ogasawara,N. (2006) The GTP-binding protein YlqF participates in the late step of 50 S ribosomal subunit assembly in Bacillus subtilis. *J Biol Chem*, **281**, 8110–8117.
42. Achila,D., Gulati,M., Jain,N. and Britton,R.A. (2012) Biochemical characterization of ribosome assembly GTPase RbgA in Bacillus subtilis. *J. Biol. Chem.*, **287**, 8417–8423.
43. Bharat,A., Jiang,M., Sullivan,S.M., Maddock,J.R. and Brown,E.D. (2006) Cooperative and critical roles for both G domains in the GTPase activity and cellular function of ribosome-associated Escherichia coli EngA. *J. Bacteriol.*, **188**, 7992–7996.
44. Zhang,X., Yan,K., Zhang,Y., Li,N., Ma,C., Li,Z., Zhang,Y., Feng,B., Liu,J., Sun,Y. *et al.* (2014) Structural insights into the function of a

unique tandem GTPase EngA in bacterial ribosome assembly. *Nucleic Acids Res.*, **42**, 13430–13439.
45. Shajani,Z., Sykes,M.T. and Williamson,J.R. (2011) Assembly of bacterial ribosomes. *Annu. Rev. Biochem.*, **80**, 501–526.
46. Sykes,M.T. and Williamson,J.R. (2009) A Complex Assembly Landscape for the 30S Ribosomal Subunit. *Annu. Rev. Biophys.*, **38**, 197–215.
47. Woodson,S.A. (2008) RNA folding and ribosome assembly. *Curr. Opin. Chem. Biol.*, **12**, 667–673.
48. Woodson,S.A. (2011) RNA folding pathways and the self-assembly of ribosomes. *Acc. Chem. Res.*, **44**, 1312–1319.
49. Mulder,A.M., Yoshioka,C., Beck,A.H., Bunner,A.E., Milligan,R.A., Potter,C.S., Carragher,B. and Williamson,J.R. (2010) Visualizing ribosome biogenesis: parallel assembly pathways for the 30S subunit. *Science*, **330**, 673–677.
50. Leidig,C., Thoms,M., Holdermann,I., Bradatsch,B., Berninghausen,O., Bange,G., Sinning,I., Hurt,E. and Beckmann,R. (2014) 60S ribosome biogenesis requires rotation of the 5S ribonucleoprotein particle. *Nat. Commun.*, **5**, 3491.

The C-terminal helix in the YjeQ zinc-finger domain catalyzes the release of RbfA during 30S ribosome subunit assembly

AJITHA JEGANATHAN, AIDA RAZI, BRETT THURLOW, and JOAQUIN ORTEGA

Department of Biochemistry and Biomedical Sciences, M.G. DeGroote Institute for Infectious Diseases Research, McMaster University, Hamilton, Ontario, Canada L8S 4K1

ABSTRACT

YjeQ (also called RsgA) and RbfA proteins in *Escherichia coli* bind to immature 30S ribosome subunits at late stages of assembly to assist folding of the decoding center. A key step for the subunit to enter the pool of actively translating ribosomes is the release of these factors. YjeQ promotes dissociation of RbfA during the final stages of maturation; however, the mechanism implementing this functional interplay has not been elucidated. YjeQ features an amino-terminal oligonucleotide/oligosaccharide binding domain, a central GTPase module and a carboxy-terminal zinc-finger domain. We found that the zinc-finger domain is comprised of two functional motifs: the region coordinating the zinc ion and a carboxy-terminal α-helix. The first motif is essential for the anchoring of YjeQ to the 30S subunit and the carboxy-terminal α-helix facilitates the removal of RbfA once the 30S subunit reaches the mature state. Furthermore, the ability of the mature 30S subunit to stimulate YjeQ GTPase activity also depends on the carboxy-terminal α-helix. Our data are consistent with a model in which YjeQ uses this carboxy-terminal α-helix as a sensor to gauge the conformation of helix 44, an essential motif of the decoding center. According to this model, the mature conformation of helix 44 is sensed by the carboxy-terminal α-helix, which in turn stimulates the YjeQ GTPase activity. Hydrolysis of GTP is believed to assist the release of YjeQ from the mature 30S subunit through a still uncharacterized mechanism. These results identify the structural determinants in YjeQ that implement the functional interplay with RbfA.

Keywords: ribosome assembly; 30S subunit; YjeQ protein; RsgA protein; RbfA protein; GTPase

INTRODUCTION

The 70S ribosome is the macromolecular complex performing protein synthesis. It is comprised of two functional subunits, the large 50S and the small 30S subunits (Ramakrishnan 2002). The 50S subunit is composed of the 23S and 5S rRNAs as well as 34 ribosomal proteins (r-proteins) (Ban et al. 2000; Harms et al. 2001). The 50S subunit houses the peptidyl transferase center (PTC), which is the catalytic site for peptide bond formation. The 30S subunit contains only one molecule of rRNA (16S rRNA) and 21 r-proteins (Wimberly et al. 2000). The functional core in the 30S subunit is the decoding center, which translates the sequence of the mRNA into protein. Considering the size and complexity of the ribosome, it is a remarkable feat that assembly of the ribosomal subunits in bacterial cells occurs with such high precision and efficiency.

A constant challenge for the cell to maintain high efficiency in the process of ribosome assembly is to ensure that the rRNA molecules stay in a productive line of folding toward the mature structure, without falling into kinetic traps (Woodson 2008, 2011; Shajani et al. 2011). In particular, the folding events involving the maturation of the decoding center in the 30S subunit and PTC in the 50S subunit, occurring at the late stages of assembly (Jomaa et al. 2011a, 2014; Guo et al. 2013; Leong et al. 2013; Li et al. 2013) have a strong tendency to fall into local energy minima. Therefore, bacterial cells have acquired a number of protein factors that are dedicated to assist the folding of these motifs critical for ribosome function (Wilson and Nierhaus 2007); however, it is still not understood how they perform their function.

There are at least four protein factors (YjeQ [or RsgA], RbfA, RimM, and Era) that assist the folding of the decoding center during the late stages of assembly of the 30S subunit. Their roles in the maturation of the functional core of the 30S subunit may entail facilitating proper 17S rRNA folding, assisting processing of the rRNA, or mediating protein–RNA interactions. Cryo-electron microscopy (cryo-EM) (Sharma et al. 2005; Datta et al. 2007; Guo et al. 2011; Jomaa et al. 2011b) revealed that at least three factors, Era, YjeQ, and RbfA bind at or in close proximity to the decoding center at sites that are not overlapping, indicating that simultaneous

Corresponding author: ortegaj@mcmaster.ca

Article published online ahead of print. Article and publication date are at http://www.rnajournal.org/cgi/doi/10.1261/rna.049171.114. Freely available online through the *RNA* Open Access option.

binding is stereochemically possible. Consistently, genetic experiments (Bylund et al. 1998, 2001; Inoue et al. 2003, 2006; Campbell and Brown 2008) suggested that these factors operate in conjunction rather than independently. Indeed, a recent study (Goto et al. 2011) described that binding of YjeQ stimulates the removal of RbfA bound to the mature 30S subunit. The RbfA protein binds to the small ribosomal subunit at the junction between the body and head, most likely when the particle is still in an immature state and alters the position of helix 44 and 45 (Datta et al. 2007). This study (Goto et al. 2011) suggested that one of the functions of YjeQ is assisting the release of RbfA and perhaps other assembly factors, once maturation of the ribosomal particle is completed. Therefore, accumulated evidence suggests that YjeQ, RbfA, RimM, and Era function together to ensure the maturation of the functional core of the 30S subunit.

Although the question here at large is how these four factors cooperate to ensure proper maturation of the decoding center, the specific focus in this study is to identify the motifs in YjeQ that implement the functional interplay between YjeQ and RbfA (Goto et al. 2011).

The YjeQ protein is a GTPase broadly conserved across most bacterial species. It exhibits slow intrinsic GTPase activity; however, interaction with the 30S subunit enhances this activity by 160-fold (Daigle and Brown 2004). YjeQ is structurally well conserved (Levdikov et al. 2004; Shin et al. 2004; Nichols et al. 2007) featuring an amino-terminal oligonucleotide/oligosaccharide binding (OB-fold) domain, a central GTPase module and a carboxy-terminal zinc-finger domain (Supplemental Fig. S1A). The OB-fold domain consists of antiparallel β-sheets that come together forming a β-barrel. In the YjeQ GTPase domain the characteristic G motifs mediating the nucleotide binding (G1 (Walker A, P-loop)-G2 (T)-G3 (Walker B)-G4 (N/TKxD)-G5 [(T/G)(C/S)A]) are circularly permutated and adopt a G4–G5–G1–G2–G3 pattern. Work in the prototype ras GTPase showed that nucleotide binding and hydrolysis leads to conformational changes typically confined to two loops in the GTPase domain known as switch I and switch II (Hall et al. 2002). Switch I in YjeQ encompass the G2-loop and it is disordered in the YjeQ structures. The G3 loop constitutes the switch II, which in this case is a long stretch of amino acids connecting the GTPase domain with the carboxy-terminal zinc-finger domain. Therefore, switch I and II are well positioned in YjeQ to propagate the conformational changes occurring as a result of the GTP hydrolysis to the upstream OB-fold and downstream zinc-finger domain, respectively. The carboxy-terminal zinc-finger domain in YjeQ is comprised of a 3^{10}-helix and a long loop containing three cysteine residues and a histidine that mediate the tetrahedral coordination of one zinc ion. Beyond this loop there are two additional α-helices. The function of the last carboxy-terminal α-helix is unclear, as it is not directly required to coordinate the zinc ion (Supplemental Fig. S1A).

It has been described that the OB-fold domain is essential for binding to the 30S subunit and GTPase stimulation (Daigle and Brown 2004), but a specific role for the GTPase and zinc-finger domains has not been assigned. Here, we found that the zinc-finger domain is comprised of two functional motifs. The region coordinating the zinc ion, which is essential for efficient binding of YjeQ to the 30S subunit and the carboxy-terminal α-helix that is necessary for the removal of RbfA from the mature 30S subunit. In addition, it has been described (Goto et al. 2011) that when the 30S subunit reaches the mature state, the GTPase activity of the bound YjeQ increases. We found that the ability of the mature 30S subunit to stimulate YjeQ GTPase activity also depends on the presence of the carboxy-terminal α-helix in the zinc-finger domain. Our data are consistent with a model in which YjeQ uses the carboxy-terminal α-helix as a sensor to gauge the conformation of helix 44, an essential motif of the decoding center that only adopts its mature conformation at the very end of the assembly process. According to this model, the carboxy-terminal α-helix senses that helix 44 has reached the mature conformation and triggers GTP hydrolysis facilitating the release of YjeQ from the mature 30S subunit through a still uncharacterized mechanism. Release of the assembly factors is necessary for the mature 30S subunit to associate with the 50S subunit and engage in translation.

RESULTS

The carboxy-terminal zinc-finger domain of YjeQ provides structural stability to the protein

To determine the specific function of the zinc-finger domain of YjeQ in assisting the assembly of the 30S subunit, we constructed three protein variants with different truncations in the carboxy-terminal region (Supplemental Fig. S1B). In the first variant (YjeQ M1), the entire zinc-finger domain was removed by introducing a stop codon in the position of Leu 278 (*Escherichia coli* numbering) located in the loop connecting this domain with the GTPase domain. For the second variant the stop codon was introduced in the position of Phe 287, right after the 3^{10}-helix, therefore removing the loop coordinating the zinc ion. Finally, for the third variant (YjeQ M3) the stop codon was introduced in the position of Lys 320 removing the carboxy-terminal α-helix, but not the loop coordinating the zinc ion.

To compare the stability of these YjeQ variants with the wild-type YjeQ protein, we performed a precipitation test in which the proteins were incubated at different temperatures and NH_4Cl concentrations (Supplemental Fig. S1C). From these experiments we concluded that in order to maintain the YjeQ variants in solution under the low salt conditions required for our binding assays with the 30S ribosome subunits (see below), the temperature had to be maintained at 16°C or lower.

In addition, to ensure that these carboxy-terminal deletions did not produce a global unfolding of the protein, the wild-type YjeQ protein and YjeQ variants were analyzed by

circular dichroism (CD) (Supplemental Fig. S2). This technique, consistent with the results from the precipitation test, showed that at a temperature of 25°C or lower the YjeQ variants were stable and properly folded. However, the carboxy-terminal zinc-finger domain of the protein was necessary for the YjeQ protein to remain structurally stable at higher temperatures.

Finally, we tested the effect of removing the zinc ion on the stability of YjeQ. Three cysteine residues (Cys 297, Cys 302, and Cys 310) and a histidine (His 305) mediate the tetrahedral coordination of one zinc ion to the carboxy-terminal domain of YjeQ (Supplemental Fig. S1A). To remove the ability of the domain to coordinate the zinc ion, Cys 297 and Cys 310 residues were mutated to alanine (YjeQ M5). We found that when expressing this variant most of the protein produced was insoluble regardless of the temperature used in the incubation of the culture (16°C, 25°C, and 37°C) (data not shown). This result suggested that in the full-length YjeQ, the presence of the zinc ion is important not only for the folding of the zinc-finger domain, but also for the proper folding of the amino-terminal OB fold and GTPase domains.

YjeQ requires the carboxy-terminal zinc-finger domain to bind the mature 30S subunit

The OB-fold domain of YjeQ has already been identified as a necessary motif for the binding of the protein to the 30S subunits and stimulation of its GTPase activity (Daigle and Brown 2004). Here, to determine the role of the zinc-finger domain of YjeQ in the binding of the protein to the small ribosome subunit, we tested the ability of the carboxy-terminal truncation variants of YjeQ (Supplemental Fig. S1B) to bind mature 30S and immature 30S subunits purified from *yjeQ* null *E. coli* cells. To this end, we used filtration assays in which a mixture of the 30S subunits (mature or immature) with YjeQ (full-length or variants) was incubated at 16°C for 15 min. After the incubation period, reactions were spun through a 100 kDa centrifugal device that retains the YjeQ protein or its variants only when bound to the ribosomal particles. The unbound fraction of protein was captured in the flow-through. However, the protein bound to the 30S subunits was retained by the filter and subsequently resuspended. Resolving these samples by SDS-PAGE allowed us to visualize the content of the flow-through and bound fractions (Fig. 1).

In this assay, one of the factors affecting the amount of binding of YjeQ to the 30S subunits is the salt concentration in the reaction buffer. Filtration assays (Supplemental Fig. S3; left panel) performed with buffers containing a concentration of NH_4Cl ranging from 60 to 600 mM showed that at 300 mM NH_4Cl, YjeQ bound to the 30S subunit at ~1:1 ratio, which is the stoichiometry that has been previously established for the 30S+YjeQ complex (Daigle and Brown 2004; Himeno et al. 2004; Guo et al. 2011; Jomaa et al. 2011b). Therefore, we used buffer containing 300 mM NH_4Cl for these filtration assays, as these conditions were optimal to measure specific binding of YjeQ to the 30S subunits and minimize any potential nonspecific binding. Under these conditions the filter did not retain YjeQ or the YjeQ protein variants when they were by themselves, thus they all appeared in the flow through upon centrifugation. Instead, the filter retained all the mature and immature 30S subunits (Fig. 1A).

Under these conditions, we first tested the ability of full-length YjeQ to bind the mature and immature 30S subunits and found that the protein bound equally well to both particles in the presence of GMP-PNP (Fig. 1B). Then, we tested the binding of the YjeQ variants to the mature 30S subunit (Fig. 1B, top panel). We found that the YjeQ M1 variant lacking the entire zinc-finger domain showed a fourfold decrease in binding to the mature 30S subunit compared with wild-type YjeQ. Similarly, the YjeQ M2 variant, containing only the first 3^{10}-helix of the zinc-finger domain, showed a fivefold decrease in binding. However, the YjeQ M3 variant that had only missing the carboxy-terminal α-helix motif showed slightly improved binding compared with wild-type YjeQ (Fig. 1B, top panel).

A caveat in the filtration assay was that not all of YjeQ M3 protein was recovered in the flow-through nor in the bound fractions. This suggested that a percentage of the YjeQ M3 protein was nonspecifically binding to the filter, despite stringent blocking of the filter with solution of bovine serum albumin (BSA). To confirm the ability of the YjeQ M3 variant to bind the mature 30S subunit a pelleting assay was performed with both proteins (Fig. 1C). In the pelleting assay, the binding reaction was laid over a sucrose cushion in the same buffer conditions used for the filtration assay and then subjected to ultracentrifugation. Protein binding to the 30S subunit was found in the pellet fraction and the unbound protein was found in the supernatant fraction. Proteins in both fractions were then visualized by SDS-PAGE. Consistent with the filtration assay (Fig. 1C), the pelleting assay showed that the binding of YjeQ M3 to the mature 30S subunit was ~1.5-fold enhanced compared to that of wild-type YjeQ (Fig. 1C). Considering that the stoichiometry of the 30S+YjeQ complex is 1:1, these results suggest that under the salt concentration used in the pelleting experiment (300 mM NH_4Cl) approximately one-third of the YjeQ M3 variant was binding the mature 30S subunit in an unspecific manner. It is plausible that exposure of a new surface in the zinc-finger domain of YjeQ upon removal of the carboxy-terminal α-helix may be causing the unspecific binding.

When analyzing the binding of the YjeQ variants to the immature subunit, the binding of the YjeQ M1 and YjeQ M2 variants only decreased by approximately twofold when compared with wild-type YjeQ. In the case of YjeQ M3, it bound to the immature 30S subunit similarly to wild-type YjeQ (Fig. 1B, bottom panel).

Overall, this data suggest that the zinc-finger domain plays an important role for efficient binding of YjeQ to the mature

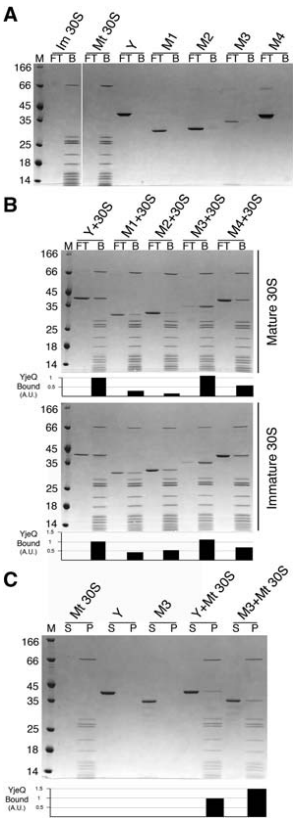

FIGURE 1. Binding of YjeQ carboxy-terminal variants to the mature and immature 30S subunits. (*A*,*B*) Ability of YjeQ (Y) and YjeQ variants (M1, M2, M3, and M4) to bind to the mature (Mt) and immature (Im) 30S subunits analyzed by filtration assays. Coomassie blue stained SDS-PAGE in *A* contains the controls for the experiment consistent in reactions containing either YjeQ (full-length or variants) or 30S subunits (mature or immature) by themselves. Reactions containing a mixture of YjeQ protein and ribosomal particles contained a fivefold molar excess of protein. Assembly mixtures were incubated for 15 min at 16°C in the presence of 1 mM GMP-PNP. Following incubation, the reactions were passed through a 100 kDa cut-off filter using centrifugation. The unbound protein was captured in the flow-through (FT) and the protein bound to the ribosomal particles (B) was retained by the filter and resuspended by an equal volume of buffer. The molecular weight marker (M) is in kDa. The flow-through and bound portions from these assays were loaded into 4%–12% bis–tris polyacrylamide gels and resolved using SDS-PAGE. (*C*) Pelleting assay of YjeQ M3 variant with the mature 30S subunit. A fivefold excess of YjeQ M3 was incubated with mature 30S subunits for 15 min at 16°C. Following the incubation, reactions were laid over a sucrose cushion and subjected to ultracentrifugation. Proteins that were unbound were collected in the supernatant (S), while proteins that bound to the 30S particle were found in the pellet (P). The molecular weight (M) is in kDa. The pellet and supernatant were resolved by 4%–12% bis–tris SDS-PAGE and stained with Coomassie blue. The bar diagrams *under* the gels in *B* and *C* indicate the binding of the YjeQ variants to the 30S subunits with respect to wild-type YjeQ (set as 1).

30S subunit, but does not require the carboxy-terminal α-helix for this function. It also suggests that the zinc-finger domain may not play as critical as a role for binding to the immature 30S subunit. In this case, efficient binding to the subunit seems to depend more on the OB-fold domain.

Lysine 298 and arginine 300 in the carboxy-terminal zinc-finger domain of YjeQ are not essential for binding to the mature 30S subunit

A previous structural study describing the cryo-EM structure of the mature 30S subunit in complex with YjeQ (Guo et al. 2011) indicates that YjeQ binds in an orientation in which the OB-fold domain interacts with helix 44 and the zinc-finger domain interacts with the head of the 30S subunit mainly through residues Lys 298 and Arg 300 (Fig. 5A, below). The electrostatic interactions between the positively charged side chains of these two amino acids and the negatively charged phosphate groups of the 16S rRNA of the ribosomal particle stabilize these contacts. To study the contribution of Lys 298 and Arg 300 for binding of YjeQ to the ribosome subunit, we mutated both residues to alanine in the full-length YjeQ protein to produce the YjeQ M4 variant (Supplemental Fig. S1B). In the precipitation test this mutant did not show any instability when exposed at 37°C (Supplemental Fig. S1C) and its CD spectra at all temperatures tested completely overlapped with that of wild-type YjeQ (Supplemental Fig. S2) indicating that the YjeQ M4 variant folds into its native conformation. When we tested the ability of the YjeQ M4 variant to bind the mature and immature 30S subunit (Fig. 1A,B), we found that the YjeQ M4 variant had only decreased binding to the mature and immature 30S subunits by twofold and 1.3-fold, respectively. This result indicated, contrary to what the cryo-EM structure suggested (Guo et al. 2011), that residues Lys 298 and Arg 300 in the zinc-finger domain of YjeQ are not essential for binding to the mature 30S subunit.

The carboxy-terminal α-helix of the zinc-finger domain is necessary for the 30S subunit-dependent GTPase activity of YjeQ

In the absence of ribosome subunits YjeQ hydrolyzes GTP slowly and exhibits a k_{cat} of 9.4 h^{-1} and a K_m for GTP of 120 μM (Daigle et al. 2002). However, association with the 30S subunit results in a 160-fold stimulation of YjeQ GTPase activity. Previous studies indicated that the first 20 amino-terminal amino acids are important for ribosome-stimulated GTPase activity of YjeQ (Daigle and Brown 2004).

Here, we tested the carboxy-terminal truncations of YjeQ to determine whether the zinc-finger domain plays any role in this activity. The initial rates of GTP hydrolysis for full-length YjeQ and YjeQ variants were measured in the presence and absence of mature and immature 30S subunits. To this end we used a malachite green assay to measure the amount

of free phosphate produced in the reaction from GTP hydrolysis. Reactions were incubated for 1 h at 25°C before they were quenched. This temperature was chosen instead of the 30°C that was used in previous studies (Daigle and Brown 2004) with YjeQ, to ensure that the YjeQ variants remained stable during the course of the reaction (Supplemental Figs. S1C, S2). The initial rate of the GTP hydrolysis was estimated from the amount of free phosphate produced in each reaction.

We found that all the carboxy-terminal truncation variants of YjeQ exhibited an intrinsic initial rate of GTP hydrolysis comparable to full-length YjeQ and that ranged from 1–4 pmol/min (Fig. 2). When the mature 30S subunit was included in the reaction, the initial rate of the full-length YjeQ increased by approximately eightfold (see Materials and Methods). However, it did not increase considerably for any of the carboxy-terminal variants of YjeQ, except for the YjeQ M4 variant that showed an initial rate comparable to wild-type YjeQ. Using the immature 30S subunit in the reactions caused less than a threefold increase in the initial rate of full-length YjeQ, but again no increase was observed for the YjeQ variants (Fig. 2). This result is consistent with previous work (Himeno et al. 2004) that show the stimulation of the YjeQ GTPase activity by the immature 30S subunits is minimal in comparison to the mature 30S subunit. However, the fold-increase in the initial rate measured for the full-length protein was substantially lower than the 160-fold stimulation that had been reported (Daigle and Brown 2004). This difference is likely caused by the lower temperature (25°C versus 30°C) incubations in our assays.

Considering these results, we interpreted that the YjeQ M1 and YjeQ M2 variants did not show an increased level in 30S subunit-dependent GTPase activity (Fig. 2), possibly because both proteins cannot efficiently bind the mature 30S particle (Fig. 1B). In addition, we found that YjeQ M3 was able to bind the mature 30S subunit, but showed no increase in 30S subunit-dependent GTPase activity (Fig. 2). These results indicate that while the carboxy-terminal α-helix in the zinc-finger domain is not required for binding, it is a necessary motif for stimulation of GTP hydrolysis by the 30S subunit.

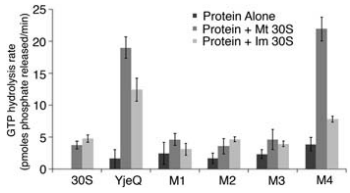

FIGURE 2. Stimulation of GTPase activity of YjeQ variants by mature and immature 30S subunits. The GTP hydrolysis rate of the YjeQ variants alone or in the presence of mature (Mt 30S) and immature 30S (Im 30S) subunits was assessed using the Malachite Green Phosphate assay as described in Materials and Methods. The GTPase hydrolysis rates plotted in the graph were determined by measuring the free phosphate produced after the reactions had been incubated for 60 min at 25°C. Standard deviations shown in the plot correspond to three replicas of the experiment.

YjeQ promotes the release of RbfA from the mature 30S subunit through the carboxy-terminal α-helix of the zinc-finger domain

Genetic and biochemical studies suggest that a function of YjeQ during maturation of the 30S subunit is assisting on the release of RbfA from the mature 30S subunit once the maturation of the particle is completed (Goto et al. 2011). It is not understood how this functional interplay is implemented and the structural determinants in YjeQ that allow the protein to perform this action. Prompted by the interesting phenotype of the YjeQ M3 variant that binds the 30S subunit without having an increase in its GTPase activity, we tested the ability of this YjeQ variant to remove RbfA and determined whether the CTE has any role in this activity.

To test the YjeQ M3 variant, we first modified the filtration assay to visualize the displacement of RbfA by full-length YjeQ. In these experiments, RbfA was first bound to the ribosomal subunits by incubating the reaction for 15 min. YjeQ was then added and incubated for an additional 15 min before the reaction was spun in the centrifugal device to separate free protein from that bound to the 30S subunits. The content in the flow through and bound portion was then analyzed by SDS-PAGE.

As in the assays testing the binding of YjeQ (Fig. 1B), the concentration of NH_4Cl in the buffer is a critical parameter influencing the binding of RbfA to the small ribosome subunits. Performing the assembly reactions in buffers containing a range of NH_4Cl concentration from 60 to 600 mM, we determined that at 60 mM NH_4Cl, RbfA bound stoichiometrically to the immature 30S subunit (Supplemental Fig. S3, right panel). Binding of RbfA to immature 30S subunits is better than to mature 30S subunits (Goto et al. 2011), therefore this analysis was done with immature particles. In the case of mature 30S subunits, binding of RbfA is substoichiometric in buffer containing 60 mM NH_4Cl (Supplemental Fig. S4A, middle panel). Consequently, the NH_4Cl concentration in these assays aiming to visualize the release of RbfA upon binding of YjeQ was maintained at 60 mM NH_4Cl, ensuring that binding of RbfA to the mature 30S subunit was still occurring (Supplemental Fig. S4, middle panel). We found that under these conditions YjeQ was able to efficiently remove RbfA from the mature 30S subunit. The removal of RbfA was very efficient in the presence of GTP (~95%) and GMP-PNP (~90%). In the presence of GDP, YjeQ displaced ~65% of the RbfA bound to the mature 30S subunit (Supplemental Fig. S4A, middle panel).

In the case of immature 30S subunits, YjeQ could not release RbfA from the immature particle, regardless of the nucleotide present in the buffer (Supplemental Fig. S4A, bottom panel). To establish that the inability of YjeQ to release RbfA

from the immature 30S subunit was not due to the low salt concentration on the buffer, this experiment was repeated also at higher salt concentration (Supplemental Fig. S4B). In this case the assembly reaction was carried out in the presence of GMP-PNP. We found that YjeQ still did not displace RbfA from the immature 30S subunits, even at the high salt concentrations and in the presence of GMP-PNP. Control filtration assays performed in parallel using YjeQ, RbfA, or both proteins in low or high salt buffer, showed that the filter did not retain the proteins by themselves or when combined in either buffer (Supplemental Fig. S4A, top panel; Supplemental Fig. S4B, left gel).

Now that a reliable assay was in place to visualize displacement of RbfA from the 30S subunit upon YjeQ binding, we tested the ability of the YjeQ M3 variant to perform this action. In this case, reactions were incubated at 25°C in order to maintain the solubility and folding of the YjeQ variant. Subsequently, the reaction was spun in a centrifugal device to perform the filtration assay. Interestingly, we found that whereas wild-type YjeQ removed 100% of the RbfA bound to the mature 30S subunit, the YjeQ M3 variant enhanced binding of RbfA by fourfold instead of removing it (Fig. 3A). Consistently with this result, when the reactions were laid over a sucrose cushion and subjected to a pelleting assay we observed a similar result (Fig. 4B). Wild-type YjeQ removed ~60% of the RbfA bound to the mature 30S subunit and the YjeQ M3 variant increased binding of RbfA by 5.5-fold. These results indicate that the carboxy-terminal α-helix in the zinc-finger domain is the structural motif implementing the ability of YjeQ to remove RbfA from the 30S subunit once the maturation is completed. Furthermore, binding of the YjeQ M3 variant lacking the carboxy-terminal α-helix seemed to induce a conformation in the mature 30S subunit that stabilized the binding of RbfA.

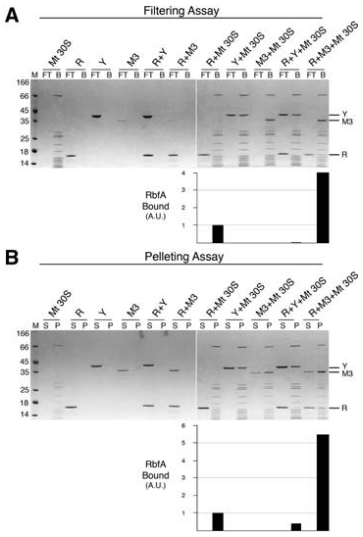

FIGURE 3. YjeQ M3 is unable to remove RbfA bound to the mature 30S subunit. (*A*) Filtration assay to test the release of RbfA (R) from the mature 30S subunit (Mt 30S) in the presence of YjeQ wild-type (Y) and YjeQ M3 variant (M3). These reactions were performed by adding the assembly factors in fivefold molar excess with respect to the 30S subunits and in the presence of GMP-PNP. Incubations were done at 25°C. Flow-through (FT) and bound (B) fractions from the filtration assay were resolved in 4%–12% bis–tris SDS-PAGE and stained with Coomassie blue. (*B*) Pelleting assay of identical reactions used in *A*. The molecular weight marker (M) is in kDa. Supernatant (S) and pellet (P) fractions from this assay were resolved in 4%–12% bis–tris SDS-PAGE and stained with Coomassie blue. The bar diagrams *under* the gels indicate the binding of the RbfA to the mature 30S subunit in each reaction. The observed binding of RbfA to the mature 30S subunit was defined as 1.

The carboxy-terminal extension of the zinc-finger domain in YjeQ is necessary for its function in vivo

The in vitro experiments described above indicated that the carboxy-terminal α-helix in the zinc-finger domain is an essential element for the 30S subunit-dependent GTPase activity of YjeQ (Fig. 2), as well as for YjeQ to promote on the release of RbfA once the maturation of the 30S subunit is completed (Fig. 3). To test whether the carboxy-terminal α-helix is necessary for YjeQ to assist in the assembly of the 30S subunits in vivo, we performed a complementation assay by expressing the YjeQ M3 variant in the *yjeQ* null strain. These cells were then tested for growth, rRNA and ribosome content. The wild-type *yjeQ* or *yjeQ m3* genes in these experiments were reintroduced in the null strain with a high-copy plasmid in which the expression is under the control of an IPTG-inducible T5 promotor (Kitagawa et al. 2005). Reintroduction of the gene in a plasmid, instead of in the chromosome eliminated the possibility of polar effects on downstream genes.

To analyze the growth, cells were grown at 25°C for up to 47 h and their optical density was measured and plotted over time (Fig. 4A). We also calculated their growth rate (Table 1). As previously described (Campbell et al. 2006; Goto et al. 2011) the *E. coli yjeQ* null strain exhibited a slow-growth phenotype (growth rate [GR] = 0.14 h^{-1}) compared to the parental strain (GR = 0.44 h^{-1}). We found that expression of wild-type YjeQ in small amounts achieved by using a low concentration (1 μM) of IPTG was sufficient to partially correct the slow-growth phenotype of the null *yjeQ* strain (GR = 0.21 h^{-1}). However, overexpression of YjeQ by using a higher concentration of IPTG (100 μM) led the cells to grow slower than the null strain (GR = 0.12 h^{-1}). This was likely the result of the toxic effect caused by an excess of YjeQ in the cells, which causes 70S subunits to dissociate (Daigle and Brown 2004; Himeno et al. 2004). Consequently to prevent the toxicity effects due to high levels of expression of YjeQ, the complementation experiments with the YjeQ M3 variant were performed using low concentrations of IPTG. Expression

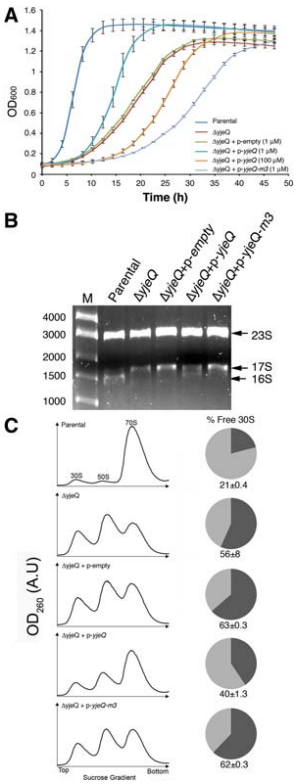

FIGURE 4. The carboxy-terminal extension of the zinc-finger domain in YjeQ is necessary for its function in vivo. (*A*) The parental strain and the *yjeQ* null strain by itself or complemented with the plasmid expressing yjeQ, YjeQ M3 variant, or the empty vector were induced at $t = 0$ h with the indicated concentration of IPTG and grown at 25°C for 47 h. Growth was monitored by measuring absorbance at 600 nm and plotted against time. Standard deviations shown in the plot correspond to three replicas of the experiment. (*B*) Total rRNA of cell cultures were analyzed when cultures reached mid-log phase represented by $OD_{600} = 0.2$. Total rRNA was extracted and resolved by electrophoresis in 0.9% synergel–0.7% agarose gel. The marker (M) is in base pairs. (*C*) Ribosome absorbance profiles from the parental strain and *yjeQ* null strain by itself or complemented with the plasmid expressing YjeQ, YjeQ M3 variant, or the empty plasmid were fractionated by ultracentrifugation in 10%–30% sucrose gradients providing the profiles shown in this panel. Peaks for the 30S, 50S subunits, and 70S ribosomes are indicated. The proportion of free 30S to bound 30S (i.e., 30S subunits in 70S complexes) in each case was calculated by integrating the areas *under* the 30S and 70S peaks of the sucrose gradient profiles. The area of the 30S peak plus one-third the area of the 70S peak corresponds to the total 30S population. The area of the 30S peak was divided by the total 30S absorbance to obtain the percentage of free 30S subunits and produce the pie charts in this panel. The standard deviations shown correspond to three replicas of the experiment. Peak area for the 30S subunit in each case was measured with respect to the area *under* the 70S peak to calculate the percentage of free 30S subunits in both strains. The calculated percentages are shown in the pie charts. The standard deviations shown correspond to three replicas of the experiment.

of the YjeQ M3 variant in this manner caused the cells to exhibit a growth rate of 0.10 h^{-1}, which is even slower than that shown by the null *yjeQ* strain. In the control experiments where cells were transformed with the empty vector we found that it had no effect on the growth rate of the null strain (Fig. 4A; Table 1).

Total rRNA from the cells tested for growth was purified and resolved by gel electrophoresis (Fig. 4B) after they had been grown to mid-log phase. We found that the majority of the rRNA purified from parental cells was mature 16S rRNA, as opposed to the null *yjeQ* cells (alone or transformed with the empty plasmid), which mainly contained precursor 17S rRNA. Cells complemented with the plasmid expressing wild-type YjeQ showed that ~50% of the accumulated rRNA had been processed into 16S rRNA. Conversely, in the cells expressing the YjeQ M3 variant most of the rRNA remained as unprocessed immature 17S rRNA (Fig. 4B).

Finally, we analyzed the ribosome profiles of the parental, null *yjeQ* cells and cells complemented with either the empty plasmid or that encoding wild-type YjeQ or the YjeQ M3 variant (Fig. 4C). The parental strain produced the expected profile with most of the particles assembled as 70S ribosomes and two small peaks representing dissociated 30S and 50S subunits. In these cells only ~21% of the total 30S subunits were free and not associated with the 50S subunit. Null *yjeQ* cells and cells transformed with the empty plasmid produced a profile in which 56% and 63%, respectively, of the total 30S subunits did not associate to form 70S ribosomes (Daigle and Brown 2004; Himeno et al. 2004). Complementation with the plasmid expressing YjeQ caused the proportion of free 30S subunits to decrease to 40%. However, the percentage of free 30S subunits in cells expressing the YjeQ M3 was even higher (62%) than that of the null *yjeQ* cells. Therefore, we concluded from the analysis of the growth, rRNA, and ribosomal content that in vivo the YjeQ M3 variant was not able to complement the slow-growth phenotype exhibited by null *yjeQ* cells. Indeed, the observed phenotypes suggest that YjeQ M3 exhibited a gain-of function that is toxic most likely due to its enhanced binding to the 30S subunit and its ability to promote binding of RbfA (instead of facilitating release). Tighter binding of YjeQ and RbfA combined most

TABLE 1. Growth rates of the *E. coli yjeQ* null strain in the YjeQ and YjeQ-M3 variant complementation assay

E. coli strains	Growth rate $k = \ln 2/DT$ (h^{-1})
Parental	0.44 ± 0.01
Δ*yjeQ*	0.14 ± 0.01
Δ*yjeQ* + p-*empty* (1 μM IPTG)	0.14 ± 0.01
Δ*yjeQ* + p-*yjeQ* (1 μM IPTG)	0.21 ± 0.01
Δ*yjeQ* + p-*yjeQ* (100 μM IPTG)	0.12 ± 0.01
Δ*yjeQ* + p-*yje-m3* (1 μM IPTG)	0.10 ± 0.01

Standard deviations were calculated from three replicas of the experiment.

likely impaired proper association of the 30S subunits with the 50S subunits to form 70S ribosomes. Consistently, we observed that the proportion of the free 30S subunits in the null *yjeQ* cells transformed with the plasmid expressing the YjeQ M3 was higher than that of the nontransfected null *yjeQ* cells.

DISCUSSION

In this study, we found that the carboxy-terminal zinc-finger domain in YjeQ is important for the overall structural stability of the protein. Interestingly, an in silico analysis of other circularly permutated GTPases (Anand et al. 2006) concluded that a consequence of repositioning the G3/switch II motif within the GTPase domain is that an anchoring carboxy-terminal domain is then required to fasten switch II and maintain its efficiency for GTP binding and hydrolysis. Our finding that the carboxy-terminal zinc-finger domain is necessary for the stability of YjeQ is consistent with this model.

In addition, we also determined that the zinc-finger domain of YjeQ is essential for the role of this protein in assisting the late stages of maturation of the 30S subunit. The presented data indicate that this domain is subdivided into two functional motifs. The part of the domain coordinating the zinc ion is the region that allows for efficient binding of the protein to the 30S subunit, whereas the carboxy-terminal α-helix is the region through which YjeQ senses the binding to the mature 30S subunit triggering GTP hydrolysis in the GTPase domain. The zinc-finger domain is attached to the GTPase domain through the switch II region, which propagates the conformational change. In addition, the carboxy-terminal α-helix is also the region that implements the functional interplay of YjeQ with RbfA and facilitates the removal of RbfA from the mature 30S subunit once maturation of the 30S subunit is completed (Goto et al. 2011).

Recent structural studies with immature 30S subunits purified at late stages of assembly (Guo et al. 2011, 2013; Jomaa et al. 2011b; Boehringer et al. 2012; Clatterbuck Soper et al. 2013; Leong et al. 2013; Yang et al. 2014) revealed that the decoding center is the last region to fold into the mature conformation during the assembly of the subunit. Multiple assembly factors, including YjeQ, RbfA, RimM, and Era, bind to this region (Sharma et al. 2005; Datta et al. 2007; Guo et al. 2011; Jomaa et al. 2011b) at the late stages of assembly and operate in conjunction to monitor the proper folding of this region and prevent immature 30S subunits from engaging in translation. During this process functional interplays between assembly factors likely occur. In principle, any of the maturation steps these proteins facilitate including rRNA folding, rRNA processing, or mediating protein–RNA interactions could be assisted by several of these proteins simultaneously, rather than by protein factors individually. In addition, functional interplays likely play an important role in ensuring that all of the assembly factors are released once the maturation process is completed. Factor release is essential for the mature 30S subunit to enter the pool of actively translating ribosomes (Shajani et al. 2011).

Although there is genetic, biochemical, and structural evidence suggesting a functional interplay between these four putative assembly factors, the specific mechanism on how they work together to assist in maturation of the decoding center remains to be described. Recently, a study (Goto et al. 2011) identified that one of the functions of YjeQ is to assist in the release of RbfA once the maturation of the 30S subunit has been completed. However, it is still not understood how this functional interplay between the two proteins is implemented. A costructure of the 30S subunit in complex with both YjeQ and RbfA that could be informative about this mechanism has not yet been obtained. Furthermore, the cryo-EM structures of the YjeQ protein in complex with the mature 30S subunit (Guo et al. 2011; Jomaa et al. 2011b) propose two conflicting binding orientations of YjeQ to the 30S subunit. Therefore, an unambiguous functional model from these structural data cannot be derived.

In this study, we found that the part of the domain coordinating the zinc ion in YjeQ is important for binding to the 30S subunit and the carboxy-terminal α-helix is essential for this factor to facilitate the release of RbfA from the mature 30S subunit. An important question is how these findings conform to the two conflicting cryo-EM structures (Guo et al. 2011; Jomaa et al. 2011b). The two cryo-EM structures showed that YjeQ binds to the 30S subunit covering the region of helix 44 forming the decoding center and also contacts the head and nearby region of the platform of the ribosomal particle (Fig. 5A,B). However, the two structures proposed a different orientation of the YjeQ protein in this complex. One of the structures (Guo et al. 2011) placed YjeQ with the OB-fold and GTPase domain contacting helix 44 and the carboxy-terminal zinc-finger domain interacting with the head (Fig. 5A, left panel). The second structure (Jomaa et al. 2011b) places YjeQ in an orientation rotated by ~180° around an axis perpendicular to the interface surface of the 30S subunit. In this structure, the OB-fold domain is the region interacting with the platform and the carboxy-terminal zinc-finger domain sits in helix 44 (Fig. 5B, left panel).

Analysis of the two structures revealed that the data presented here are difficult to reconcile with the cryo-EM map where the zinc-finger domain contacts the head domain (Guo et al. 2011). According to this model, only three amino acids within the loop coordinating the zinc ion are close enough to interact with the phosphate–oxygen backbone of the rRNA in the head of the 30S subunit (Lys 298 and Arg 300) or r-protein S13 (Tyr 299) (Fig. 5A, right panel). In this structure, the rest of the zinc-finger domain, including the carboxy-terminal α-helix does not directly contact with either the head or the platform. Only Arg 331 in the carboxy-terminal α-helix comes close to the backbone of helix 24 (Fig. 5A, right panel). Our mutational study indicates

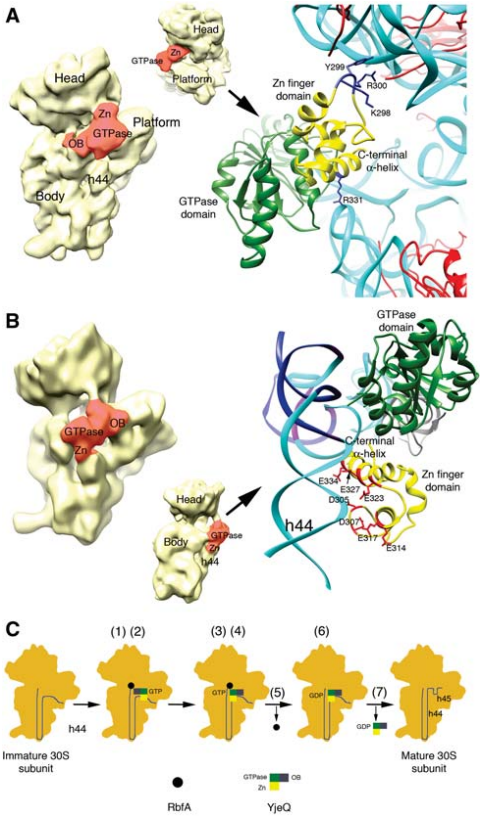

FIGURE 5. Interaction of the zinc-finger domain of YjeQ with the 30S subunit and working model for the functional interplay between YjeQ and RbfA. Structures of the 30S+YjeQ complex as described in Guo et al. (2011) (*A*) and Jomaa et al. (2011b) (*B*). The panel in the *left* shows a view of the entire complex. Landmarks and domains of the YjeQ protein are labeled. Area colored in red represents the YjeQ protein bound to the 30S subunit. The panel in the *right* shows a zoomed in view of the complex in the area of interaction of the zinc-finger domain with the 30S subunit. The rRNA is colored in cyan except for some nucleotides (*B*) that are colored in dark blue. A corresponding density for these nucleotides does not exist in the cryo-EM map of the 30S+YjeQ complex (Jomaa et al. 2011b). The side chains of important residues for this interaction are labeled. Structures shown were obtained from the EMDB (EMD-1884 and EMD-1895) and PDB (2YKR and 4A2I). Images of the structures were prepared with UCSF Chimera software (Pettersen et al. 2004). (*C*) Proposed model for the functional interplay between YjeQ and RbfA. The model explains the mechanism through which YjeQ facilitates the release of RbfA once the maturation of the 30S subunit is completed. Numbers in brackets refer to the steps of the model described in the text.

that the part of the domain coordinating the zinc ion is essential for YjeQ to bind the mature 30S subunit. Additionally, we found that mutating two (Lys 298 and Arg 300) out of the three residues that come into close contact with the head of the 30S subunit did not abolish binding (Fig. 1B). Therefore, it is difficult to envision how the carboxy-terminal α-helix could facilitate the release of RbfA from the mature 30S subunit with the zinc-finger domain in this location and having minimal interactions with the ribosome (Fig. 5A, right panel).

In the second cryo-EM structure (Jomaa et al. 2011b), the zinc-finger domain of YjeQ sits in the upper domain of helix 44 near the decoding center (Fig. 5B). In this location, negatively charged residues in the surface of the loop region coordinating the zinc ion and more importantly the carboxy-terminal α-helix face the negatively charged phosphate–oxygen backbone of nucleotides in helix 44 (Fig. 5B, right panel). This charge distribution in the two motifs of the zinc-finger domain generates electrostatic repulsion with helix 44 causing a displacement of the upper domain of the helix from its mature conformation (Fig. 5B, right panel). It is possible that the carboxy-terminal α-helix in YjeQ facilitates the release of RbfA from the mature 30S subunit by preventing the upper domain of helix 44 to adopt the mature conformation.

RbfA binds in the neck region of the 30S subunit (Datta et al. 2007) also causing a displacement of the upper domain of helix 44 and helix 45. The cryo-EM structure of the 30S subunit in complex with RbfA shows that upon binding, these motifs surround RbfA and lock the protein deeply into the cleft between the head and body. Considering that complexes in this cryo-EM study were prepared with a 10- to 40-fold excess of RbfA with respect to the 30S subunits (Datta et al. 2007), it is plausible that the conformation visualized by cryo-EM represent a "trapped" state of RbfA bound to the mature 30S subunit with the displaced helix 44 and 45 blocking the release of the factor. One of our findings in this study was that substantial binding of YjeQ to the immature 30S subunit is still observed in the absence of the zinc-finger domain (Fig. 1C). Taking all these data into consideration, we propose the following model (Fig. 5C) to explain the functional interplay between YjeQ and RbfA in mediating the maturation of the decoding center. (1) RbfA first binds in the neck region of the immature 30S subunit, which at this point still exhibits the part of helix 44 forming the decoding center in an immature state. (2) RbfA assists in the recruitment of YjeQ, which initially binds to the 30S subunit largely through the OB-fold domain. (3) As the upper domain of helix 44 continues to fold into its mature state, the region in this helix forming the binding site for the zinc-finger domain of YjeQ adopt the proper conformation to allow YjeQ to bind the 30S subunit through both the OB-fold and zinc-finger domains. This is likely the conformation shown by one of the cryo-EM structures (Jomaa et al. 2011b). (4) Binding of YjeQ through the zinc-finger domain to the 30S subunit prevents the upper domain of helix 44 to fold over the bound RbfA and lock this factor in the "trapped" state shown by the cryo-EM map of the 30S+RbfA complex (Datta et al. 2007). (5) By maintaining the upper domain of helix 44 in

a non-native conformation, YjeQ facilitates the release of RbfA. (6) Release of RbfA is sensed by the carboxy-terminal α-helix, activating hydrolysis of the GTP molecule bound to YjeQ. (7) The reduced affinity of YjeQ-GDP for the 30S facilitates the dissociation of YjeQ from the mature subunit through a still uncharacterized mechanism, allowing the upper domain of helix 44 to adopt the conformation observed in the decoding center of the mature subunit. Dissociation of YjeQ also uncovers essential intersubunit bridges (B2a and B3) allowing the mature 30S subunit to associate with the 50S subunit and engage in protein translation.

An important consideration regarding our experimental set up to analyze the YjeQ-induced release of RbfA is that it does not completely mimic the sequence of events most likely occurring in the cell (Fig. 5C). Mainly, in our assays we bound RbfA directly to the mature 30S subunit and then YjeQ was added to test RbfA release. In the cell, it is most likely that RbfA would bind to the immature 30S subunit (instead to the mature 30S subunit) and YjeQ-induced release would take place once this subunit has evolved and becomes a mature subunit. Unfortunately, attempts of starting our reactions with the immature 30S subunit in complex with RbfA and maturing these subunits in vitro to then test the release of RbfA with YjeQ were unsuccessful. Nevertheless, it is likely that the binding mode of RbfA to the mature 30S subunit in our in vitro assays closely resembles that existing in the analogous complex in vivo. Consequently, conclusions withdrawn from these binding assays most likely apply to the maturation process occurring in vivo. In this regard, future efforts to determine the structure of mature and immature 30S subunits in complex with RbfA and YjeQ will be important to visualize the conformational changes suggested by the model described above and how the implementation of the functional interplay between YjeQ and RbfA occurs.

MATERIALS AND METHODS

Cell strains and protein overexpression clones

Parental *Escherichia coli* K-12 (BW25113) and *E. coli* Δ*yjeQ* strains were obtained from the Keio collection (Baba et al. 2006).

The pDEST17-*yjeQ* plasmid used to overexpress wild-type YjeQ protein with an amino-terminal His_6 tag cleavable by TEV protease was produced as previously described (Jomaa et al. 2011b). The pDEST17-*yjeQM1*, pDEST17-*yjeQM2*, pDEST17-*yjeQM3*, and pDEST17-*yjeQM4* plasmids used to overexpress the YjeQ carboxy-terminal deletion variants were generated by using the QuikChange II XL Site-Directed Mutagenesis Kit (Agilent Technologies). To this end, the parental pDEST17-*yjeQ* plasmid was used as the template for site-directed mutagenesis reactions that introduced a stop codon in the position of L278 (YjeQM1), F287 (YjeQM2), K320 (YjeQM3) or to create the point mutations K298A and R300A (YjeQM4). The Q5 Site-Directed Mutagenesis Kit (New England Biolabs) was used to produce the pDEST17-*yjeQM5* plasmid containing mutations C297A and C310A. In this case, we used the same template plasmid as the other mutants.

Overexpression of RbfA was obtained using the pET15b-*rbfA* plasmid. To produce this plasmid the sequence of the *rbfA* gene (NCBI reference: NC_007779.1) was optimized for overexpression in *E. coli* cells using the GeneOptimizer software and subsequently synthesized (Life Technologies; Thermo Fisher Scientific) with a NdeI and a BamHI site in the 5′ and 3′ ends of the gene, respectively. The gene was cloned into the carrier pMA-T plasmid using the SfiI and SfiI cloning sites and subsequently subcloned into the final expression vector pET15b using the NdeI and a BamHI restriction sites. The resulting pET15b-*rbfA* plasmid produces the RbfA protein with an amino-terminal His_6 tag cleavable by thrombin.

We used sequencing (MOBIX, McMaster University) to validate all overexpression clones.

Protein overexpression and purification

Wild-type YjeQ protein and the constructed variants (YjeQ M1, YjeQ M2, YjeQ M3, YjeQ M4, and YjeQ M5) were overexpressed as amino-terminal His_6-tag proteins by transforming *E. coli* BL21-A1 cells with the corresponding expression plasmids constructed to produce these proteins (see above). Typically, 1 L of cells were grown in LB medium at 37°C to an OD_{600} of 0.6 and expression was induced with 0.2% L-arabinose. Wild-type YjeQ and YjeQ M4 were induced for 3 h at 37°C, whereas YjeQ M1, YjeQ M2, and YjeQ M3 were induced for 16 h at 16°C due to the instability and low solubility of the proteins at 37°C. In the case of the YjeQ M5 variant, expression was tested at 16 h at 16°C, 5 h at 25°C, and 3 h at 37°C. Cells were harvested after induction by centrifugation at 8500*g* for 15 min. The cell pellets were then washed with 1× PBS buffer (137 mM NaCl, 2.7 mM KCl, 8.1 mM Na_2HPO_4, 1.76 mM KH_2PO_4 at pH 7.4), centrifuged at 1400*g* for 20 min and resuspended in 20 mL of lysis buffer (50 mM Tris–HCl at pH 8.0, 10% [w/v] sucrose, 100 mM NaCl). The cell suspension was passed through the French press three consecutive times at 20,000 lb/in^2 to lyse the cells. Lysate was separated from cell debris by centrifugation at 30,000*g* for 40 min and NaCl was added to the clarified lysate to bring the concentration to 0.5 M. The lysate was then filtered with a 0.45 µm filter and loaded onto a HiTrap Metal Chelating column (GE Healthcare Life Sciences) equilibrated with 50 mM Tris–HCl at pH 8.0, 0.5 M NaCl and 5% [v/v] glycerol. The column was washed with buffer containing concentrations of imidazole of 45 mM and 90 mM. Finally, proteins were eluted by increasing the concentration of imidazole in the buffer to 240 mM. The purity of fractions was monitored by 15% SDS-PAGE. Fractions with pure protein were collected and dialyzed overnight at 4°C against buffer containing 50 mM Tris–HCl at pH 8.0 and 5% [v/v] glycerol. For YjeQ M1, YjeQ M2, and YjeQ M3, the dialysis buffer also included 120 mM NaCl to increase protein solubility.

The amino-terminal His_6-tag was removed by digestion with purified tobacco etch virus (TEV) protease during the previous overnight dialysis step. To this end, 0.05 mg of TEV protease per milligram of YjeQ was added to the pooled and dialyzed fractions containing the wild-type or YjeQ variants. Following digestion and dialysis, the reaction was loaded onto the HiTrap Metal Chelating column (GE Healthcare Life Sciences) previously equilibrated with 50 mM Tris–HCl at pH 8.0, 60 mM imidazole, 0.2 M NaCl, and 5% [v/v] glycerol. The flow through containing the untagged protein was recovered and purity of fractions showing cleaved protein was monitored by 15% SDS-PAGE. Fractions with

pure, cleaved protein were dialyzed overnight at 4°C against buffer containing 50 mM Tris–HCl at pH 8.0 and 5% [v/v] glycerol. For YjeQ M1, YjeQ M2, and YjeQ M3 the dialysis buffer also included 120 mM NaCl. Pure proteins were concentrated using a 10 kDa-cutoff filter (Amicon). Proteins were frozen in liquid nitrogen and stored at −80°C.

The RbfA protein containing an amino-terminal His_6-tag was overexpressed in *E. coli* BL21-DE3 cells transformed with the pET15b-*rbfA* plasmid. One liter of cells was grown in LB medium at 37°C to an OD_{600} of 0.6 and then induced with 1 mM isopropyl β-D-1-thiogalactopyranoside (IPTG) for 3 h at 37°C. Following induction, cells were harvested and lysed using the same protocol and buffers as in the case of the YjeQ protein. The first step of purification of RbfA included a HiTrap Metal Chelating column (GE Healthcare Life Sciences) that was performed in an identical manner to the YjeQ purification except that the column washes before elution were done with buffers containing 30 and 75 mM imidazole. Fractions containing RbfA protein were collected, pooled, and dialyzed overnight at 4°C against buffer containing 50 mM Tris–HCl at pH 8.0 and 5% [v/v] glycerol. Dialyzed RbfA was then loaded onto a HiTrap Q HP Anion Exchange column (GE Healthcare Life Sciences) previously equilibrated with 50 mM Tris–HCl at pH 8.0 and 5% [v/v] glycerol. Nonspecifically bound proteins were washed with 50 mM NaCl and RbfA was eluted by increasing the NaCl concentration to 100 mM. Purity of the fractions was monitored by 15% SDS-PAGE. Fractions with pure RbfA were dialyzed overnight at 4°C against buffer containing 50 mM Tris–HCl at pH 8.0 and 5% [v/v] glycerol and concentrated using a 10 kDa-cutoff filter (Amicon). Purified RbfA was frozen in liquid nitrogen and stored at −80°C. The amino-terminal His_6-tag in RbfA was not removed in order to facilitate visualization of the protein in the binding assays with the 30S ribosomal subunits (see below).

Purification of 30S ribosomal subunits

Parental (BW25113) and Δ*yjeQ E. coli* cells were used as the source for purification of the mature and immature 30S ribosomal subunits. We used centrifugation over sucrose cushions and gradients as previously described (Jomaa et al. 2011a) to purify both ribosomal particles from these cells (Supplemental Fig. S5A). In the case of the mature 30S subunits, sucrose gradients loaded with ribosomal particles from parental cells were resolved under "dissociating" conditions (buffer containing 1.1 mM magnesium acetate) that leads to the dissociation of the 70S subunits and allows for an efficient purification of mature 30S subunits. Under "associating conditions" (buffer containing 10 mM magnesium acetate), the parental strain yielded a characteristic ribosome profile with the majority of 30S subunits assembled as mature 70S particles, establishing that these cells have a normal wild-type phenotype (Supplemental Fig. S5A). Immature 30S subunits were purified from Δ*yjeQ*. In this case, sucrose gradients loaded with purified ribosomes were resolved under "associating conditions." These cells typically accumulate a large proportion of free immature 30S subunits (~39%) (Supplemental Fig. S3A), thus these conditions allowed us to obtain a homogeneous preparation of immature subunits without contaminating mature 30S subunits.

The rRNA analysis of 30S subunits from parental and Δ*yjeQ E. coli* cells was performed to verify that our purifications of 30S subunits consisted of mature and immature 30S subunits, respectively (Supplemental Fig. S5B). For each preparation, we took ~10–50 pmol of purified ribosome subunits and used the RNeasy Mini Kit (Qiagen) to purify the rRNA following manufacturer's protocols. Subsequently, purified rRNA samples from the fractions corresponding to the 30S, 50S, and 70S peaks in the sucrose gradients were resolved in a 0.9% synergel–0.7% agarose gel using previously described methods (Wachi et al. 1999). This approach allows for the separation during electrophoresis of the 23S, 17S, and 16S rRNAs during electrophoresis. The preparations of mature and immature 30S subunits did not contain any 23S rRNA indicating the absence of 50S subunit contamination. The purification of 30S subunits from parental cells showed the presence of 16S rRNA indicating that it mainly contained mature 30S subunits. Instead, the 30S subunits purified from Δ*yjeQ* cells contained exclusively 17S rRNA, which is the precursor form of the mature 16S rRNA, indicating that the 30S subunits in these preparations were immature. The Δ*yjeQ* cells also contained small amounts of 16S rRNA, but it was incorporated into 30S subunits that were associated to the 50S subunit and appeared in the 70S peak of the gradient.

Circular dichroism spectroscopy

CD spectra for each YjeQ protein were collected using a Circular Dichroism Spectrometer Model 410 (Aviv Biomedical, Inc.). Spectral scans were performed from 260 to 200 nm, with step resolution and bandwidth of 1.0 nm. A 1-mm-path-length quartz cuvette was used for the measurements. The spectra for each protein and each temperature (4°C, 16°C, 25°C, and 37°C) are an average from three consecutive scans obtained during a 15-min incubation period. Protein solutions were prepared at a concentration of 0.5 mg/mL in Binding Buffer 300 (10 mM Tris–HCl at pH 8.0, 7 mM magnesium acetate, 300 mM NH_4Cl, and 1 mM dithiothreitol [DTT]). The machine units of millidegrees ellipticity were used to calculate the mean residue molar ellipticity in [θ] using the following equation:

$$[\theta](\mathrm{deg}\cdot\mathrm{cm}^2\bullet\mathrm{dmol}^{-1}) = \mathrm{Ellipticity(mged)}\bullet 10^6/\mathrm{Pathlength(mm)} \bullet[\mathrm{Protein(mM)}]\bullet n$$

(n is the number of peptide bonds in the protein).

Binding assays

Reactions for filtration assays to detect binding of YjeQ and RbfA to mature and immature 30S subunits were prepared by mixing 200 pmol of protein (YjeQ, YjeQ variants, and/or RbfA) with 40 pmol of 30S subunit in a 100 µL reaction in either Binding Buffer 60 (10 mM Tris–HCl at pH 8.0, 7 mM magnesium acetate, 60 mM NH_4Cl, 1 mM DTT, and 1 mM GMP-PNP) or Binding Buffer 300 (10 mM Tris–HCl at pH 8.0, 7 mM magnesium acetate, 300 mM NH_4Cl, 1 mM DTT, and 1 mM GMP-PNP). The concentration of each protein assembly factor in this reaction was fivefold that of the ribosomal particle. Nucleotide (GMP-PNP, GDP, or GTP) was added where indicated to a final concentration of 1 mM. Reactions were incubated at 16°C, 25°C, or 37°C for 15 min followed by centrifugation in a 100 kDa Nanosep Centrifugal Devices (PALL). In cases where YjeQ was added following a 15 min incubation of RbfA with the ribosomal particle, the binding reaction was allowed to proceed

for another 15 min. Prior to loading the binding reactions in the 100 kDA Nanosep Centrifugal Devices (PALL), its filter membrane was blocked by loading 500 µL of 1% [w/v] BSA and washed twice with 500 µL of RNase free water. Reactions were spun at 12,000*g* for 10 min to separate 30S particles and 30S-bound proteins that were retained by the filter from unbound proteins in flow-through (FT). The flow-through was collected and the filter was washed gently twice with 100 µL of Binding Buffer 60 or 300, followed by a 5 min spin at 12,000*g*. Finally, the 30S particles and 30S-bound proteins retained by the filter were vigorously resuspended in 100 µL of Binding Buffer 60 or 300 and collected as the bound fraction (B). To resolve the flow-through and bound fractions, 30 µL of sample were mixed with 6× SDS-PAGE loading buffer and loaded into a 4%–12% Criterion XT Bis–tris gel (Bio-Rad). Samples were run in XT MOPS buffer (Bio-Rad). Gels were stained with Coomassie blue.

In the case of the pelleting assays, reactions were prepared by mixing 250 pmol of protein (YjeQ, YjeQ variants, and/or RbfA) with 50 pmol of 30S particle in a 50 µL reaction in either Binding Buffer 60 or Binding Buffer 300. The final concentration of GMP-PNP in the binding reactions containing YjeQ and YjeQ variants was 2 mM. Reactions were incubated at 16°C, 25°C, or 37°C for 15 min. In cases where RbfA was added following a 15 min incubation of YjeQ with the ribosomal particle, the binding reaction was allowed to proceed for another 15 min. Following incubation, reactions were laid over a 150 µL 1.1 M sucrose cushion in either Binding Buffer 60 or 300 and spun for 250,000*g* for 5 h. The supernatant (S) containing free protein that did not pellet with the 30S subunits was collected. The pellet (P) containing the 30S particles and 30S-bound proteins was resuspended in 200 µL of Binding Buffer 60 or 300. To resolve the supernatant and pellet fractions, 30 µL of sample was mixed with 6× SDS-PAGE loading buffer and loaded into a 4%–12% Criterion XT Bis–tris gel (Bio-Rad). Samples were run in XT MOPS buffer (Bio-Rad). Gels were stained with Coomassie blue.

Image Lab (V5) software (Bio-rad) was used to perform a densitometry analysis on the Coomassie stained gels for relative quantification of assembly factors binding to 30S subunits. Specifically, the lanes were automatically detected using a background subtraction with a disc size of 5 mm. Bands were then automatically detected using high sensitivity settings (sensitivity: 5, size scale: 7, noise filter: 4, shoulder: 1) followed by manual adjustment of both lanes and bands to ensure accurate measurements. The quantity tools implemented with the Image Lab software package were used to determine the relative amounts of each assembly factor in the bound portion (YjeQ or RbfA) to the S4 protein within the same lane. Binding of wild-type YjeQ or RbfA to the mature or immature 30S subunit was considered as 1 and all other binding interactions were quantified with respect to this value. Prior to the quantification of the bands for YjeQ, YjeQ, variants and RbfA, their intensity was normalized to account for small differences in the amount of binding reaction loaded in the gel. To this end, we used the band for r-protein S4, which should have constant intensity in all binding reactions regardless of whether mature or immature 30S subunits were used. The r-protein S4 is not partially depleted in the immature 30S subunits purified from the Δ*yjeQ E. coli* cells.

GTPase activity assays

The intrinsic initial rates of GTP hydrolysis of the full-length YjeQ and YjeQ variants were measured by incubating each protein (100 nM) with GTP (250 µM) at 25°C for 60 min and then measuring the release of free phosphate using the Malachite Green Phosphate Assay Kit (BioAssay Systems). The reactions were initiated by adding GTP to the proteins in reaction buffer containing 10 mM Tris–HCl at pH 8.0, 7 mM magnesium acetate, 300 mM NH_4Cl, and 1 mM DTT. In those cases where the stimulation of the GTPase activity of YjeQ or YjeQ variants by the 30S particles was measured, the sample also contained 100 nM of 30S particle before GTP was added. Volume of the reactions was 80 µL. Reactions were terminated by addition of 20 µL of the malachite green reagent and an additional incubation of 15 min at 25°C before monitoring color formation by measuring the absorbance at 620 nm. Values were plotted against a standard curve of free phosphate in the same reaction buffer. The amount of phosphate produced by the reaction containing only buffer and GTP was considered background and was subtracted from each reaction. To calculate the fold-increase of the initial rate, the background level of GTP hydrolysis of the 30S particle by itself was subtracted from the value obtained for the reaction containing YjeQ and the 30S subunit. Reactions were run in a 96-well plate and readings were done with the Infinite M1000 multiplate reader (TECAN). Average and standard deviation values were derived from three replicas of each reaction. We determined that under the conditions used to measure GTPase activity, the amount of free phosphate produced in the reactions was within the linear range of the assay.

Culture growth conditions

The growth rate of the null *yjeQ* and parental *E. coli* (BW25113) strains was determined by growing the cells at 25°C for 47 h with shaking. Culture density was monitored by measuring the optical density at 600 nm (OD_{600}) in a Sunrise 96-well plate reader (TECAN) and plotted using Magellan (TECAN). Doubling times were calculated according to the formula $DT = (t2 - t1) \times [\log 2/(\log OD_{600}@t2/\log OD_{600}@t1)]$ and expressed in hours. Growth rates were calculated as $k = \ln 2/DT$ and expressed in h^{-1}.

The growth curves were produced by inoculating 200 µL of LB media from overnight cultures at 1:100 dilutions. To reintroduce the YjeQ or YjeQ M3 variant, we used the high-copy plasmid pCA24N. The pCA24N-empty and pCA24N-*yjeQ* plasmids were purified from the ASKA collection, which contains a complete set of open reading frame clones of *E. coli* (Kitagawa et al. 2005). The pCA24N-*yjeQ* plasmid expresses the amino-terminal histidine-tagged YjeQ under the control of the IPTG-inducible promoter $P_{T5\text{-}lac}$. The pCA24N-*yjeQM3* plasmid was constructed from the pCA24N-*yjeQ* plasmid using QuikChange II XL Site-Directed Mutagenesis Kit (Agilent Technologies) to introduce a stop codon in the position of Lys 320. We used standard protocols (Sambrook et al. 1989) to transform these plasmids into the Δ*yjeQ* cells before proceeding to obtain the growth curves as described above. In the cultures where we wanted to express YjeQ or the YjeQ M3 variant (or pCA24N-empty plasmid) the LB media contained either 1 µM or 100 µM IPTG as specified.

To obtain the ribosome profiles and analyze the rRNA content of these cells, LB cultures (1 L) were grown at 25°C to an OD_{600} of 0.2. In the case of the strains containing the pCA24N-empty plasmid or that encoding for YjeQ or YjeQ M3 variant, we added IPTG to a concentration of 1 µM. Following growth, 10 mL of culture were pelleted by centrifugation at 1400*g* for 20 min and processed to

purify the rRNA. Total rRNA was analyzed by extracting rRNA from the cell pellet with the RNeasy Mini Kit (Qiagen). The concentration of purified rRNA was measured by absorbance at A_{260}, where 1 absorbance unit was equivalent to 40 µg/mL of RNA. Approximately 0.8 µg of purified rRNA was loaded on a 0.9% synergel–0.7% agarose gel, using methods described previously to separate 23S, 17S, and 16S rRNA (Wachi et al. 1999).

The remainder of the cultures were harvested by spinning the cells at 8500*g* for 15 min to obtain ribosome profiles. Pellets were washed and resuspended with 20 mL of Buffer A (10 mM Tris–HCl at pH 7.5, 10 mM $MgCl_2$, and 60 mM KCl), divided into three conical tubes and then centrifuged at 1400*g* for 15 min. Each pellet was resuspended in 6 mL of Lysis buffer (10 mM Tris–HCl at pH 7.5, 10 mM $MgCl_2$, and 60 mM KCl, 0.5 % [v/v] Tween 20, 1 mM DTT, 1 tablet/10 mL complete mini Protease Inhibitor Cocktail [Roche]), and 20 µL of RNase Free DNAse (Invitrogren). The cell suspension was lysed by passing it through the French press three consecutive times at 20,000 lb/in^2 and clarified by centrifuging at 19,000*g* for 10 min. Ribosomes were pelleted by centrifuging the clarified lysate at 125,000*g* for 1 h 52 min. The ribosomal pellet was rinsed with 1 mL of Buffer B (20 mM Tris–HCl at pH 7.5, 6 mM $MgCl_2$, 30 mM NH_4Cl, and 1 mM DTT) and resuspended in 3 mL of this same buffer for 30 min on ice. An equal amount of Buffer C (20 mM Tris–HCl at pH 7.5, 6 mM $MgCl_2$, 800 mM NH_4Cl, and 1 mM DTT) was added and further incubated on ice for 1 h. The mixture was clarified by centrifuging at 19,000*g* for 10 min and subsequently ribosomes were pelleted by centrifuging at 125,000*g* for 1 h 52 min. The ribosomal pellet was rinsed with 700 µL of Buffer D (20 mM Tris–HCl at pH 7.5, 10 mM $MgCl_2$, 30 mM NH_4Cl, and 1 mM DTT) and resuspended in 700 µL of the same buffer for 1 h. The mixture was clarified by centrifuging at 19,000*g* for 10 min and 10 A_{260} units were laid on top of 10 mL 10%–30% sucrose gradients made with Buffer E (20 mM Tris–HCl at pH 7.5, 10 mM $MgCl_2$, 50 mM NH_4Cl, and 1 mM DTT). Gradients were centrifuged at 43,000*g* for 16 h using a Beckman SW41 Ti swinging-bucket rotor. Gradients were then fractioned using a Brandel fractionator apparatus and an AKTAprime purification system (GE Healthcare). The elution peaks of the ribosomal subunits were monitored by absorbance at A_{260}.

SUPPLEMENTAL MATERIAL

Supplemental material is available for this article.

ACKNOWLEDGMENTS

We are grateful to Vivian Leong for technical assistance. This work was supported by a grant from the National Science and Engineering Research Council of Canada (RGPIN288327-12) to J.O. The funders had no role in study design, data collection and analysis, decision to publish, or preparation of the manuscript.

Received November 28, 2014; accepted March 22, 2015.

REFERENCES

Anand B, Verma SK, Prakash B. 2006. Structural stabilization of GTP-binding domains in circularly permuted GTPases: implications for RNA binding. *Nucleic Acids Res* **34:** 2196–2205.

Baba T, Ara T, Hasegawa M, Takai Y, Okumura Y, Baba M, Datsenko KA, Tomita M, Wanner BL, Mori H. 2006. Construction of *Escherichia coli* K-12 in-frame, single-gene knockout mutants: the Keio collection. *Mol Syst Biol* **2:** 2006.0008.

Ban N, Nissen P, Hansen J, Moore PB, Steitz TA. 2000. The complete atomic structure of the large ribosomal subunit at 2.4 Å resolution. *Science* **289:** 905–920.

Boehringer D, O'Farrell HC, Rife JP, Ban N. 2012. Structural insights into methyltransferase KsgA function in 30S ribosomal subunit biogenesis. *J Biol Chem* **287:** 10453–10459.

Bylund GO, Wipemo LC, Lundberg LA, Wikstrom PM. 1998. RimM and RbfA are essential for efficient processing of 16S rRNA in *Escherichia coli*. *J Bacteriol* **180:** 73–82.

Bylund GO, Lovgren JM, Wikstrom PM. 2001. Characterization of mutations in the *metY-nusA-infB* operon that suppress the slow growth of a Δ*rimM* mutant. *J Bacteriol* **183:** 6095–6106.

Campbell TL, Brown ED. 2008. Genetic interaction screens with ordered overexpression and deletion clone sets implicate the *Escherichia coli* GTPase YjeQ in late ribosome biogenesis. *J Bacteriol* **190:** 2537–2545.

Campbell TL, Henderson J, Heinrichs DE, Brown ED. 2006. The *yjeQ* gene is required for virulence of *Staphylococcus aureus*. *Infect Immun* **74:** 4918–4921.

Clatterbuck Soper SF, Dator RP, Limbach PA, Woodson SA. 2013. In vivo X-ray footprinting of pre-30S ribosomes reveals chaperone-dependent remodeling of late assembly intermediates. *Mol Cell* **52:** 506–516.

Daigle DM, Brown ED. 2004. Studies of the interaction of *Escherichia coli* YjeQ with the ribosome in vitro. *J Bacteriol* **186:** 1381–1387.

Daigle DM, Rossi L, Berghuis AM, Aravind L, Koonin EV, Brown ED. 2002. YjeQ, an essential, conserved, uncharacterized protein from *Escherichia coli*, is an unusual GTPase with circularly permuted G-motifs and marked burst kinetics. *Biochemistry* **41:** 11109–11117.

Datta PP, Wilson DN, Kawazoe M, Swami NK, Kaminishi T, Sharma MR, Booth TM, Takemoto C, Fucini P, Yokoyama S, et al. 2007. Structural aspects of RbfA action during small ribosomal subunit assembly. *Mol Cell* **28:** 434–445.

Goto S, Kato S, Kimura T, Muto A, Himeno H. 2011. RsgA releases RbfA from 30S ribosome during a late stage of ribosome biosynthesis. *EMBO J* **30:** 104–114.

Guo Q, Yuan Y, Xu Y, Feng B, Liu L, Chen K, Sun M, Yang Z, Lei J, Gao N. 2011. Structural basis for the function of a small GTPase RsgA on the 30S ribosomal subunit maturation revealed by cryoelectron microscopy. *Proc Natl Acad Sci* **108:** 13100–13105.

Guo Q, Goto S, Chen Y, Feng B, Xu Y, Muto A, Himeno H, Deng H, Lei J, Gao N. 2013. Dissecting the *in vivo* assembly of the 30S ribosomal subunit reveals the role of RimM and general features of the assembly process. *Nucleic Acids Res* **41:** 2609–2620.

Hall BE, Bar-Sagi D, Nassar N. 2002. The structural basis for the transition from Ras-GTP to Ras-GDP. *Proc Natl Acad Sci* **99:** 12138–12142.

Harms J, Schluenzen F, Zarivach R, Bashan A, Gat S, Agmon I, Bartels H, Franceschi F, Yonath A. 2001. High resolution structure of the large ribosomal subunit from a mesophilic eubacterium. *Cell* **107:** 679–688.

Himeno H, Hanawa-Suetsugu K, Kimura T, Takagi K, Sugiyama W, Shirata S, Mikami T, Odagiri F, Osanai Y, Watanabe D, et al. 2004. A novel GTPase activated by the small subunit of ribosome. *Nucleic Acids Res* **32:** 5303–5309.

Inoue K, Alsina J, Chen J, Inouye M. 2003. Suppression of defective ribosome assembly in a rbfA deletion mutant by overexpression of Era, an essential GTPase in *Escherichia coli*. *Mol Microbiol* **48:** 1005–1016.

Inoue K, Chen J, Tan Q, Inouye M. 2006. Era and RbfA have overlapping function in ribosome biogenesis in *Escherichia coli*. *J Mol Microbiol Biotechnol* **11:** 41–52.

Jomaa A, Stewart G, Martin-Benito J, Zielke R, Campbell TL, Maddock JR, Brown ED, Ortega J. 2011a. Understanding ribosome

assembly: the structure of in vivo assembled immature 30S subunits revealed by cryo-electron microscopy. *RNA* **17:** 697–709.

Jomaa A, Stewart G, Mears JA, Kireeva I, Brown ED, Ortega J. 2011b. Cryo-electron microscopy structure of the 30S subunit in complex with the YjeQ biogenesis factor. *RNA* **17:** 2026–2038.

Jomaa A, Jain N, Davis JH, Williamson JR, Britton RA, Ortega J. 2014. Functional domains of the 50S subunit mature late in the assembly process. *Nucleic Acids Res* **42:** 3419–3435.

Kitagawa M, Ara T, Arifuzzaman M, Ioka-Nakamichi T, Inamoto E, Toyonaga H, Mori H. 2005. Complete set of ORF clones of *Escherichia coli* ASKA library (a complete set of *E. coli* K-12 ORF archive): unique resources for biological research. *DNA Res* **12:** 291–299.

Leong V, Kent M, Jomaa A, Ortega J. 2013. *Escherichia coli rimM* and *yjeQ* null strains accumulate immature 30S subunits of similar structure and protein complement. *RNA* **19:** 789–802.

Levdikov VM, Blagova EV, Brannigan JA, Cladiere L, Antson AA, Isupov MN, Séror SJ, Wilkinson AJ. 2004. The crystal structure of YloQ, a circularly permuted GTPase essential for *Bacillus subtilis* viability. *J Mol Biol* **340:** 767–782.

Li N, Chen Y, Guo Q, Zhang Y, Yuan Y, Ma C, Deng H, Lei J, Gao N. 2013. Cryo-EM structures of the late-stage assembly intermediates of the bacterial 50S ribosomal subunit. *Nucleic Acids Res* **41:** 7073–7083.

Nichols CE, Johnson C, Lamb HK, Lockyer M, Charles IG, Hawkins AR, Stammers DK. 2007. Structure of the ribosomal interacting GTPase YjeQ from the enterobacterial species *Salmonella typhimurium*. *Acta Crystallogr Sect F Struct Biol Cryst Commun* **63:** 922–928.

Pettersen EF, Goddard TD, Huang CC, Couch GS, Greenblatt DM, Meng EC, Ferrin TE. 2004. UCSF Chimera—a visualization system for exploratory research and analysis. *J Comput Chem* **25:** 1605–1612.

Ramakrishnan V. 2002. Ribosome structure and the mechanism of translation. *Cell* **108:** 557–572.

Sambrook J, Fritsch EF, Maniatis T. 1989. *Molecular cloning: a laboratory manual*. Cold Spring Harbor Laboratory Press, Cold Spring Harbor, NY.

Shajani Z, Sykes MT, Williamson JR. 2011. Assembly of bacterial ribosomes. *Annu Rev Biochem* **80:** 501–526.

Sharma MR, Barat C, Wilson DN, Booth TM, Kawazoe M, Hori-Takemoto C, Shirouzu M, Yokoyama S, Fucini P, Agrawal RK. 2005. Interaction of Era with the 30S ribosomal subunit implications for 30S subunit assembly. *Mol Cell* **18:** 319–329.

Shin DH, Lou Y, Jancarik J, Yokota H, Kim R, Kim SH. 2004. Crystal structure of YjeQ from *Thermotoga maritima* contains a circularly permuted GTPase domain. *Proc Natl Acad Sci* **101:** 13198–13203.

Wachi M, Umitsuki G, Shimizu M, Takada A, Nagai K. 1999. *Escherichia coli* cafA gene encodes a novel RNase, designated as RNase G, involved in processing of the 5′ end of 16S rRNA. *Biochem Biophys Res Commun* **259:** 483–488.

Wilson DN, Nierhaus KH. 2007. The weird and wonderful world of bacterial ribosome regulation. *Crit Rev Biochem Mol Biol* **42:** 187–219.

Wimberly BT, Brodersen DE, Clemons WM Jr, Morgan-Warren RJ, Carter AP, Vonrhein C, Hartsch T, Ramakrishnan V. 2000. Structure of the 30S ribosomal subunit. *Nature* **407:** 327–339.

Woodson SA. 2008. RNA folding and ribosome assembly. *Curr Opin Chem Biol* **12:** 667–673.

Woodson SA. 2011. RNA folding pathways and the self-assembly of ribosomes. *Acc Chem Res* **44:** 1312–1319.

Yang Z, Guo Q, Goto S, Chen Y, Li N, Yan K, Zhang Y, Muto A, Deng H, Himeno H, et al. 2014. Structural insights into the assembly of the 30S ribosomal subunit *in vivo*: functional role of S5 and location of the 17S rRNA precursor sequence. *Protein Cell* **5:** 394–407.